Online Single Particle Chemical Characterization Of Aerosol Populations in Remote Environments

by

Matthew J. Gunsch

A dissertation submitted in partial fulfillment
of the requirements for the degree of
Doctor of Philosophy
(Chemistry)
in the University of Michigan
2017

Doctoral Committee:

Assistant Professor Kerri A. Pratt, Chair
Assistant Professor Andrew P. Ault
Associate Professor J. Timothy Dvonch
Associate Professor Brandon T. Ruotolo

Matthew J. Gunsch

gunsch@umich.edu

ORCID iD: 0000-0003-2472-8621

ACKNOWLEDGEMENTS

I first need to thank my advisor, Dr. Kerri Pratt, for all of your guidance and mentorship over the past four years. You provided me with the tools, expertise, and mentorship needed to accomplish all that I have throughout my time in your lab, and for that I will always be thankful. Without your hard work and dedication as an advisor, none of this would have been possible.

I also would like to acknowledge my dissertation committee, Dr. Andrew Ault, Dr. Brandon Rutolo, and Dr. J. Timothy Dvonch for their helpful advice on my research. I would individually like to thank Dr. Ault, who has collaborated on many of the projects discussed within this thesis and provided extensive guidance and feedback on much of my work.

I wouldn't have made it through these past years without the help of both past and present labmates, especially Eric Boone, Nate May, Stephen McNamara, Garrett Welshofer, Rachel Kirpes, Peter Peterson, Siyuan Wang and Ryan Cook. I should also acknowledge the Ault lab, particularly, Becky Craig, Amy Bondy and Dan Gardner, for all of their help over the years. Eric started out with me as two of Kerri's first graduate students, and as my deskmate for many years he was always there to answer my Igor questions, even if he eventually limited me to five a day. Peter eventually took over for Eric as my desk mate, and provided me with any assistance I needed with data processing in Microsoft Excel, particularly how to exit out of it and open up Matlab like a real scientist. Nate was vital in getting the TSI ATOFMS up and running for our first field campaign to UMBS in 2014, and without his hard work we would not have been able to collect the data presented in Chapter 3 of this thesis. Stephen, Garrett and Ryan were always there when I needed some help while building the A-ATOFMS, either to do some heavy lifting or just making sure I hadn't lost my mind yet. Ryan and I also had the high honor of representing the University of Michigan in the 2016 Heroes of the Storm collegiate tournament, where we proceeded to win zero games. Rachel provided invaluable microscopy assistance and collected all of the microscopy data presented in Chapter 5, and was always there to discuss how Fran McCaffery was the best coach to ever be in the MAAC. Finally, Siyuan (along with many of the

others listed here) was always there for some of my tri-weekly visits to Panda Express, where he questioned what exactly was “Beijing Beef”. Almost all of us joined at least one of the team we put together for the various rec sports, where we were all reminded why we chose to go into the sciences. Seriously though, I couldn’t have made it through graduate school without any of you, and I cannot thank you enough for everything you’ve helped me achieve over the past years. You all are great labmates, and even better friends.

The atmospheric science field is a very collaborate one, so I need to acknowledge all of the assistance I’ve received on individual chapters. There are full acknowledgements following each chapter on this thesis, but I wanted to give particular thanks to the following: **Chapter 2** – I cannot thank Dr. Kimberly Prather, Joe Mayer, and the rest of the Prather lab enough for all of the assistance they gave us while building the A-ATOFMS. Dr. Prather graciously provided us with all of the schematics for the A-ATOFMS, without which we would not have been able to successfully construct the A-ATOFMS. **Chapter 3 and 4** – Our 2014 field campaign would not have been possible without the combined efforts of the Pratt and Ault labs, or without the support of the University of Michigan Biological Station. We also received generous funding from UMBS as well as the University of Michigan’s MCubed program. This was a collaborative campaign with Dr. Tim VanReken’s group out of Washington State University, who provided valuable AMS data presented in Chapter 3. **Chapter 5 and 6** – I must thank the generous funding provided by NOAA and DOE ARM, making our 2015 field campaign to Utqiaġvik, Alaska and our 2016 field campaign to Oliktok Point, Alaska possible. These were collaborative campaigns with Dr. Rebecca Sheesley’s lab out of Baylor University, and I need to thank her students Dr. Tate Barrett and Claire Moffett for all of their assistance as well.

Last, but most important, I need to thank my family for all of their encouragement throughout my entire academic career. My parents, Mark and Tami, have been the most supportive parents anyone could ask for, and provided me with tremendous amounts of guidance since my first day of school 22 years ago. Without them, I wouldn’t have been able to make to where I am today. My brothers, Mark and Ryan, always took an interest in my work, even though I was the nerdy brother. I also need to thank my Grandma for all of the love she has sent my way while I’ve been away from home (I promise we will make it to Pizza Hut when I get home!). Finally, my girlfriend Casey has been there for me since we met four years ago and supported me every step

of the way through graduate school. She is one of the most understanding and caring people I've met, and I couldn't imagine being here without her.

TABLE OF CONTENTS

LIST OF FIGURES

LIST OF TABLES

LIST OF APPENDICES

ABSTRACT

Atmospheric aerosols have significant impacts on air quality, climate, and human health, yet analytical and logistical challenges have limited our ability to measure these aerosol particles, particularly in remote regions. In this dissertation, individual atmospheric particles were chemically characterized in rural northern Michigan and remote northern Alaska for the first time. To enable this measurements, Chapter 2 details the construction and characterization of an updated aircraft-capable aerosol time-of-flight mass spectrometer (A-ATOFMS), capable of measuring size-resolved chemical composition of 0.07 – 1.6 μm individual particles up to 40 Hz with lower mass (~25 kg saved) and power (~600 W saved) consumption than the previous A-ATOFMS. Chapter 3 discusses size-resolved chemical composition of atmospheric aerosols in northern Michigan while the site was influenced by Canadian wildfire, urban, and local forest air masses. Throughout the study, long-range transported biomass burning aerosols were the cores of particles primarily consisting, by mass, of secondary organic aerosol from the oxidation of volatile organic compounds emitted from both wildfires and forests. In Chapter 4, we identified 14 periods of ultrafine particle growth at the same field site. Urban air mass influence during the daytime led to the highest observed growth rates, likely due to increased atmospheric oxidant levels producing condensable material. Nighttime wildfire air masses were likely influenced by increased SO_2 and NO_2 in the plumes leading to NO_3 radical oxidation. TEM-EDX showed contributions from sulfur, carbon, and oxygen down to 20 nm particles, suggesting contributions from H_2SO_4 and SOA. As particle growth was previously thought to be suppressed in this isoprene-rich forest, these measurements represent a source of particles not previously considered in this environment.

Chapters 5 – 6 discuss the results from field campaigns conducted in the Alaskan Arctic. In Chapter 5, I show results of A-ATOFMS and scanning electron microscopy with energy-dispersive x-ray spectroscopy (SEM-EDX) analyses of atmospheric particles transported to Utqiaġvik, AK from the Prudhoe Bay oil fields, located hundreds of kilometers to the east, in

comparison to the pristine Arctic Ocean background. During Arctic Ocean influence, fresh sea spray aerosol (SSA) was the primary contributor to aerosol number concentrations, compared to transported organic carbon and aged SSA particles during Prudhoe Bay air masses. Chapter 6 details the 2016 field campaign within the Prudhoe Bay oil fields, where we deployed the A-ATOFMS to characterize local oil field combustion plumes and the overall oil field background aerosol population; these were the first single particle measurements within an Arctic oil field. Diesel and natural gas combustion were the major influences on the aerosol population, with unique amine-containing particles identified from the processing of natural gas. Overall, the results from these field campaigns, aided by the newly constructed A-ATOFMS, provided new insights into the chemical composition of local and transported atmospheric particles on rural and remote environments influenced by the changing climate.

Chapter 1. Introduction

1.1. Characteristics of Atmospheric Particulate Matter

Atmospheric particles, especially particulate matter less than 2.5 μm in diameter ($PM_{2.5}$), can impact climate, health and air quality (Pöschl, 2005; Calvo et al., 2013; Pöschl and Shiraiwa, 2015). Atmospheric particle number distributions show the majority of particles are less than 100 nm, though contributions by mass are primarily between 100 – 1000 nm (Seinfeld and Pandis, 2016). Particles less than 100 nm will have a larger impact on health due to their ability to travel further into the body and enter the lungs and bloodstream (Brook et al., 2004; Pope and Dockery, 2006). $PM_{2.5}$ can originate from natural sources, such as the ocean, or anthropogenic sources, such as vehicular combustion. Particulate matter is classified as primary, or directly emitted from a source such as forest fires, or secondary, formed in-situ in the atmosphere from species such as sulfuric acid and low volatility biogenic gases (Pöschl, 2005; Kulmala et al., 2004; Sipila et al., 2010; Jayne et al., 2000; Jokinen et al., 2015). $PM_{2.5}$ directly impacts the climate either by absorbing or scattering incoming solar radiation, or indirectly by acting as cloud condensation nuclei (CCN) or ice nuclei (IN) (IPCC, 2013). Increased levels of $PM_{2.5}$ are also linked to negative health effects (Pope and Dockery, 2006). Particles of different chemical composition have vastly different impacts. For example, a hygroscopic particle, such as sea salt, will act much more readily as a CCN and have a larger indirect effect on the climate (O'Dowd et al., 1997). On the other hand, soot particles will readily absorb incoming solar radiation, leading to a warming effect (Koch et al., 2009; Bond et al., 2013; Moffet and Prather, 2009); whereas, other particle types, such as ammonium sulfate, will readily scatter the incoming light and lead to a cooling effect (Kiehl and Briegleb, 1993; Haywood and Boucher, 2000).

$PM_{2.5}$ impacts are not limited to the area surrounding their source, and $PM_{2.5}$ can be transported to influence locations hundreds of kilometers away (Uno et al., 2009). Transported emissions will impact the aerosol populations in these locations, which can lead remote areas to be out of compliance with National Ambient Air Quality Standards (NAAQS) standards

(Dreessen et al., 2016; National Research Council and National Academies, 2010). Characterizing the impact of these transported particles and the changes in their properties occurring during transport is necessary to predict air quality and climate changes (Calvo et al., 2013). During transport, particles can undergo heterogeneous reactions and gas-particle partitioning, forming secondary species such as water, ammonium, nitrate, sulfate, and oxidized organic carbon (Moffet and Prather, 2009; Riemer and West, 2013). This leads to internally mixed particles, where different chemical species are within the same particle, or externally mixed particles, where chemical species are contained within different particles (Riemer and West, 2013; Ault and Axson, 2017). Changes in particulate chemical composition impacts properties such as reactivity, hygroscopicity, toxicity, scattering and absorption (Pöschl, 2005; Brook et al., 2004; Calvo et al., 2013; Fierce et al., 2016; Furutani et al., 2008). However, assessing the impacts of individual particle mixing state is complex. Many modeling and field studies have found that when sulfate or oxidized organic carbon is internally mixed with soot, particle absorption is increased (e.g. Knox et al., 2009; Liu et al., 2015; Moffet and Prather, 2009; Ramanathan and Carmichael, 2008); however, other studies have found that there may not be significant enhancement of absorption (e.g. Cappa et al., 2012; Healy et al., 2015). Therefore, obtaining measurements of particle mixing state and associated particle properties is essential for understanding the complex impacts of aerosols on climate (Matsui et al., 2013; Bauer et al., 2013).

1.2. Impacts of Climate Change on Natural and Anthropogenic Aerosol Production

While climate change has been impacting areas around the globe for decades, this dissertation will focus on two distinct impacts of climate change. First, increased wildfire activity has been impacting the United States and Canada due to increasing temperatures in wildfire-active regions (Gillett et al., 2004; Knorr et al., 2016; Liu et al., 2010; Veira et al., 2016). Wildfires emit large quantities of $PM_{2.5}$, primarily organic carbon particles, which can have impacts on surrounding areas as well as areas far away through long range transport (Hudson et al., 2004; Pratt et al., 2010). They are also a major contributor of volatile organic compounds (VOCs), which can undergo oxidization and form secondary organic aerosol (SOA) through condensation onto existing particles (Jaffe and Wigder, 2012; Andreae and Merlet, 2001). In fact, models predict that on a national level wildfire emissions are currently the largest

contributor of SOA to $PM_{2.5}$ by mass (Jathar et al., 2014). Ozone is also often produced within these plumes, which can lead to areas far away from the source being out of compliance with ozone regulatory standards (Hu et al., 2008; Jaffe and Wigder, 2012; Lu et al., 2016). With wildfire activity expected to continue increasing due to increasing temperatures and precipitation changes (Liu et al., 2010), it is important to characterize the contributions of long-range transported wildfire emissions to the upper Midwest US atmosphere in order to inform air quality modeling efforts (Smith and Mueller, 2010).

Elevated global temperatures have also made the Arctic more vulnerable to an increase in oil and gas extraction; the melting of Arctic sea ice (Overland and Wang, 2013; Wang and Overland, 2015) has made the area more accessible for increased shipping traffic and extraction activities (Harsem et al., 2015; Allison and Bassett, 2015). With 30% of the world's undiscovered gas and 13% of undiscovered oil thought to be in the Arctic (Gautier et al., 2009), increased access to the open waters is making this area very attractive for further oil and gas extraction activities, adding local pollutants to the atmosphere. The major PM emissions from oil and gas extraction are soot and organic carbon (Peters et al., 2011). Modeling conducted by Sand et al. (2013) predicted that soot emitted within the Arctic will have as much as a factor of five greater warming impact compared to transported soot. With soot estimated to be under predicted by models in the Arctic by a factor of 2.5 (Koch et al., 2009; Bond et al., 2013), accurately quantifying soot, along with other particulate emissions, is critical to fully understand the impacts that oil and gas extraction emissions will have on the Arctic.

1.3. Measurements of Bulk Aerosol Properties

The measurement of atmospheric particles is a challenge due to their complex and evolving nature. Their chemical composition, and therefore properties, is constantly changing, as particles can react with other species in the atmosphere, such as oxidants, and have species partition between gas and particle phases. The chemical composition of particles can be determined through bulk or single particle measurements (Figure 1.1., Prather et al., 2008). One of the most common online bulk measurement techniques is the Aerodyne aerosol mass spectrometer (AMS), where particles are collected onto a tungsten filament where they undergo thermal particle vaporization and electron impact ionization (Jimenez et al., 2003; Jayne et al., 2000). The AMS typically measures size-resolved chemical composition of non-refractory PM less than

1 micron in diameter (PM_1), with collection of mass spectra at a rate of up to 100 Hz and typical data reporting intervals of 1 – 5 minutes. Offline bulk measurements are typically achieved through filter-based sampling, followed by extraction and analysis using methods such as gas or liquid chromatography coupled with mass spectrometers (Pratt and Prather, 2012a). Since offline measurements are not completed in real-time, artifacts can occur, such as the evaporation of semivolatile aerosol components, as well as heterogeneous reactions on the filters. Also, time resolution is limited by how often the filter is changed, typically multiple hours to days. High time resolution is necessary to observe changes in particles due to rapidly changing conditions, such as shifts in wind direction. As these are bulk measurement techniques, they provide an average chemical composition of the particles and can identify contributing sources using tracer compounds (e.g. Sheesley et al., 2004), but the characteristics of each individual particle cannot be isolated. Also, a major drawback of bulk measurements is the inability to measure individual particle mixing state. Using single particle measurement techniques, individual particle mixing states can be determined through both offline and online techniques.

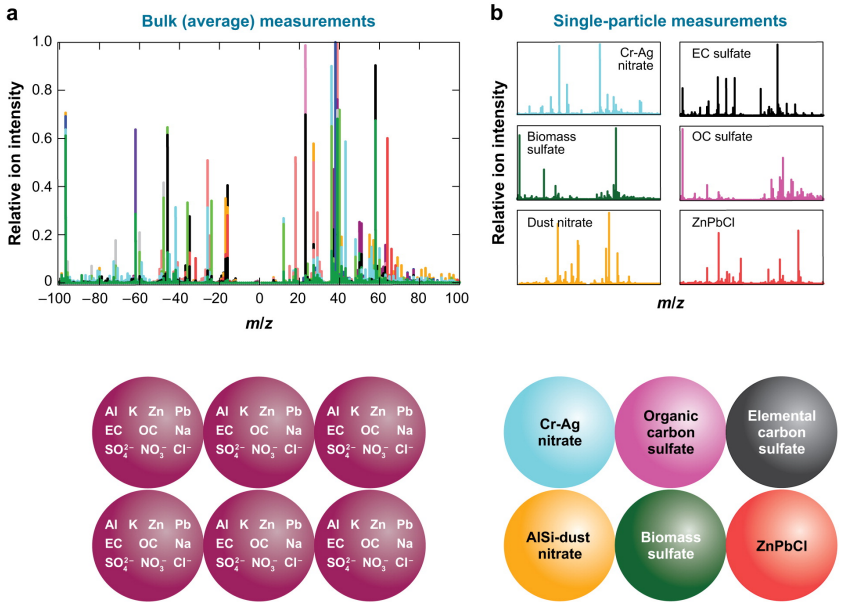

Figure 1.1. Comparison of mass spectra obtained using (a) bulk ensemble analysis versus (b) single-particle analysis. The interpretations of the bulk versus single-particle analyses are shown below. (Figure 1.1 reprinted with permission from Prather, K.A., Hatch, C.D., Grassian, V.H. Analysis of Atmospheric Aerosols. *Annual Review of Analytical Chemistry,* 2008. 1:16.1-16.30.)

1.4. Off-line Chemical Characterization of Individual Aerosol Particles

For offline single particle measurements, particles are collected on substrates using an impactor, such as a multiple orifice uniform deposition impactor (MOUDI, MSP Corp.) or a microanalysis particle sampler (MPS, California Instruments). These types of impactors collect particles on size-resolved stages, allowing analysis to be focused on certain particle size ranges. Applying offline single particle measurements of these collected particles, particle morphology and the distribution of chemical species within each particle can be measured (Ault and Axson, 2017). In addition, non-destructive techniques allow for the same samples to undergo multiple analyses. Many different types of offline single particle measurements are commonly used, including electronic spectroscopy, x-ray techniques, optical microscopy, and vibrational spectroscopy, detailed thoroughly in a recent review by Ault and Axson (2017). This dissertation utilizes electronic spectroscopy, particularly scanning electron microscopy (SEM) and transmission electron microscopy (TEM), both coupled with energy dispersive X-ray (EDX) spectroscopy.

SEM can collect detailed morphological images of single particles down to ~100 nm (Laskin and Cowin, 2001). These images result from the interaction of the particle with a beam of electrons (Ault and Axson, 2017). Computer-controlled SEM automates the collection of these particle images, allowing for substantially more particles to be analyzed with ease (Laskin and Cowin, 2001). TEM has much greater spatial resolution than SEM, allowing for the analysis of ~20 nm particles (Prather et al., 2013); however, it has not yet been automated making the collection of a large number of particles time consuming. When SEM and TEM are coupled with EDX, semi-quantitative chemical information can be obtained by measuring element specific X-rays emitted during interactions between the particle and the electron beam. By rastering across the entire particle, spatially-resolved (<10 nm) chemical composition can be measured (Conny and Norris, 2011). This allows for not only the measurement of individual particle mixing state, but where these species are located within individual particles as well. Elemental mapping can give information on the heterogeneity of the particles, which influence particle properties, such as the ability to scatter and absorb radiation, particle toxicity, and particle reactivity (Conny and Norris, 2011). Both SEM-EDX and TEM-EDX have been used to analyze particles from both field and laboratory studies around the world (e.g. Niemi et al., 2006; Ault et al., 2013; Ault et al., 2014; Gunsch et al., 2017; Adachi and Buseck, 2008; Krueger et al., 2004). However, these

offline techniques require samples to be impacted on substrate, which can change particle morphology through spreading, splattering or fragmenting. These samples also need to be transported and then stored for periods of days to years, which could potentially impact the chemical composition of the particles due to chemical reactions occurring on these particles after collection.

1.5. On-line Chemical Characterization of Individual Aerosol Particles through Single Particle Mass Spectrometry

Almost 50 years ago, the ideal aerosol instrument was described as one that can simultaneously measure the size and chemical composition of aerosol particles in real-time (Friedlander, 1970). This idea began to be realized in the 1980's, when an instrument capable of these measurements was first proposed (Marijnissen et al., 1988), followed by their development in the early 1990's (Prather et al., 1994; Hinz et al., 1994). While there are many different single particle mass spectrometers in use today, both commercially and custom built, most share common characteristics (Pratt and Prather, 2012b; Murphy, 2007). All single particle mass spectrometers have an inlet, either an aerodynamic lens or nozzle, for aerosols to enter and be focused into a tight beam in the instrument. This is typically, though not always, followed by a particle sizing region, either using a one laser configuration that sizes particles based on scattered light, or two lasers which measure the velocity of the particle based on the transit time between them, which can be calibrated to standards of known particle size. Finally, the particles enter a time-of-flight mass spectrometer, where the particles undergo laser desorption and ionization, with either single or dual polarity mass spectra collected by the mass analyzer. Previous reviews have described these instruments in detail (Noble and Prather, 2000; Pratt and Prather, 2012b; Murphy, 2007); here, a brief description of some common single particle mass spectrometer designs is provided.

1.5.1. Aerosol Time-of-Flight Mass Spectrometer (ATOFMS)

The ATOFMS was originally designed in Kimberly Prather's lab in the early 1990's at the University of California – Riverside, and it was one of the first online single particle mass spectrometers developed (Prather et al., 1994). While it has undergone decades of refinement, the basic operating principles have stayed the same. A thorough description of the instrument can

be found in Chapter 2. Briefly, particles enter the instrument through a nozzle or aerodynamic lens system, accelerating the particles to terminal velocity and focusing them in a beam. They continue into the sizing region of the instrument, where particle velocity is measured based on the time it takes to traverse two continuous wave lasers spaced a set distance apart. This can be calibrated to particle diameter based on the velocity of polystyrene latex spheres of a known size and density. The particles then continue into the time-of-flight mass spectrometer, where the particle is desorbed and ionized by a 266nm Nd:YAG laser triggered based on the particle velocity calculated in the sizing region, producing both positive and negative ion mass spectra for each particle.

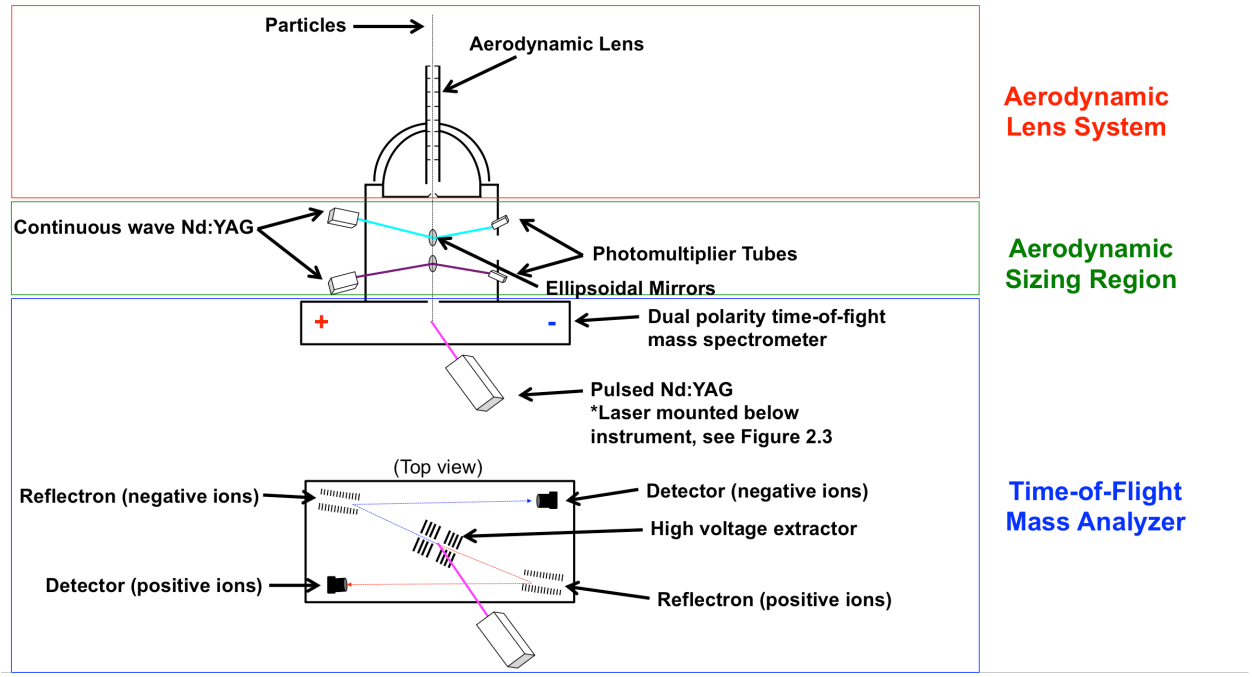

Figure 1.2. Simplified schematic of A-ATOFMS with notable regions outlined. See Chapter 2 for detailed description.

The ATOFMS has undergone five major revisions following the first ATOFMS described in 1994 (Prather et al., 1994). In 1997, the second generation of the ATOFMS was finished, resulting in dual polarity mass spectra and a field portable instrument (Gard et al., 1997). This was followed by a third generation in 1999, used as a prototype for the TSI 3800, the first commercially available ATOFMS. In 2009, a description of the fourth generation ATOFMS

was published, a much more compact ATOFMS (reduction of volume by 57%, length by 69% and weight by 33%) and the first ATOFMS capable of operation on an aircraft (A-ATOFMS, Figure 1.2.) (Pratt et al., 2009b). The A-ATOFMS utilizes a Z-configuration dual polarity time-of-flight mass spectrometer, greatly reducing the overall footprint of the flight tubes, while also increasing ion transmission and resolution. A fifth generation ATOFMS was recently built in the Pratt lab based on the design of the A-ATOFMS and is described in Chapter 2 of this thesis. To date, the ATOFMS has been used in numerous ground, flight and ship-based field campaigns around the world (e.g. Pratt et al., 2009a; Silva et al., 1999; Liu et al., 2003; Qin et al., 2012; Gunsch et al., 2017; Sierau et al., 2014).

Table 1.1. Comparison of single particle mass spectrometers, with published work in the last five years.

Instrument	Inlet Type	Aerodynamic Size Range (μm)	Particle Sizing Method	Ionization Method	Single or Dual Polarity Mass Spectrometer	Notes	References
Nozzle ATOFMS	Nozzle	0.2 - 3.0	Aerosol time of flight	266 nm Nd:YAG (20 Hz)	Dual	Prototype for TSI 3800 ATOFMS	Gard et al., 1997
UF-ATOFMS	Aerodynamic lens	0.05 - 0.3	Aerosol time of flight	266 nm Nd:YAG (20 Hz)	Dual	First ATOFMS with aerodynamic lens	Su et al., 2004
A-ATOFMS (Prather Lab)	Aerodynamic lens	0.09 - 1.2	Aerosol time of flight	266 nm Nd:YAG (50 Hz)	Dual	Capable of use in aircraft.	Pratt et al., 2009
A-ATOFMS (supermicron aerosol lens)	Aerodynamic lens	4.0 - 10	Aerosol time of flight	266 nm Nd:YAG (50 Hz)	Dual	New aerodynamic lens on previous A-ATOFMS	Cahill et al., 2014
A-ATOFMS (Pratt Lab)	Aerodynamic lens	0.07 - 1.6	Aerosol time of flight	266 nm Nd:YAG (100 Hz)	Dual	Based on design of previous A-ATOFMS.	Chapter 2, this thesis
PALMS	Aerodynamic lens	0.15 - 2.0	Aerosol time of flight	193 nm excimer	Single	Capable of use in NASA WB-57F and NOAA P3 aircraft.	Thomson et al., 2000 Cziczo et al., 2006
SPLAT II	Aerodynamic lens	0.05 - 3.0	Aerosol time of flight	two step CO2 (10.6 μm) and UV (193 nm)	Dual	miniSPLAT was developed with reduced footprint.	Zelenyuk et al., 2009 Zelenyuk et al., 2015
NAMS	Aerodynamic lens	0.01 - 0.03	Ion trap	532 nm Nd:YAG	Single	Particles are not sized, however size can be selected by quadrupole.	Wang et al., 2006 Horan et al., 2017
LAMPAS-3	Aerodynamic lens or nozzle	0.2 - 2.5	aerosol time of flight	337 nm laser	Dual	Previous models include LAMPAS and LAMPAS-2	Hinz et al., 2011
ALABAMA	Aerodynamic lens	0.15 - 0.9	aerosol time of flight	266 nm Nd:YAG (5 Hz)	Dual	Particle sizing uses fiber optic lasers.	Brand et al., 2009
SPAMS 3.0	Aerodynamic lens	0.1 - 12*	laser light scattering	248 nm excimer	Dual	Commercially available from Livermore Instruments. *Characterization not available	Livemoreinstruments.com
SPAMS 0515-R	Aerodynamic lens	0.25 - 2.0	aerosol time of flight	266 nm Nd:YAG (50 HZ)	Dual	Commercially available from Hexin Mass Spectrometry	Li et al., 2011
LAAPTOF	Aerodynamic lens	0.1 - 1.0	aerosol time of flight	193 nm excimer	Dual	Commercially available from Aeromegt, GmbH	Gemayel et al., 2017

1.5.2. Other Single Particle Mass Spectrometers

The design of single particle mass spectrometers has varied since their initial conception (Table 1.1). Two notable examples of different designs are the Particle Analysis by Laser Mass Spectrometry (PALMS) and the Single Particle Laser Ablation Time-of-flight mass spectrometer (SPLAT). The PALMS was developed by Daniel Murphy at the National Oceanic and

Atmospheric Administration Earth Research Laboratory (NOAA ERL) and obtains single polarity (either positive or negative ion) mass spectra for individual particles 0.3 – 16 μm in diameter (Murphy and Thomson, 1995). Particles enter the PALMS through a differentially pumped inlet, perpendicular to the scattering and ionization laser. Particles pass through and scatter a 532 nm continuous wave laser, and the scattered light is collected and used to obtain the approximate diameter of the particles. This is also used as a trigger for the 193 nm excimer laser, which desorbs and ionizes individual particles. Unlike the 266 nm Nd:YAG desorption and ionization (DI) laser used on the ATOFMS, an excimer laser does not require a flash lamp to charge and can therefore immediately fire following particle detection. However, the 193 nm excimer laser causes a higher degree of fragmentation of compounds compared to the 266 nm laser, limiting the information obtained about particle chemistry, particularly for organic compounds (Murphy, 2007). As the 193 nm laser operates at high photon energy (6.42 eV) compared to the 266 nm laser (4.66 eV), mass spectrometers incorporating the 193 nm laser are able to characterize species that are unable to be ionized by the 266 nm laser, such as ammonium sulfate, allowing more quantitative characterization (Murphy, 2007). However, increased fragmentation of organic compounds occur (Murphy, 2007; Pratt and Prather, 2012b). In later versions of the PALMS (Thomson et al., 2000), the inlet was replaced with an aerodynamic lens in order to increase the transmission of smaller particles (yet limiting particle analysis to 0.2 – 3 μm), and the 532 nm Nd:YAG laser was split into two beams to provide particle velocity based on particle transit time, similar to the ATOFMS. Sizing particles using transit time between two lasers has been shown to be the more accurate measurement of size compared to the collection of scattered light due to variance in the amount of scattered light based on the spatial orientation of the particle when it scatters the laser beam (Murphy, 2007). This later version of the PALMS is also an aircraft compatible single particle mass spectrometer (SPMS) similar to the A-ATOFMS; however it can only be installed into the nose of the NASA WB-57F research plane or the wing pod of the NOAA P-3, limiting the availability to only these planes.

The SPLAT was developed in Alla Zelenyuk's lab at Pacific Northwest National Laboratory (PNNL) in 2005, and it has since undergone two revisions (SPLAT II and miniSPLAT, both aircraft capable instruments) (Zelenyuk and Imre, 2005; Zelenyuk et al., 2009; Zelenyuk et al., 2015). Similar to the ATOFMS, the SPLAT uses an aerodynamic lens for the inlet and two continuous wave lasers for particle sizing. Instead of an Nd:YAG, the SPLAT typically utilizes a

combination of a pulsed CO_2 infrared (9.4 μm) laser to vaporize semi-volatile species and an excimer (193 nm) laser to ionize the resulting plume as well as non-volatile components, in order to reduce fragmentation of organic compounds. SPLAT II and miniSPLAT both follow these same general principles with a reduced footprint. SPLAT and SPLAT II both produce single polarity (either positive or negative) mass spectra, whereas miniSPLAT uses a Z-configuration dual-polarity time-of-flight mass spectrometer, similar to the A-ATOFMS.

Various other single particle mass spectrometers are in use today, all roughly based on one of the designs above. The Rapid Single Particle Mass Spectrometer (RSMS) was one of the first SPMS instruments, however, it did not include particle sizing (Carson et al., 1995). It later underwent revisions (RSMS-II) to include particle sizing (Phares et al., 2002); however presently it has been repurposed as the Nano Aerosol Mass Spectrometer (NAMS), capable of measuring the chemical composition (but not size) of individual particles less than 10 nm (Horan et al., 2017; Pennington and Johnston, 2012; Wang and Johnston, 2006; Wang et al., 2006). The LAser Mass analyzer for Particles in the Airborne State (LAMPAS) was developed around the same time as the original ATOFMS (Hinz et al., 1994) and was notably the first SPMS to collect dual polarity mass spectra (Trimborn et al., 2000). It has since undergone two major revisions (LAMPAS 2 and LAMPAS 3), reducing the volume of the instrument in order to fit into a single 19" rack typically used on aircraft missions (Trimborn et al., 2000; Hinz et al., 2011). The Aircraft-based Laser Ablation Aerosol Mass Spectrometer (ALABAMA) is one of the most recently developed single particle mass spectrometer, which operates on similar principles to the ATOFMS (Brands et al., 2011). Several commercial SPMS are now sold today, including the Laser Ablation of Aerosol Particles Time of Flight Mass Spectrometer (LAAPTOF, AeroMegt GmbH), Livermore Instrument's Single Particle Aerosol Mass Spectrometer 3.0 (SPAMS 3.0), and Hexin Mass Spectrometry's Single Particle Aerosol Mass Spectrometer (SPAMS 0515-R). The LAAPTOF follows a similar design of the PALMS using a split 532 nm continuous wave laser for sizing and a 193 nm excimer laser for particle ablation. The SPAMS 3.0 and SPAMS 0515-R operate similar to the ATOFMS and use a 266 nm laser for particle ablation triggered based on particle velocity.

1.6. Goals of Dissertation

This dissertation focuses on using single particle chemical composition to investigate aerosol populations in rural environments impacted by the changing climate. Chapter 2 details the design and operation of the newest aircraft-capable aerosol time-of-flight mass spectrometer (A-ATOFMS), built in the Pratt Lab. Chapter 3 describes the characterization of long-range transported aerosols in remote northern Michigan using the TSI 3800 ATOFMS. Chapter 4 details how these same long-range influences impact particle growth in remote northern Michigan, with these particle growth events characterized using aerosol size distribution instrumentation and chemically characterized through TEM-EDX of individual particles. Chapter 5 describes the size-resolved chemical characterization of individual atmospheric particles from within the Prudhoe Bay oil fields located in the Arctic, using the newest A-ATOFMS. Chapter 6 details the chemical characterization of particles transported from Prudhoe Bay to Utqiaġvik, AK, located over 250 km away, using A-ATOFMS and SEM-EDX. Finally, Chapter 7 concludes the dissertation and discusses the future directions of on-going projects. Appendix 1 contains FAA certification documents necessary for the use of the A-ATOFMS within aircraft.

1.7. References

Adachi, K., and Buseck, P.: Internally mixed soot, sulfates, and organic matter in aerosol particles from Mexico City, Atmos. Chem. Phys., 8, 6469-6481, 2008.

Allison, E. H., and Bassett, H. R.: Climate change in the oceans: Human impacts and responses, Science, 350, 778-782, 2015.

Andreae, M. O., and Merlet, P.: Emission of trace gases and aerosols from biomass burning, Global biogeochemical cycles, 15, 955-966, 2001.

Ault, A. P., Guasco, T. L., Ryder, O. S., Baltrusaitis, J., Cuadra-Rodriguez, L. A., Collins, D. B., Ruppel, M. J., Bertram, T. H., Prather, K. A., and Grassian, V. H.: Inside versus outside: Ion redistribution in nitric acid reacted sea spray aerosol particles as determined by single particle analysis, J. Am. Chem. Soc., 135, 14528-14531, 2013.

Ault, A. P., Guasco, T. L., Baltrusaitis, J., Ryder, O. S., Trueblood, J. V., Collins, D. B., Ruppel, M. J., Cuadra-Rodriguez, L. A., Prather, K. A., and Grassian, V. H.: Heterogeneous reactivity of nitric acid with nascent sea spray aerosol: Large differences observed between and within individual particles, J. Phys. Chem. Lett., 5, 2493-2500, 2014.

Ault, A. P., and Axson, J. L.: Atmospheric Aerosol Chemistry: Spectroscopic and Microscopic Advances, Anal. Chem., 89, 430-452, 2017.

Bauer, S. E., Ault, A., and Prather, K. A.: Evaluation of aerosol mixing state classes in the GISS modelE - MATRIX climate model using single - particle mass spectrometry measurements, J. Geophys. Res-Atmos., 118, 9834-9844, 2013.

Bond, T. C., Doherty, S. J., Fahey, D., Forster, P., Berntsen, T., DeAngelo, B., Flanner, M., Ghan, S., Kärcher, B., and Koch, D.: Bounding the role of black carbon in the climate system: A scientific assessment, J. Geophys. Res-Atmos., 118, 5380-5552, 2013.

Brands, M., Kamphus, M., Böttger, T., Schneider, J., Drewnick, F., Roth, A., Curtius, J., Voigt, C., Borbon, A., and Beekmann, M.: Characterization of a newly developed aircraft-based laser ablation aerosol mass spectrometer (ALABAMA) and first field deployment in urban pollution plumes over Paris during MEGAPOLI 2009, Aerosol. Sci. Technol., 45, 46-64, 2011.

Brook, R. D., Franklin, B., Cascio, W., Hong, Y., Howard, G., Lipsett, M., Luepker, R., Mittleman, M., Samet, J., and Smith, S. C.: Air pollution and cardiovascular disease, Circulation, 109, 2655-2671, 2004.

Calvo, A., Alves, C., Castro, A., Pont, V., Vicente, A., and Fraile, R.: Research on aerosol sources and chemical composition: past, current and emerging issues, Atmospheric Research, 120, 1-28, 2013.

Cappa, C. D., Onasch, T. B., Massoli, P., Worsnop, D. R., Bates, T. S., Cross, E. S., Davidovits, P., Hakala, J., Hayden, K. L., and Jobson, B. T.: Radiative absorption enhancements due to the mixing state of atmospheric black carbon, Science, 337, 1078-1081, 2012.

Carson, P. G., Neubauer, K. R., Johnston, M. V., and Wexler, A. S.: On-line chemical analysis of aerosols by rapid single-particle mass spectrometry, J. Aerosol. Sci., 26, 535-545, 1995.

Conny, J. M., and Norris, G. A.: Scanning electron microanalysis and analytical challenges of mapping elements in urban atmospheric particles, Environ. Sci. Technol., 45, 7380-7386, 2011.

Dreessen, J., Sullivan, J., and Delgado, R.: Observations and Impacts of Transported Canadian Wildfire Smoke on Ozone and Aerosol Air Quality in the Maryland Region on 9-12 June, 2015, J. Air Waste Manage. Assoc., 66, 842-862, 2016.

Fierce, L., Bond, T. C., Bauer, S. E., Mena, F., and Riemer, N.: Black carbon absorption at the global scale is affected by particle-scale diversity in composition, Nat. Commun., 7, 2016.

Friedlander, S.: The characterization of aerosols distributed with respect to size and chemical composition, J. Aerosol. Sci., 1, 295-307, 1970.

Furutani, H., Dall'osto, M., Roberts, G. C., and Prather, K. A.: Assessment of the relative importance of atmospheric aging on CCN activity derived from field observations, Atmos. Environ., 42, 3130-3142, 2008.

Gard, E., Mayer, J. E., Morrical, B. D., Dienes, T., Fergenson, D. P., and Prather, K. A.: Real-time analysis of individual atmospheric aerosol particles: Design and performance of a portable ATOFMS, Anal. Chem., 69, 4083-4091, 1997.

Gautier, D. L., Bird, K. J., Charpentier, R. R., Grantz, A., Houseknecht, D. W., Klett, T. R., Moore, T. E., Pitman, J. K., Schenk, C. J., and Schuenemeyer, J. H.: Assessment of undiscovered oil and gas in the Arctic, Science, 324, 1175-1179, 2009.

Gillett, N., Weaver, A., Zwiers, F., and Flannigan, M.: Detecting the effect of climate change on Canadian forest fires, Geophys. Res. Lett., 31, L18211, 2004.

Gunsch, M. J., Kirpes, R. M., Kolesar, K. R., Barrett, T. E., China, S., Sheesley, R. J., Laskin, A., Wiedensohler, A., Tuch, T., and Pratt, K. A.: Contributions of Transported Prudhoe Bay Oilfield Emissions to the Aerosol Population in Utqiaġvik, Alaska, Atmos. Chem. Phys. Discuss., 2017, 1-29, 10.5194/acp-2017-453, 2017.

Harsem, Ø., Heen, K., Rodrigues, J., and Vassdal, T.: Oil exploration and sea ice projections in the Arctic, Polar. Rec., 51, 91-106, 2015.

Haywood, J., and Boucher, O.: Estimates of the direct and indirect radiative forcing due to tropospheric aerosols: A review, Rev. Geophys., 38, 513-543, 2000.

Healy, R. M., Wang, J. M., Jeong, C. H., Lee, A. K., Willis, M. D., Jaroudi, E., Zimmerman, N., Hilker, N., Murphy, M., and Eckhardt, S.: Light‐absorbing properties of ambient black carbon and brown carbon from fossil fuel and biomass burning sources, J. Geophys. Res-Atmos., 120, 6619-6633, 2015.

Hinz, K.-P., Kaufmann, R., and Spengler, B.: Laser-induced mass analysis of single particles in the airborne state, Anal. Chem., 66, 2071-2076, 1994.

Hinz, K.-P., Gelhausen, E., Schäfer, K.-C., Takats, Z., and Spengler, B.: Characterization of surgical aerosols by the compact single-particle mass spectrometer LAMPAS 3, Analytical and bioanalytical chemistry, 401, 3165-3172, 2011.

Horan, A. J., Krasnomowitz, J. M., and Johnston, M. V.: Particle Size and Chemical Composition Effects on Elemental Analysis with the Nano Aerosol Mass Spectrometer, Aerosol. Sci. Technol., 00-00, 2017.

Hu, Y., Odman, M. T., Chang, M. E., Jackson, W., Lee, S., Edgerton, E. S., Baumann, K., and Russell, A. G.: Simulation of air quality impacts from prescribed fires on an urban area, Environ. Sci. Technol., 42, 3676-3682, 2008.

Hudson, P. K., Murphy, D. M., Cziczo, D. J., Thomson, D. S., De Gouw, J. A., Warneke, C., Holloway, J., Jost, H. J., and Hübler, G.: Biomass‐burning particle measurements: Characteristic composition and chemical processing, J. Geophys. Res-Atmos., 109, D23S27, 2004.

IPCC: IPCC, 2013: climate change 2013: the physical science basis. Contribution of working group I to the fifth assessment report of the intergovernmental panel on climate change, edited by: Stocker, T., Qin, D., Plattner, G., Tignor, M., Allen, S., Boschung, J., Nauels, A., Xia, Y., Bex, B., and Midgley, B., Cambridge University Press, 2013.

Jaffe, D. A., and Wigder, N. L.: Ozone production from wildfires: A critical review, Atmos. Environ., 51, 1-10, 2012.

Jathar, S. H., Gordon, T. D., Hennigan, C. J., Pye, H. O., Pouliot, G., Adams, P. J., Donahue, N. M., and Robinson, A. L.: Unspeciated organic emissions from combustion sources and their influence on the secondary organic aerosol budget in the United States, Proc. Natl. Acad. Sci., 111, 10473-10478, 2014.

Jayne, J. T., Leard, D. C., Zhang, X., Davidovits, P., Smith, K. A., Kolb, C. E., and Worsnop, D. R.: Development of an aerosol mass spectrometer for size and composition analysis of submicron particles, Aerosol. Sci. Technol., 33, 49-70, 2000.

Jimenez, J. L., Jayne, J. T., Shi, Q., Kolb, C. E., Worsnop, D. R., Yourshaw, I., Seinfeld, J. H., Flagan, R. C., Zhang, X., and Smith, K. A.: Ambient aerosol sampling using the aerodyne aerosol mass spectrometer, J. Geophys. Res-Atmos., 108, 8425, 2003.

Jokinen, T., Berndt, T., Makkonen, R., Kerminen, V. M., Junninen, H., Paasonen, P., Stratmann, F., Herrmann, H., Guenther, A. B., Worsnop, D. R., Kulmala, M., Ehn, M., and Sipila, M.: Production of extremely low volatile organic compounds from biogenic emissions: Measured yields and atmospheric implications, Proc. Natl. Acad. Sci., 112, 7123-7128, 10.1073/pnas.1423977112, 2015.

Kiehl, J., and Briegleb, B.: The relative roles of sulfate aerosols and greenhouse gases in climate forcing, Science, 260, 311-314, 1993.

Knorr, W., Jiang, L., and Arneth, A.: Climate, CO2 and human population impacts on global wildfire emissions, Biogeosciences, 13, 267-282, 2016.

Knox, A., Evans, G., Brook, J., Yao, X., Jeong, C.-H., Godri, K., Sabaliauskas, K., and Slowik, J.: Mass absorption cross-section of ambient black carbon aerosol in relation to chemical age, Aerosol. Sci. Technol., 43, 522-532, 2009.

Koch, D., Schulz, M., Kinne, S., McNaughton, C., Spackman, J., Balkanski, Y., Bauer, S., Berntsen, T., Bond, T. C., and Boucher, O.: Evaluation of black carbon estimations in global aerosol models, Atmos. Chem. Phys., 9, 9001-9026, 2009.

Krueger, B. J., Grassian, V. H., Cowin, J. P., and Laskin, A.: Heterogeneous chemistry of individual mineral dust particles from different dust source regions: the importance of particle mineralogy, Atmos. Environ., 38, 6253-6261, 2004.

Kulmala, M., Vehkamäki, H., Petäjä, T., Dal Maso, M., Lauri, A., Kerminen, V.-M., Birmili, W., and McMurry, P. H.: Formation and growth rates of ultrafine atmospheric particles: a review of observations, J. Aerosol. Sci., 35, 143-176, 2004.

Laskin, A., and Cowin, J. P.: Automated single-particle SEM/EDX analysis of submicrometer particles down to 0.1 μm, Anal. Chem., 73, 1023-1029, 2001.

Liu, D. Y., Wenzel, R. J., and Prather, K. A.: Aerosol time‐of‐flight mass spectrometry during the Atlanta Supersite Experiment: 1. Measurements, J. Geophys. Res-Atmos., 108, 2003.

Liu, S., Aiken, A. C., Gorkowski, K., Dubey, M. K., Cappa, C. D., Williams, L. R., Herndon, S. C., Massoli, P., Fortner, E. C., and Chhabra, P. S.: Enhanced light absorption by mixed source black and brown carbon particles in UK winter, Nat. Commun., 6, 2015.

Liu, Y., Stanturf, J., and Goodrick, S.: Trends in global wildfire potential in a changing climate, Forest. Ecol. Manag., 259, 685-697, 2010.

Lu, X., Zhang, L., Yue, X., Zhang, J., Jaffe, D. A., Stohl, A., Zhao, Y., and Shao, J.: Wildfire influences on the variability and trend of summer surface ozone in the mountainous western United States, Atmos. Chem. Phys., 16, 14687-14702, 2016.

Marijnissen, J., Scarlett, B., and Verheijen, P.: Proposed on-line aerosol analysis combining size determination, laser-induced fragmentation and time-of-flight mass spectroscopy, J. Aerosol. Sci., 19, 1307-1310, 1988.

Matsui, H., Koike, M., Kondo, Y., Moteki, N., Fast, J. D., and Zaveri, R. A.: Development and validation of a black carbon mixing state resolved three‐dimensional model: Aging processes and radiative impact, J. Geophys. Res-Atmos., 118, 2304-2326, 2013.

Moffet, R. C., and Prather, K. A.: In-situ measurements of the mixing state and optical properties of soot with implications for radiative forcing estimates, Proc. Natl. Acad. Sci., 106, 11872-11877, 2009.

Murphy, D., and Thomson, D.: Laser ionization mass spectroscopy of single aerosol particles, Aerosol. Sci. Technol., 22, 237-249, 1995.

Murphy, D. M.: The design of single particle laser mass spectrometers, Mass Spectrom. Rev., 26, 150-165, 2007.

National Research Council, and National Academies: Global sources of local pollution: an assessment of long-range transport of key air pollutants to and from the United States, xiii, 234 p., National Academies Press, Washington, D.C., xiii, 234 p. pp., 2010.

Niemi, J., Saarikoski, S., Tervahattu, H., Mäkelä, T., Hillamo, R., Vehkamäki, H., Sogacheva, L., and Kulmala, M.: Changes in background aerosol composition in Finland during polluted and clean periods studied by TEM/EDX individual particle analysis, Atmos. Chem. Phys., 6, 5049-5066, 2006.

Noble, C. A., and Prather, K. A.: Real‐time single particle mass spectrometry: A historical review of a quarter century of the chemical analysis of aerosols, Mass Spectrom. Rev., 19, 248-274, 2000.

O'Dowd, C. D., Smith, M. H., Consterdine, I. E., and Lowe, J. A.: Marine aerosol, sea-salt, and the marine sulphur cycle: A short review, Atmos. Environ., 31, 73-80, 1997.

Overland, J. E., and Wang, M.: When will the summer Arctic be nearly sea ice free?, Geophys. Res. Lett., 40, 2097-2101, 2013.

Pennington, M. R., and Johnston, M. V.: Trapping charged nanoparticles in the nano aerosol mass spectrometer (NAMS), International Journal of Mass Spectrometry, 311, 64-71, 2012.

Peters, G., Nilssen, T., Lindholt, L., Eide, M., Glomsrød, S., Eide, L., and Fuglestvedt, J.: Future emissions from shipping and petroleum activities in the Arctic, Atmos. Chem. Phys., 11, 5305-5320, 2011.

Phares, D. J., Rhoads, K. P., and Wexler, A. S.: Performance of a single ultrafine particle mass spectrometer, Aerosol. Sci. Technol., 36, 583-592, 2002.

Pope, C. A., and Dockery, D. W.: Health effects of fine particulate air pollution: lines that connect, J. Air Waste Manage. Assoc., 56, 709-742, 2006.

Pöschl, U.: Atmospheric Aerosols: Composition, Transformation, Climate and Health Effects, Angew. Chen. Int. Ed., 44, 7520 - 7540, 2005.

Pöschl, U., and Shiraiwa, M.: Multiphase chemistry at the atmosphere–biosphere interface influencing climate and public health in the anthropocene, Chem. Rev., 115, 4440-4475, 2015.

Prather, K. A., Nordmeyer, T., and Salt, K.: Real-time characterization of individual aerosol particles using time-of-flight mass spectrometry, Anal. Chem., 66, 1403-1407, 1994.

Prather, K. A., Hatch, C. D., and Grassian, V. H.: Analysis of atmospheric aerosols, Annu. Rev. Anal. Chem., 1, 485-514, 2008.

Prather, K. A., Bertram, T. H., Grassian, V. H., Deane, G. B., Stokes, M. D., DeMott, P. J., Aluwihare, L. I., Palenik, B. P., Azam, F., and Seinfeld, J. H.: Bringing the ocean into the laboratory to probe the chemical complexity of sea spray aerosol, Proc. Natl. Acad. Sci., 110, 7550-7555, 2013.

Pratt, K. A., DeMott, P. J., French, J. R., Wang, Z., Westphal, D. L., Heymsfield, A. J., Twohy, C. H., Prenni, A. J., and Prather, K. A.: In situ detection of biological particles in cloud ice-crystals, Nat. Geosci., 2, 398-401, 2009a.

Pratt, K. A., Mayer, J. E., Holecek, J. C., Moffet, R. C., Sanchez, R. O., Rebotier, T. P., Furutani, H., Gonin, M., Fuhrer, K., and Su, Y.: Development and characterization of an aircraft aerosol time-of-flight mass spectrometer, Anal. Chem., 81, 1792-1800, 2009b.

Pratt, K. A., Heymsfield, A. J., Twohy, C. H., Murphy, S. M., DeMott, P. J., Hudson, J. G., Subramanian, R., Wang, Z., Seinfeld, J. H., and Prather, K. A.: In situ chemical characterization of aged biomass-burning aerosols impacting cold wave clouds, J. Atmos. Sci., 67, 2451-2468, 2010.

Pratt, K. A., and Prather, K. A.: Mass spectrometry of atmospheric aerosols－Recent developments and applications. Part I: Off‐line mass spectrometry techniques, Mass Spectrom. Rev., 31, 1-16, 2012a.

Pratt, K. A., and Prather, K. A.: Mass spectrometry of atmospheric aerosols－Recent developments and applications. Part II: On‐line mass spectrometry techniques, Mass Spectrom. Rev., 31, 17-48, 2012b.

Qin, X., Pratt, K. A., Shields, L. G., Toner, S. M., and Prather, K. A.: Seasonal comparisons of single-particle chemical mixing state in Riverside, CA, Atmos. Environ., 59, 587-596, 2012.

Ramanathan, V., and Carmichael, G.: Global and regional climate changes due to black carbon, Nat. Geosci., 1, 221-227, 2008.

Riemer, N., and West, M.: Quantifying aerosol mixing state with entropy and diversity measures, Atmos. Chem. Phys., 13, 11423-11439, 2013.

Sand, M., Berntsen, T. K., Seland, Ø., and Kristjánsson, J. E.: Arctic surface temperature change to emissions of black carbon within Arctic or midlatitudes, J. Geophys. Res-Atmos., 118, 7788-7798, 2013.

Sheesley, R. J., Schauer, J. J., Bean, E., and Kenski, D.: Trends in secondary organic aerosol at a remote site in Michigan's upper peninsula, Environ. Sci. Technol., 38, 6491-6500, 2004.

Sierau, B., Chang, R.-W., Leck, C., Paatero, J., and Lohmann, U.: Single-particle characterization of the high-Arctic summertime aerosol, Atmos. Chem. Phys., 14, 7409-7430, 2014.

Silva, P. J., Liu, D.-Y., Noble, C. A., and Prather, K. A.: Size and chemical characterization of individual particles resulting from biomass burning of local Southern California species, Environ. Sci. Technol., 33, 3068-3076, 1999.

Sipila, M., Berndt, T., Petaja, T., Brus, D., Vanhanen, J., Stratmann, F., Patokoski, J., Mauldin, R. L., Hyvarinen, A. P., Lihavainen, H., and Kulmala, M.: The role of sulfuric acid in atmospheric nucleation, Science, 327, 1243-1246, 10.1126/science.1180315, 2010.

Smith, S., and Mueller, S.: Modeling natural emissions in the Community Multiscale Air Quality (CMAQ) Model–I: building an emissions data base, Atmos. Chem. Phys., 10, 4931-4952, 2010.

Thomson, D. S., Schein, M. E., and Murphy, D. M.: Particle analysis by laser mass spectrometry WB-57F instrument overview, Aerosol. Sci. Technol., 33, 153-169, 2000.

Trimborn, A., Hinz, K.-P., and Spengler, B.: Online analysis of atmospheric particles with a transportable laser mass spectrometer, Aerosol. Sci. Technol., 33, 191-201, 2000.

Uno, I., Eguchi, K., Yumimoto, K., Takemura, T., Shimizu, A., Uematsu, M., Liu, Z., Wang, Z., Hara, Y., and Sugimoto, N.: Asian dust transported one full circuit around the globe, Nat. Geosci., 2, 557-560, 2009.

Veira, A., Lasslop, G., and Kloster, S.: Wildfires in a warmer climate: Emission fluxes, emission heights, and black carbon concentrations in 2090–2099, J. Geophys. Res-Atmos., 121, 3195-3223, 2016.

Wang, M., and Overland, J. E.: Projected future duration of the sea-ice-free season in the Alaskan Arctic, Prog. Oceanogr., 136, 50-59, 2015.

Wang, S., and Johnston, M. V.: Airborne nanoparticle characterization with a digital ion trap–reflectron time of flight mass spectrometer, International Journal of Mass Spectrometry, 258, 50-57, 2006.

Wang, S., Zordan, C. A., and Johnston, M. V.: Chemical characterization of individual, airborne sub-10-nm particles and molecules, Anal. Chem., 78, 1750-1754, 2006.

Zelenyuk, A., and Imre, D.: Single particle laser ablation time-of-flight mass spectrometer: an introduction to SPLAT, Aerosol. Sci. Technol., 39, 554-568, 2005.

Zelenyuk, A., Yang, J., Choi, E., and Imre, D.: SPLAT II: An aircraft compatible, ultra-sensitive, high precision instrument for in-situ characterization of the size and composition of fine and ultrafine particles, Aerosol. Sci. Technol., 43, 411-424, 2009.

Zelenyuk, A., Imre, D., Wilson, J., Zhang, Z., Wang, J., and Mueller, K.: Airborne single particle mass spectrometers (SPLAT II & miniSPLAT) and new software for data visualization and analysis in a geo-spatial context, Journal of The American Society for Mass Spectrometry, 26, 257-270, 2015.

Chapter 2.
Construction and Characterization of a Second Generation Aircraft Aerosol Time-of-Flight Mass Spectrometer

2.1 Introduction

The aerosol time-of-flight mass spectrometer, a single particle mass spectrometer developed by Kimberly Prather's labs at the University of California – Riverside and San Diego, measures the size and chemical composition of individual aerosol particles in real-time (Cahill et al., 2014; Gard et al., 1997; Prather et al., 1994; Pratt et al., 2009b; Su et al., 2004). The ATOFMS provides dual-polarity time-of-flight mass spectra for individual particles from 50 nm to 10 μm, depending on the configuration (Cahill et al., 2014; Gard et al., 1997; Pratt et al., 2009b; Su et al., 2004). The description of a compact, aircraft-capable version of the ATOFMS was published in 2009 (Pratt et al., 2009b),; the A-ATOFMS features reduced footprint and weight, while increasing performance, and has been used for numerous ground and aircraft-based studies (e.g. Creamean et al., 2013; Pratt et al., 2009a). As part of this dissertation, an updated version of this A-ATOFMS was constructed, using upgraded technology and lower wavelength sizing lasers, increasing characterization down to 70 nm particles, and doubling the maximum theoretical data collection rate while lowering the weight and power consumption of the instrument. In this chapter, the design, upgrades, and performance of the updated A-ATOFMS, built in the Pratt Lab, are discussed. This updated A-ATOFMS was deployed during 2015 and 2016 to the Alaskan Arctic (Chapters 5 and 6), providing valuable insights onto particulate matter contributions from Arctic oil and gas extraction.

2.2 Experimental

2.2.1. Design of the A-ATOFMS

A field-capable instrument requires a high data acquisition rate in order to obtain the necessary time resolution to distinguish different atmospheric sources that quickly pass (e.g.

moving plume, nearby vehicles, etc.). Atmospheric aerosols enter the A-ATOFMS (Figures 1.2 and 2.1) through a 1.5 mCi ^{210}Po neutralizer (3 x Staticmaster 1400, Amstat Industries Inc, custom built enclosure), which imparts a Boltzmann distribution of charges on the aerosol

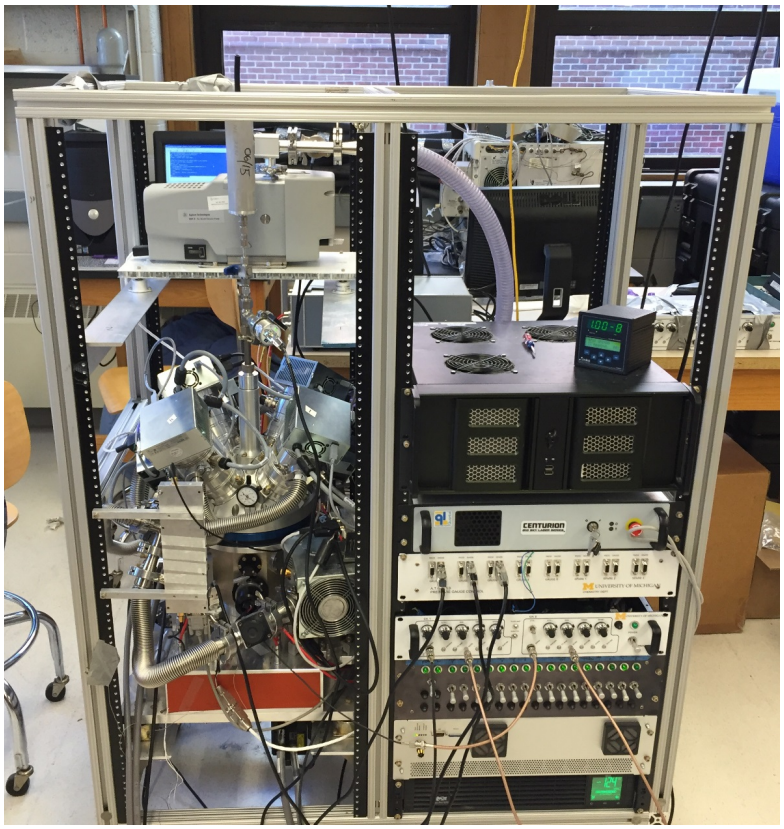

Figure 2.1. Picture of the A-ATOFMS within the Pratt Lab.

population. Particles then pass through an orifice with an opening of 75 - 100 µm, depending on the aerodynamic lens system in use (Section 2.3.2.1), at ~0.1 L/min. Particles continue into the aerodynamic lens system (ALS), consisting of a relaxation chamber, orifice disks of varying sizes, and an accelerating nozzle, which collimates the particles into a tight beam. Two aerodynamic lens systems were constructed and tested with the A-ATOFMS: one with a cylindrical relaxation region and six orifices of decreasing internal diameter (ALS A) and one with a conical relaxation region and seven orifices spaced 30 mm apart (ALS B). A conical relaxation region is preferable as it limits losses of large particles impacting onto the walls (Zhang et al., 2004). When using ALS B during both aircraft and ground studies, a pressure-controlled inlet based on the design of Bahreini et al. (2008) needs to be used in order to set the upstream pressure to 4.8 torr. The aerodynamic lens system is installed within a moveable dome,

which allows for adjustment to the alignment of the aerodynamic lens. A stationary dome can also be used, which removes this adjustment ability while increasing the overall stability and decreasing the weight of the instrument; however, initial tests indicated that our aerodynamic lens requires the adjustment from the moveable dome to transmit the particles down the center of the light scattering region. Four Agilent TwisTorr 84 turbomolecular pumps, operating at 66 L/s, are used on the dome, replacing the previous Agilent V70 pumps. These pumps have reduced weight (~2 lbs less each, including the controller) and power consumption (~0.2 amps less each). While it is optimal to use four turbomolecular pumps for pumping the dome, the instrument can function with only two of these pumps active (though it increases the stress on the active pumps). This allows for greater flexibility for weight restrictions during flight campaigns. A Pirani Vacuum Sensor Series 917 (MKS) is used to monitor the pressure of this region. The particle beam exits the dome through a 1.0 mm diameter skimmer and continues into the particle sizing region of the instrument.

The particle sizing region consists of two orthogonal continuous wave lasers, focused using plano-convex lenses (KPX055-C, Newport), vertically spaced 6 cm apart. The particle beam travels perpendicular to the two lasers and as a particle passes by the first laser beam from a 50 mW 488nm laser (OBIS, Coherent Inc.), the scattered light is focused using an elliptical mirror (Optiforms) onto a photomultiplier tube (PMT, U10721-110, Hamamatsu). The scattering signal is amplified to a +5V square wave and sent to the timing circuit, beginning a timing sequence. The particle continues and scatters the light of a 50 mW 405 nm laser (OBIS, Coherent, Inc) with the scattered light similarly focused into a second PMT, the action of which triggers stopping the timing sequence. In the future, the scattered light waveform will be optionally collected using a digitizer (Express OSCAR 12-bit, GaGe) to further investigate particle density and refractive index (Moffet and Prather, 2005). Particle velocity is calculated by the time it takes the particle to traverse the 6 cm spacing of the two lasers. Particle velocity is then converted to particle vacuum aerodynamic diameter by applying a calibration of the velocities of polystyrene latex spheres (Polysciences, Inc.), with known diameter, shape, and density, using a 5^{th} power polynomial (Figure 2.2). Below 300 nm, particle velocity is fit to a power regression (Figure 2.2). For a quick fit to visualize the data in real-time within the A-ATOFMS software, the particle diameter calibration curve is fit to a power regression. The

particle sizing region is pumped by one TwisTorr 84 (Agilent), and the pressure is monitored by a 925 MicroPirani (MKS).

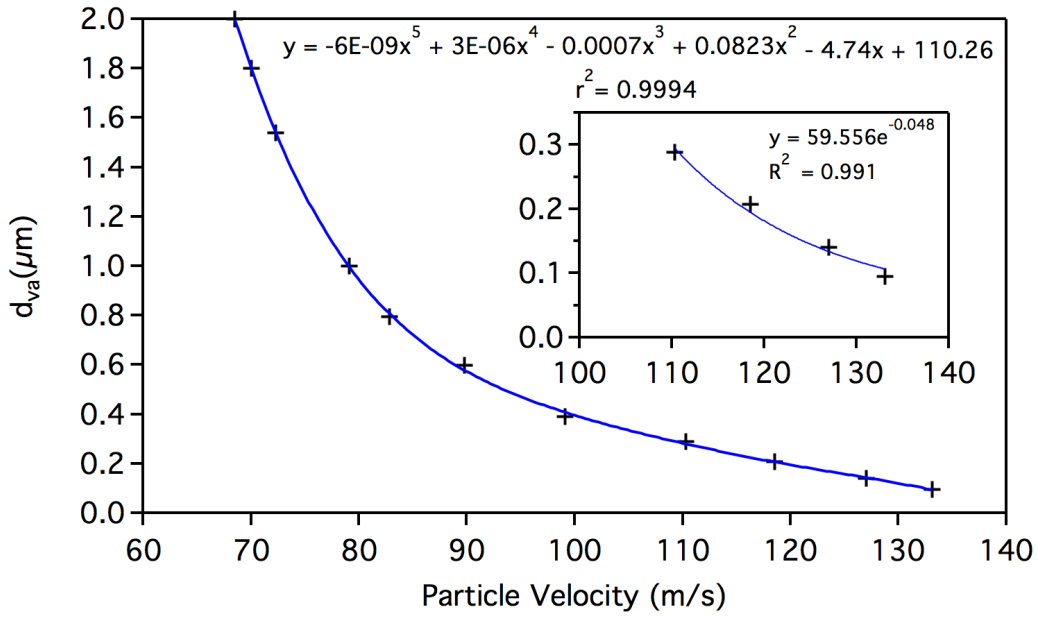

Figure 2.2. Particle diameter calibration of ALS 1 using atomized PSLs. A 5th order polynomial is fit to PSLs from 0.090 – 1.6 μm (vacuum aerodynamic diameter). Note: When using size calibration data during data processing, 11 significant figures should be used to ensure software applies the correct calibration.

The particle beam exits the particle sizing region and enters the mass spectrometer, a second generation Z-configuration dual-polarity reflectron time-of-flight mass spectrometer (ZTOF, Tofwerk). The ZTOF is separated from the aerodynamic sizing region by a ball valve, allowing the ZTOF to be isolated in case of vacuum loss. Based on particle velocity, a Q-switched 100 Hz 266 nm Nd:YAG laser (Centurion, Quantel Inc), operating at ~1 mJ, is triggered by the timing circuit to desorb and ionize the single particle. A series of pins and jumpers have been added to the timing circuit to control the Nd:YAG laser makeup pulses, replacing the previous dial. These makeup pulses just fire the LED within the Nd:YAG laser, keeping it warmed up in low particle concentrations. However, these makeup pulses can interfere with "real" laser shots, leading to missed particles. These jumpers allow the timing circuit to be pre-programmed with up to nine unique pulse rates, easily configurable through the programmable port on the back of the timing circuit. This pulse rate should be set as low as

possible while ensuring that the laser fires at ~1 mJ, in order to minimize the number of particles missed during these make-up pulses.

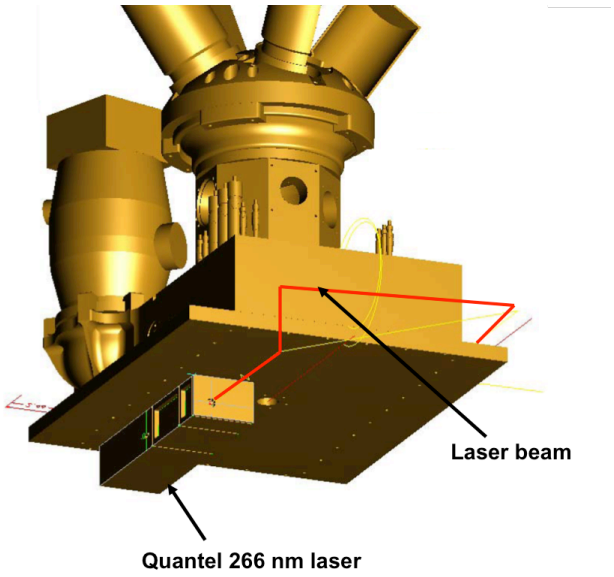

Figure 2.3. Position of the laser beneath the A-ATOFMS. The laser beam path is drawn below the instrument in red.

The laser is positioned underneath the mass spectrometer (Figure 2.3), and the laser beam is directed to the ZTOF using four 12.5 mm Nd:YAG laser line mirrors (47-980, Edmund Optics) and focused using a plano-convex lens (SPX025AR.10, Newport). The positive and negative ions are extracted using a pulsed (triggered) high voltage (+/- 2.8 kV) and accelerated into field free drift regions. Ions are focused within reflectrons into second field free regions and onto 25 mm bipolar time-of-flight ion detectors, each made up of an microchannel plate (MCP), scintillator, and photomultiplier tube (PMT). Positive and negative ion mass spectra (see example individual particle mass spectra in Figure 2.4) are collected by two data acquisition cards (U1071-001, Agilent Technologies), with each polarity collected onto two channels (one attenuated, one unattenuated) for a greater dynamic range of signal. These data acquisition cards are triggered by the Q-switch of the Nd:YAG laser, and the data is processed using custom software programmed in LabVIEW and C. The mass spectrometer is pumped by an Agilent TwisTorr 304 (220 L/s), capable of operating with a lower backing pressure (0.75 torr), compared the previous Agilent V301. This has allowed the entire instrument to be backed by a single Agilent IDP-3 dry scroll (60 L/min), isolated from the instrument by four vibration dampeners (T22-AB-5, Barry Controls). The entire instrument is situated on similar vibration

dampeners, discussed in Section 2.2.2. This pump is oil-free and therefore requires minimal maintenance, only needing the tip seals replaced every ~20,000 run hours, or when the ultimate pressure starts decreasing.

The A-ATOFMS is powered by a custom built power distribution unit (PDU), with 17 locking switches and independent fuses, to provide power to individual components. The PDU itself is plugged into a 1500 VA (1350 W) uninterruptable power supply (UPS), capable of running the entire instrument for ~10 minutes. While this provides a short amount of time to allow the instrument to be properly shut down and sealed in case of power loss, the UPS is primarily needed to bridge the brief power outage when switching from ground power to aircraft power. From the UPS, the entire A-ATOFMS is run from a single NEMA 5-15P plug and can plug into standard electric outlets, with a maximum power draw of 1100 W, ~400 W less than the original A-ATOFMS (Pratt et al., 2009b). During normal operation (without pressure controlled inlet), the new A-ATOFMS draws only 840 W, ~600 W less than the original A-ATOFMS (Pratt et al., 2009b).

2.2.2. Aircraft Specifications

In order for the A-ATOFMS to operate on most research aircraft, the instrument needs to undergo FAA approval on the design, construction, and components of the instrument. The previous A-ATOFMS has undergone this approval process, and the current A-ATOFMS will undergo approval before the first flight campaign. In order to be approved for flight, the structural design must conform to all guidelines listed in within the *National Science Foundation/National Center for Atmospheric Research (NSF/NCAR) High-performance*

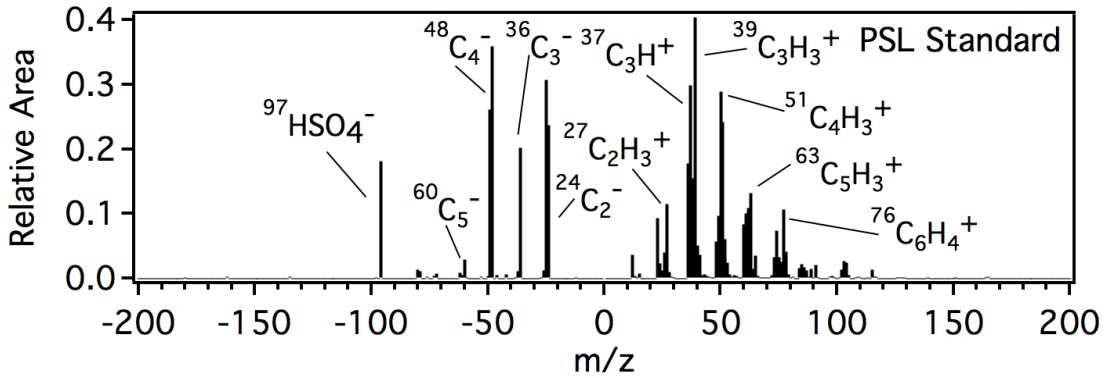

Figure 2.4. Dual-polarity mass spectrum of a 300 nm polystyrene latex sphere (PSL) standard collected by the A-ATOFMS.

Instrumented Airborne Platform for Environmental Research (HIAPER) Investigator Handbook and *NSF/NCAR C-130 Investigator Handbook*, limiting hazards and ensuring the instrument can perform during flight. For example, the updated A-ATOFMS now uses an air-cooled Nd:YAG laser instead of a water cooled one, limiting this potential hazard. In addition, the instrument must be able to handle all loads imposed by emergency landings, in-flight lift and drag forces, and gust loads. The preferred material for aircraft flight is aluminum primarily due to a high strength to weight ratio. Therefore, the body of the A-ATOFMS is constructed out of machined 6061 aluminum alloy and assembled using various cadmium-plated fasteners which conform to Military Specifications (MS) and National Aerospace Standards (NAS). To protect the instrument from vibrations during use, cadmium-plated lock nuts were used for all fasteners not directly attached to the body, and helicoil-inserts were used for the rest of the fasteners directly attached to the body of the A-ATOFMS in order to strengthen the threaded holes. Also to isolate the instrument from the influence of external vibration, the entire A-ATOFMS body is attached to the rack by four vibration dampeners (T64-AB-80, Barry Controls).

In addition to structural requirements, all custom-built electrical systems must conform to the guidelines stated in the *FAA Advisor Circulars: Chapter 11 – Aircraft Electrical Systems* of *AC 43.13-1B – Acceptable Methods, Techniques, and Practices – Aircraft Inspection and Repair*. Briefly, this indicates that all wiring must be self-extinguishing and made of an approved material, typically a fluoropolymer. For the A-ATOFMS, all internal custom wiring is made out of tinned copper insulated by ethylene tetrafluoroethylene (ETFE), as described in military specification *MIL-W-22759*. Power cables were constructed out of silver-coated copper insulated with polytetrafluoroethylene (PTFE), as described in military specification *MIL-W-16878*. BNC signal cables consist of a conductor made out of silver covered copper clad steel, dielectric material of PTFE, silver covered copper shields and a fluorinated ethylene propylene (FEP) jacket, as described in military specification *MIL-DTL-17*. RS-232 signal cables have a low smoke zero halogen (LSZH) insulation specifically designed for use within aircrafts. Commercially purchased electronics that have not undergone modification are exempt from these specifications. These include the computer, monitor, all laser power supplies, and ZTOF-MS power supply. All power connectors have been designed to use MS locking circular power connectors, approved for use within aircraft.

2.2.3. Instrument Characterization

In order to assess the performance of the aerodynamic lens system in a controlled environment, as well as calibrate particle velocity and size, a set of standards were used. A ~150 mL water solution of NIST-calibrated polystyrene latex spheres (PSLs, Polysciences) of known diameter (90 – 2000 nm) and density (1 g/mL) were aerosolized using a custom-built Collison atomizer and passed through two silica diffusion driers to remove particle water (relative humidity following driers is ~ 20 – 40%). For characterizing aerodynamic lens transmission, the atomized PSL flow was split between the ATOFMS, a scanning mobility particle sizer (SMPS 3082, TSI Inc.), and an aerodynamic particle sizer (APS 3321, TSI Inc.) in order to compare the atomized particle number concentration to the ATOFMS measured particle number concentration.

2.3. Results and Discussion

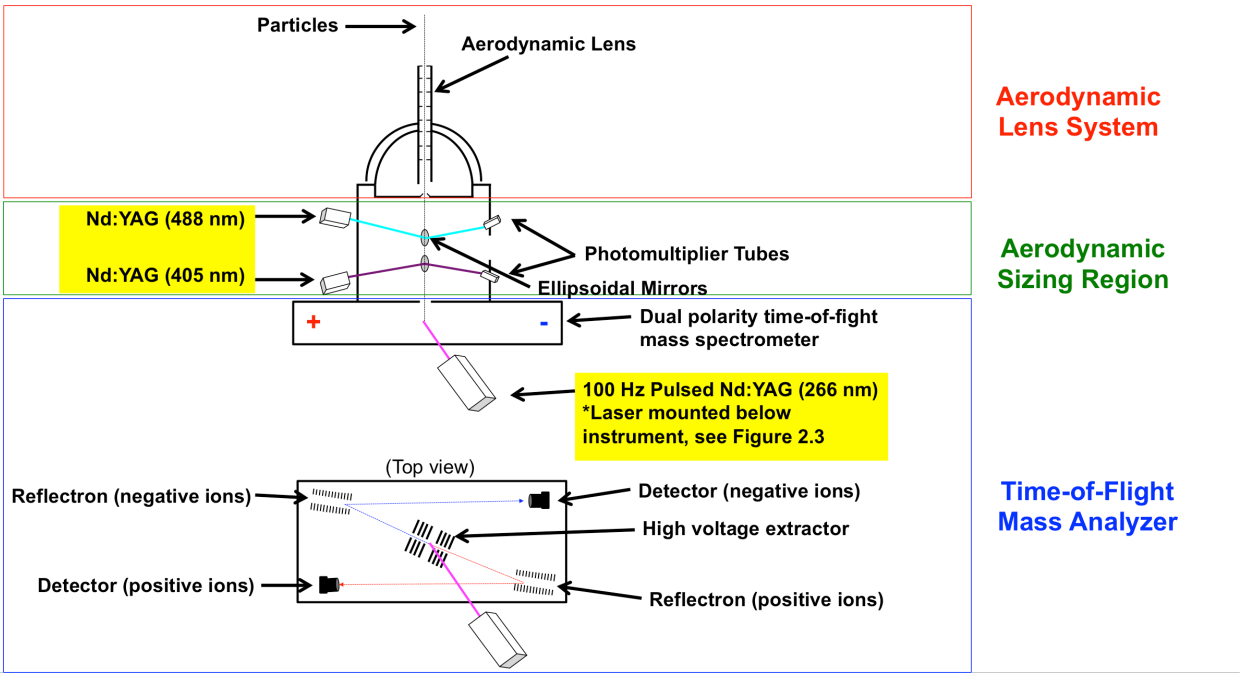

Figure 2.5. Schematic of A-ATOFMS with notable regions outlined. Upgraded lasers are highlighted in yellow.

2.3.1. Design Modifications

2.3.1.1. Improved Light Scattering Region

The light scattering region was optimized for improved detection of ultrafine (<0.1 μm) particles. Previously, two 50 mW continuous wave 532 nm solid-state lasers (JDS Uniphase) were used in this region. These were expensive lasers that are now difficult to acquire if one were to fail while the instrument was in use. These have been replaced with 50 mW Coherent OBIS lasers, one 405 nm and one 488 nm, which had many added benefits (Figure 2.5). First, the OBIS lasers are more compact (~38 mm less in length) and weigh less (~0.5 kg less). Also, using smaller wavelengths takes advantage of scattering intensity being proportional to λ^{-4} (Bohren and Huffman, 2008), such that a 405 nm laser has 3x greater scattering than 532 nm, for example. The photomultiplier tubes (PMT) have also been upgraded to a newer model (H-10721, Hamamatsu) that have a higher quantum efficiency, leading to greater signal associated with the scattered light. The timing circuit has been redesigned using modern components and now incorporates a second PMT output channel, which gives an attenuated signal in order to accurately measure the light scattered by individual particles without saturating the signal, as previously occurred. This will allow the instrument to be used to measure chemically-resolved single-particle refractive index and density (Moffet and Prather (2005) with increased accuracy as both an attenuated and non-attenuated signal will be able to be collected. This collection should also be improved by the implementation of two scattering laser wavelengths (488 nm and 405 nm). Previous studies (Moffet and Prather, 2005, 2009) that used two 532 nm lasers found that scattering curves for particles greater than 600 nm began to "tip over" at characteristic refractive index and density values, allowing for these properties to be determined for these size particles. In contrast, particles smaller than 600 nm in diameter showed a single curve, such that refractive indices and densities could not be determined. Therefore, with the new lasers, we will be able to probe smaller particles with the 405 nm laser, as scattered light increases by λ^{-4}, and larger particles with the 488 nm laser, without saturating the signal. In addition, the interior of the light scattering region was black anodized, limiting interference from stray light for more accurate light scattering signal collection.

2.3.1.2. Improved Mass Spectrometer

Upgrades were also made to the Z-configuration dual-polarity reflectron time-of-flight mass spectrometer (ZTOF). First, the ZTOF power supply was upgraded by Tofwerk, leading to a significant reduction in weight (~4.5 kg). The ion optics within the ZTOF were also upgraded with the newer technology available during this build, though the mass resolving power of the positive (~500 at *m/z* 100) and negative spectra (~800 at *m/z* -100) are still similar to the previous A-ATOFMS (Pratt et al., 2009b). Finally, a high voltage pulser has been added to the ZTOF ion extraction plates, which is synced with the Q-switch on the ionization laser, pulsing the voltages as soon as the laser is fired.

The original 50 Hz Ultra CFR 266nm laser (Big Sky Laser/Quantel) was replaced with a 100 Hz Centurion 266nm laser (Quantel) (Figure 2.5). The Centurion is an air-cooled solid-state laser, which eliminates the need for a flash lamp (can burn out or break) and water cooling (hazard for aircraft operation), leading to an overall more reliable laser both on the ground and during flight. In addition, the laser is now controlled directly through the computer, allowing for streamlined control of the instrument through the updated custom software. The 100 Hz fire rate allows the instrument to analyze more particles as it is not limited by the previous 50 Hz fire rate. Laboratory studies show an increased maximum rate of data collection (Section 2.3.2).

2.3.2. Performance

2.3.2.1. Transmission and Scattering Efficiency

In order to characterize the two aerodynamic lens systems used on the A-ATOFMS, particle transmission and scattering efficiency was compared to previous modeled (transmission only) and experimental (transmission + scattering, Pratt et al., 2009) results. Particle transmission and scattering efficiency is defined as the percentage of particles that are focused within the ALS and subsequently scatter the light of both sizing lasers, Modeling of the aerodynamic lens system A (ALS A), based on previous designs (Liu et al., 1995a, b), indicates that particle transmission less than 600 nm should be close to 100%, and decrease to ~25% by 1000 nm and 10% by 3000 nm (Wang and McMurry, 2006). However, even if 100% of the particles are transmitted through the lens, the A-ATOFMS still needs to be able to detect the particles within the aerodynamic sizing region. Therefore, in practice, the transmission and scattering efficiency is much less, as not all particles traverse in a straight line between the two lasers and smaller particles do not

scatter enough light from the continuous wave lasers to be detected by the PMTs. The scattering efficiency curve for the aerodynamic lens system on the current and previous A-ATOFMS instruments, as well as the modeled transmission efficiency (Wang and McMurry, 2006) are shown in Figure 2.6. Similar to the previous A-ATOFMS (Pratt et al., 2009), the transmission and scattering efficiency minimum was 0.2% for 90 nm PSLs and increased to a maximum of 60% at 800 nm. Above 800 nm the transmission begins to decline, reaching a minimum of 5% at 3 µm. Ambient soot, which is not spherical and can therefore scatter more light per its vacuum aerodynamic diameter, was observed down to 70 nm (Chapter 6); however, attempts to run PSLs smaller than 90 nm have not been made. While the transmission curves for the two A-ATOFMS instruments deviate some above 1.5 µm, the mode diameter for the atmospheric aerosol

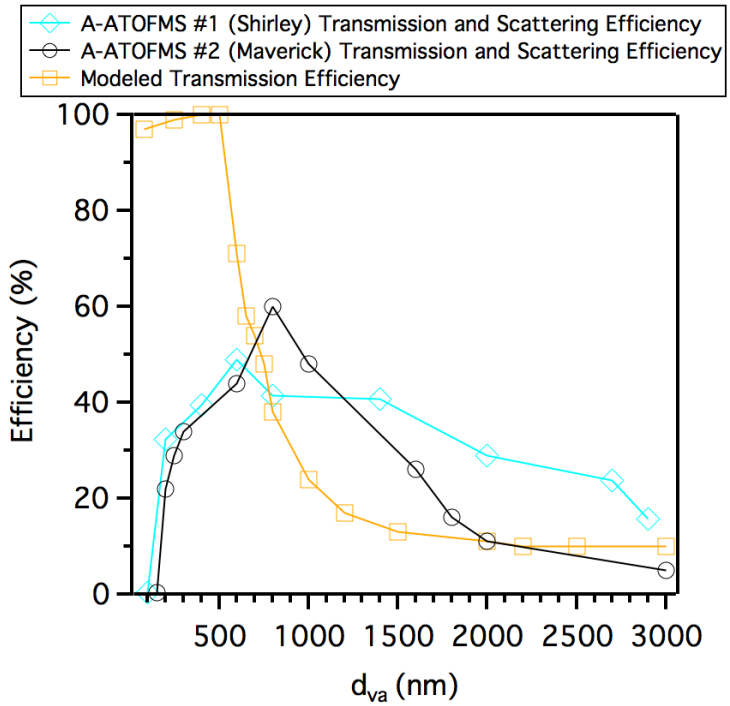

Figure 2.6. A-ATOFMS (#2, "Maverick", University of Michigan) scattering efficiency compared to the previous A-ATOFMS (#1, "Shirley", University of California, San Diego; Pratt et al., 2009) and modeled transmission (Wang and McMurry, 2006).

population is <0.2 µm; therefore, this inconsistency (likely due to minute differences in machining of the aerodynamic lens system) is not expected to significantly impact ambient aerosol sampling and characterization.

Aerodynamic lens system B (ALS B) has not previously been fully characterized; however, it has been used in past aircraft-based field campaigns by the Prather Lab (Cazorla et al., 2013; Creamean et al., 2013). Since ALS B uses a conical relaxation chamber, fewer larger particles should be lost through impaction compared to a cylindrical chamber. Also, ALS B is designed for use in flight, and therefore a pressure-controlled inlet, based on the design of Bahreini et al. (2008), was constructed and is necessary to set the pressure of the relaxation region at 4.8 torr to ensure the lens focuses as designed. Future work includes fully characterizing the transmission efficiency of this aerodynamic lens system.

2.3.2.2. Single-particle Mass Spectral Acquisition Rate

The A-ATOFMS is run by custom LabVIEW instrumental software, and drivers have been upgraded for use with Windows 7, increasing the overall software performance and data collection rate. When configured for maximum data acquisition rate, the previous version of the A-ATOFMS needed 33.5 ms to detect, read, and save both positive and negative mass spectra of individual particles for a maximum theoretical collection rate of 30 Hz; however, Pratt et al. (2009b) noted that observed collection rates were slower due to non-ideal particle spacing. For the new A-ATOFMS, the upgraded software, computer, and electronics have lowered the time needed to collect positive and negative spectra to 15 ms, doubling the previous maximum theoretical collection rate to 67 Hz when configured for maximum data collection. With real-time instrument and online analysis displays active, the new A-ATOFMS needs 25 ms for each hit particle, providing a maximum acquisition rate of 40 Hz, over 4 times the previous A-ATOFMS (120 ms, or 8.3 Hz).

2.4. Conclusions

An updated version of the field transportable and aircraft capable A-ATOFMS was constructed, based on the design of Pratt et al. (2009b). Two aerodynamic lens systems were characterized for this new A-ATOFMS, allowing for flexibility on studies that require the analysis of smaller (0.07 – 1.6 μm) particles (ALS #1) or larger particles (~0.1 – 2.5 μm) (ALS #2). Also, as the previous A-ATOFMS was built over 10 years ago, major technological upgrades were made to the instrument, including upgrading the computer, lasers, pumps, and mass spectrometer, reducing the weight by 23 kg and power by 400 W. Decreased sizing laser wavelengths, along with a black anodized light scattering region, has improved the lower limits of particle characterization to 70 nm. In addition, upgrades to the data acquisition computer and

Nd:YAG laser increased the maximum theoretical mass spectral acquisition rate from 30 Hz to 67 Hz. As the majority of atmospheric aerosol particles are less than 100 nm by number and aircraft deployments require fast data acquisition for spatially resolved measurements, these improvements this will allow for a more complete characterization of aerosol populations while deployed in the field. The newly constructed A-ATOFMS has already been deployed to remote Alaska during 2015 and 2016 (Chapters 5 and 6), collecting valuable data on the impacts of Arctic oil and gas extraction activities.

2.5. Acknowledgements

The authors gratefully acknowledge Kim Prather and Joe Mayer (University of California, San Diego) for providing the schematics of the original A-ATOFMS, without which this build would not have been possible. Jack Cahill, Hashim Al-Mashat, and the rest of the Prather lab are also thanked for answering questions during the A-ATOFMS construction. Urs Rohner (Tofwerk) is thanked for assistance with ZTOF voltage tuning and troubleshooting. Stephen McNamara, Garrett Welshofer, Ryan Cook, and the rest of the Pratt Lab are thanked for their assistance during the assembly of the instrument. Assistance with the A-ATOFMS software and electronics development was provided by Ryan Miller (University of Michigan Space Physics Research Laboratory), Jon Ameel, Rebekah Andrews, and Katherine De Los Santos (University of Michigan Physics Department).

2.6. References

Bahreini, R., Dunlea, E.J., Matthew, B.M., Simons, C., Docherty, K.S., DeCarlo, P.F., Jimenez, J.L., Brock, C.A., Middlebrook, A.M., 2008. Design and operation of a pressure-controlled inlet for airborne sampling with an aerodynamic aerosol lens. Aerosol. Sci. Technol. 42, 465-471.

Bohren, C.F., Huffman, D.R., 2008. Absorption and scattering of light by small particles. John Wiley & Sons.

Cahill, J.F., Darlington, T.K., Wang, X., Mayer, J., Spencer, M.T., Holecek, J.C., Reed, B.E., Prather, K.A., 2014. Development of a high-pressure aerodynamic lens for focusing large particles (4–10 μm) into the aerosol time-of-flight mass spectrometer. Aerosol. Sci. Technol. 48, 948-956.

Cazorla, A., Bahadur, R., Suski, K., Cahill, J.F., Chand, D., Schmid, B., Ramanathan, V., Prather, K., 2013. Relating aerosol absorption due to soot, organic carbon, and dust to emission sources determined from in-situ chemical measurements. Atmos. Chem. Phys. 13, 9337-9350.

Creamean, J.M., Suski, K.J., Rosenfeld, D., Cazorla, A., DeMott, P.J., Sullivan, R.C., White, A.B., Ralph, F.M., Minnis, P., Comstock, J.M., 2013. Dust and biological aerosols from the Sahara and Asia influence precipitation in the western US. Science 339, 1572-1578.

Gard, E., Mayer, J.E., Morrical, B.D., Dienes, T., Fergenson, D.P., Prather, K.A., 1997. Real-time analysis of individual atmospheric aerosol particles: Design and performance of a portable ATOFMS. Anal. Chem. 69, 4083-4091.

Liu, P., Ziemann, P.J., Kittelson, D.B., McMurry, P.H., 1995a. Generating particle beams of controlled dimensions and divergence: I. Theory of particle motion in aerodynamic lenses and nozzle expansions. Aerosol. Sci. Technol. 22, 293-313.

Liu, P., Ziemann, P.J., Kittelson, D.B., McMurry, P.H., 1995b. Generating particle beams of controlled dimensions and divergence: II. Experimental evaluation of particle motion in aerodynamic lenses and nozzle expansions. Aerosol. Sci. Technol. 22, 314-324.

Moffet, R.C., Prather, K.A., 2005. Extending ATOFMS measurements to include refractive index and density. Anal. Chem. 77, 6535-6541.

Moffet, R.C., Prather, K.A., 2009. In-situ measurements of the mixing state and optical properties of soot with implications for radiative forcing estimates. Proc. Natl. Acad. Sci. 106, 11872-11877.

Prather, K.A., Nordmeyer, T., Salt, K., 1994. Real-time characterization of individual aerosol particles using time-of-flight mass spectrometry. Anal. Chem. 66, 1403-1407.

Pratt, K.A., DeMott, P.J., French, J.R., Wang, Z., Westphal, D.L., Heymsfield, A.J., Twohy, C.H., Prenni, A.J., Prather, K.A., 2009a. In situ detection of biological particles in cloud ice-crystals. Nat. Geosci. 2, 398-401.

Pratt, K.A., Mayer, J.E., Holecek, J.C., Moffet, R.C., Sanchez, R.O., Rebotier, T.P., Furutani, H., Gonin, M., Fuhrer, K., Su, Y., 2009b. Development and characterization of an aircraft aerosol time-of-flight mass spectrometer. Anal. Chem. 81, 1792-1800.

Su, Y., Sipin, M.F., Furutani, H., Prather, K.A., 2004. Development and characterization of an aerosol time-of-flight mass spectrometer with increased detection efficiency. Anal. Chem. 76, 712-719.

Wang, X., McMurry, P.H., 2006. A design tool for aerodynamic lens systems. Aerosol. Sci. Technol. 40, 320-334.

Zhang, X., Smith, K.A., Worsnop, D.R., Jimenez, J.L., Jayne, J.T., Kolb, C.E., Morris, J., Davidovits, P., 2004. Numerical characterization of particle beam collimation: part II integrated aerodynamic-lens–nozzle system. Aerosol. Sci. Technol. 38, 619-638.

Chapter 3.

Ubiquitous Influence of Wildfire Emissions and Secondary Organic Aerosol on Summertime Atmospheric Aerosol in the Forested Great Lakes Region

Accepted to *Atmos. Chem. Phys. Discuss.*

3.1. Introduction

Atmospheric particulate matter less than 2.5 μm in diameter ($PM_{2.5}$) has significant impacts on air quality, climate, and human health (Calvo et al., 2013; Pöschl and Shiraiwa, 2015). Atmospheric particles directly affect climate by scattering incoming solar radiation and indirectly by acting as cloud condensation (CCN) and ice nuclei (IN) (IPCC, 2013). Increased levels of $PM_{2.5}$ are also linked to increased health risks, particularly respiratory and cardiovascular diseases (Brook et al., 2004; Pope and Dockery, 2006). Particles can impact areas hundreds of kilometers from their sources through long-range transport, with residence times of up to two weeks depending on particle size and chemical composition (Uno et al., 2009). Determining the impact of the long-range transported particles, as well as how they are transformed in the atmosphere during transport, is a critical topic to accurately predict their air quality and climate effects (Ault et al., 2011; Creamean et al., 2013). During transport, particles undergo heterogeneous reactions and gas-particle partitioning, aging the particles and leading primary particles (e.g., soot) to become internally mixed with secondary species, including water, ammonium, nitrate, sulfate, and oxidized organic carbon, thus changing the chemical composition of individual particles (Moffet and Prather, 2009; Riemer and West, 2013). These aging processes are particularly important since chemical composition is directly related to particle properties, including reactivity, hygroscopicity, toxicity, scattering, and absorption properties (Brook et al., 2004; Calvo et al., 2013; Fierce et al., 2016; Pöschl, 2005). Particle properties also differ based on the distribution of chemical species, or mixing state, within a population of particles – whether various chemical species are contained within a single particle

(internally mixed) or within different particles (externally mixed). Particle mixing state representation in models is particularly important (Bauer et al., 2013), especially for predicting aerosol impacts on the climate (Fierce et al., 2016; Matsui et al., 2013).

Long-range transport of atmospheric particles can contribute to both remote and populated locations being out of compliance with air quality regulations (National Research Council and National Academies, 2010). For example, elevated aerosol mass and ozone in Europe, eastern Canada, and northeastern United States has been attributed to transported Canadian wildfire emissions (Colarco et al., 2004; Dempsey, 2013; Dreessen et al., 2016; Dutkiewicz et al., 2011; Forster et al., 2001; Kang et al., 2014; Miller et al., 2011; Müller et al., 2005; Wang et al., 2010b). A multi-day exceedance of the National Ambient Air Quality Standard for ozone in Maryland during the summer of 2015 was attributed to Canadian wildfire emissions (Dreessen et al., 2016). Similarly, elevated $PM_{2.5}$ observed in New York and Wisconsin has been attributed to Ohio River Valley emissions. Transported pollutants can impact biogenic secondary organic aerosol (SOA) formation in remote locations (Carlton et al., 2010; Emanuelsson et al., 2013; Rattanavaraha et al., 2016; Xu et al., 2015). Finally, prior and on-going studies through the IMPROVE program in rural locations throughout North America have investigated both transported and local contributions to the aerosol populations (Hand et al., 2011). Uncertainty in the contributions of long-range aerosols and limited measurements in remote areas can lead to inaccuracies in modeling of aerosol source contributions.

Relatively few studies have chemically characterized atmospheric aerosols in the rural Great Lakes region of the United States (Bullard et al., 2017; Jeong et al., 2011; Kim et al., 2005; Kim et al., 2007; Kundu and Stone, 2014; Sheesley et al., 2004; Sjostedt et al., 2011; Zhang et al., 2009). Except for the major metropolitan areas of Detroit (MI), Chicago (IL), Minneapolis (MN), and Milwaukee (WI), much of the land is characterized by rural agricultural areas and remote forests without significant anthropogenic emissions. A study in the upper peninsula of Michigan conducted by Sheesley et al. (2004) observed major contributions from secondary organic aerosol from both biogenic and anthropogenic volatile organic compound (VOC) oxidation in the summer. Studies across rural Illinois and Ohio found major atmospheric contributions from secondary sulfate, nitrate, and organic carbon, consistent with aerosol aging during transport (Kim et al., 2005; Kim et al., 2007; Zhang et al., 2009), though these locations were much less forested than the more northern Great Lakes regions. Kundu and Stone (2014)

measured composition and sources at rural locations in Iowa, identifying major PM mass contributions from biomass burning, combustion, and dust. Jeong et al. (2011) and (Sjostedt et al., 2011) identified contributions from secondary organic aerosol, elemental carbon, and dust in rural Harrow, Ontario, downwind of Detroit and Windsor. The scarcity of measurement data in the rural Great Lakes region provides limited opportunities for model evaluation and requires assumptions of background primary aerosol.

In remote regions, there are challenges in distinguishing and identifying primary and secondary aerosol sources, particularly for bulk methods (Pratt and Prather, 2012). Single-particle mass spectrometry allows the identification of particle sources through comparisons with source 'fingerprints' and particle aging through characterization of individual particle chemical mixing state (Pratt and Prather, 2009, 2012). Therefore, to apportion the sources of the aerosol population influencing remote northern Michigan, single particle mass spectrometry measurements were conducted during July 2014 at the University of Michigan Biological Station (UMBS) near Pellston, MI. In this study, individual particle chemical composition, measured in real-time using single-particle mass spectrometry, was used to identify the sources and secondary processing of transported particles at UMBS. In addition, high resolution aerosol mass spectrometry (HR-AMS) measured chemically-resolved mass concentrations of non-refractory aerosol (organics, sulfate, nitrate, ammonium, and chloride) to provide complementary mass-based characterization of the transported particles at UMBS.

3.2. Methods

3.2.1. Field Site and Instrumentation

Atmospheric measurements were conducted from July 13-24, 2014 at the University of Michigan Biological Station (UMBS) near Pellston, MI, a 10,000-acre, remote, forested location with little local pollution (Carroll et al., 2001). The closest major cities are Milwaukee (370 kilometers southwest), Detroit (385 kilometers south), and Chicago (466 kilometers southwest). Instrumentation was located within a laboratory at the base of the Program for Research on Oxidants: Photochemistry, Emissions, and Transport (PROPHET) tower, a 30-meter tall sampling tower (45°33'31"N, 84°42'52"W) (Carroll et al., 2001). Air was sampled from 34 m above ground level (~14 m above the forest canopy) through foam-insulated 1.09-cm I.D. copper tubing at a flow rate of 9.25 L min^{-1} (laminar) with a residence time of 15 s. This tubing was

connected to a shared sampling manifold at the base of the tower, allowing individual instruments to each have a dedicated sampling line while limiting particle loss.

An aerosol time-of-flight mass spectrometer (ATOFMS model 3800, TSI, Inc., Shoreview, MN) (Dall'Osto et al., 2004; Gard et al., 1997), described briefly below, was used to measure the size and chemical composition of individual atmospheric particles ranging from 0.5 – 2.0 μm in vacuum aerodynamic diameter (d_{va}) (Section 3.2.2). An Aerodyne high resolution aerosol mass spectrometer (HR-AMS) (DeCarlo et al., 2006) measured chemically-resolved mass concentrations of non-refractory fine particulate material (nominal vacuum aerodynamic diameter range of 0.05 – 1.0 μm) from July 15–24, 2014. Concentrations for major composition classes (organics, sulfate, nitrate, ammonium, and chloride) are reported here. The operation of the HR-AMS followed standard practice as described elsewhere (Allan et al., 2004; Allan et al., 2003; Jayne et al., 2000; Jimenez et al., 2003); the sampling resolution for the UMBS observations was 2.5 min. Data were analyzed using SQUIRREL (version 1.60) and the high resolution analysis software tool PIKA (version 1.20) (Sueper, 2010), with the concentrations corrected based on the estimated composition-dependent collection efficiency (Middlebrook et al., 2012). Additional instrumentation included an ozone analyzer (Thermo Scientific model 49), a scanning mobility particle sizer spectrometer (SMPS, TSI model 3936) with a sheath flow rate of 4 L/min and an aerosol flow rate of 0.4 L/min for measuring size-resolved number concentrations of mobility diameter particles 12-600 nm, and an aerodynamic particle sizer spectrometer (APS, TSI model 3321) for measuring size-resolved number concentrations of 0.5-19 μm aerodynamic diameter particles. SMPS and APS size distributions were merged to give a continuous aerosol distribution from 0.01-2.5 μm (aerodynamic diameter) using previously established methods (Khlystov et al., 2004), assuming a density of 1.5 g cm^{-3} and shape factor of 1.

3.2.2. Aerosol Time-of-Flight Mass Spectrometer

Using the ATOFMS, 11,430 individual atmospheric particles ranging from 0.5 – 2 μm in d_{va} were chemically analyzed from July 13-24, 2014. The design and operation of the ATOFMS has been described in detail elsewhere (Dall'Osto et al., 2004; Su et al., 2004). Briefly, particles are focused through an aerodynamic lens system and optically detected by two 532 nm continuous wave lasers spaced 6 cm apart. Particle aerodynamic diameter is obtained from

particle speed by calibration using spherical polystyrene latex spheres (0.4 – 2.5 μm, Polysciences, Inc.) of known diameter and density. Particles are individually desorbed and ionized by a 266 nm Nd:YAG laser that was operated at ~1.2 mJ and the resulting ions enter a dual-polarity reflectron time-of-flight mass spectrometer. Positive and negative ion mass spectra corresponding to the same individual particles are collected. Mass spectral peak lists for individual particles were generated using TSI MS-Analyze software.

The individual particle mass spectra were analyzed using YAADA (yaada.org), a software toolkit for MATLAB. Particles were clustered in YAADA using the ART-2a algorithm with a vigilance factor of 0.80 and a learning rate of 0.05 for 20 iterations (Song et al., 1999). The top 50 clusters were manually classified into five particle types, described in Section 3.3.1 These top 50 clusters contained 92% of the 11,430 particle mass spectra collected and are the focus of the manuscript. Particle identification was based on characteristic ATOFMS mass spectral signatures previously described (Pastor et al., 2003; Qin et al., 2012; Silva et al., 1999). The errors associated with number fractions for each particle types were calculated using binomial statistics.

To obtain chemically-resolved particle number and mass concentrations, ATOFMS particle counts were scaled with the APS size-resolved particle number concentration data using the method of Qin et al. (2006) to account for size-dependent particle transmission in the inlet. Briefly, ratios of APS number concentration to ATOFMS non-scaled number concentration were calculated every three hours for each individual size bin defined by the APS for use as a scaling factor. This scaling factor was then multiplied by the corresponding ATOFMS number concentration, providing size and chemically-resolved particle number concentrations for each of the four particle types. These number concentrations were then converted to mass concentrations using assumed spherical shape and compositionally-specific densities. The following densities were applied for the four particle types: 1.5 g cm^{-3} for biomass burning, 1.5 g cm^{-3} for salts, and 1.25 g cm^{-3} for organic carbon-sulfate (OC-sulfate), and elemental carbon/organic carbon – sulfate (ECOC-sulfate) particles (Moffet et al., 2008; Spencer et al., 2007).

3.3. Results and Discussion

3.3.1. Overview

The UMBS campaign (July 13-24, 2014) was characterized by air masses from three primary directions: north, northwest, and southwest (Figures A.1 and A.2), representative of periods observed during previous UMBS summer studies (Cooper et al., 2001; VanReken et al., 2015). Analysis of NOAA HYSPLIT backward air mass trajectories showed four distinct air mass time periods (Figure A.2). From July 13–15, air primarily came from northwestern Canada. From July 15–17, the wind shifted and came from directly north crossing over Lake Superior and Lake Michigan before arriving at the field site. In contrast, from July 17–22 the air came mainly from south-southwest of the field site, crossing over the major metropolitan areas of Chicago and Milwaukee followed by Lake Michigan. Finally, from July 23–24, air came from the north-northwest of the field site, crossing Lake Superior and Lake Michigan from northern Canada (Figure A.2). During summer 2009, VanReken et al. (2015) found that 60% of the air masses came from north/northwest of UMBS, similar to this study (57%). Air came from southern polluted regions 43% of the time during our study, compared to 29% during July-August 2009 (VanReken et al., 2015).

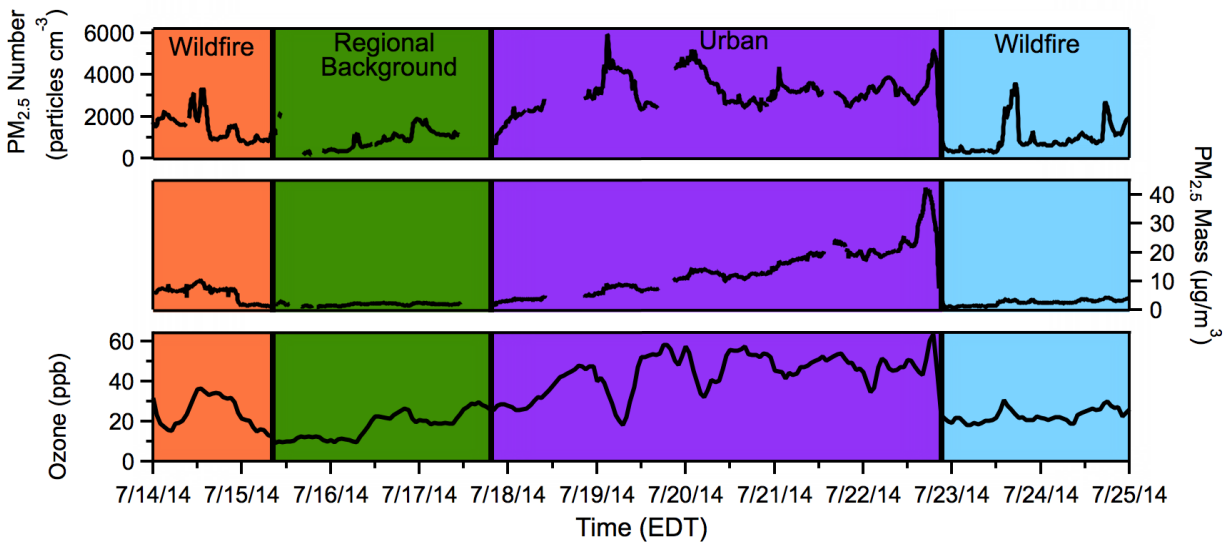

Figure 3.1. Time-resolved $PM_{2.5}$ number and mass concentrations and ozone mole ratios during the different periods of air mass influence. Periods without data are due to instrument down time. Colors of the different time periods correspond to the colors of the corresponding HYSPLIT backward air mass trajectories in Figure A.2.

Total $PM_{2.5}$ number, $PM_{2.5}$ mass, and ozone concentrations ranged from 143 to 6,031 particles cm^{-3} (average ± standard deviation: 1,822 ± 1,181 particles cm^{-3}), 1 to 43 $\mu g/m^3$ (average ± standard deviation: 8 ± 8 $\mu g/m^3$) and 9 to 63 ppb (average ± standard deviation: 32 ±

14 ppb), respectively (Figure 3.1). Maximum concentrations were detected when the air arrived from the southwestern urban areas, and the minimum values were observed for air masses from the north during remote air transport (Figure 3.1). Previously, VanReken et al. (2015) observed an 85% increase in particle number concentration when air originating from these southwestern urban areas impacted UMBS. These results suggest a wide range of sources affecting the field site, which were directly observed by the ATOFMS. Here, we examine the influences of wildfires (Section 3.3.3) and urban pollution (Section 3.3.4) on summertime aerosol chemical composition, compared to remote background (Section 3.3.2), at UMBS.

Major individual particle types observed by ATOFMS included biomass burning, organic carbon-sulfate (OC-sulfate), and elemental carbon/organic carbon-sulfate (ECOC-sulfate) (Figure 3.2). Biomass burning particles were characterized by intense peaks at *m/z* 39 (K^+) and -97 (HSO_4^-), as well as less intense peaks at *m/z* 12 (C^+), 18 (NH_4^+), and 27 ($C_2H_3^+$) (Pratt et al., 2010). Biomass burning particles also contained a peak at *m/z* 43 ($C_2H_3O^+$), a marker for oxidized OC on particles, which is addressed further in section 3.3.3. Biomass burning was the most prominent particle type, comprising ~80% of submicron (0.5 – 1.0 μm) and ~50% of supermicron (1 – 2 μm) particles, by number, throughout the study, with number fraction varying according to the level of influence from wildfires. OC-sulfate particles contributed ~7% by number to submicron (0.5 – 1.0 μm) particles and ~8% by number to supermicron (1.0 – 2.0 μm) particles and were characterized by intense peaks at *m/z* 27 ($C_2H_3^+$), 39 ($C_3H_3^+/K^+$), +/-43 ($C_2H_3O^{+/-}$), and -97 (HSO_4^-). OC-sulfate particles can originate from a variety of sources including primary vehicular emissions (Toner et al., 2008) and secondary organic sources (Pratt and Prather, 2009). The intense *m/z* 43 (most intense OC-sulfate particle ion peak) is indicative of significant SOA coatings on combustion particles, including biomass burning (Pratt and Prather, 2009). ECOC-sulfate particles, characterized by C_n^+ fragment peaks, observed at *m/z* 12 (C^+), 24 (C_2^+), 36 (C_3^+), 48 (C_4^+), etc., as well as markers at *m/z* 27 ($C_2H_3^+$), 18 (NH_4^+), and -97 (HSO_4^-), are attributed to vehicular emissions (Toner et al., 2008; Toner et al., 2006) and contributed ~5% by number to both sub- and supermicron particles with the majority observed on July 22 during an urban-influenced air mass. In addition to the previously mentioned combustion and secondary particles, Na and Ca salts internally mixed with nitrate were episodically detected, primarily during July 16–18 and July 24–25. These salts may have

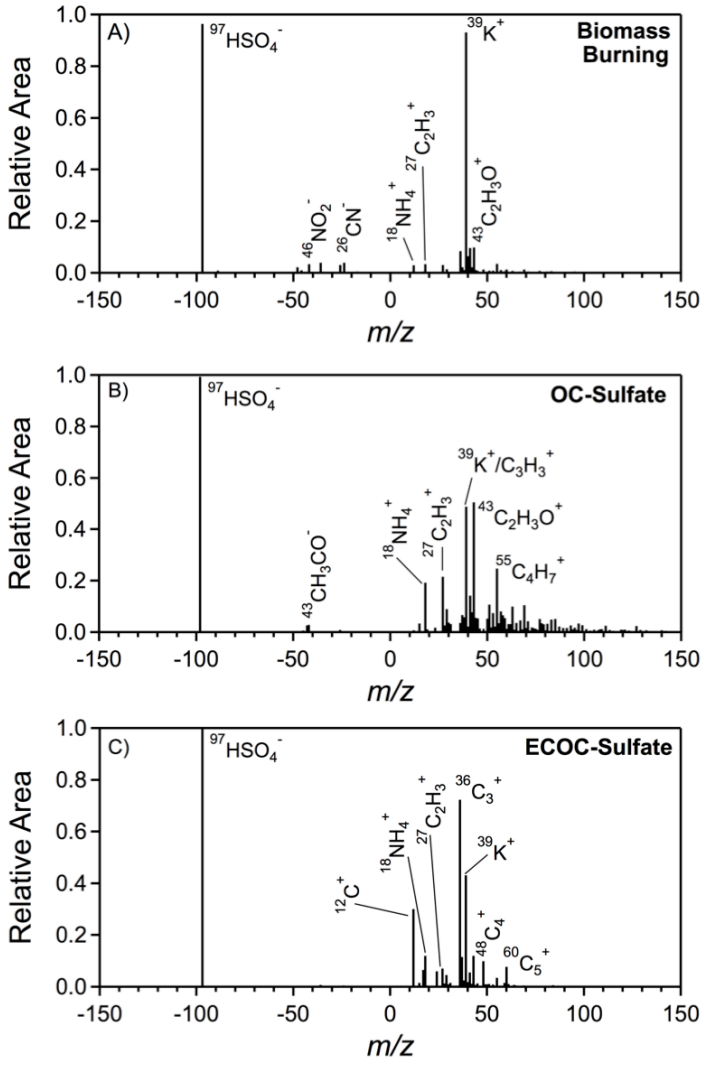

Figure 3.2. Average positive and negative ion single-particle mass spectra (ATOFMS), with characteristic peaks labeled, for the dominant aged combustion particle types observed: (A) biomass burning, (B) OC-sulfate, and (C) ECOC-sulfate.

originated from the Great Lakes (Axson et al., 2016) and/or seawater and are the focus of an upcoming manuscript.

PM_1 mass measured by the HR-AMS was on average 73% organics (7.8 μg/m^3) throughout the study, with a substantial contribution from oxidized organics as determined by an average HR-AMS O/C ratio of 0.84 and through the ATOFMS oxidized organic carbon ion marker *m/z* 43, $C_2H_3O^+$ (Aiken et al., 2008; Qin et al., 2012). O/C ratios between 0.6 – 1 are commonly associated with low volatility oxidized organic aerosol (LV-OOA) that has undergone extensive aging (Jimenez et al., 2009), consistent with the single-particle observation that SOA coated the major particle types. Also consistent with atmospheric processing during long-range

transport, 92% of all 0.5 – 2.0 µm particles, by number, were measured by the ATOFMS to be internally mixed with secondary species, including sulfate (HSO_4^-, *m/z* -97), nitrate (NO_2^-, *m/z* -46 and/or NO_3^-, *m/z* -62), ammonium (NH_4^+, *m/z* 18), and/or oxidized OC ($C_3H_2O^-$, *m/z* -43 or $C_3H_2O^+$, *m/z* 43) (Qin et al., 2012). On average, sulfate comprised 20% (2.2 µg/m^3) of the total PM_1 mass measured by HR-AMS.

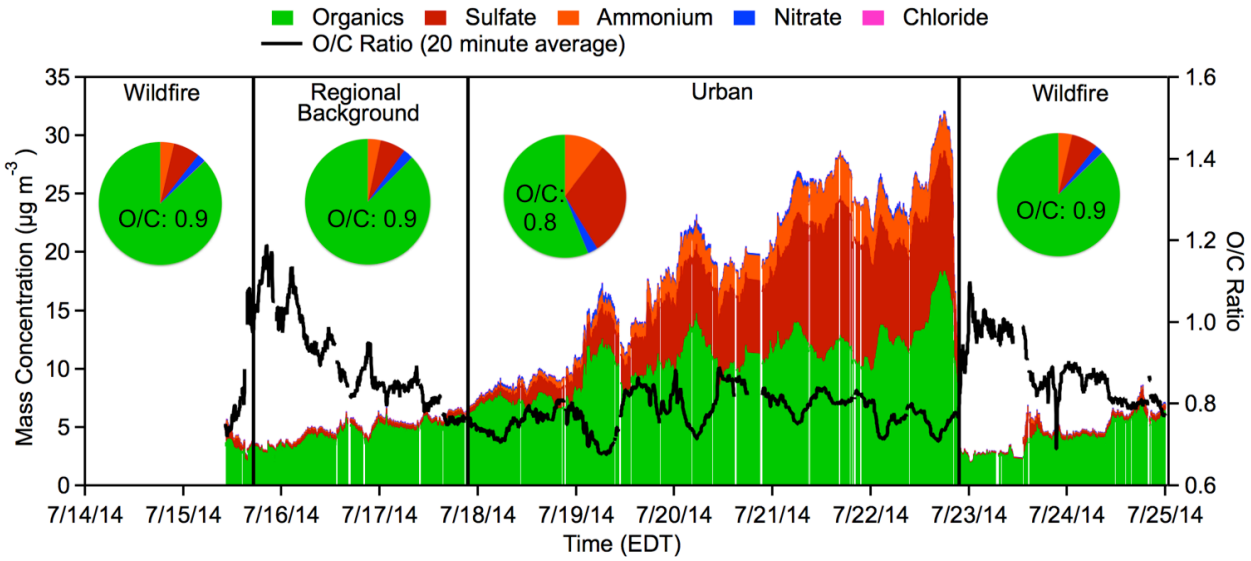

Figure 3.3. PM_1 non-refractory chemically speciated mass concentrations, as well as O/C ratios (20 min averages), measured by HR-AMS. Periods of influence are notated and separated by solid vertical lines. Pie charts represent the average mass fractions for each air mass period, with average O/C ratio inset.

3.3.2. Remote Background Air Mass Influence

From July 15-17, air arrived at UMBS originating from rural northern Canada. The average $PM_{2.5}$ number concentration was 903 ± 499 particles cm^{-3} (range of 143 - 2163 particles cm^{-3}, Figure 3.1) and average $PM_{2.5}$ mass concentration was 1.9 ± 0.4 µg/m^3 with a particle mode of 82 nm (Figure 3.1 and S3). The average ozone concentration was 17 ± 6 ppb (Figure 3.1). With a lack of direct wildfire influence (Figure 3.4), 61 ± 1% of the 0.5 – 2.0 µm particles, by number, were classified by ATOFMS as aged biomass burning aerosols, relatively similar to the background biomass burning particle influence reported by Hudson et al. (2004) and Pratt et al. (2010) for the United States free troposphere (33-52% by number). Biomass burning particles were internally mixed with oxidized OC (80 ± 2%, by number) or mixed with sulfate (85 ± 2%). Nitrate was internally mixed with 8 ± 2%, by number of biomass burning particles and 33 ± 3%,

by number, of OC-sulfate particles. It is likely that, while the observed biomass burning particles have a small potassium-rich (biomass burning) core, they are primarily SOA by mass (Moffet et al., 2010; Pratt and Prather, 2009) (Section 3.3.3). The HR-AMS showed average PM_1 organic mass concentrations of 4.4 μg/m^3, with minimal contribution from sulfate (0.3 μg/m^3), as well as nitrate and ammonium (both less than 0.1 μg/m^3 on average) (Figure 3.3).

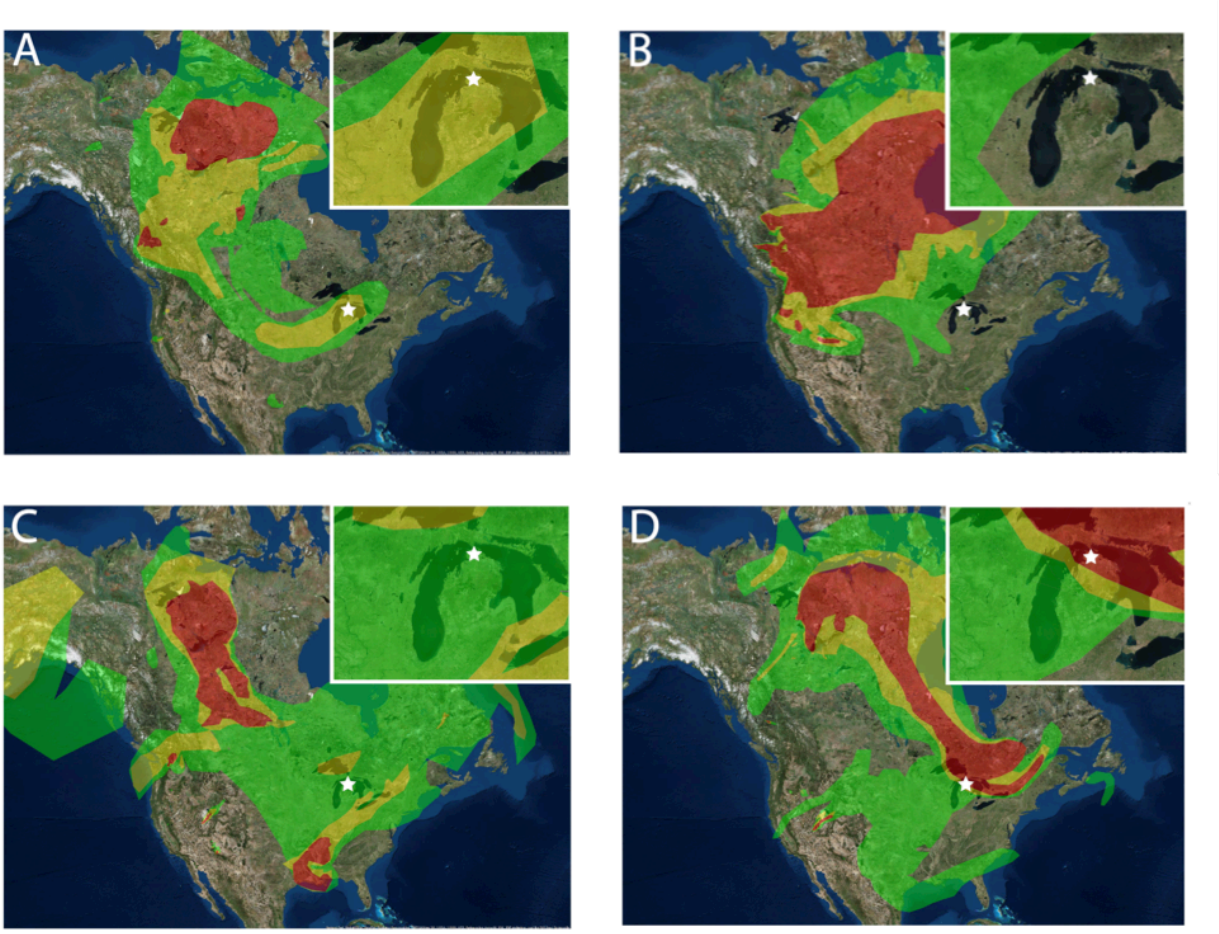

Figure 3.4. Representative NOAA HMS smoke maps for four representative days during the time periods of different air influence: (A) July 14, wildfire influence; (B) July 16, remote background influence; (C) July 21, Urban influence; (D) July 24, wildfire influence. Inset enlarges the state of Michigan to clearly display smoke influence on the field site, shown as a star.

The significant internal mixing of oxidized OC combined with the significant organic mass loading (average HR-AMS O/C ratio of 0.9) is consistent with high SOA mass on the particles (Aiken et al., 2008). Previous studies in rural and forested environments found similarly high O/C during periods of non-polluted air and attributed this to regional SOA formation (Jimenez et al., 2009; Raatikainen et al., 2010; Sjostedt et al., 2011; Sun et al., 2009). There was

a notable spike in O/C on July 15 – 16 to 1.2, indicative very highly oxidized organics. O/C ratios of this magnitude have previously been observed at the remote Whistler Mountain, where organic aerosol O/C ratios up to ~1.3 where observed during organic aerosol accumulation events (Sun et al., 2009). Sheesley et al. (2004) found that SOA, primarily biogenic-derived, contributed over 90% of the total organic carbon mass observed during the summer at the Seney National Wildlife Refuge in northern Michigan, located 120 km northwest of UMBS. Notably, ultrafine particle growth was observed at UMBS on July 16 during this high O/C ratio spike (Gunsch et al., 2017). The air arriving during this period was not under the influence of wildfires (Section 3.3.3) or urban areas (Section 3.3.4), and is therefore expected to be representative of remote background conditions.

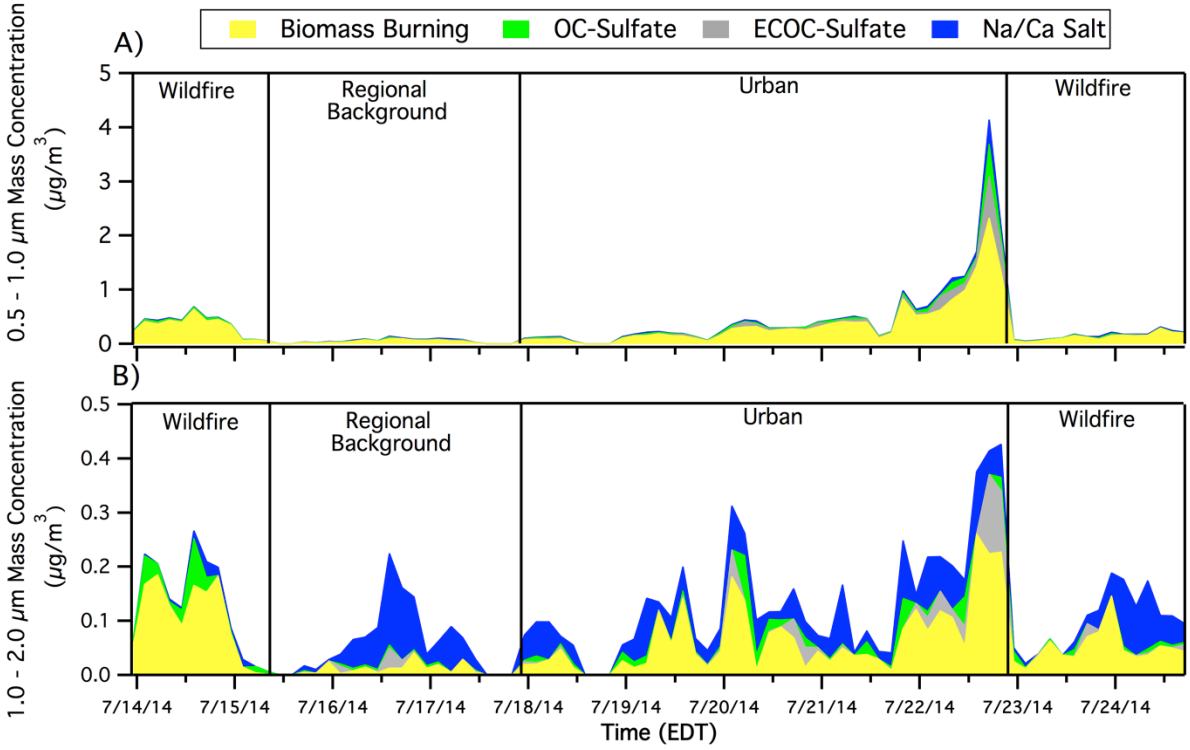

Figure 3.5. Three hour binned mass concentrations of (A) 0.5 – 1.0 µm and (B) 1.0 – 2.0 µm particle types, as measured by ATOFMS. Gaps in the data correspond to periods when APS data were not available for scaling.

3.3.3. Wildfire Influence

From July 13-15 and July 24 mid-day through July 25, the NOAA Hazard Mapping System (HMS) Smoke Product (Rolph et al., 2009) indicated that smoke plumes originating from

wildfires within the Northwest Territories (Canada) directly influenced UMBS (Figure 3.4). According to the Canadian Interagency Forest Fire Centre, over 5,500 km^2 of land burned within the Northwest Territories during July 2014 (CIFFC, 2014). Canadian wildfires are a major source of global $PM_{2.5}$, with estimates of ~1.6 Tg yr^{-1} emitted to the atmosphere (Wiedinmyer et al., 2006). Average $PM_{2.5}$ number and concentrations during these two wildfire influence periods were statistically higher (t-test, $\alpha = 0.05$) at 1400 ± 800 particles cm^{-3} (range of 147 – 4832 particles cm^{-3}, Figure 3.1) and 5.4 ± 2.6 $\mu g/m^3$ (range of 1.3 – 10.5 $\mu g/m^3$, Figure 3.1), respectively, compared to the background period (Section 3.3.2). The particle mode during wildfire influence was 80 nm, similar to background periods (Figure A.3). Ozone was also elevated during July 13-15 reaching as high as 35 ppb, compared to an average of 10 ppb during the background period (Figure 3.1). During these periods, the air masses did not pass over any major urban areas (Figure A.2), making ozone production within the smoke plume during transport the likely source (Jaffe and Wigder, 2012). Ozone did not increase during the July 24 smoke plume, staying near the average for the study (25 ± 12 ppb) with a concentration of 26 ± 3 ppb (Figure 3.1). While an ozone increase is often observed for aged wildfire plumes, an increase does not always occur during wildfire influence, such as when low NO_x levels within plumes, potentially due to smoldering combustion, limit the production of ozone (Jaffe and Wigder, 2012).

During the wildfire influenced periods, 88 ± 1% of the measured 0.5 – 2.0 μm particles, by number, were biomass burning particles, with an average mass concentration of 0.42 $\mu g/m^3$ (Figure 3.5) and a maximum of 0.80 $\mu g/m^3$ occurring during the early afternoon of July 14 when the heaviest wildfire smoke was reported by the NOAA smoke product (Figure 3.4A). Minor contributions of OC-sulfate particles (8 ± 1% by number) were also measured. The OC-sulfate particle mass spectra (Figure 3.2B) showed that 75 ± 5%, by number, contained potassium (K^+, *m/z* 39), suggesting that these were highly aged biomass burning particles coated by SOA such that the typical biomass burning mass spectral signature had been masked, as observed previously by Pratt and Prather (2009) using a thermodenuder. These OC-sulfate particles featured a dominant intense *m/z* 43 ($C_2H_3O^+$) ion peak, indicating that these particles were heavily coated with SOA. During the afternoon event on July 24, PM_1 organic mass concentrations measured by HR-AMS nearly doubled from 2.5 ± 0.1 $\mu g/m^3$ before the event to 4.5 ± 0.3 $\mu g/m^3$ during the event (Figure 3.3), accounting for ~90% of the total PM_1 mass

concentration. The HR-AMS O/C ratio was 0.8 during wildfire periods, consistent with biomass burning particles heavily coated with SOA (Aiken et al., 2008), as also observed by 95 ± 1%, by number, of the biomass burning and OC-sulfate particles, measured by ATOFMS during these periods, featuring the oxidized OC ion marker (*m/z* 43, $C_2H_3O^+$) (Figure 3.6). Freshly emitted biomass burning has a O/C ratio of ~0.2, which can increase to ~0.6 in only a few hours as oxidized material condenses onto the particles (Grieshop et al., 2009; Pratt et al., 2011). As the wildfire air masses measured during the present study were transported over multiple days over Canadian forests, biogenic SOA, from condensation of monoterpene oxidation products (Slowik et al., 2010), likely contributed to the observed O/C ratio of 0.8 at UMBS.

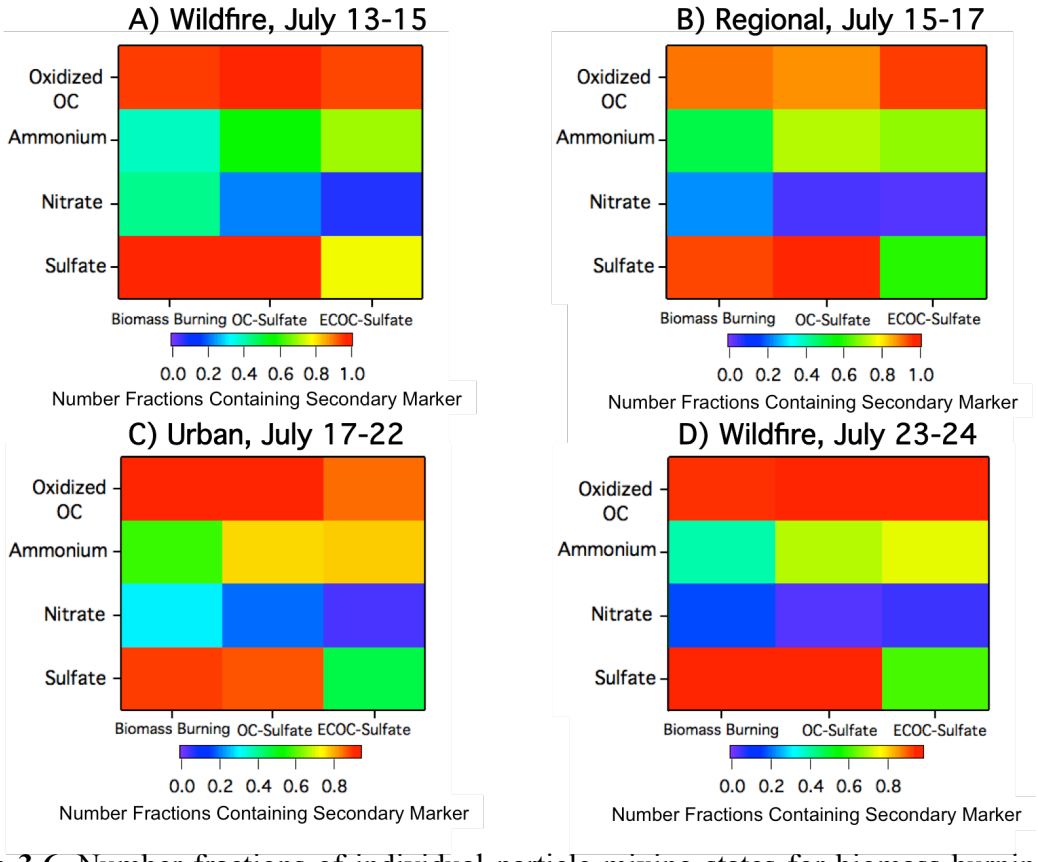

Figure 3.6. Number fractions of individual particle mixing states for biomass burning, OC-sulfate and ECOC-sulfate particle types during: (A) Wildfire influence between July 13-15, (B) Clean air from northern Canada between July 15-17, (C) Mix of wildfire and urban influences from July 17-22, (D) Mix of clean air and Canadian wildfires between July 23-24. Species observed include oxidized OC ($C_2H_3O^+$, *m/z* 43), ammonium (NH_4^+, *m/z* 18), nitrate (NO_2^-, *m/z* -46, and/or NO_3^-, m/*z* -62), and sulfate (HSO_4^-, *m/z* -97).

During transport of the biomass burning aerosols, accumulation of sulfate also occurred, with 97 ± 1%, by number, of biomass burning particles internally mixed with sulfate (*m/z* -97, HSO_4^-) (Figure 3.6). HR-AMS measured PM_1 sulfate also increased from less than 0.1 μg/m^3 to 2 μg/m^3 after mid-day July 24 (Figure 3.3). Increases in particulate sulfate mass have been observed during wildfire plume aging (DeBell et al., 2004; Pratt et al., 2010). In comparison, the HR-AMS measured limited amounts of PM_1 ammonium (~2% of total mass, 0.2 μg/m^3) during the wildfire event on July 24 (Figure 3.3). However, ammonium was internally mixed in 38 ± 2%, by number, of biomass burning and 68 ± 2%, by number, of OC-sulfate particles (Figure 3.6). This result indicates that while ammonium was present within many particles, it was a minor fraction of the particle mass. Nitrate was also internally mixed with 43 ± 2% of biomass burning particles, by number, and 17 ± 2%, by number, of OC-sulfate particles (Figure 3.6), and the HR-AMS only measured ~1% of PM_1 mass to be nitrate (0.06 μg/m^3). Therefore, it is likely that the ammonium was present in the form of ammonium sulfate internally mixed with biomass burning and OC-sulfate.

3.3.4. Urban Air Mass Influence

From July 17-22, UMBS was influenced by air masses from the southwest, passing over the major metropolitan areas of Chicago and Milwaukee before arriving at the site (Figure A.2) after transport times of 24-36 hours. The average ozone concentration was elevated at an average of 41 ± 12 ppb similar to previous measurements by Cooper et al. (2001) at UMBS when under the direct influence of urban pollution (Figure 3.1). The $PM_{2.5}$ number and mass concentration for this period were 2,700 ± 900 particles cm^{-3} (range of 414 – 6,031 particles cm^{-3}) and 14 ± 8 μg/m^3 (range of 2 – 43 μg/m^3), respectively, the highest for the study (Figure 3.1). The particle mode of 69 nm was also the smallest of the study (Figure A.3). VanReken et al. (2015) previously observed the highest particle number concentrations (3,000 ± 1,300 particles cm^{-3}) at UMBS during the influence of southern air masses. Wildfire smoke influence was present during this period as shown by the NOAA smoke product (Figure 3.4C). However, unlike during the previous periods, this smoke originated mainly from the southern United States (active fires were located in Tennessee, Arkansas, and Missouri). Biomass burning particles measured by ATOFMS steadily increased in mass concentration throughout this period (Figure 3.5), with a notable spike in the mass concentration on July 22 observed in both the submicron (2.3 μg/m^3)

and supermicron (0.3 μg/m^3) size ranges (Figure 3.5). Overall, during urban influence, biomass burning particles accounted for 72 ± 2% of the particles by number and ~30% of the total mass concentration (Figure 3.5). The biomass burning particles were aged, as shown by internal mixtures of sulfate (88 ± 2%, by number), oxidized OC (92 ± 1%, by number), ammonium (58 ± 2%, by number), and nitrate (30 ± 2%, by number) (Figure 3.6). The greatest internal mixing with ammonium was observed during this period. The HR-AMS also measured the highest average ammonium mass concentration during this period of 1.6 μg/m^3, accounting for 10% of the total PM_1 particle mass (Figure 3.3). Agricultural activities, both crop and livestock, located to the south and southwest of the field site (Paulot et al., 2014; Stephen and Aneja, 2008) may be the source of the elevated ammonium levels.

ECOC-sulfate and OC-sulfate particles comprised the second most prominent particle types measured by ATOFMS during this urban-influenced period at 12 ± 1% and 9 ± 1% of the submicron (0.5 – 1.0 μm) particles, by number, and an average of 0.08 μg/m^3 and 0.03 μg/m^3, respectively (Figure 3.5). The influence of urban vehicular combustion resulted in the increased levels of measured ECOC-sulfate particles (Toner et al., 2008; Toner et al., 2006), compared to non-urban influenced periods (2 ± 1% by number). HR-AMS PM_1 mass concentrations (Figure 3.3) showed increased organic mass during urban influence with an average mass concentration of 9.7 μg/m^3 (Figure 3.3), likely due to a mixture of biomass burning, anthropogenic, and biogenic organic aerosol. The average HR-AMS O/C ratio during the urban period was the lowest of the study (0.78), likely due to increased contributions from hydrocarbon-like organic aerosol from urban vehicle combustion emissions (Aiken et al., 2008), in contrast to primarily oxidized organic aerosol during regional background periods (Jimenez et al., 2009). An increase in less oxidized organic aerosol was similarly observed in rural Ontario when the site was influenced by urban air masses from Detroit, compared to remote air masses (Sjostedt et al., 2011). The ECOC-sulfate and OC-sulfate particles were highly aged, with ~75%, by number, of each particle type internally mixed with ammonium, consistent with particle aging during transport (Figure 3.6C). Ammonium (1.6 μg/m^3) and sulfate (4.9 μg/m^3) comprised over 40% of the total PM_1 mass measured by the HR-AMS during these periods, likely in the form of ammonium sulfate (Figure 3.3). Urban influenced air masses had the highest mass concentration of sulfate (up to 10 μg/m^3) measured throughout the study. In contrast, there was little presence of nitrate internally mixed in the ECOC-sulfate (4 ± 2% by number) and OC-sulfate (19 ± 5% by

number) particles (Figure 3.6), and nitrate only comprised 1% (0.2 μg/m^3) of the total PM_1 mass concentration from the urban influence (Figure 3.3).

3.4. Conclusions

Source apportionment of atmospheric particles in the summertime was conducted at the forested University of Michigan Biological Station, located in remote northern Michigan. The field site was impacted by air masses from three distinct areas: remote background, northwestern Canada, and southwestern urban areas. July 2014 was one of the most active burning seasons for the Northwest Territories in over two decades with a total of 10,643 km^2 of land burned, significantly more than the ten-year (1,944 km^2) and twenty-five year (2,423 km^2) averages (CIFFC, 2014). The increased wildfire activity noticeably impacted northern Michigan, as the presence of biomass burning particles was ubiquitous throughout the study and made up the majority of measured particle number and mass concentrations. While air also came from urban areas southwest of UMBS, aged biomass burning particles dominated particle number concentrations due to wildfire influences from the southern United States. Due to the urban influence, these air masses had the highest mass contributions of sulfate (over 50 times the background) detected during the entire study. The accumulation of soluble secondary species, including sulfate and nitrate, increases the CCN ability of biomass burning particles (Furutani et al., 2008; Petters et al., 2009; Wang et al., 2010a), illustrating the importance of transported wildfire emissions.

While biomass burning particles were the most dominant particle core detected, SOA was a major contributor to particle mass during the study. On average, the HR-AMS organic aerosol O/C ratio was 0.84, indicative of highly oxidized organic carbon (Aiken et al., 2008). During remote background periods, internal mixing of oxidized OC combined with the significant PM_1 organic mass loading is indicative of the high mass loading of biogenic SOA in the forested region (Sheesley et al., 2004). During wildfire-influenced air masses, organics contributed ~90% to the PM_1 mass, with SOA internally mixed with biomass burning and OC-sulfate particles, indicating that SOA from both biogenic VOC oxidation and wildfire combustion is a major source of OC in the region. Models under-predict OC in this region, and Jathar et al. (2014) indicates that on a national level, models predict biomass burning is the largest combustion contributor to SOA by mass, consistent with the significant influence of wildfires during this work.

Modeling studies have called for further investigations of wildfire emissions and areas they affect in order to reduce uncertainty within models due to limited data, particularly when modeling interactions between wildfire plumes and urban emissions. Wildfire plume ozone production can lead to areas far from the original source to be out of compliance with regulatory standards, demonstrating the importance to be able to accurately model ozone production (Hu et al., 2008; Jaffe and Wigder, 2012; Lu et al., 2016). Also, as described here, particles aged through transport show internal mixtures of nitrate, sulfate and oxidized organics, which can lead to increased CCN activity (Furutani et al., 2008). With wildfires expected to increase in both intensity and frequency due to climate change (Gillett et al., 2004; Knorr et al., 2016; Liu et al., 2010; Veira et al., 2016), the contributions of long-range transported biomass burning emissions to the upper Midwest US atmosphere are expected to increase, such that air quality modeling efforts will need to supplement their existing emissions to account for the expected increase in wildfire emissions (Smith and Mueller, 2010).

3.5. Acknowledgements

Funding for the UMBS study was provided by University of Michigan MCubed Program and UMBS graduate fellowships for M. Gunsch, N. May, and D. Gardner. Matthew Gunsch and Nathaniel May ran the ATOFMS during the study. Daniel Gardner assisted in the operation the SMPS and APS. Miao Wen, Courtney Bottenus, and Timothy VanReken provided AMS and meteorological data. Support for T. VanReken and M. Wen was provided by the U.S. Department of Energy Early Career Research Program (award no. SC0003899). Steven Bertman provided support and assistance at the PROPHET tower. The ATOFMS used throughout the study was provided by Philip Hopke. Jennifer Dean (Washington University) is thanked for her assistance during the field study. We also thank the Pratt and Ault Groups for assistance on the field study. The authors gratefully acknowledge the NOAA Air Resources Laboratory (ARL) for the provision of the HYSPLIT transport and dispersion model and READY website (http://www.ready.noaa.gov) used in this publication. The authors also gratefully acknowledge the NOAA Office of Satellite and Product Operations for the use of the Hazard Mapping System Smoke Product (http://www.ospo.noaa.gov/Products/land/hms.html).

3.6. References

Aiken, A.C., Decarlo, P.F., Kroll, J.H., Worsnop, D.R., Huffman, J.A., Docherty, K.S., Ulbrich, I.M., Mohr, C., Kimmel, J.R., Sueper, D., 2008. O/C and OM/OC ratios of primary, secondary, and ambient organic aerosols with high-resolution time-of-flight aerosol mass spectrometry. Environ. Sci. Technol. 42, 4478-4485.

Allan, J.D., Delia, A.E., Coe, H., Bower, K.N., Alfarra, M.R., Jimenez, J.L., Middlebrook, A.M., Drewnick, F., Onasch, T.B., Canagaratna, M.R., 2004. A generalised method for the extraction of chemically resolved mass spectra from Aerodyne aerosol mass spectrometer data. J. Aerosol. Sci. 35, 909-922.

Allan, J.D., Jimenez, J.L., Williams, P.I., Alfarra, M.R., Bower, K.N., Jayne, J.T., Coe, H., Worsnop, D.R., 2003. Quantitative sampling using an Aerodyne aerosol mass spectrometer 1. Techniques of data interpretation and error analysis. J. Geophys. Res-Atmos. 108, 4090.

Ault, A.P., Williams, C.R., White, A.B., Neiman, P.J., Creamean, J.M., Gaston, C.J., Ralph, F.M., Prather, K.A., 2011. Detection of Asian dust in California orographic precipitation. J. Geophys. Res-Atmos. 116.

Axson, J.L., May, N.W., Colón-Bernal, I.D., Pratt, K.A., Ault, A.P., 2016. Lake Spray Aerosol: A Chemical Signature from Individual Ambient Particles. Environ. Sci. Technol. 50, 9835 - 9845.

Bauer, S.E., Ault, A., Prather, K.A., 2013. Evaluation of aerosol mixing state classes in the GISS modelE ‐ MATRIX climate model using single ‐ particle mass spectrometry measurements. J. Geophys. Res-Atmos. 118, 9834-9844.

Brook, R.D., Franklin, B., Cascio, W., Hong, Y., Howard, G., Lipsett, M., Luepker, R., Mittleman, M., Samet, J., Smith, S.C., 2004. Air pollution and cardiovascular disease. Circulation 109, 2655-2671.

Bullard, R.L., Singh, A., Anderson, S.M., Lehmann, C.M., Stanier, C.O., 2017. 10-Month characterization of the aerosol number size distribution and related air quality and meteorology at the Bondville, IL Midwestern background site. Atmos. Environ.

Calvo, A., Alves, C., Castro, A., Pont, V., Vicente, A., Fraile, R., 2013. Research on aerosol sources and chemical composition: past, current and emerging issues. Atmospheric Research 120, 1-28.

Carlton, A.G., Pinder, R.W., Bhave, P.V., Pouliot, G.A., 2010. To what extent can biogenic SOA be controlled? Environ. Sci. Technol. 44, 3376-3380.

Carroll, M.A., Bertman, S.B., Shepson, P.B., 2001. Overview of the Program for Research on Oxidants: Photochemistry, Emissions, and Transport (PROPHET) summer 1998 measurements intensive. J. Geophys. Res-Atmos. 106, 24275-24288.

Canadian Interagency Forest Fire Centre, National Wildland Fire Situation Report. Accessed July 2016. http://www.ciffc.ca.

Colarco, P., Schoeberl, M., Doddridge, B., Marufu, L., Torres, O., Welton, E., 2004. Transport of smoke from Canadian forest fires to the surface near Washington, DC: Injection height, entrainment, and optical properties. J. Geophys. Res-Atmos. 109, D06203.

Cooper, O., Moody, J., Thornberry, T., Town, M., Carroll, M., 2001. PROPHET 1998 meteorological overview and air‐mass classification. J. Geophys. Res-Atmos. 106, 24289-24299.

Creamean, J.M., Suski, K.J., Rosenfeld, D., Cazorla, A., DeMott, P.J., Sullivan, R.C., White, A.B., Ralph, F.M., Minnis, P., Comstock, J.M., 2013. Dust and biological aerosols from the Sahara and Asia influence precipitation in the western US. Science 339, 1572-1578.

Dall'Osto, M., Beddows, D., Kinnersley, R.P., Harrison, R.M., Donovan, R.J., Heal, M.R., 2004. Characterization of individual airborne particles by using aerosol time‐of‐flight mass spectrometry at Mace Head, Ireland. J. Geophys. Res-Atmos. 109.

DeBell, L.J., Talbot, R.W., Dibb, J.E., Munger, J.W., Fischer, E.V., Frolking, S.E., 2004. A major regional air pollution event in the northeastern United States caused by extensive forest fires in Quebec, Canada. J. Geophys. Res-Atmos. 109, D19305.

DeCarlo, P.F., Kimmel, J.R., Trimborn, A., Northway, M.J., Jayne, J.T., Aiken, A.C., Gonin, M., Fuhrer, K., Horvath, T., Docherty, K.S., 2006. Field-deployable, high-resolution, time-of-flight aerosol mass spectrometer. Anal. Chem. 78, 8281-8289.

Dempsey, F., 2013. Forest fire effects on air quality in Ontario: Evaluation of several recent examples. B. Am. Meteorol. Soc. 94, 1059-1064.

Dreessen, J., Sullivan, J., Delgado, R., 2016. Observations and Impacts of Transported Canadian Wildfire Smoke on Ozone and Aerosol Air Quality in the Maryland Region on 9-12 June, 2015. J. Air Waste Manage. Assoc. 66, 842-862.

Dutkiewicz, V.A., Husain, L., Roychowdhury, U.K., Demerjian, K.L., 2011. Impact of Canadian wildfire smoke on air quality at two rural sites in NY State. Atmos. Environ. 45, 2028-2033.

Emanuelsson, E.U., Hallquist, M., Kristensen, K., Glasius, M., Bohn, B., Fuchs, H., Kammer, B., Kiendler-Scharr, A., Nehr, S., Rubach, F., 2013. Formation of anthropogenic secondary organic aerosol (SOA) and its influence on biogenic SOA properties. Atmos. Chem. Phys. 13, 2837-2855.

Fierce, L., Bond, T.C., Bauer, S.E., Mena, F., Riemer, N., 2016. Black carbon absorption at the global scale is affected by particle-scale diversity in composition. Nat. Commun. 7.

Forster, C., Wandinger, U., Wotawa, G., James, P., Mattis, I., Althausen, D., Simmonds, P., O'Doherty, S., Jennings, S.G., Kleefeld, C., 2001. Transport of boreal forest fire emissions from Canada to Europe. J. Geophys. Res-Atmos. 106, 22887-22906.

Furutani, H., Dall'osto, M., Roberts, G.C., Prather, K.A., 2008. Assessment of the relative importance of atmospheric aging on CCN activity derived from field observations. Atmos. Environ. 42, 3130-3142.

Gard, E., Mayer, J.E., Morrical, B.D., Dienes, T., Fergenson, D.P., Prather, K.A., 1997. Real-time analysis of individual atmospheric aerosol particles: Design and performance of a portable ATOFMS. Anal. Chem. 69, 4083-4091.

Gillett, N., Weaver, A., Zwiers, F., Flannigan, M., 2004. Detecting the effect of climate change on Canadian forest fires. Geophys. Res. Lett. 31, L18211.

Grieshop, A., Donahue, N., Robinson, A., 2009. Laboratory investigation of photochemical oxidation of organic aerosol from wood fires 2: analysis of aerosol mass spectrometer data. Atmos. Chem. Phys. 9, 2227-2240.

Gunsch, M.J., Schmidt, S., Gardner, D.J., Bondy, A.L., May, N., Bertman, S.B., Pratt, K.A., Ault, A.P., 2017. Particle Growth in an Isoprene-Rich Forest: Influences of Urban, Wildfire, and Biogenic Precursors. Submitted to Atmospheric Environment.

Hand, J., Copeland, S., Day, D., Dillner, A., Indresand, H., Malm, W., McDade, C., Moore, C., Pitchford, M., Schichtel, B., 2011. Spatial and seasonal patterns and temporal variability of haze and its constituents in the United States: IMPROVE Report V, June 2011.

Hu, Y., Odman, M.T., Chang, M.E., Jackson, W., Lee, S., Edgerton, E.S., Baumann, K., Russell, A.G., 2008. Simulation of air quality impacts from prescribed fires on an urban area. Environ. Sci. Technol. 42, 3676-3682.

Hudson, P.K., Murphy, D.M., Cziczo, D.J., Thomson, D.S., De Gouw, J.A., Warneke, C., Holloway, J., Jost, H.J., Hübler, G., 2004. Biomass‐burning particle measurements: Characteristic composition and chemical processing. J. Geophys. Res-Atmos. 109, D23S27.

IPCC, 2013. IPCC, 2013: climate change 2013: the physical science basis. Contribution of working group I to the fifth assessment report of the intergovernmental panel on climate change. Cambridge University Press.

Jaffe, D.A., Wigder, N.L., 2012. Ozone production from wildfires: A critical review. Atmos. Environ. 51, 1-10.

Jathar, S.H., Gordon, T.D., Hennigan, C.J., Pye, H.O., Pouliot, G., Adams, P.J., Donahue, N.M., Robinson, A.L., 2014. Unspeciated organic emissions from combustion sources and their influence on the secondary organic aerosol budget in the United States. Proc. Natl. Acad. Sci. 111, 10473-10478.

Jayne, J.T., Leard, D.C., Zhang, X., Davidovits, P., Smith, K.A., Kolb, C.E., Worsnop, D.R., 2000. Development of an aerosol mass spectrometer for size and composition analysis of submicron particles. Aerosol. Sci. Technol. 33, 49-70.

Jeong, C.-H., McGuire, M.L., Godri, K.J., Slowik, J.G., Rehbein, P., Evans, G., 2011. Quantification of aerosol chemical composition using continuous single particle measurements. Atmos. Chem. Phys. 11, 7027-7044.

Jimenez, J., Canagaratna, M., Donahue, N., Prevot, A., Zhang, Q., Kroll, J.H., DeCarlo, P.F., Allan, J.D., Coe, H., Ng, N., 2009. Evolution of organic aerosols in the atmosphere. Science 326, 1525-1529.

Jimenez, J.L., Jayne, J.T., Shi, Q., Kolb, C.E., Worsnop, D.R., Yourshaw, I., Seinfeld, J.H., Flagan, R.C., Zhang, X., Smith, K.A., 2003. Ambient aerosol sampling using the aerodyne aerosol mass spectrometer. J. Geophys. Res-Atmos. 108, 8425.

Kang, C.-M., Gold, D., Koutrakis, P., 2014. Downwind O 3 and PM 2.5 speciation during the wildfires in 2002 and 2010. Atmos. Environ. 95, 511-519.

Khlystov, A., Stanier, C., Pandis, S., 2004. An algorithm for combining electrical mobility and aerodynamic size distributions data when measuring ambient aerosol. Aerosol. Sci. Technol. 38, 229-238.

Kim, E., Hopke, P.K., Kenski, D.M., Koerber, M., 2005. Sources of fine particles in a rural midwestern US area. Environ. Sci. Technol. 39, 4953-4960.

Kim, M., Deshpande, S.R., Crist, K.C., 2007. Source apportionment of fine particulate matter (PM2.5) at a rural Ohio River Valley site. Atmos. Environ. 41, 9231-9243.

Knorr, W., Jiang, L., Arneth, A., 2016. Climate, CO2 and human population impacts on global wildfire emissions. Biogeosciences 13, 267-282.

Kundu, S., Stone, E.A., 2014. Composition and sources of fine particulate matter across urban and rural sites in the Midwestern United States. Env. Sci. Process. Impact 16, 1360-1370.

Liu, Y., Stanturf, J., Goodrick, S., 2010. Trends in global wildfire potential in a changing climate. Forest. Ecol. Manag. 259, 685-697.

Lu, X., Zhang, L., Yue, X., Zhang, J., Jaffe, D.A., Stohl, A., Zhao, Y., Shao, J., 2016. Wildfire influences on the variability and trend of summer surface ozone in the mountainous western United States. Atmos. Chem. Phys. 16, 14687-14702.

Matsui, H., Koike, M., Kondo, Y., Moteki, N., Fast, J.D., Zaveri, R.A., 2013. Development and validation of a black carbon mixing state resolved three‐dimensional model: Aging processes and radiative impact. J. Geophys. Res-Atmos. 118, 2304-2326.

Middlebrook, A.M., Bahreini, R., Jimenez, J.L., Canagaratna, M.R., 2012. Evaluation of composition-dependent collection efficiencies for the aerodyne aerosol mass spectrometer using field data. Aerosol. Sci. Technol. 46, 258-271.

Miller, D.J., Sun, K., Zondlo, M.A., Kanter, D., Dubovik, O., Welton, E.J., Winker, D.M., Ginoux, P., 2011. Assessing boreal forest fire smoke aerosol impacts on US air quality: A case study using multiple data sets. J. Geophys. Res-Atmos. 116.

Moffet, R.C., Henn, T.R., Tivanski, A.V., Hopkins, R.J., Desyaterik, Y., Kilcoyne, A., Tyliszczak, T., Fast, J., Barnard, J., Shutthanandan, V., 2010. Microscopic characterization of carbonaceous aerosol particle aging in the outflow from Mexico City. Atmos. Chem. Phys. 10, 961-976.

Moffet, R.C., Prather, K.A., 2009. In-situ measurements of the mixing state and optical properties of soot with implications for radiative forcing estimates. Proc. Natl. Acad. Sci. 106, 11872-11877.

Moffet, R.C., Qin, X., Rebotier, T., Furutani, H., Prather, K.A., 2008. Chemically segregated optical and microphysical properties of ambient aerosols measured in a single‐particle mass spectrometer. J. Geophys. Res-Atmos. 113, D12213.

Müller, D., Mattis, I., Wandinger, U., Ansmann, A., Althausen, D., Stohl, A., 2005. Raman lidar observations of aged Siberian and Canadian forest fire smoke in the free troposphere over Germany in 2003: Microphysical particle characterization. J. Geophys. Res-Atmos. 110.

National Research Council, National Academies, 2010. Global sources of local pollution: an assessment of long-range transport of key air pollutants to and from the United States. National Academies Press, Washington, D.C.

Pastor, S.H., Allen, J.O., Hughes, L.S., Bhave, P., Cass, G.R., Prather, K.A., 2003. Ambient single particle analysis in Riverside, California by aerosol time-of-flight mass spectrometry during the SCOS97-NARSTO. Atmos. Environ. 37, 239-258.

Paulot, F., Jacob, D.J., Pinder, R., Bash, J., Travis, K., Henze, D., 2014. Ammonia emissions in the United States, European Union, and China derived by high‐resolution inversion of ammonium wet deposition data: Interpretation with a new agricultural emissions inventory (MASAGE_NH3). J. Geophys. Res-Atmos. 119, 4343-4364.

Petters, M.D., Carrico, C.M., Kreidenweis, S.M., Prenni, A.J., DeMott, P.J., Collett, J.L., Moosmueller, H., 2009. Cloud condensation nucleation activity of biomass burning aerosol. J. Geophys. Res-Atmos. 114.

Pope, C.A., Dockery, D.W., 2006. Health effects of fine particulate air pollution: lines that connect. J. Air Waste Manage. Assoc. 56, 709-742.

Pöschl, U., 2005. Atmospheric Aerosols: Composition, Transformation, Climate and Health Effects. Angew. Chen. Int. Ed. 44, 7520 - 7540.

Pöschl, U., Shiraiwa, M., 2015. Multiphase chemistry at the atmosphere–biosphere interface influencing climate and public health in the anthropocene. Chem. Rev. 115, 4440-4475.

Pratt, K., Murphy, S., Subramanian, R., DeMott, P., Kok, G., Campos, T., Rogers, D., Prenni, A., Heymsfield, A., Seinfeld, J., 2011. Flight-based chemical characterization of biomass burning aerosols within two prescribed burn smoke plumes. Atmos. Chem. Phys. 11, 12549-12565.

Pratt, K.A., Heymsfield, A.J., Twohy, C.H., Murphy, S.M., DeMott, P.J., Hudson, J.G., Subramanian, R., Wang, Z., Seinfeld, J.H., Prather, K.A., 2010. In situ chemical characterization of aged biomass-burning aerosols impacting cold wave clouds. J. Atmos. Sci. 67, 2451-2468.

Pratt, K.A., Prather, K.A., 2009. Real-time, single-particle volatility, size, and chemical composition measurements of aged urban aerosols. Environ. Sci. Technol. 43, 8276-8282.

Pratt, K.A., Prather, K.A., 2012. Mass spectrometry of atmospheric aerosols—Recent developments and applications. Part II: On‐line mass spectrometry techniques. Mass Spectrom. Rev. 31, 17-48.

Qin, X., Bhave, P.V., Prather, K.A., 2006. Comparison of two methods for obtaining quantitative mass concentrations from aerosol time-of-flight mass spectrometry measurements. Anal. Chem. 78, 6169-6178.

Qin, X., Pratt, K.A., Shields, L.G., Toner, S.M., Prather, K.A., 2012. Seasonal comparisons of single-particle chemical mixing state in Riverside, CA. Atmos. Environ. 59, 587-596.

Raatikainen, T., Vaattovaara, P., Tiitta, P., Miettinen, P., Rautiainen, J., Ehn, M., Kulmala, M., Laaksonen, A., Worsnop, D.R., 2010. Physicochemical properties and origin of organic

groups detected in boreal forest using an aerosol mass spectrometer. Atmos. Chem. Phys. 10, 2063-2077.

Rattanavaraha, W., Chu, K., Budisulistiorini, S.H., Riva, M., Lin, Y.-H., Edgerton, E.S., Baumann, K., Shaw, S.L., Guo, H., King, L., 2016. Assessing the impact of anthropogenic pollution on isoprene-derived secondary organic aerosol formation in PM 2.5 collected from the Birmingham, Alabama, ground site during the 2013 Southern Oxidant and Aerosol Study. Atmos. Chem. Phys. 16, 4897-4914.

Riemer, N., West, M., 2013. Quantifying aerosol mixing state with entropy and diversity measures. Atmos. Chem. Phys. 13, 11423-11439.

Rolph, G.D., Draxler, R.R., Stein, A.F., Taylor, A., Ruminski, M.G., Kondragunta, S., Zeng, J., Huang, H.-C., Manikin, G., McQueen, J.T., 2009. Description and verification of the NOAA smoke forecasting system: the 2007 fire season. Weather Forecast. 24, 361-378.

Sheesley, R.J., Schauer, J.J., Bean, E., Kenski, D., 2004. Trends in secondary organic aerosol at a remote site in Michigan's upper peninsula. Environ. Sci. Technol. 38, 6491-6500.

Silva, P.J., Liu, D.-Y., Noble, C.A., Prather, K.A., 1999. Size and chemical characterization of individual particles resulting from biomass burning of local Southern California species. Environ. Sci. Technol. 33, 3068-3076.

Sjostedt, S., Slowik, J., Brook, J., Chang, R.-W., Mihele, C., Stroud, C., Vlasenko, A., Abbatt, J., 2011. Diurnally resolved particulate and VOC measurements at a rural site: indication of significant biogenic secondary organic aerosol formation. Atmos. Chem. Phys. 11, 5745-5760.

Slowik, J., Stroud, C., Bottenheim, J., Brickell, P., Chang, R.-W., Liggio, J., Makar, P., Martin, R., Moran, M., Shantz, N., 2010. Characterization of a large biogenic secondary organic aerosol event from eastern Canadian forests. Atmos. Chem. Phys. 10, 2825-2845.

Smith, S., Mueller, S., 2010. Modeling natural emissions in the Community Multiscale Air Quality (CMAQ) Model–I: building an emissions data base. Atmos. Chem. Phys. 10, 4931-4952.

Song, X.-H., Hopke, P.K., Fergenson, D.P., Prather, K.A., 1999. Classification of single particles analyzed by ATOFMS using an artificial neural network, ART-2A. Anal. Chem. 71, 860-865.

Spencer, M.T., Shields, L.G., Prather, K.A., 2007. Simultaneous measurement of the effective density and chemical composition of ambient aerosol particles. Environ. Sci. Technol. 41, 1303-1309.

Stephen, K., Aneja, V.P., 2008. Trends in agricultural ammonia emissions and ammonium concentrations in precipitation over the Southeast and Midwest United States. Atmos. Environ. 42, 3238-3252.

Su, Y., Sipin, M.F., Furutani, H., Prather, K.A., 2004. Development and characterization of an aerosol time-of-flight mass spectrometer with increased detection efficiency. Anal. Chem. 76, 712-719.

Sueper, D., 2010. ToF-AMS analysis software. Available at: http://cires1.colorado.edu/jimenez-group/ToFAMSResources/ToFSoftware/index.html.

Sun, Y., Zhang, Q., Macdonald, A.M., Hayden, K., Li, S.M., Liggio, J., Liu, P.S.K., Anlauf, K.G., Leaitch, W.R., Steffen, A., Cubison, M., Worsnop, D.R., van Donkelaar, A., Martin, R.V., 2009. Size-resolved aerosol chemistry on Whistler Mountain, Canada with a high-resolution aerosol mass spectrometer during INTEX-B. Atmos. Chem. Phys. 9, 3095-3111.

Toner, S.M., Shields, L.G., Sodeman, D.A., Prather, K.A., 2008. Using mass spectral source signatures to apportion exhaust particles from gasoline and diesel powered vehicles in a freeway study using UF-ATOFMS. Atmos. Environ. 42, 568-581.

Toner, S.M., Sodeman, D.A., Prather, K.A., 2006. Single particle characterization of ultrafine and accumulation mode particles from heavy duty diesel vehicles using aerosol time-of-flight mass spectrometry. Environ. Sci. Technol. 40, 3912-3921.

Uno, I., Eguchi, K., Yumimoto, K., Takemura, T., Shimizu, A., Uematsu, M., Liu, Z., Wang, Z., Hara, Y., Sugimoto, N., 2009. Asian dust transported one full circuit around the globe. Nat. Geosci. 2, 557-560.

VanReken, T., Mwaniki, G., Wallace, H., Pressley, S., Erickson, M., Jobson, B., Lamb, B., 2015. Influence of air mass origin on aerosol properties at a remote Michigan forest site. Atmos. Environ. 107, 35-43.

Veira, A., Lasslop, G., Kloster, S., 2016. Wildfires in a warmer climate: Emission fluxes, emission heights, and black carbon concentrations in 2090–2099. J. Geophys. Res-Atmos. 121, 3195-3223.

Wang, J., Cubison, M., Aiken, A., Jimenez, J., Collins, D., 2010a. The importance of aerosol mixing state and size-resolved composition on CCN concentration and the variation of the importance with atmospheric aging of aerosols. Atmos. Chem. Phys. 10, 7267-7283.

Wang, Y., Huang, J., Zananski, T.J., Hopke, P.K., Holsen, T.M., 2010b. Impacts of the Canadian forest fires on atmospheric mercury and carbonaceous particles in northern New York. Environ. Sci. Technol. 44, 8435-8440.

Wiedinmyer, C., Quayle, B., Geron, C., Belote, A., McKenzie, D., Zhang, X., O'Neill, S., Wynne, K.K., 2006. Estimating emissions from fires in North America for air quality modeling. Atmos. Environ. 40, 3419-3432.

Xu, L., Guo, H., Boyd, C.M., Klein, M., Bougiatioti, A., Cerully, K.M., Hite, J.R., Isaacman-VanWertz, G., Kreisberg, N.M., Knote, C., 2015. Effects of anthropogenic emissions on aerosol formation from isoprene and monoterpenes in the southeastern United States. Proc. Natl. Acad. Sci. 112, 37-42.

Zhang, Y., Sheesley, R.J., Schauer, J.J., Lewandowski, M., Jaoui, M., Offenberg, J.H., Kleindienst, T.E., Edney, E.O., 2009. Source apportionment of primary and secondary organic aerosols using positive matrix factorization (PMF) of molecular markers. Atmos. Environ. 43, 5567-5574.

Chapter 4.
Particle Growth in an Isoprene-Rich Forest: Influences of Urban, Wildfire, and Biogenic Precursors

Submitted to *Atmos. Environ.*

4.1. Introduction

New particle formation and growth (NPFG) has been identified as an important (Gordon et al., 2016; Jokinen et al., 2015b; Kulmala et al., 2014; Kulmala et al., 2000), but uncertain (Pierce and Adams, 2007, 2009b), contributor to global aerosol concentrations. Growth events, where newly formed particles increase in size through condensation, impact climate by acting as cloud condensation nuclei (CCN) (Laaksonen et al., 2005; Merikanto et al., 2009; Pierce and Adams, 2009a; Sotiropoulou et al., 2006), thereby modifying cloud properties and leading to cooling through the indirect effect (Ruehl et al., 2016). Through model simulations, Gordon et al. (2016) suggested that biogenic NPFG events are the source of 50-100% of particles by number within 500 m of the surface over large swaths of North America, from interior Alaska to the northern Great Lakes region, with these particles increasing CCN concentrations by 3-40% and altering the cloud albedo effect by up to 0.5 W/m^2. Growth events have been observed in forested (e.g. Creamean et al., 2011; Dal Maso et al., 2005; Yu et al., 2015), urban (e.g. Salimi et al., 2017; Wang et al., 2013), marine (e.g. Allan et al., 2015; Sipila et al., 2016), and polar regions (e.g. Weller et al., 2015; Willis et al., 2016), as well as in the free troposphere (e.g. Bianchi et al., 2016; Rose et al., 2015). However, there have been few studies in the upper Midwest United States (Kanawade et al., 2011; Lee et al., 2008; Pierce et al., 2014; Twohy et al., 2002).

Nucleated particles are formed in-situ in the atmosphere from stable molecular clusters (Zhang, 2010), including a variety of chemical species, such as sulfuric acid (Sipila et al., 2010;

Zhang et al., 2004), low volatility oxidized biogenic gases (Jokinen et al., 2015b; Troestl et al., 2016), organic (including amine) salts (Barsanti et al., 2009; Jen et al., 2016; Smith et al., 2010), iodine-containing gases (Allan et al., 2015; Sipila et al., 2016), and gaseous ions (Kirkby et al., 2016). In particular, low volatility oxidation products of biogenic volatile organic compounds (BVOCs), including monoterpenes and sesquiterpenes, are thought to play an important role in new particle formation due to the prevalence of events in forested regions (Laaksonen et al., 2008). Growth events have been observed in boreal forests (Mäkelä et al., 1997; Sellegri et al., 2005), European coniferous forests (Gonser et al., 2014; Manninen et al., 2010), African savanna forests (Laakso et al., 2008; Vakkari et al., 2011), and deciduous forests (Jung et al., 2013; Manninen et al., 2010; Pryor et al., 2011), all of which have significant concentrations of BVOCs. The oxidants present prior to and during growth events also impact the formation of low volatility species, with OH oxidation dominating during the day and NO_3 at night (Brown et al., 2006; Ziemann and Atkinson, 2012). In addition to precursor and oxidant concentrations, key factors determining whether a growth event will occur are background aerosol concentration (condensation sink) (Dal Maso et al., 2002), season (Kulmala et al., 2004), and radiation (George et al., 2015; Zhang et al., 2011). While the majority of growth events are observed during the daytime (Kulmala et al., 2014; Kulmala et al., 2004), some events have been measured at night (Lee et al., 2008; Salimi et al., 2017). Also, while most growth events have been observed during clean conditions in remote areas, growth events can also begin due to the influence of transported emissions from long-range sources, including urban areas (Chandra et al., 2016; Salma et al., 2016; Venzac et al., 2008; Yue et al., 2013) and wildfires (Bein et al., 2008). Given the wide range of chemical and atmospheric variables that can impact growth events, studies are needed that compare events that occur during different atmospheric conditions at the same location.

Growth rate is a key variable once particle growth is occurring, as this determines the time necessary for particles to reach a size where nucleated particles can act as CCN. While H_2SO_4 is a key gaseous precursor for NPF (Kulmala and Laaksonen, 1990; Kulmala et al., 2004; Sipila et al., 2010), nucleation growth rates (J) are typically faster than can be explained by binary nucleation of H_2SO_4 and water vapor (Jokinen et al., 2015b; Kulmala et al., 2014; Kulmala et al., 2012; Kulmala et al., 2004; Sipila et al., 2016). In some locations, growth rates are seasonally dependent (Kulmala et al., 2004; Yu et al., 2015), but a great deal of uncertainty remains due to significant interannual variation (Kanawade et al., 2011; Yu et al., 2015). Growth

rates are strongly related to the concentration and chemical form of low volatility materials present (Laaksonen et al., 2008). However, there are limited measurements of growth rates for growth events with different gaseous precursors and oxidants at the same site, particularly in northern portions of North America where growth events are expected to contribute substantially to CCN concentrations (Gordon et al., 2016).

A potential complicating factor for growth events in forested regions is that isoprene has been speculated to suppress growth events. For the summer of 2009 in northern Michigan, Kanawade et al. (2011) credited isoprene suppression leading to a lack new particle formation events at UMBS, though growth of ultrafine aerosol was observed on a few occasion from ~20 nm particles that were too small to have been regionally transported. This hypothesis was based on results from a laboratory chamber experiment, where a lack of nucleation was attributed to the high reactivity of isoprene with the hydroxyl radical, inhibiting nucleation (Kiendler-Scharr et al., 2009). However, many other studies (e.g. Jokinen et al., 2015a; Kourtchev et al., 2005; Limbeck et al., 2003) have observed that isoprene could potentially enhance new particle formation and growth instead of inhibiting it. Therefore, it is important to investigate particle growth events in isoprene-rich environments.

At the University of Michigan Biological Station (UMBS) in northern Michigan, the Program for Research on Oxidants PHotochemistry, Emissions and Transport (PROPHET) tower is located within a temperate mixed-deciduous forest, dominated by isoprene emissions (Ortega et al., 2007), and representative of north-central US and south-central Canada (Carroll et al., 2001; VanReken et al., 2015). Herein, frequent ultrafine particle growth events at UMBS during summer 2014 are reported. Particle size distributions, individual particle chemical composition, meteorological parameters, and air mass trajectories were examined from June 24 – August 2, 2014 to understand the conditions that led to particle growth. This paper highlights particle growth occurring during three unique air mass types within the same forest: transported urban air masses, transported wildfire-influenced air masses, and stagnant local air masses rich in isoprene from the surrounding forest.

4.2. Methods

Atmospheric sampling was conducted between June 24 and August 2, 2014 at UMBS near Pellston, Michigan (45°33'31"N, 84°42'52"W). UMBS is a remote 40 km^2 research forest with little local pollution. The forest is dominated by aspen (61%), northern hardwoods (17%),

and upland conifers (13%), with an average canopy height of 22.5 m (VanReken et al., 2015). Major nearby metropolitan areas include Milwaukee (370 km southwest), Detroit (385 km south-southeast), and Chicago (466 km south-southwest).

Instruments were located within the PROPHET laboratory adjacent to a 31 m tall outdoor tower. Above canopy air was sampled from 34 m (~12 m above the forest canopy) through an insulated 1.1 cm ID copper tubing inlet using a cylindrical sampling manifold with dedicated lines for each instrument. Sampled air had a residence time from the top of the tower to the instruments of ~15 s. Meteorological data were obtained from the UMBS AmeriFlux tower at a height of 46 m, located 100 m to the northeast of PROPHET, and are detailed in the Supplemental Information (SI). Tropospheric NO_2 column data were obtained from Global Ozone Monitoring Experiment–2 (GOME-2) data products (Boersma et al., 2004).

Particle size distributions were measured using two scanning mobility particle sizer (SMPS) instruments. From June 24 – July 20, a SMPS 3936 system (TSI Inc., model 3080 electrostatic classifier, model 3081 long differential mobility analyzer, model 3025A condensation particle counter) was used, and from July 10 – August 2, a SMPS 3938 system (TSI Inc., model 3082 electrostatic classifier, model 3081A long differential mobility analyzer, and a model 3775 condensation particle counter) was used. Both SMPS systems used a sheath flow rate of 4 L/min and an aerosol flow rate of 0.4 L/min, allowing for the detection of particles from 11.5 nm – 603.4 nm (electrical mobility diameter). A correction factor was derived for data reported by the SMPS 3936 and the SMPS 3938 for each size bin to account for any instrumental differences, allowing for the direct comparison of the concentrations reported by the two instruments. Details of the comparison between the measurements of the two SMPS systems (Figure B.1), including the derived size-dependent correction factor (Figure B.2), are available in the SI. During the 10-day period when both SMPS systems were present, the SMPS 3938 sampled above the forest canopy at 34 m, and the SMPS 3936 sampled at ~3 m above ground level through 0.5 cm ID copper tubing with a residence time of ~2 s. A particle concentration gradient was not observed between these two sampling heights (Figure B.1), and therefore, the analysis presented focuses only on above canopy sampling that was available throughout the study. It should be noted that new particle formation occurs at ~1 nm (Zhang, 2010), while the lower limit of the SMPS systems used herein is 11 nm. Thus, since only particle growth is

directly observed, the events are referred to as growth events, even though the likely origin of the particles is nucleation.

Particle samples for transmission electron microscopy (TEM) were collected using a micro-orifice uniform deposition impactor (MOUDI, model 110, MSP Corp.), sampling at 30 L/min. In order to prevent particle overloading on the substrates, the MOUDI flow was diluted to 10 L/min, with the remaining 20 L/min comprised of particle-free air sampled through a HEPA capsule (Pall Laboratory). Particles were impacted on 200 mesh carbon type B with Formvar grids (Ted Pella Inc.) and analyzed at the Michigan Center for Materials Characterization (MC^2) at the University of Michigan. A JEOL 2100 probe-corrected analytical electron microscope equipped with a zirconated tungsten thermal field emission tip operating at 200 kV and a high angle annular dark field (HAADF) detector were used for analysis. The microscope was equipped with an energy dispersive X-ray (EDX) detector (EDAX, Inc.), and EDX spectra from individual particles were collected and analyzed to determine their elemental composition.

In order to investigate the air masses impacting the site, the NOAA Hybrid Single Particle Lagrangian Integrated Trajectory (HYSPLIT) model was run for each growth event at a starting height of 100 m to obtain 72 h backward air mass trajectories, allowing particle growth events to be classified based on air mass origin at the onset of the event (Stein et al., 2015). The NOAA Hazard Mapping System Fire and Smoke Product was also used to probe the influence of wildfire smoke emissions on the field site (Rolph et al., 2009). This product is produced as daily images using MODIS satellite imagery to locate wildfire smoke plumes.

4.3. Results & Discussion

A typical particle growth event was defined as having a starting particle mobility diameter mode less than 40 nm with consistent growth over at least three subsequent hours. From June 24 – August 2, 2014, 14 particle growth events occurred over 31% of the sampling days (Table 4.1). Growth rates ranged from 0.8 – 10.2 nm h^{-1} (Table 4.1), consistent with previous observations of particle growth in the mid-latitudes (Holmes, 2007; Kulmala et al., 2004). Example growth events are shown in Figure 4.1, and all events are detailed in Table 4.1. Particle growth event frequency was higher here than during the summer 2009 Community Atmosphere-Biosphere Interactions Experiment (CABINEX) at the PROPHET tower, when particle growth occurred on 6% of sampling days at the same site (Kanawade et al., 2011; Yu et al., 2015). However, during CABINEX, there were lower than average temperatures (22°C during

CABINEX, compared to the UMBS July average of 26°C and August average of 25°C), due in part to increased cloud coverage (Bryan et al., 2012; Steiner et al., 2011), which limited the amount of incoming solar radiation and inhibited photochemical reactions needed for particle growth (Zhang et al., 2011). In addition, greater summertime Canadian wildfire activity occurred in 2014 (46,000 km^2 burned) compared to 2009 (8,500 km^2 burned) (CIFFC, 2017), contributing to the wildfire-influenced particle growth events observed in this study, as discussed in Section 4.3.3.

Table 4.1. Characteristics of the 14 particle growth events observed at UMBS.

Event Number	Event Start (EDT)	Event End (EDT)	Start Diameter (nm)	Stop Diameter (nm)	Growth Rate (nm h^{-1})
Urban (Midday)					
3	6/29/14 14:05	6/30/14 0:00	17	62	4.5
4	7/1/14 11:54	7/1/14 14:30	20	41	8.1
5	7/2/14 8:50	7/2/14 15:05	38	67	4.6
6	7/5/14 15:00	7/5/14 18:20	23	57	10.2
11	7/16/14 10:25	7/16/14 23:45	36	59	1.7
14	7/25/14 12:00	7/25/14 17:40	19	69	8.8
Wildfire (Nighttime)					
2	6/25/14 17:10	6/26/14 1:40	25	71	5.4
7	7/7/14 17:35	7/8/14 7:25	35	61	1.9
8	7/9/14 20:00	7/10/14 4:15	32	66	4.1
10	7/13/14 16:45	7/14/14 9:30	32	57	1.5
12	7/22/14 22:20	7/23/14 10:55	38	87	3.9
13	7/24/14 22:00	7/25/14 1:00	15	24	3.0
Forested/Stagnant (Multiday)					
1	6/25/14 7:10	6/26/14 12:35	50	115	2.2
9	7/11/14 0:10	7/13/14 7:00	47	91	0.8

Each particle growth event observed in the present study was preceded by low particle concentrations, typically due to increased particle scavenging from rain or passing cold fronts (Nilsson et al., 2001). This creates favorable conditions for nucleation, as there are fewer existing aerosols for low volatility gases to condense on. The condensation sink (CS), a measure of how fast condensable vapor condenses onto existing aerosols, was calculated using the method described by Dal Maso et al. (2002) and particle number size distributions. The CS varied by a factor of 35 during the study (2×10^{-4} to 7×10^{-2} s^{-1}, Figure 4.2), a similar range to the forested study described by Dal Maso et al. (2002). This low CS is favorable for NPF and particle growth (e.g. Chandra et al., 2016; Dal Maso et al., 2002; Gordon et al., 2016; Riipinen et al., 2007). As

shown in Figure 4.2, growth events typically began during CS minima with an average initial CS of 2 x 10^{-3} s^{-1}, compared to an average of 6.0 x 10^{-3} s^{-1} during non-event periods. As the events progressed, the CS typically increased as the particles grew to larger sizes and provided a surface for condensation.

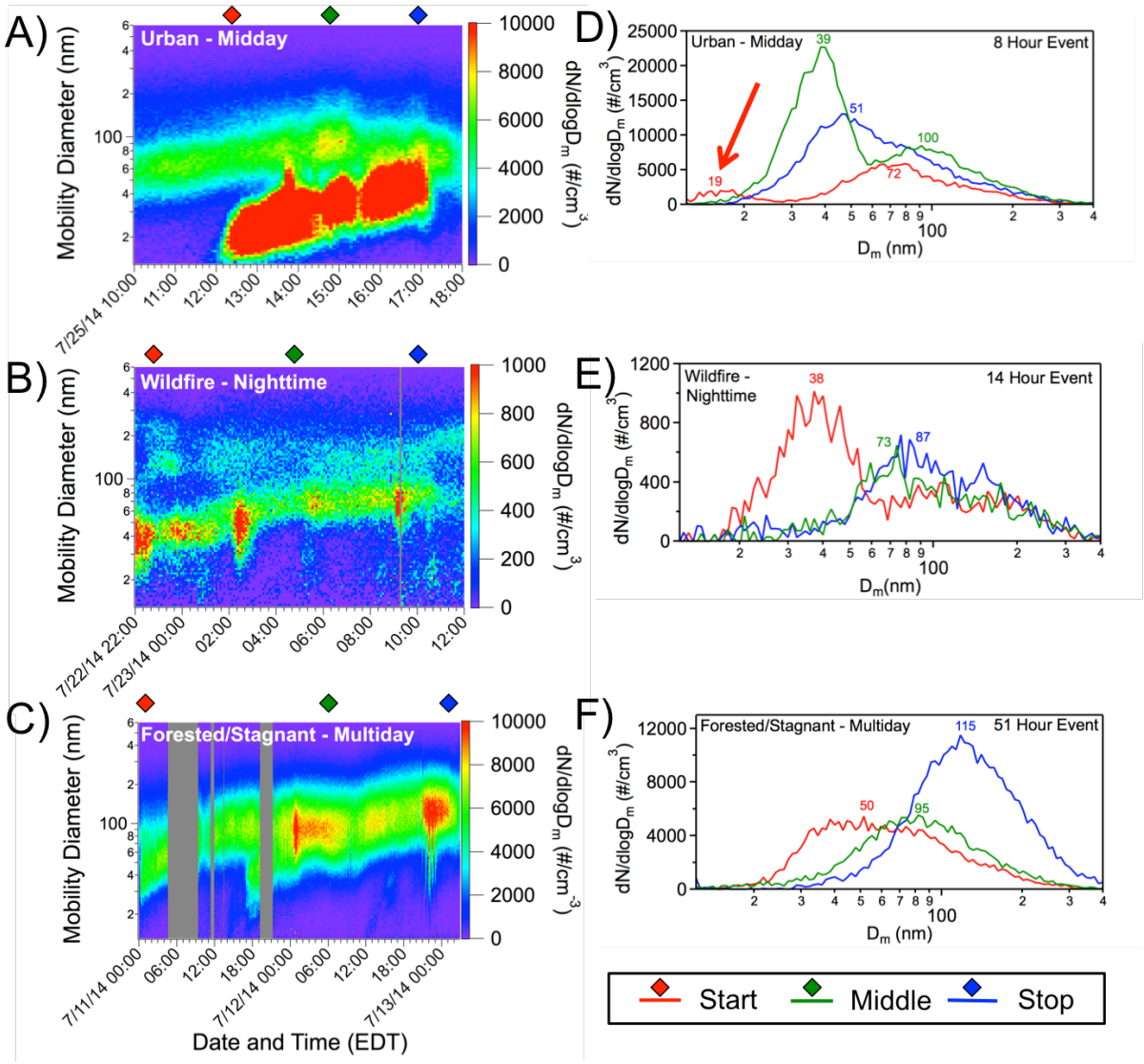

Figure 4.1. (Left) Example time-resolved aerosol size distributions for representative (A) midday, (B) nighttime, and (C) multiday growth events. (Right) Corresponding aerosol size distributions (D, E, and F) are shown for the start (red), middle (green), and end (blue) of each event, with the particle size mode notated above each trace. The timing of selected aerosol size distributions are indicated by diamonds on the temporal size distribution plot. A red arrow in plot D indicates the first of the two modes in that size distribution. Time periods without data are indicated in gray.

The 14 growth events occurred while the field site was influenced by air masses from three unique locations: 1) urban areas to the southwest, 2) wildfires from the northwest, and 3) stagnant air local to the forest field site. Four of the 14 events began midday (12:00 EDT +/- 3 h) and were classified as urban air mass influenced events. Two additional events began midday (#5 and #11), but were not influenced by urban air masses. Five events began at night (20:00 EDT +/- 3 h) and were classified as wildfire air mass influenced events. One additional event (#2) began at night, but was not under wildfire air mass influence. Although the general starting diameter cut-off for a particle growth event was defined as 40 nm, there were two unique cases identified as stagnant/forested (multiday) events where growth began at 7:10 EDT and 00:10 EDT, respectively, and lasted for greater than 24 h with observed starting diameters of 50 nm. Figure 4.1 shows the progression of the aerosol size distributions during example growth events for each air mass type, Figure 4.3 shows the progression of the particle modes during each of the 14 events, and Figure 4.4 shows average growth rate during each event type. Across all event types, particle growth rates were generally dependent on initial particle diameter, with smaller particles growing faster than particles with larger starting diameters (Figure B.3). The event categories and characteristics are discussed in detail in the following sections.

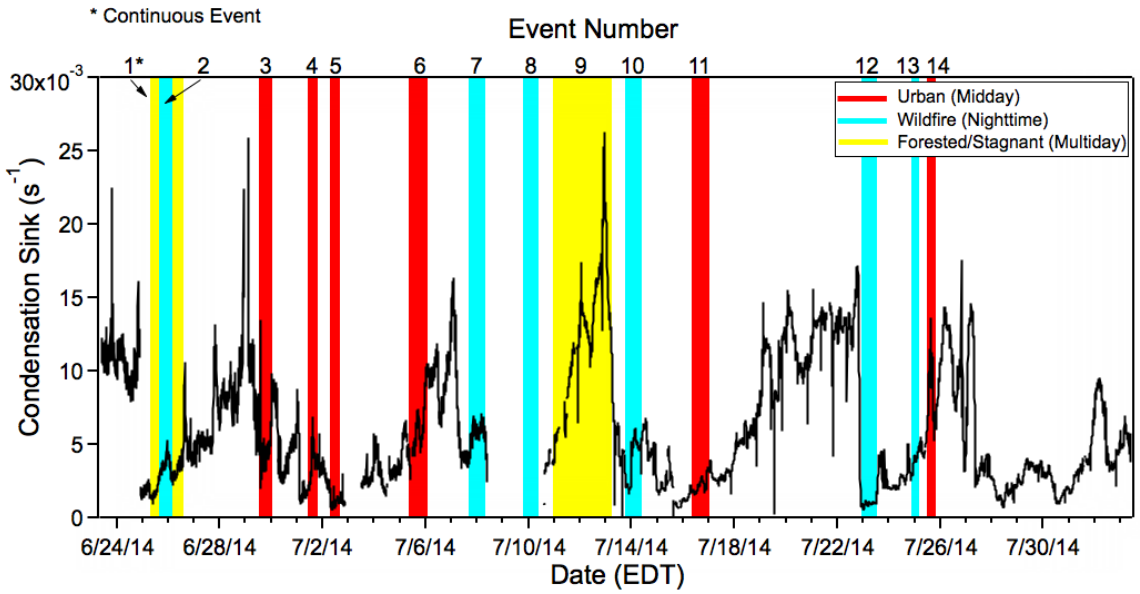

Figure 4.2. Calculated condensation sink (CS) as a function of time, with colored bars representing the duration of individual growth events and their classification. Event numbers are denoted at the top of the plot above each bar, and an asterisk indicates the continuous nature of event #1 after the conclusion of event #2 (Figure B.9).

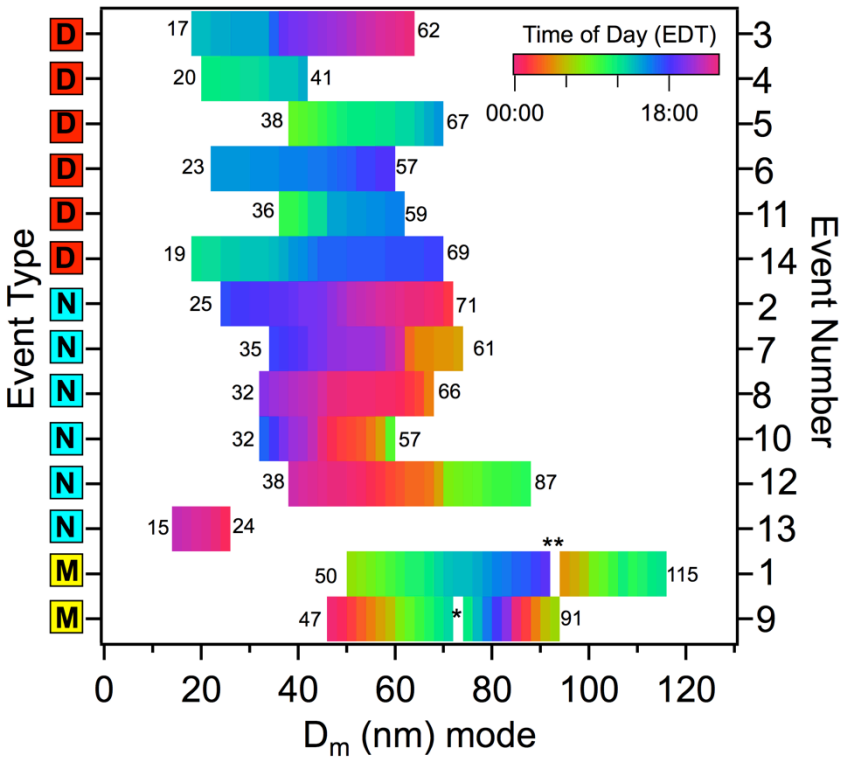

Figure 4.3. Progression of particle size modes during each growth event. Start and end mobility diameters are notated for each growth event, as well as the classification as a midday (D), nighttime (N), or multiday (M) event. Detailed characteristics of each event are located in Table 4.1. Events 1** and 9* include 10 h and 23 h, respectively, of stagnant nighttime periods, when particle growth appeared to pause.

4.3.1. Urban (Midday) Events

The four urban (midday) events occurred when air masses were transported from metropolitan areas, including Chicago and Milwaukee, with transport times of 12 to 24 h (Figure 4.5). They had an average growth rate of 8 ± 2 nm h^{-1}, the fastest of the three event types (Figure 4.4). Two additional midday growth events (#5, #11) not influenced by urban air masses had slower growth (3 ± 2 nm h^{-1}), likely due to limited influence from the urban precursors O_3 and NO_x. Average mid-day (12:00 EDT +/- 3 h) incident radiation was also higher during growth event days (748 ± 108 W m^{-2}) compared to non-event days (623 ± 92 W m^{-2}) (Figure B.4). Previous measurements at UMBS have indicated that elevated O_3 and NO_x levels are present during periods of urban influence (Thornberry et al., 2001). During the urban events in this study, increased transported tropospheric (column) NO_2 was also observed during these events

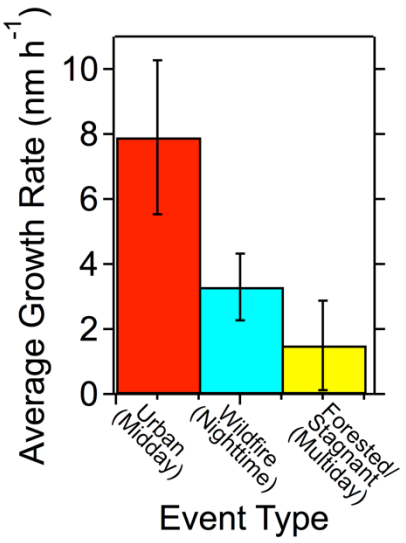

Figure 4.4. Average particle growth rates and 95% confidence interval (error bars) for urban (midday), wildfire (nighttime), and forested/stagnant (multiday) influenced growth events at UMBS.

(Figures 4.5 and B.5). Additionally, since these events not only occurred during midday, but on days with high solar radiation, it is expected that OH reactions with BVOCs emitted from the forest likely contributed to the production of semi-volatile organic compounds (Zhang et al., 2011), which condense onto particles. In the daytime at UMBS, isoprene dominates these OH reactions with minor contributions from monoterpenes and sesquiterpenes (Ortega et al., 2007). Therefore, it is expected that the midday growth events occurred through photochemical reactions likely driven by increased levels of anthropogenic oxidants reacting with local BVOCs and transported anthropogenic VOCs. Similar growth events were characterized during a campaign in California, where growth was driven by the condensation of oxidized organics and ammonium sulfate from the mixing of biogenic and urban emissions (Setyan et al., 2014; Shilling et al., 2013).

When considering climate impacts of particles from growth events, single particle composition and mixing state is a key factor (Ault and Axson, 2017; Craig et al., 2017). In the analysis of individual particles during an example urban (midday) event, large carbon and oxygen peaks, indicative of oxidized organics likely from BVOC photooxidation, were observed using TEM-EDX (Figure 4.6), though elemental concentrations were not quantitative since carbon and oxygen are also present from the TEM substrate (Ault et al., 2013; Guasco et al., 2013; Shen et al., 2016). TEM-EDX also showed significant contributions from sulfur (Figure 4.6), and composition was uniform enough to suggest a mostly internal mixture. Based on these observations, it is possible that sulfuric acid formed within the urban air mass, as previously observed by Kanawade et al. (2011) at UMBS, and contributed to particle growth (Zhang et al., 2011). Amines or ammonium may have also contributed to the observed particle growth, however nitrogen-containing species are difficult to detect by EDX (Laskin et al., 2002). Other studies have also observed similar contributions from organics and sulfate within both individual and bulk nucleated particles during a growth event (Bzdek and Johnston, 2010) and in submicron

particles at the UMBS site (Craig et al., 2015). Therefore, it is likely that the combination of H_2SO_4 and BVOC photooxidation, followed by subsequent gas-particle partitioning, contributed to particle growth and led to the highest average growth rate (8 ± 2 nm h^{-1}; maximum 10.2 nm h^{-1}, Table 4.1) observed in this study.

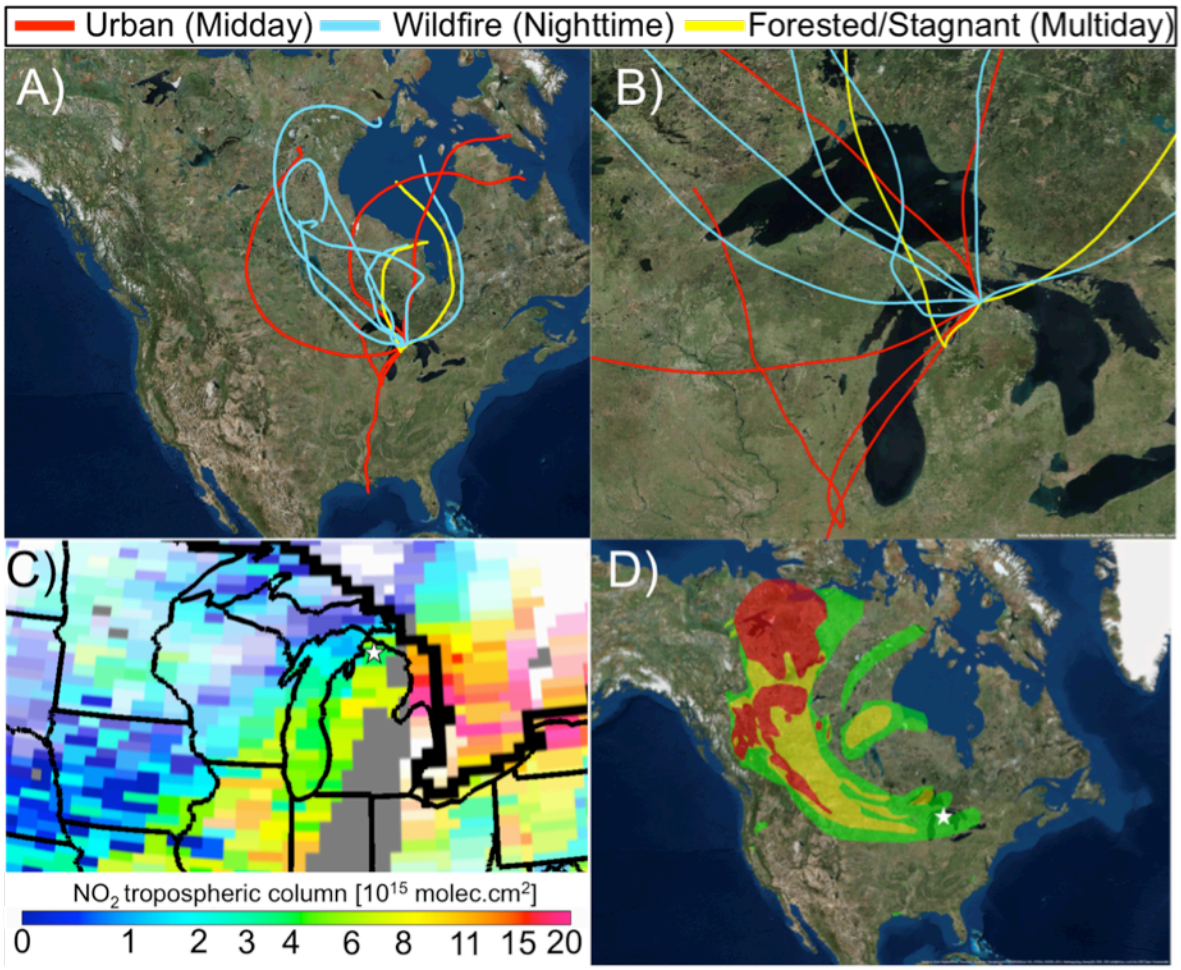

Figure 4.5. (A) and (B) NOAA HYSPLIT backward air mass trajectories (72 h) for the start of each growth event. (C) Tropospheric column NO_2 from TEMIS GOME-2 for July 1, 2014 (Urban – Midday event). (D) NOAA HMS smoke maps for July 13, 2014 (Wildfire - Nighttime event). Smoke coverage is categorized as heavy (red), medium (yellow), and light (green). Field site is indicated by white star, and state/international boundaries are indicated in black lines. Areas outside satellite field of view are depicted in gray. Map imagery for (A), (B) and (D) was provided by ArcGIS 10.3.1 with World Imagery basemap (Sources: Esri, DigitalGlobe, GeoEye, Earthstar Geographics, CNES/Airbus DS, USDA, USGS, AeroGRID, IGN, and the GIS User Community).

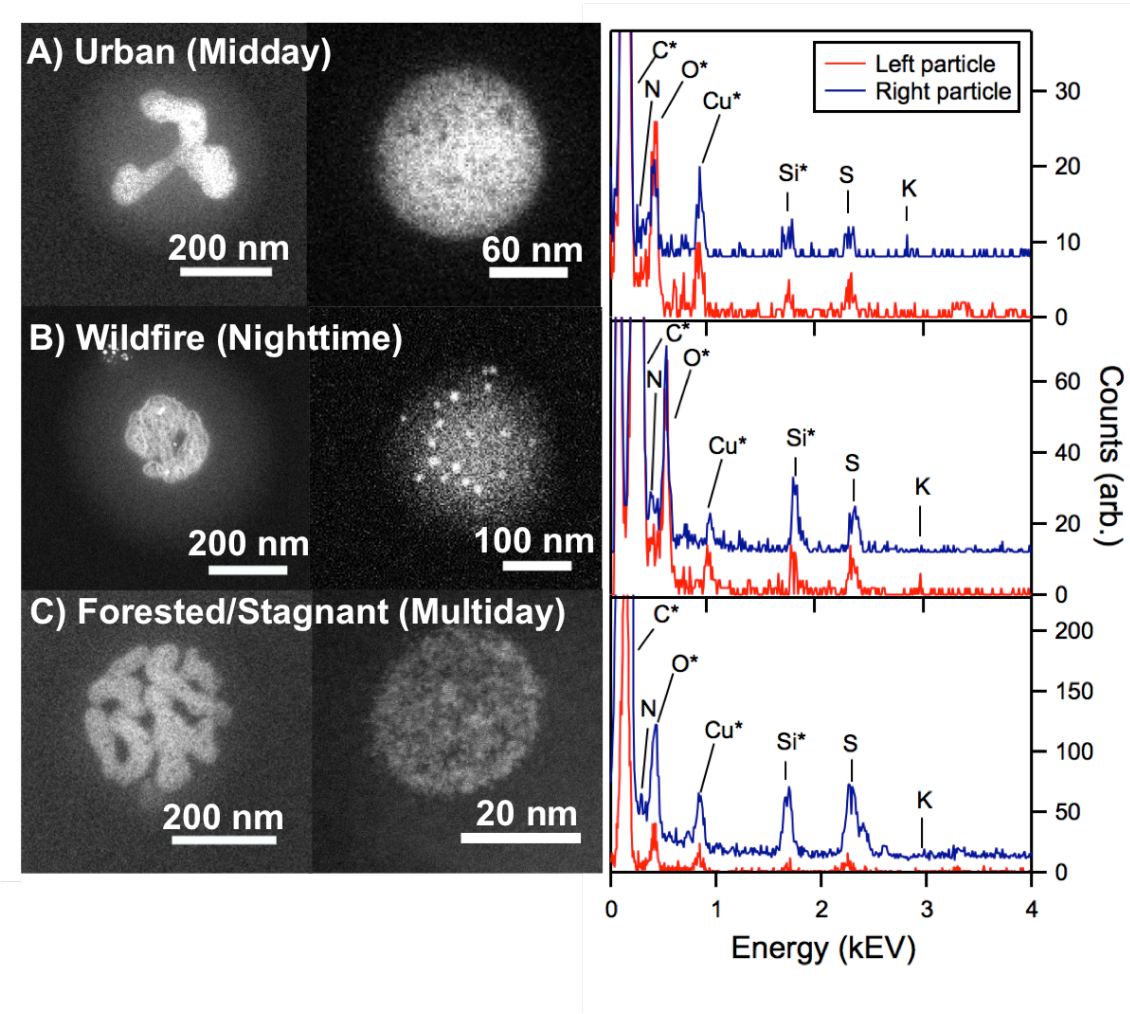

Figure 4.6. Example TEM dark field images (left) and EDX spectra (right) of individual particles collected during: A) urban (midday) growth event (July 12, 2014), B) wildfire (nighttime) growth event (July 25, 2014), and C) forested/stagnant (multiday) growth event (July 24, 2014). Note the carbon peak is off scale, and asterisks indicate interference from the substrate or detector.

4.3.2. Wildfire (Nighttime) Events

Six events began during reduced solar radiation between 16:45 – 22:20 EDT (Table 4.1), with an average growth rate of 3 ± 2 nm h^{-1} (Figure 4.4). While nighttime particle growth has been observed in previous mid-latitude studies (e.g. Lee et al., 2008; Ortega et al., 2012; Russell et al., 2007; Suni et al., 2008), it is less common compared to daytime particle growth (Zhang et al., 2011). Five of the six nighttime events occurred during the influence of northwest Canadian air masses which passed over active wildfires, with smoke observed over UMBS as indicated by

the NOAA Hazard Mapping System (HMS) Smoke and Fire Product (Figures 4.5 and B.7, as well as Gunsch et al., 2017). All five of the wildfire-influenced nighttime events were preceded by cold fronts, which led to decreased particle number concentrations and surface area (average CS of 4 x 10^{-3} s^{-1}). The only nighttime event that did not occur during wildfire influence (Figure B.7, event #2) was likely influenced by similar conditions as the multiday events and is therefore discussed in Section 4.3.3.

NPFG events during wildfire influence have been observed in other locations, including Pittsburgh, PA under summertime Canadian wildfire influence; however, these events occurred during periods of solar radiation maxima and were driven by photochemical reactions (Bein et al., 2008). Wildfire plumes are rich in SO_2 and NO_x (Jaffe and Wigder, 2012; Viswanathan et al., 2006) and Lee et al. (2008) hypothesized that nighttime oxidants such as NO_3 could oxidize SO_2 to H_2SO_4 at night, which would therefore contribute to particle growth. In addition to growth by H_2SO_4, these air mass trajectories came from areas of high monoterpene emissions (Guenther et al., 1995), which upon NO_3 oxidation could contribute to particle growth (Lee et al., 2008). Similar to the urban (midday) events, TEM-EDX confirmed the presence of sulfur, as well as oxygen and carbon, within 100 nm and 200 nm particles collected during nighttime growth at UMBS (Figure 4.5), indicating similar contributions from H_2SO_4 and oxidized BVOCs.

As previously measured nighttime particle growth occurred during nighttime with NO_2 mole ratios as high as 15 ppbv (Rollins et al., 2012), elevated NO_x would likely be needed at UMBS for nighttime particle growth to occur. UMBS is typically a low NO_x environment, with average [NO] of 67 ppt and average [NO_2] of 1.2 ppb (Griffith et al., 2013; Pratt et al., 2012). Previously modeled summer nighttime NO_3 levels at UMBS are <1.5 x 10^7 molecules cm^{-3} (Pratt et al., 2012). Jaffe and Wigder (2012) point out that NO_x in wildfire plumes can impact areas far away from the source by regeneration through the decomposition of peroxyacetyl nitrate (PAN), a NO_x reservoir species, effectively extending the lifetime of NO_x. In fact, a recent study conducted in Maryland measured elevated NO_x in air masses impacted by Canadian wildfires 3,100 km away (Dreessen et al., 2016). Therefore, NO_3 oxidation of monoterpenes and SO_2 appears to be the most likely mechanism driving the observed growth events. However, a more comprehensive study including precursor and oxidant measurements is needed to fully understand the nighttime particle growth mechanism during wildfire influence.

During summer 2009 CABINEX at UMBS, Kanawade et al. (2011) detected a small number of nighttime growth events and suggested influence from transported ultrafine particles (3-10 nm) from urban air to the southwest. However, the short lifetimes of particles in this size range (roughly minutes), due to condensation and coagulation (Hinds, 2012; Seinfeld and Pandis, 2016; Williams et al., 2002), make it unlikely that such small particles would survive the 30-35 h transport from downwind urban environments without undergoing growth. An alternative theory proposed here suggests that the nighttime CABINEX growth events observed by Kanawade et al. (2011) were actually due to Canadian wildfire influence, as shown in Figure B.8, similar to the nighttime events observed in the present study. Kanawade et al. (2011) reported elevated NO_x, SO_2, and H_2SO_4 mole ratios during the growth events, consistent with both urban and wildfire influences. Kanawade et al. (2011) also observed a similar spike in SO_2 and H_2SO_4 during daytime urban influence on July 5, 2009; however, a growth event was not observed, further supporting the role of wildfires and NO_3 chemistry in nighttime events.

4.3.3. Forested/Stagnant (Multiday) Events

Two particle growth events lasted longer than 24 h with starting diameters of 50 nm, larger than the previously discussed growth events (average starting diameter 28 ± 9 nm). These multiday events had the slowest average growth rate (2 ± 1 nm h^{-1}) compared to the other 12 events (4 ± 2 nm h^{-1}). A second mode (classified as event #2) appeared during the evening period of the first multi-day event (#1) and lasted until the morning (Figure B.9). No wildfire or urban influence was observed during these events. Average NO_x (NO = ~70 ppt and NO_2 = ~0.5 ppb for summer 2009) (Griffith et al., 2013) and O_3 levels (~28 ppb for summer 2009) at UMBS are expected to be lower than when the site is under urban (Cooper et al., 2001; Gunsch et al., 2017); or wildfire (Gunsch et al., 2017; Jaffe and Wigder, 2012) influence, suggesting that lower oxidant levels may play a role in reduced growth during stagnant events. As shown in Figure 4.2, these multiday events began at a similarly low CS compared to midday and nighttime events. As the multiday events progressed for 29 and 55 h, respectively, the CS increased to the highest levels detected during the campaign (9.2 x 10^{-3} s^{-1}). Meteorological conditions, including wind direction, wind speed, and temperature, were stable for the duration of each event (Figure B.6), and the events were uninterrupted by external factors, such as precipitation, that could impact the aerosol size distribution. On average, wind speed was slower during multiday (1.9 ± 0.7 m/s)

compared to midday (2.8 ± 0.7 m/s) growth events, leading to more stagnant conditions. The growth rate varied diurnally, with the highest growth rate observed during the daytime (~3 nm h^{-1}) and growth stopping (~0 nm h^{-1}) at night (20:00 – 06:00 EDT), when the lack of solar radiation halts photochemical reactions. Due to the stagnant air, growth restarted the following morning upon sunrise.

As the air was relatively stagnant throughout these events, local BVOCs emitted within the forest, including isoprene, monoterpenes, and sesquiterpenes (Ortega et al., 2007), were the main sources of VOCs present. Therefore, BVOC oxidation products were the likely source of condensable material. EDX spectra of ultrafine (~20 nm) and fine (~200 nm) mode example particles from multi-day growth events indicate large contributions from carbon, oxygen, and sulfur (Figure 4.6). These measurements are consistent with the presence of condensed secondary organic aerosol (SOA) and sulfate observed during previous NPFG events (Bzdek and Johnston, 2010).

Similar multiday growth events were previously observed by Pierce et al. (2012) at Whistler Mountain, also a pristine, forested site. Without influence from anthropogenic sources on this remote environment, SO_2 was below 0.05 ppb (method limit of detection) during the Whistler Mountain study, and therefore, the authors attributed the observed particle growth to BVOC oxidation products. Pierce et al. (2012; 2011) simulated the observed continuous growth by assuming that the SOA was essentially non-volatile with a saturation vapor concentration of 10^{-3} μg m^{-3}.

4.4. Conclusion

In forested northern Michigan during summer 2014, 14 particle growth events were observed during three different air mass conditions: urban influence, wildfire influence, and forested/stagnant conditions over multiple days. Six growth events began midday, with four of the six events under the influence of urban air masses. Increased oxidants within urban air masses, combined with elevated radiation, likely led to BVOC photochemical oxidation and particle growth. Mixing of urban oxidants and BVOCs in forested environments has previously been shown to increase SOA formation and particle growth (Setyan et al., 2014; Shilling et al., 2013). Six growth events occurred during the nighttime, with five of these occurring under the influence of transported Canadian wildfires, suggesting that elevated SO_2 and NO_x levels in the

smoke plumes likely resulted in increased NO_3 levels, for reaction with SO_2 and monoterpenes for the production of condensable species. Similar wildfire influence in summer 2009 at UMBS may have contributed to the growth events described by Kanawade et al. (2011). Given the frequent impact of Canadian wildfires on air quality in the midwest and northeast US and the expected increase in fires due to warming climate (Gillett et al., 2004; Knorr et al., 2016; Liu et al., 2010; Veira et al., 2016), particle growth during these wildfire-influenced nighttime events should be considered in future climate and air quality modeling assessments. Finally, two events occurred over multiple days during stagnant conditions influenced by regional forest BVOC emissions. Example particles measured during all growth event types contained sulfur, carbon, and oxygen, consistent with H_2SO_4 and SOA contribution to particle growth within this forested environment.

4.5. Acknowledgements

Funding for M. Gunsch, N. May, and D. Gardner was provided by the University of Michigan MCubed Program and UMBS graduate fellowships. Funding for S. Schmidt was provided by the National Science Foundation through an REU at UMBS (AGS-1262634). The JEOL 2100 TEM used in this work is maintained by the Michigan Center for Materials Characterization (MC^2) through the support of the University of Michigan College of Engineering and NSF grant (#DMR-0723032). Additionally, the authors acknowledge Dr. Kai Sun for assistance with TEM-EDX. We also acknowledge the UMBS AmeriFlux site for the meteorological data. Funding for AmeriFlux data resources was provided by the U.S. Department of Energy's Office of Science. We acknowledge the free use of tropospheric NO_2 column data from the OMI sensor (www.temis.nl). The authors gratefully acknowledge the NOAA Air Resources Laboratory (ARL) for the provision of the HYSPLIT transport and dispersion model and READY website (http://www.ready.noaa.gov) used in this publication.

4.6. References

Allan, J.D., Williams, P.I., Najera, J., Whitehead, J.D., Flynn, M.J., Taylor, J.W., Liu, D., Darbyshire, E., Carpenter, L.J., Chance, R., Andrews, S.J., Hackenberg, S.C., McFiggans, G., 2015. Iodine observed in new particle formation events in the Arctic atmosphere during ACCACIA. Atmos. Chem. Phys. 15, 5599-5609.

Ault, A.P., Axson, J.L., 2017. Atmospheric Aerosol Chemistry: Spectroscopic and Microscopic Advances. Anal. Chem. 89, 430-452.

Ault, A.P., Moffet, R.C., Baltrusaitis, J., Collins, D.B., Ruppel, M.J., Cuadra-Rodriguez, L.A., Zhao, D., Guasco, T.L., Ebben, C.J., Geiger, F.M., Bertram, T.H., Prather, K.A., Grassian, V.H., 2013. Size-dependent changes in sea spray serosol composition and properties with different seawater conditions. Environ. Sci. Technol. 47, 5603-5612.

Barsanti, K.C., McMurry, P.H., Smith, J.N., 2009. The potential contribution of organic salts to new particle growth. Atmos. Chem. Phys. 9, 2949-2957.

Bein, K.J., Zhao, Y., Johnston, M.V., Wexler, A.S., 2008. Interactions between boreal wildfire and urban emissions. J. Geophys. Res-Atmos. 113, D07304.

Bianchi, F., Trostl, J., Junninen, H., Frege, C., Henne, S., Hoyle, C.R., Molteni, U., Herrmann, E., Adamov, A., Bukowiecki, N., Chen, X., Duplissy, J., Gysel, M., Hutterli, M., Kangasluoma, J., Kontkanen, J., Kuerten, A., Manninen, H.E., Muench, S., Perakyla, O., Petaja, T., Rondo, L., Williamson, C., Weingartner, E., Curtius, J., Worsnop, D.R., Kulmala, M., Dommen, J., Baltensperger, U., 2016. New particle formation in the free troposphere: A question of chemistry and timing. Science 352, 1109-1112.

Boersma, K., Eskes, H., Brinksma, E., 2004. Error analysis for tropospheric NO2 retrieval from space. J. Geophys. Res-Atmos. 109, D04311.

Brown, S., Ryerson, T., Wollny, A., Brock, C., Peltier, R., Sullivan, A., Weber, R., Dube, W., Trainer, M., Meagher, J., 2006. Variability in nocturnal nitrogen oxide processing and its role in regional air quality. Science 311, 67-70.

Bryan, A., Bertman, S., Carroll, M., Dusanter, S., Edwards, G., Forkel, R., Griffith, S., Guenther, A., Hansen, R., Helmig, D., 2012. In-canopy gas-phase chemistry during CABINEX 2009: sensitivity of a 1-D canopy model to vertical mixing and isoprene chemistry. Atmos. Chem. Phys. 12, 8829-8849.

Bzdek, B.R., Johnston, M.V., 2010. New particle formation and growth in the troposphere. ACS Publications.

Carroll, M.A., Bertman, S.B., Shepson, P.B., 2001. Overview of the Program for Research on Oxidants: Photochemistry, Emissions, and Transport (PROPHET) summer 1998 measurements intensive. J. Geophys. Res-Atmos. 106, 24275-24288.

Canadian Interagency Forest Fire Centre, National Wildland Fire Situation Report. Accessed June 2017. http://www.ciffc.ca.

Chandra, I., Kim, S., Seto, T., Otani, Y., Takami, A., Yoshino, A., Irei, S., Park, K., Takamura, T., Kaneyasu, N., 2016. New particle formation under the influence of the long-range transport of air pollutants in East Asia. Atmos. Environ. 141, 30-40.

Cooper, O., Moody, J., Thornberry, T., Town, M., Carroll, M., 2001. PROPHET 1998 meteorological overview and air□mass classification. J. Geophys. Res-Atmos. 106, 24289-24299.

Craig, R.L., Bondy, A.L., Ault, A.P., 2015. Surface Enhanced Raman Spectroscopy Enables Observations of Previously Undetectable Secondary Organic Aerosol Components at the Individual Particle Level. Anal. Chem. 87, 7510-7514.

Craig, R.L., Bondy, A.L., Ault, A.P., 2017. Computer-Controlled Raman Microspectroscopy (CC-Raman): A Method for the Rapid Characterization of Individual Atmospheric Aerosol Particles. Aerosol Sci. Technol., 00-00.

Creamean, J.M., Ault, A.P., Ten Hoeve, J.E., Jacobson, M.Z., Roberts, G.C., Prather, K.A., 2011. Measurements of Aerosol Chemistry during New Particle Formation Events at a Remote Rural Mountain Site. Environ. Sci. Technol. 45, 8208-8216.

Dal Maso, M., Kulmala, M., Lehtinen, K., Mäkelä, J., Aalto, P., O'Dowd, C., 2002. Condensation and coagulation sinks and formation of nucleation mode particles in coastal and boreal forest boundary layers. J. Geophys. Res-Atmos. 107, 8097.

Dal Maso, M., Kulmala, M., Riipinen, I., Wagner, R., Hussein, T., Aalto, P.P., Lehtinen, K.E., 2005. Formation and growth of fresh atmospheric aerosols: eight years of aerosol size distribution data from SMEAR II, Hyytiala, Finland. Boreal. Environ. Res. 10, 323.

Dreessen, J., Sullivan, J., Delgado, R., 2016. Observations and Impacts of Transported Canadian Wildfire Smoke on Ozone and Aerosol Air Quality in the Maryland Region on 9-12 June, 2015. J. Air Waste Manage. Assoc. 66, 842-862.

George, C., Ammann, M., D'Anna, B., Donaldson, D., Nizkorodov, S.A., 2015. Heterogeneous photochemistry in the atmosphere. Chem. Rev. 115, 4218-4258.

Gillett, N., Weaver, A., Zwiers, F., Flannigan, M., 2004. Detecting the effect of climate change on Canadian forest fires. Geophys. Res. Lett. 31, L18211.

Gonser, S., Klein, F., Birmili, W., Größ, J., Kulmala, M., Manninen, H., Wiedensohler, A., Held, A., 2014. Ion–particle interactions during particle formation and growth at a coniferous forest site in central Europe. Atmos. Chem. Phys. 14, 10547-10563.

Gordon, H., Sengupta, K., Rap, A., Duplissy, J., Frege, C., Williamson, C., Heinritzi, M., Simon, M., Yan, C., Almeida, J., Trostl, J., Nieminen, T., Ortega, I.K., Wagner, R., Dunne, E.M., Adamov, A., Amorim, A., Bernhammer, A.K., Bianchi, F., Breitenlechner, M., Brilke, S., Chen, X.M., Craven, J.S., Dias, A., Ehrhart, S., Fischer, L., Flagan, R.C., Franchin, A., Fuchs, C., Guida, R., Hakala, J., Hoyle, C.R., Jokinen, T., Junninen, H., Kangasluoma, J., Kim, J., Kirkby, J., Krapf, M., Kurten, A., Laaksonen, A., Lehtipalo, K., Makhmutov, V., Mathot, S., Molteni, U., Monks, S.A., Onnela, A., Perakyla, O., Piel, F., Petaja, T., Praplanh, A.P., Pringle, K.J., Richards, N.A.D., Rissanen, M.P., Rondo, L., Sarnela, N., Schobesberger, S., Scott, C.E., Seinfeldo, J.H., Sharma, S., Sipila, M., Steiner, G., Stozhkov, Y., Stratmann, F., Tome, A., Virtanen, A., Vogel, A.L., Wagner, A.C., Wagner, P.E., Weingartner, E., Wimmer, D., Winkler, P.M., Ye, P.L., Zhang, X., Hansel, A., Dommen, J., Donahue, N.M., Worsnop, D.R., Baltensperger, U., Kulmala, M., Curtius, J., Carslaw, K.S., 2016. Reduced anthropogenic aerosol radiative forcing caused by biogenic new particle formation. Proc. Natl. Acad. Sci. 113, 12053-12058.

Griffith, S., Hansen, R., Dusanter, S., Stevens, P., Alaghmand, M., Bertman, S., Carroll, M., Erickson, M., Galloway, M., Grossberg, N., 2013. OH and HO 2 radical chemistry during PROPHET 2008 and CABINEX 2009–Part 1: Measurements and model comparison. Atmos. Chem. Phys. 13, 5403-5423.

Guasco, T.L., Cuadra-Rodriguez, L.A., Pedler, B.E., Ault, A.P., Collins, D.B., Zhao, D., Kim, M.J., Ruppel, M.J., Wilson, S.C., Pomeroy, R.S., Grassian, V.H., Azam, F., Bertram, T.H., Prather, K.A., 2013. Transition Metal Associations with Primary Biological Particles in Sea Spray Aerosol Generated in a Wave Channel. Environ. Sci. Technol. 48, 1324-1333.

Guenther, A., Hewitt, C.N., Erickson, D., Fall, R., Geron, C., Graedel, T., Harley, P., Klinger, L., Lerdau, M., McKay, W., 1995. A global model of natural volatile organic compound emissions. J. Geophys. Res-Atmos. 100, 8873-8892.

Gunsch, M.J., May, N.W., Gardner, D., Wen, M., Dean, J., VanReken, T.M., Bertman, S.B., Hopke, P.K., Ault, A.P., Pratt, K.A., 2017. Ubiquitous Influence of Wildfire Emissions on Summertime Atmospheric Aerosol in the Forested Great Lakes Region. In preparation for Atmospheric Environment.

Hinds, W.C., 2012. Aerosol technology: properties, behavior, and measurement of airborne particles. John Wiley & Sons, New York, NY, USA.

Holmes, N.S., 2007. A review of particle formation events and growth in the atmosphere in the various environments and discussion of mechanistic implications. Atmos. Environ. 41, 2183-2201.

Jaffe, D.A., Wigder, N.L., 2012. Ozone production from wildfires: A critical review. Atmos. Environ. 51, 1-10.

Jen, C.N., Bachman, R., Zhao, J., McMurry, P.H., Hanson, D.R., 2016. Diamine-sulfuric acid reactions are a potent source of new particle formation. Geophys. Res. Lett. 43, 867-873.

Jokinen, T., Berndt, T., Makkonen, R., Kerminen, V.-M., Junninen, H., Paasonen, P., Stratmann, F., Herrmann, H., Guenther, A.B., Worsnop, D.R., 2015a. Production of extremely low volatile organic compounds from biogenic emissions: Measured yields and atmospheric implications. Proc. Natl. Acad. Sci. 112, 7123-7128.

Jokinen, T., Berndt, T., Makkonen, R., Kerminen, V.M., Junninen, H., Paasonen, P., Stratmann, F., Herrmann, H., Guenther, A.B., Worsnop, D.R., Kulmala, M., Ehn, M., Sipila, M., 2015b. Production of extremely low volatile organic compounds from biogenic emissions: Measured yields and atmospheric implications. Proc. Natl. Acad. Sci. 112, 7123-7128.

Jung, J., Miyazaki, Y., Kawamura, K., 2013. Different characteristics of new particle formation between urban and deciduous forest sites in Northern Japan during the summers of 2010–2011. Atmos. Chem. Phys. 13, 51-68.

Kanawade, V., Jobson, B.T., Guenther, A., Erupe, M., Pressley, S., Tripathi, S., Lee, S.-H., 2011. Isoprene suppression of new particle formation in a mixed deciduous forest. Atmos. Chem. Phys. 11, 6013-6027.

Kiendler-Scharr, A., Wildt, J., Dal Maso, M., Hohaus, T., Kleist, E., Mentel, T.F., Tillmann, R., Uerlings, R., Schurr, U., Wahner, A., 2009. New particle formation in forests inhibited by isoprene emissions. Nature 461, 381-384.

Kirkby, J., Duplissy, J., Sengupta, K., Frege, C., Gordon, H., Williamson, C., Heinritzi, M., Simon, M., Yan, C., Almeida, J., Troestl, J., Nieminen, T., Ortega, I.K., Wagner, R., Adamov, A., Amorim, A., Bernhammer, A.-K., Bianchi, F., Breitenlechner, M., Brilke, S., Chen, X., Craven, J., Dias, A., Ehrhart, S., Flagan, R.C., Franchin, A., Fuchs, C., Guida, R., Hakala, J., Hoyle, C.R., Jokinen, T., Junninen, H., Kangasluoma, J., Kim, J., Krapf, M., Kuerten, A., Laaksonen, A., Lehtipalo, K., Makhmutov, V., Mathot, S., Molteni, U., Onnela, A., Peraekylae, O., Piel, F., Petaejae, T., Praplan, A.P., Pringle, K., Rap, A., Richards, N.A.D., Riipinen, I., Rissanen, M.P., Rondo, L., Sarnela, N., Schobesberger, S., Scott, C.E., Seinfeld, J.H., Sipilae, M., Steiner, G., Stozhkov, Y., Stratmann, F., Tome, A., Virtanen, A., Vogel, A.L., Wagner, A.C., Wagner, P.E., Weingartner, E., Wimmer, D., Winkler, P.M., Ye, P., Zhang, X., Hansel, A., Dommen, J., Donahue, N.M., Worsnop, D.R., Baltensperger, U., Kulmala, M., Carslaw, K.S., Curtius, J., 2016. Ion-induced nucleation of pure biogenic particles. Nature 533, 521-526.

Knorr, W., Jiang, L., Arneth, A., 2016. Climate, CO2 and human population impacts on global wildfire emissions. Biogeosciences 13, 267-282.

Kourtchev, I., Ruuskanen, T., Maenhaut, W., Kulmala, M., Claeys, M., 2005. Observation of 2-methyltetrols and related photo-oxidation products of isoprene in boreal forest aerosols from Hyytiälä, Finland. Atmos. Chem. Phys. 5, 2761-2770.

Kulmala, M., Laaksonen, A., 1990. Binary nucleation of water–sulfuric acid system: Comparison of classical theories with different H2SO4 saturation vapor pressures. J. Chem. Phys. 93, 696-701.

Kulmala, M., Petaja, T., Ehn, M., Thornton, J., Sipila, M., Worsnop, D.R., Kerminen, V.M., 2014. Chemistry of Atmospheric Nucleation: On the Recent Advances on Precursor Characterization and Atmospheric Cluster Composition in Connection with Atmospheric New Particle Formation. Annu. Rev. Phys. Chem. 65, 21-37.

Kulmala, M., Petaja, T., Nieminen, T., Sipila, M., Manninen, H.E., Lehtipalo, K., Dal Maso, M., Aalto, P.P., Junninen, H., Paasonen, P., Riipinen, I., Lehtinen, K.E.J., Laaksonen, A., Kerminen, V.-M., 2012. Measurement of the nucleation of atmospheric aerosol particles. Nat. Protoc. 7, 1651-1667.

Kulmala, M., Pirjola, U., Makela, J.M., 2000. Stable sulphate clusters as a source of new atmospheric particles. Nature 404, 66-69.

Kulmala, M., Vehkamäki, H., Petäjä, T., Dal Maso, M., Lauri, A., Kerminen, V.-M., Birmili, W., McMurry, P.H., 2004. Formation and growth rates of ultrafine atmospheric particles: a review of observations. J. Aerosol. Sci. 35, 143-176.

Laakso, L., Laakso, H., Aalto, P., Keronen, P., Petaja, T., Nieminen, T., Pohja, T., Siivola, E., Kulmala, M., Kgabi, N., 2008. Basic characteristics of atmospheric particles, trace gases and meteorology in a relatively clean Southern African Savannah environment. Atmos. Chem. Phys. Discuss. 8, 6313-6353.

Laaksonen, A., Hamed, A., Joutsensaari, J., Hiltunen, L., Cavalli, F., Junkermann, W., Asmi, A., Fuzzi, S., Facchini, M.C., 2005. Cloud condensation nucleus production from nucleation events at a highly polluted region. Geophys. Res. Lett. 32, L06812.

Laaksonen, A., Kulmala, M., O'Dowd, C., Joutsensaari, J., Vaattovaara, P., Mikkonen, S., Lehtinen, K., Sogacheva, L., Maso, M.D., Aalto, P., 2008. The role of VOC oxidation products in continental new particle formation. Atmos. Chem. Phys. 8, 2657-2665.

Laskin, A., Iedema, M.J., Cowin, J.P., 2002. Quantitative time-resolved monitoring of nitrate formation in sea salt particles using a CCSEM/EDX single particle analysis. Environ. Sci. Technol. 36, 4948-4955.

Lee, S.H., Young, L.H., Benson, D.R., Suni, T., Kulmala, M., Junninen, H., Campos, T.L., Rogers, D.C., Jensen, J., 2008. Observations of nighttime new particle formation in the troposphere. J. Geophys. Res-Atmos. 113, D10210.

Limbeck, A., Kulmala, M., Puxbaum, H., 2003. Secondary organic aerosol formation in the atmosphere via heterogeneous reaction of gaseous isoprene on acidic particles. Geophys. Res. Lett. 30, 1996.

Liu, Y., Stanturf, J., Goodrick, S., 2010. Trends in global wildfire potential in a changing climate. Forest. Ecol. Manag. 259, 685-697.

Mäkelä, J., Aalto, P., Jokinen, V., Pohja, T., Nissinen, A., Palmroth, S., Markkanen, T., Seitsonen, K., Lihavainen, H., Kulmala, M., 1997. Observations of ultrafine aerosol particle formation and growth in boreal forest. Geophys. Res. Lett. 24, 1219-1222.

Manninen, H., Nieminen, T., Asmi, E., Gagné, S., Häkkinen, S., Lehtipalo, K., Aalto, P., Vana, M., Mirme, A., Mirme, S., 2010. EUCAARI ion spectrometer measurements at 12 European sites–analysis of new particle formation events. Atmos. Chem. Phys. 10, 7907-7927.

Merikanto, J., Spracklen, D., Mann, G., Pickering, S., Carslaw, K., 2009. Impact of nucleation on global CCN. Atmos. Chem. Phys. 9, 8601-8616.

Nilsson, E., Paatero, J., Boy, M., 2001. Effects of air masses and synoptic weather on aerosol formation in the continental boundary layer. Tellus B 53, 462-478.

Ortega, I., Suni, T., Boy, M., Grönholm, T., Manninen, H., Nieminen, T., Ehn, M., Junninen, H., Hakola, H., Hellén, H., 2012. New insights into nocturnal nucleation. Atmos. Chem. Phys. 12, 4297-4312.

Ortega, J., Helmig, D., Guenther, A., Harley, P., Pressley, S., Vogel, C., 2007. Flux estimates and OH reaction potential of reactive biogenic volatile organic compounds (BVOCs) from a mixed northern hardwood forest. Atmos. Environ. 41, 5479-5495.

Pierce, J., Adams, P., 2009a. Uncertainty in global CCN concentrations from uncertain aerosol nucleation and primary emission rates. Atmos. Chem. Phys. 9, 1339-1356.

Pierce, J., Leaitch, W., Liggio, J., Westervelt, D., Wainwright, C., Abbatt, J., Ahlm, L., Al-Basheer, W., Cziczo, D., Hayden, K., 2012. Nucleation and condensational growth to CCN sizes during a sustained pristine biogenic SOA event in a forested mountain valley. Atmos. Chem. Phys. 12, 3147-3163.

Pierce, J., Riipinen, I., Kulmala, M., Ehn, M., Petäjä, T., Junninen, H., Worsnop, D., Donahue, N., 2011. Quantification of the volatility of secondary organic compounds in ultrafine particles during nucleation events. Atmos. Chem. Phys. 11, 9019-9036.

Pierce, J., Westervelt, D., Atwood, S., Barnes, E., Leaitch, W., 2014. New-particle formation, growth and climate-relevant particle production in Egbert, Canada: analysis from 1 year of size-distribution observations. Atmos. Chem. Phys. 14, 8647-8663.

Pierce, J.R., Adams, P.J., 2007. Efficiency of cloud condensation nuclei formation from ultrafine particles. Atmos. Chem. Phys. 7, 1367-1379.

Pierce, J.R., Adams, P.J., 2009b. Uncertainty in global CCN concentrations from uncertain aerosol nucleation and primary emission rates. Atmos. Chem. Phys. 9, 1339-1356.

Pratt, K., Mielke, L., Shepson, P., Bryan, A., Steiner, A., Ortega, J., Daly, R., Helmig, D., Vogel, C., Griffith, S., 2012. Contributions of individual reactive biogenic volatile organic compounds to organic nitrates above a mixed forest. Atmos. Chem. Phys 12, 10125-10142.

Pryor, S., Barthelmie, R., Sørensen, L.L., McGrath, J., Hopke, P., Petäjä, T., 2011. Spatial and vertical extent of nucleation events in the Midwestern USA: insights from the Nucleation In ForesTs (NIFTy) experiment. Atmos. Chem. Phys. 11, 1641-1657.

Riipinen, I., Sihto, S.-L., Kulmala, M., Arnold, F., Maso, M.D., Birmili, W., Saarnio, K., Teinilä, K., Kerminen, V.-M., Laaksonen, A., 2007. Connections between atmospheric sulphuric acid and new particle formation during QUEST III–IV campaigns in Heidelberg and Hyytiälä. Atmos. Chem. Phys. 7, 1899-1914.

Rollins, A., Browne, E., Min, K., Pusede, S., Wooldridge, P., Gentner, D., Goldstein, A., Liu, S., Day, D., Russell, L., 2012. Evidence for NOx control over nighttime SOA formation. Science 337, 1210-1212.

Rolph, G.D., Draxler, R.R., Stein, A.F., Taylor, A., Ruminski, M.G., Kondragunta, S., Zeng, J., Huang, H.-C., Manikin, G., McQueen, J.T., 2009. Description and verification of the NOAA smoke forecasting system: the 2007 fire season. Weather Forecast. 24, 361-378.

Rose, C., Sellegri, K., Velarde, F., Moreno, I., Ramonet, M., Weinhold, K., Krejci, R., Ginot, P., Andrade, M., Wiedensohler, A., 2015. Frequent nucleation events at the high altitude station of Chacaltaya (5240 m asl), Bolivia. Atmos. Environ. 102, 18-29.

Ruehl, C.R., Davies, J.F., Wilson, K.R., 2016. An interfacial mechanism for cloud droplet formation on organic aerosols. Science 351, 1447-1450.

Russell, L., Mensah, A., Fischer, E., Sive, B., Varner, R., Keene, W., Stutz, J., Pszenny, A., 2007. Nanoparticle growth following photochemical α□and β□pinene oxidation at Appledore Island during International Consortium for Research on Transport and Transformation/Chemistry of Halogens at the Isles of Shoals 2004. J. Geophys. Res-Atmos. 112, D10S21.

Salimi, F., Rahman, M.M., Clifford, S., Ristovski, Z., Morawska, L., 2017. Nocturnal new particle formation events in urban environment. Atmos. Chem. Phys. 17, 521-530.

Salma, I., Németh, Z., Kerminen, V.-M., Aalto, P., Nieminen, T., Weidinger, T., Molnár, Á., Imre, K., Kulmala, M., 2016. Regional effect on urban atmospheric nucleation. Atmos. Chem. Phys. 16, 8715-8728.

Seinfeld, J.H., Pandis, S.N., 2016. Atmospheric chemistry and physics: from air pollution to climate change. John Wiley & Sons, Hoboken, New Jersey.

Sellegri, K., Hanke, M., Umann, B., Arnold, F., Kulmala, M., 2005. Measurements of organic gases during aerosol formation events in the boreal forest atmosphere during QUEST. Atmos. Chem. Phys. 5, 373-384.

Setyan, A., Song, C., Merkel, M., Knighton, W., Onasch, T.B., Canagaratna, M., Worsnop, D.R., Wiedensohler, A., Shilling, J.E., Zhang, Q., 2014. Chemistry of new particle growth in mixed urban and biogenic emissions–insights from CARES. Atmos. Chem. Phys. 14, 6477-6494.

Shen, H., Peters, T.M., Casuccio, G.S., Lersch, T.L., West, R.R., Kumar, A., Kumar, N., Ault, A.P., 2016. Elevated concentrations of lead in particulate matter on the neighborhood-scale in Delhi, India as determined by single particle analysis. Environ. Sci. Technol. 50, 4961-4970.

Shilling, J.E., Zaveri, R.A., Fast, J.D., Kleinman, L., Alexander, M., Canagaratna, M.R., Fortner, E., Hubbe, J.M., Jayne, J.T., Sedlacek, A., 2013. Enhanced SOA formation from mixed anthropogenic and biogenic emissions during the CARES campaign. Atmos. Chem. Phys. 13, 2091-2113.

Sipila, M., Berndt, T., Petaja, T., Brus, D., Vanhanen, J., Stratmann, F., Patokoski, J., Mauldin, R.L., Hyvarinen, A.P., Lihavainen, H., Kulmala, M., 2010. The role of sulfuric acid in atmospheric nucleation. Science 327, 1243-1246.

Sipila, M., Sarnela, N., Jokinen, T., Henschel, H., Junninen, H., Kontkanen, J., Richters, S., Kangasluoma, J., Franchin, A., Perakyla, O., Rissanen, M.P., Ehn, M., Vehkamaki, H., Kurten, T., Berndt, T., Petaja, T., Worsnop, D., Ceburnis, D., Kerminen, V.M., Kulmala, M., O'Dowd, C., 2016. Molecular-scale evidence of aerosol particle formation via sequential addition of HIO3. Nature 537, 532-534.

Smith, J.N., Barsanti, K.C., Friedli, H.R., Ehn, M., Kulmala, M., Collins, D.R., Scheckman, J.H., Williams, B.J., McMurry, P.H., 2010. Observations of aminium salts in atmospheric nanoparticles and possible climatic implications. Proc. Natl. Acad. Sci. U. S. A. 107, 6634-6639.

Sotiropoulou, R., Tagaris, E., Pilinis, C., Anttila, T., Kulmala, M., 2006. Modeling new particle formation during air pollution episodes: Impacts on aerosol and cloud condensation nuclei. Aerosol. Sci. Technol. 40, 557-572.

Stein, A., Draxler, R.R., Rolph, G.D., Stunder, B.J., Cohen, M., Ngan, F., 2015. NOAA's HYSPLIT atmospheric transport and dispersion modeling system. B. Am. Meteorol. Soc. 96, 2059-2077.

Steiner, A., Pressley, S., Botros, A., Jones, E., Chung, S., Edburg, S., 2011. Analysis of coherent structures and atmosphere-canopy coupling strength during the CABINEX field campaign. Atmos. Chem. Phys. 11, 11921-11936.

Suni, T., Kulmala, M., Hirsikko, A., Bergman, T., Laakso, L., Aalto, P., Leuning, R., Cleugh, H., Zegelin, S., Hughes, D., 2008. Formation and characteristics of ions and charged aerosol particles in a native Australian Eucalypt forest. Atmos. Chem. Phys. 8, 129-139.

Thornberry, T., Carroll, M.A., Keeler, G.J., Sillman, S., Bertman, S.B., Pippin, M.R., Ostling, K., Grossenbacher, J.W., Shepson, P.B., Cooper, O.R., 2001. Observations of reactive oxidized nitrogen and speciation of NO y during the PROPHET summer 1998 intensive. J. Geophys. Res-Atmos. 106, 24359-24386.

Troestl, J., Chuang, W.K., Gordon, H., Heinritzi, M., Yan, C., Molteni, U., Ahlm, L., Frege, C., Bianchi, F., Wagner, R., Simon, M., Lehtipalo, K., Williamson, C., Craven, J.S., Duplissy, J., Adamov, A., Almeida, J., Bernhammer, A.-K., Breitenlechner, M., Brilke, S., Dias, A., Ehrhart, S., Flagan, R.C., Franchin, A., Fuchs, C., Guida, R., Gysel, M., Hansel, A., Hoyle, C.R., Jokinen, T., Junninen, H., Kangasluoma, J., Keskinen, H., Kim, J., Krapf, M., Kuerten, A., Laaksonen, A., Lawler, M., Leiminger, M., Mathot, S., Moehler, O., Nieminen, T., Onnela, A., Petaejae, T., Piel, F.M., Miettinen, P., Rissanen, M.P., Rondo, L., Sarnela, N., Schobesberger, S., Sengupta, K., Sipilae, M., Smith, J.N., Steiner, G., Tome, A., Virtanen, A., Wagner, A.C., Weingartner, E., Wimmer, D., Winkler, P.M., Ye, P., Carslaw, K.S., Curtius, J., Dommen, J., Kirkby, J., Kulmala, M., Riipinen, I., Worsnop, D.R., Donahue, N.M., Baltensperger, U., 2016. The role of low-volatility organic compounds in initial particle growth in the atmosphere. Nature 533, 527-531.

Twohy, C.H., Clement, C.F., Gandrud, B.W., Weinheimer, A.J., Campos, T.L., Baumgardner, D., Brune, W.H., Faloona, I., Sachse, G.W., Vay, S.A., 2002. Deep convection as a source of new particles in the midlatitude upper troposphere. J. Geophys. Res-Atmos. 107.

Vakkari, V., Laakso, H., Kulmala, M., Laaksonen, A., Mabaso, D., Molefe, M., Kgabi, N., Laakso, L., 2011. New particle formation events in semi-clean South African savannah. Atmos. Chem. Phys. 11, 3333-3346.

VanReken, T., Mwaniki, G., Wallace, H., Pressley, S., Erickson, M., Jobson, B., Lamb, B., 2015. Influence of air mass origin on aerosol properties at a remote Michigan forest site. Atmos. Environ. 107, 35-43.

Veira, A., Lasslop, G., Kloster, S., 2016. Wildfires in a warmer climate: Emission fluxes, emission heights, and black carbon concentrations in 2090–2099. J. Geophys. Res-Atmos. 121, 3195-3223.

Venzac, H., Sellegri, K., Laj, P., Villani, P., Bonasoni, P., Marinoni, A., Cristofanelli, P., Calzolari, F., Fuzzi, S., Decesari, S., 2008. High frequency new particle formation in the Himalayas. Proc. Natl. Acad. Sci. 105, 15666-15671.

Viswanathan, S., Eria, L., Diunugala, N., Johnson, J., McClean, C., 2006. An analysis of effects of San Diego wildfire on ambient air quality. J. Air Waste Manage. Assoc. 56, 56-67.

Wang, Z., Hu, M., Sun, J., Wu, Z., Yue, D., Shen, X., Zhang, Y., Pei, X., Cheng, Y., Wiedensohler, A., 2013. Characteristics of regional new particle formation in urban and regional background environments in the North China Plain. Atmos. Chem. Phys. 13, 12495-12506.

Weller, R., Schmidt, K., Teinilä, K., Hillamo, R., 2015. Natural new particle formation at the coastal Antarctic site Neumayer. Atmos. Chem. Phys. 15, 11399-11410.

Williams, J., Reus, M.d., Krejci, R., Fischer, H., Ström, J., 2002. Application of the variability-size relationship to atmospheric aerosol studies: estimating aerosol lifetimes and ages. Atmos. Chem. Phys. 2, 133-145.

Willis, M.D., Burkart, J., Thomas, J.L., Köllner, F., Schneider, J., Bozem, H., Hoor, P.M., Aliabadi, A.A., Schulz, H., Herber, A.B., 2016. Growth of nucleation mode particles in the summertime Arctic: a case study. Atmos. Chem. Phys. 15, 7663-7679.

Yu, F., Luo, G., Pryor, S., Pillai, P., Lee, S., Ortega, J., Schwab, J., Hallar, A., Leaitch, W., Aneja, V., 2015. Spring and summer contrast in new particle formation over nine forest areas in North America. Atmos. Chem. Phys. 15, 13993-14003.

Yue, D., Hu, M., Wang, Z., Wen, M., Guo, S., Zhong, L., Wiedensohler, A., Zhang, Y., 2013. Comparison of particle number size distributions and new particle formation between the urban and rural sites in the PRD region, China. Atmos. Environ. 76, 181-188.

Zhang, R., Khalizov, A., Wang, L., Hu, M., Xu, W., 2011. Nucleation and growth of nanoparticles in the atmosphere. Chem. Rev. 112, 1957-2011.

Zhang, R.Y., 2010. Getting to the Critical Nucleus of Aerosol Formation. Science 328, 1366-1367.

Zhang, R.Y., Suh, I., Zhao, J., Zhang, D., Fortner, E.C., Tie, X.X., Molina, L.T., Molina, M.J., 2004. Atmospheric new particle formation enhanced by organic acids. Science 304, 1487-1490.

Ziemann, P.J., Atkinson, R., 2012. Kinetics, products, and mechanisms of secondary organic aerosol formation. Chem. Soc. Rev. 41, 6582-6605.

Chapter 5.
Contributions of Transported Prudhoe Bay Oil Field Emissions to the Aerosol Population in Utqiaġvik, Alaska

Atmos. Chem. Phys., 17, 10879-10892, 2017. https://doi.org/10.5194/acp-17-10879-2017

5.1. Introduction

The Arctic is experiencing dramatic climate change with sea ice extent declining rapidly and complete summertime sea ice loss expected by 2050 (Wang and Overland, 2015; Overland and Wang, 2013). With 30% of the world's undiscovered natural gas and 13% of undiscovered oil thought to be located in the Arctic (Gautier et al., 2009), increasing open water makes previously inaccessible areas of the Arctic available for oil and gas development and shipping (Harsem et al., 2015; Allison and Bassett, 2015). These oil and gas extraction activities add pollutants, including particulate matter (PM), volatile organic compounds (VOCs), SO_2, and NO_x, to the Arctic atmosphere (Peters et al., 2011), thereby influencing climate. The Arctic aerosol population is characterized by a maximum mass loading in the winter, due to transported pollutants from the mid-latitudes, and a minimum in the summer, when local sources, including sea spray aerosol, dominate (Quinn et al., 2002; Quinn et al., 2007). However, there is limited knowledge of aerosols produced within the Arctic, particularly in the context of changing emissions from both natural and anthropogenic sources (Arnold et al., 2016).

Modeling by Peters et al. (2011) estimates that Arctic oil and gas extraction during 2004 contributed 47 kilotons (kt) of PM emissions, with 15 kt corresponding to black carbon (BC) and 16 kt attributed to organic carbon (OC). The majority of emissions originated in western Russia (~41 kt in 2004); activities within the Alaskan Arctic, primarily the Prudhoe Bay oil fields,

contributed 6 kt during 2004 (Peters et al., 2011). Prudhoe Bay is the third largest oil field and tenth largest gas field in the US by estimated production as of 2013 (EIA, 2015). The majority of PM emitted by US Arctic oil and gas extraction sources (turbine gas combustion, diesel emissions from generators and vehicles, and flaring (Stohl et al., 2013)) in 2004 corresponded to BC (1.9 kt) and OC (2.0 kt) (Peters et al., 2011). With new drilling operations opening due to reduced sea ice coverage, Peters et al. (2011) estimate US contributions increasing up to 10 kt of primary PM (including 3.3 kt BC and 3.5 kt OC) by 2030 and 17 kt of PM (including 5.3 kt BC and 5.7 kt OC) by 2050. In addition to directly emitted PM, drilling operations can emit aerosol precursors (NO_x, SO_2, and VOCs), and alter oxidant levels, which can lead to the formation of secondary aerosol, as well as contribute to new particle formation (Peters et al., 2011; Volkamer et al., 2006; Roiger et al., 2015; Kolesar et al., 2017; Jaffe et al., 1995).

BC is estimated to have a warming effect on the Arctic atmosphere (e.g. Flanner, 2013; Sand et al., 2013a; Sharma et al., 2013; Bond et al., 2013; Flanner et al., 2007). Modeling predicts local Arctic BC emissions to cause as much as a factor of five greater increase in Arctic warming compared to BC transported from the lower latitudes (Sand et al., 2013b). Koch et al. (2009) suggested that Arctic BC concentrations are under-predicted by a variety of models by an average factor of 2.5, which may be improved by more accurately incorporating local BC sources (Flanner, 2013). However, few studies have measured PM emitted from oil and gas extraction in the Arctic. Measurements of BC from 1977 – 1997 in Utqiaġvik showed contributions from Russian oil fields year round (Polissar et al., 1999; Polissar et al., 2001), similar to the recent results of Barrett et al. (2015) at Utqiaġvik during December 2012 – March 2013 when transported particles from Russian oil fields were observed. Barrett et al. (2015) also measured regional Arctic BC from both fossil fuel combustion and biomass burning. The Arctic Climate Change, Economy, and Society (ACCESS) aircraft field campaign recently investigated emissions from oil and gas extraction in the Norwegian Arctic and measured increased BC, among other pollutants, compared to the Arctic background while sampling within plumes from oil and gas extraction facilities (Roiger et al., 2015). Also, Brock et al. (2011) conducted aircraft measurements of Prudhoe Bay emissions and detected increased PM, including OC and BC. Stohl et al. (2013) modeled BC contributions from flaring due to Arctic oil and gas extraction and determined that it contributed 42% of the annual surface soot concentrations in the Arctic.

With only these limited measurements available, further characterization of combustion emissions from oil and gas extraction activities are needed to further improve simulations.

During transport, primary aerosol can undergo chemical aging and accumulate secondary species, such as sulfate, nitrate, ammonium, oxidized organic carbon, and water, impacting both chemical composition and particle properties, such as light absorption and scattering, hygroscopicity, toxicity, and chemical reactivity (Moffet and Prather, 2009; Pöschl, 2005). Combustion particles in particular are co-emitted with VOCs and can rapidly undergo aging and accumulate these secondary organic species (Petzold et al., 2005). The distribution of these secondary species across the aerosol population determines aerosol climate impacts (Prather et al., 2008). It is currently not clear whether light absorption by a BC particle is enhanced by sulfate or organic coatings (e.g., Chung and Seinfeld, 2005; Jacobson, 2001; Moffet and Prather, 2009; Knox et al., 2009; Liu et al., 2015; Cappa et al., 2012; Healy et al., 2015). In contrast, pure sulfate particles (i.e., without BC (soot) inclusions) primarily scatter light (Haywood and Boucher, 2000). In addition, soot particles internally mixed with nitrate and sulfate have been shown to have increased CCN-activity (Bond et al., 2013). Ambient aerosol populations typically vary between internal mixtures, with multiple chemical species contained within a single particle, and external mixtures, with multiple chemical species present as separate particles (Prather et al., 2008). Therefore, it is important to determine the influence of Prudhoe Bay emissions on downwind aerosol chemical composition and mixing state of the individual particles in order to better understand and predict the effects of oil and gas extraction activities on the Arctic aerosol population and climate.

To investigate particle chemical composition and sources in the coastal Alaskan Arctic, sampling was conducted at Utqiaġvik, Alaska, a location influenced by Prudhoe Bay (Jaffe et al., 1995) and the Arctic Ocean (Quinn et al., 2002) in August – September 2015. On-line aerosol time-of-flight mass spectrometry (ATOFMS) and off-line computer controlled scanning electron microscopy with energy dispersive X-ray spectroscopy (CCSEM-EDX) analyses provided size-resolved individual particle chemical composition. The impacts of transported Prudhoe Bay oil field emissions on aerosol size distributions, primary combustion particle contributions, and secondary aerosol formation are compared to the background Arctic aerosol composition.

5.2. Methods

Atmospheric aerosol sampling was conducted over a period of August 21 – September 30, 2015 at a field site (71°16’30"N, 156°38'26"W), on the Barrow Environmental Observatory, located 4 km southeast of the town of Utqiaġvik, AK. Aerosol sampling occurred 4.5 m above ground level through 1.4 cm ID copper tubing at a flow rate of 17 Lpm through a PM_{10} (PM less than 10 μm) teflon-coated aluminum cyclone (URG-2000-30ENB, URG Corp., Chapel Hill, NC). A stainless steel cylindrical manifold (ID 8.9 cm) split the flow to dedicated insulated sampling lines for each instrument. Meteorological data, including wind speed, wind direction, relative humidity, and temperature, were obtained from the National Oceanic and Atmospheric Administration (NOAA) Earth System Research Laboratory (ESRL) Global Monitoring Division (GMD) long-term monitoring station (NOAA Barrow Observatory, 71°19’40”N, 156°38’20”W), located 5.5 km across flat tundra to the northeast of the aerosol sampling site. On-line measurements of aerosol absorption at seven wavelengths, including 880 nm, were completed using an aethalometer to obtain BC mass concentrations. BC concentrations were calculated, at 5 – 10 minute time resolution, using a portable aethalometer (Model AE42, Magee Scientific, Berkeley, CA). The aethalometer was outfitted with a seven wavelength source and $PM_{2.5}$ inlet. The sample is collected on a quartz fiber filter tape and the optical analysis (wavelengths ranging from 370 to 950 nm) is performed continuously.

5.2.1. Air Mass Classification

Backward air mass trajectories were calculated using the NOAA Hybrid Single Particle Lagrangian Integrated Trajectory (HYSPLIT) Model (Stein et al., 2015). A final height of 50 m AGL was used for arrival at the field site, and a new trajectory was calculated every 8 h and modeled the preceding 48 h. Trajectories originated from three major directions: north/northeast, southeast, and to the west (Figure 5.1). Based on these trajectories, air masses were classified into three areas of influence. Air masses that originated in the Beaufort Sea to the north/northeast of the site were classified as Arctic Ocean influenced periods. Air masses from the southeast that crossed over the Prudhoe Bay oil fields were classified as Prudhoe Bay influenced air masses, based on a previous study of air mass transport from Prudhoe Bay to Utqiaġvik (Kolesar et al., 2017). Air masses that originated from the west were primarily influenced by the town of Utqiaġvik and classified as local influence.

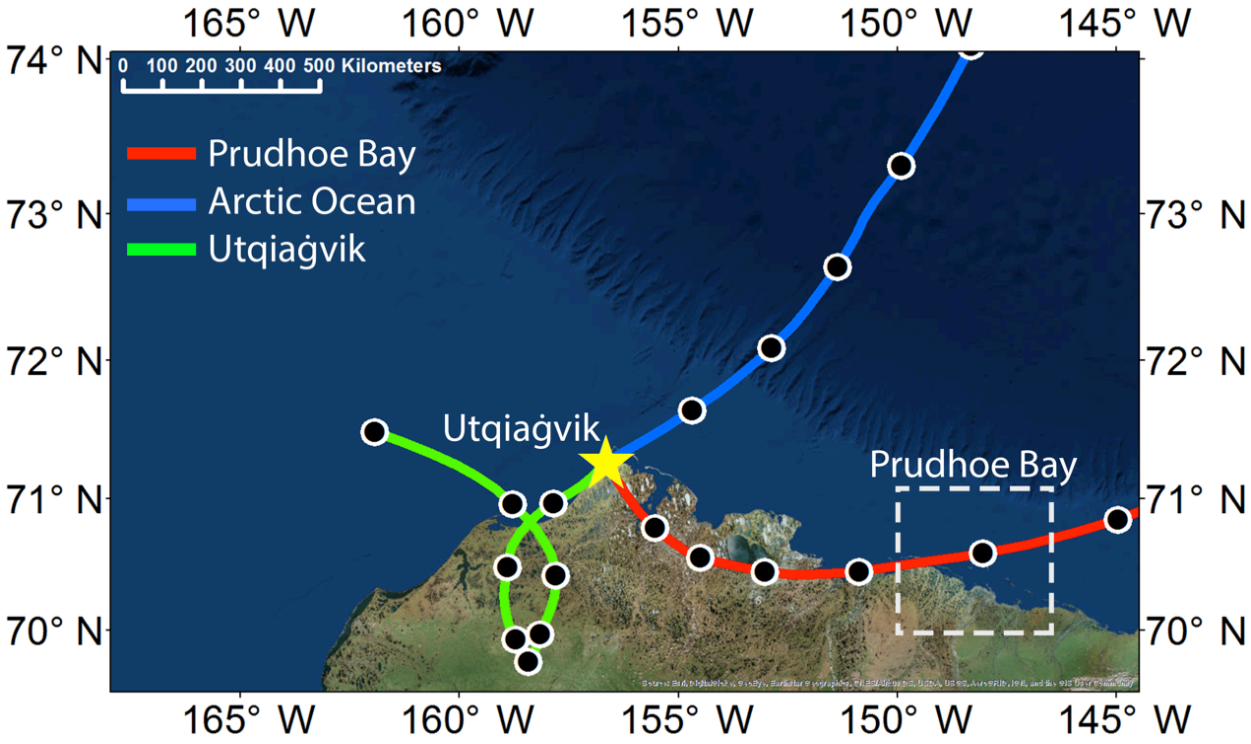

Figure 5.1. Average 48 h HYSPLIT backward air mass trajectories for three major areas of influence: Prudhoe Bay, the ice-free Arctic Ocean, and the town of Utqiaġvik. 6 h time intervals are indicated by black circles. The Utqiaġvik, AK sampling site is indicated by the yellow star, and the area of the greatest Prudhoe Bay emissions influence is indicated by the white dashed square as defined by Kolesar et al. (2017). The map background was provided by ArcGIS 10.3.1 with the World Imagery basemap (Sources: Esri, DigitalGlobe, Earthstar Geographics, CNES/Airbus DS, GeoEye, USDA FSA, USGS, Getmapping, Aerogrid, IGN, IGP, and the GIS User Community).

5.2.2. Particle Number Distributions

A scanning mobility particle sizer (SMPS, model 3082, TSI Inc., Shoreview, MN) was located at the field site from August 21 – September 20, 2015 for online measurements of size-resolved particle number concentrations from 13 – 746 nm (mobility diameter). Additionally, long-term measurements of particle number size distributions (10 – 810 nm mobility diameter) from the NOAA Barrow Observatory were collected with a TROPOS-type mobility particle size spectrometer (Wiedensohler et al., 2012) to determine daily average particle number concentrations and size distributions in August and September for the available years of 2008, 2009, 2013, and 2014. Time periods when the wind direction was between 170 and 330° were excluded from daily averages because of the influence from the town of Utqiaġvik. In addition, short (< 1 h) bursts of ultrafine particles during clean time periods were excluded due to the

likely short-term influence from local vehicle emissions. For the long-term data, the daily averages were classified according to air mass source region using 48 h backward air mass trajectories and then averaged over a month-long period.

5.2.3. Computer-Controlled Scanning Electron Microscopy with Energy Dispersive X-Ray Spectroscopy

From August 21-September 30, 2015, 0.07 – 5.0 μm particles were collected during 8 h sampling periods (00:00 – 08:00, 08:00 – 16:00, 16:00 – 00:00 AKDT) on aluminum foil substrates (MSP Corp., Shoreview, MN) and transmission electron microscopy (TEM) grids (carbon Type-B Formvar film copper grids, Ted Pella Inc., Redding, CA) using a three-stage impactor (MPS-3, California Measurements, Sierra Madre, CA) with aerodynamic diameter size cuts of 0.07 – 0.4 μm, 0.4 –2.8 μm, and 2.8 – 5 μm, respectively. Individual particles were analyzed using computer-controlled scanning electron microscopy with energy dispersive X-ray spectroscopy (CCSEM-EDX). A FEI Quanta environmental SEM with a field emission gun (FEG) operating at 20 keV with a high-angle annular dark field (HAADF) detector collected SEM images and morphological data (including diameter, perimeter, and projected area) of individual particles 0.13 – 4.0 μm projected area diameter (Laskin et al., 2006; Laskin et al., 2012). The instrument is equipped with an EDX spectrometer (EDAX Inc., Mahwah, NJ) to measure X-ray spectra of elements with atomic numbers higher than Be, providing the relative atomic abundance of elements C, N, O, Na, Mg, Al, Si, P, S, Cl, K, Ca, Ti, V, Fe, and Zn. Additional CCSEM-EDX analysis was conducted using the same method with an FEI Helios 650 Nanolab SEM/FIB (focused ion beam) with an FEG operating at 20 keV using HAADF and through-the-lens detectors with an EDX spectrometer.

K-means cluster analysis was conducted over EDX spectra from 13,972 individual particles analyzed by the Quanta instrument and 5,121 particles analyzed by the Helios instrument, resulting in 50 clusters from each data set. These clusters were then regrouped into seven main particle classes based on elemental composition, described in Section 5.3.2 and the supplemental information. For periods corresponding to Arctic Ocean air mass influence, SEM images and EDX spectra were obtained for 2,869 particles from four samples which coincided with ATOFMS sampling: September 8, 2015 (00:00 – 08:00 and 08:00 – 16:00 AKDT), September 9, 2015 00:00 – 08:00, and September 15, 2015 00:00 – 08:00. For periods of Prudhoe Bay air mass influence, 1,997 particles from two samples which coincide with

ATOFMS sampling (September 23, 2015 00:00 – 08:00 and 08:00 – 16:00) were analyzed. Error resulting from number fraction for different particle types were calculated using binomial statistics, and the minimum number of particles for a representative sample are between ~300 - 1,000 (Willis et al., 2002).

5.2.4 Aerosol Time-of-Flight Mass Spectrometer (ATOFMS)

An aerosol time-of-flight mass spectrometer (ATOFMS) measured the size and chemical composition of individual aerosol particles (0.2 – 1.5 μm) in real-time from September 8 – 30, 2015. The ATOFMS used in the current study is based on the design of Pratt et al. (2009) with modifications as described below. Briefly, particles are focused using an aerodynamic lens system, and particle velocity is measured by the transit time between two continuous wave lasers, 405 nm and 488 nm (OBIX LX, Coherent, Inc., Santa Clara, CA), spaced 6 cm apart. Vacuum aerodynamic particle diameter (d_{va}) is calculated based on particle velocity from polystyrene latex sphere standards of known diameter (90 nm – 1.5 μm) and density (1 g cm^{-3}). Particles enter a dual-polarity reflectron time-of-flight mass spectrometer (Tofwerk AG, Thun, Switzerland) and are desorbed and ionized by a Q-switched 100 Hz 266 nm Nd:YAG laser (Centurion, Quantel USA, Bozeman, MT) operated at 0.8 – 1.0 mJ, resulting in positive and negative ion mass spectra of laser-ablated individual particles. Mass spectral peak lists were created in custom software developed in LabVIEW and MATLAB. Prior to ATOFMS sampling, particles were dried in-line using two silica gel diffusion driers. Despite this, negative ion mass spectra were present for only 53% of the detected particles due to the accumulation of particulate water which suppresses negative ion formation (Neubauer et al., 1997), as commonly observed for marine environments (Spencer et al., 2008).

The ATOFMS collected dual-polarity mass spectra of 496 individual particles with aerodynamic diameters of 0.2 – 1.5 μm from September 8-30, 2016. In addition to low ambient particle concentrations impacting the data collection rate, an instrumental issue with the time-of-flight mass analyzer, which has since been fixed, led to a significantly reduced particle hit rate (fraction of mass spectra collected per number of particles sized within the instrument) of less than 1%; however, laboratory tests showed that the quality of the mass spectra collected were not affected. Individual mass spectra were analyzed using YAADA, a custom software toolkit for MATLAB (Allen, 2004). Mass spectra were clustered based on the presence and intensity of ion peaks within individual mass spectra using an ART-2a algorithm, with a vigilance factor of 0.8

and a learning rate of 0.05 for 20 iterations (Song et al., 1999). Mass spectral peaks were identified based on the most probable *m/z* considering previous laboratory and field studies (Toner et al., 2008; Pratt et al., 2011; Ault et al., 2013; Qin et al., 2012; Rehbein et al., 2011). The resulting clusters were manually combined into five groups, each representing an individual particle type (Section 5.3.2 and supplemental information). Due to the small sample number of particles, 100% of the measured particles were clustered either by ART-2a or manually. Despite the low number of collected mass spectra, the observed particle types are consistent with previous Arctic surface-based ATOFMS measurements by Sierau et al. (2014), who also obtained a similar number of mass spectra in part due to low particle number concentrations in the summertime Arctic boundary layer. The errors associated with number fractions for different particle types were calculated using binomial statistics.

5.3. Results and Discussion

5.3.1. Air Masses from the Arctic Ocean and Prudhoe Bay Oil Fields

The prevailing wind direction at Utqiaġvik is from the northeast across the Beaufort Sea (Searby and Hunter, 1971). Based on backward air mass trajectories (Figure 5.1) and wind direction (Figure C.1), 70% of the days between August 21 – September 30, 2015 were influenced by the Arctic Ocean (~6 km northeast), with 10% of days influenced by the Prudhoe Bay oil fields (~300 km southeast) and 20% influenced by the town of Utqiaġvik (~5 km northwest). Prudhoe Bay air masses traveled along the coast and were therefore influenced by both tundra and the Beaufort Sea, in addition to the emissions from the Prudhoe Bay oil fields. Here we discuss the influences from the two main source regions of interest, the Arctic Ocean and Prudhoe Bay, on atmospheric particle number and chemical composition.

From August 21 to September 20, 2015, the average number concentration of 13 – 746 nm particles during Arctic Ocean influenced air masses (130 ± 1 particles cm^{-3} with standard error of the mean) was nearly five times less than the average number concentration of the Prudhoe Bay influenced air masses (920 ± 4 particles cm^{-3} with standard error of the mean) characterized on August 24 – 25 (Figure 5.2 and C.2). Aerosol number distributions for time periods classified as Arctic Ocean and Prudhoe Bay are shown in Figure C.2; corresponding median and 25^{th} and 75^{th} percentile aerosol number distributions for both time periods are shown in Figure C.3. Notably, the average particle mode diameter of 27 ± 4 nm during Prudhoe Bay influence was smaller than the average particle mode diameter of 76 ± 40 nm during Arctic

Ocean influenced air masses, illustrating that the majority of the additional particles in the Prudhoe Bay air mass were less than 30 nm in diameter (Figure 5.2). Particles smaller than ~50 nm are often associated with combustion emissions, either from primary particles or nucleated particles within the emission plume, but can also be indicative of regional new particle formation. However, regional new particle formation would typically be followed by particle growth (Kulmala et al., 2004), which was not observed (Figure C.2). Rather, this ultrafine particle mode was sustained over multiple hours (Figure C.2), which also eliminates the possibility that these were from local vehicle emissions.

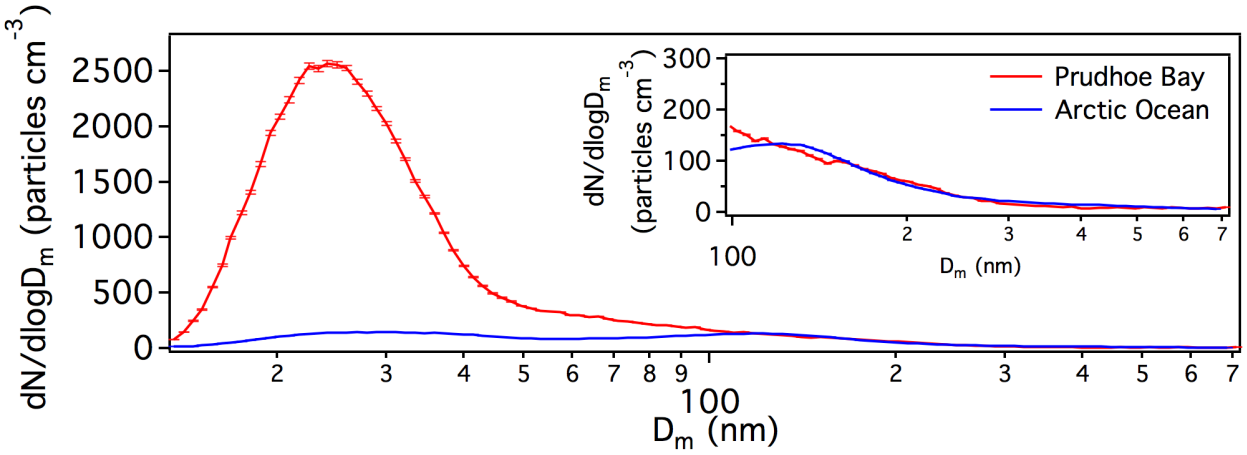

Figure 5.2. Average, and standard error of the mean, particle number size (14 – 746 nm mobility diameter) distributions during Prudhoe Bay and Arctic Ocean influenced air masses from August 21 – September 20, 2015, with the above 100 nm distributions inset. The full time series of the time-varying aerosol distribution is shown in Figure C.2.

The condensation sink, a measure of how fast molecules will condense onto existing particles (Lehtinen et al., 2003), was calculated during the 2015 study Prudhoe Bay air mass periods using the method of Dal Maso et al. (2002). The average condensation sink was 6 x 10^{-4} s^{-1}, over an order of magnitude lower than typically observed at mid-latitude and boreal forest sites (e.g. Jung et al., 2013; Dal Maso et al., 2002; Kulmala et al., 2001). Based on the simulations by Fierce et al. (2015), particle growth during transport for particles ~30 – 50 nm would take ~1 – 7 days, if coagulation-dominated due to limited condensable material. Particle growth was not observed during this study, suggesting that sufficient condensable material was not available for an observable change in particle diameter. Therefore, particles of this size could potentially be transported from Prudhoe Bay to Utqiaġvik during the average 21 ± 7 h transit time. Given the lack of primary ultrafine aerosol sources between Utqiaġvik and Prudhoe Bay, it

is suggested that these particles were likely transported from Prudhoe Bay. During semi-continuous measurements between January 2008 and July 2015, Kolesar et al. (2017) previously observed Prudhoe Bay air masses to preferentially exhibit particle growth, compared to Arctic Ocean air masses. However, particle growth was not observed to occur within all Prudhoe Bay air masses during the summer, and particle growth events were not observed in September in Utqiaġvik (Kolesar et al., 2017).

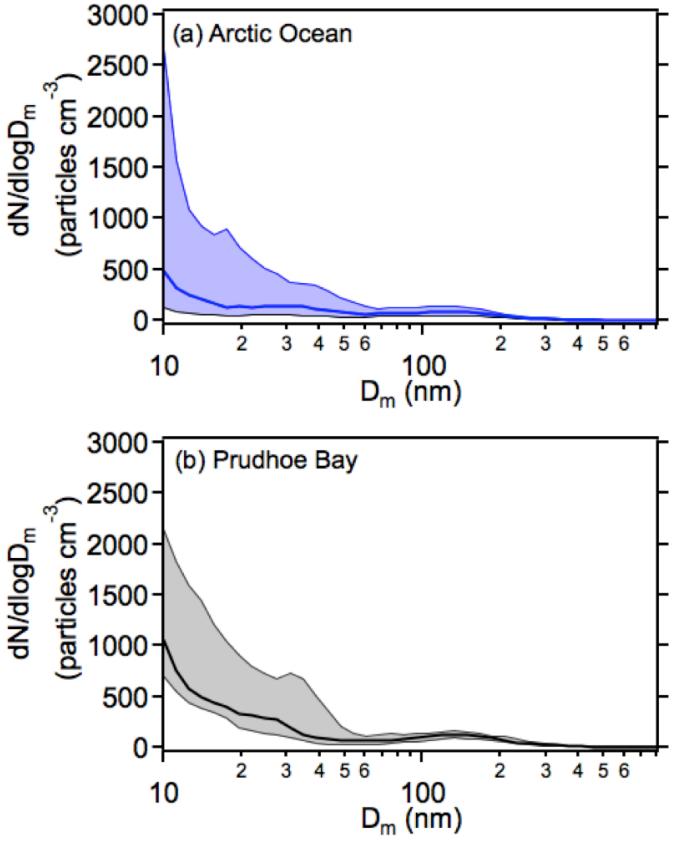

Figure 5.3. Particle number distribution (10 – 810 nm mobility diameter) for (a) Arctic Ocean and (b) Prudhoe Bay air masses observed for August-September 2008, 2009, 2013, and 2014 (median shown by the solid line, 25th and 75th percentiles shaded) at the NOAA Barrow Observatory.

Multi-year measurements of particle number size distributions were also compared for Arctic Ocean and Prudhoe Bay influenced air masses for the months of August and September (Figure 5.3). Prudhoe Bay air masses had a significantly (95% confidence interval) higher median concentration (407 particles cm^{-3}) compared to Arctic Ocean air masses (294 particles cm^{-3}), similar to the trends observed during the 2015 study. The median particle concentration within Arctic Ocean air masses is similar to the median particle number concentrations during

August at Station Nord, Greenland (227 particles cm^{-3}, Nguyen et al., 2016) and Alert, Canada (~160 particles cm^{-3}; Croft et al., 2016), during September at Tiksi, Russia (222 particles cm^{-3}; Asmi et al., 2016), and within the range of observations onboard the Swedish icebreaker *Oden* from July – September during multiple central Arctic Ocean studies when the air masses were exposed to the open ocean (90 – 210 particles cm-3; Heintzenberg et al., 2015). However, the median particle number concentration during August in Tiksi, Russia (383 particles cm^{-3}) is similar to the median concentration of Prudhoe Bay influenced air masses (407 particles cm^{-3}) even though the elevated number concentrations in Tiksi are due to biogenic influence leading to new particle formation and growth (Asmi et al., 2016).

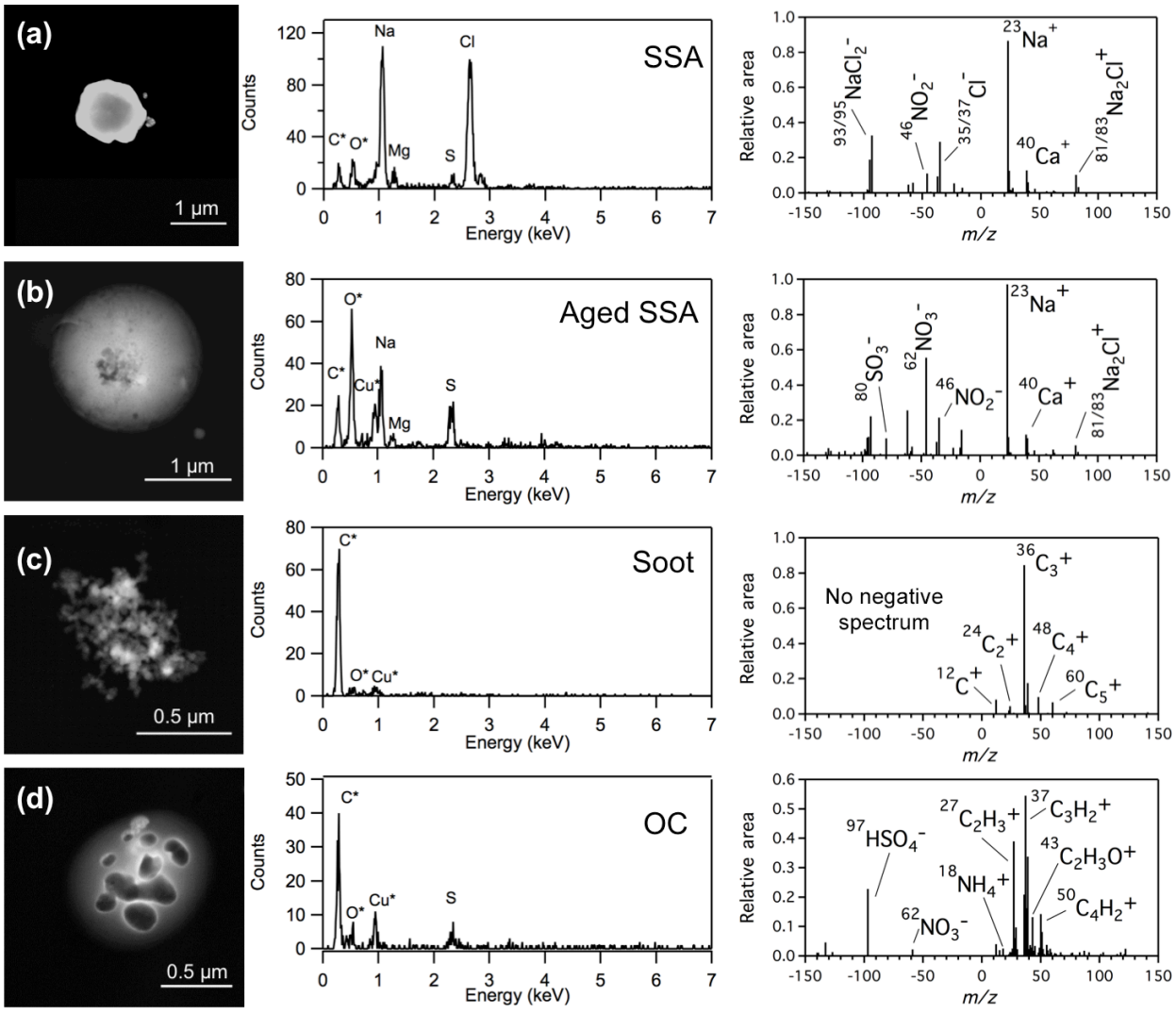

Figure 5.4. Representative SEM images (left) and EDX spectra (middle), as well as average ATOFMS mass spectra (right), for the major particle types observed: (a) Sea Spray Aerosol (SSA), (b) Partially Aged SSA, (c) Soot, (d) Organic Carbon (OC).

For the multi-year measurements, the median Arctic Ocean influenced particle size distribution has three modes (10 nm, 35 nm, 118 nm), similar to observations during August at Alert, Canada (Croft et al., 2016), Station Nord, Greenland (Nguyen et al., 2016), and Ny-Ålesund, Svalbard (Tunved et al., 2013). The Prudhoe Bay air mass median size distribution also has a clear accumulation mode ~150 nm that is typical of summertime background Arctic aerosol seen in the previously mentioned studies. A two-sample Kolmogorov-Smirnov test on Prudhoe Bay and Arctic Ocean influenced distributions from both the multi-year and 2015 study concluded that the two distributions are not significantly different ($p = 0.05$) above 100 nm, despite chemical differences described below.

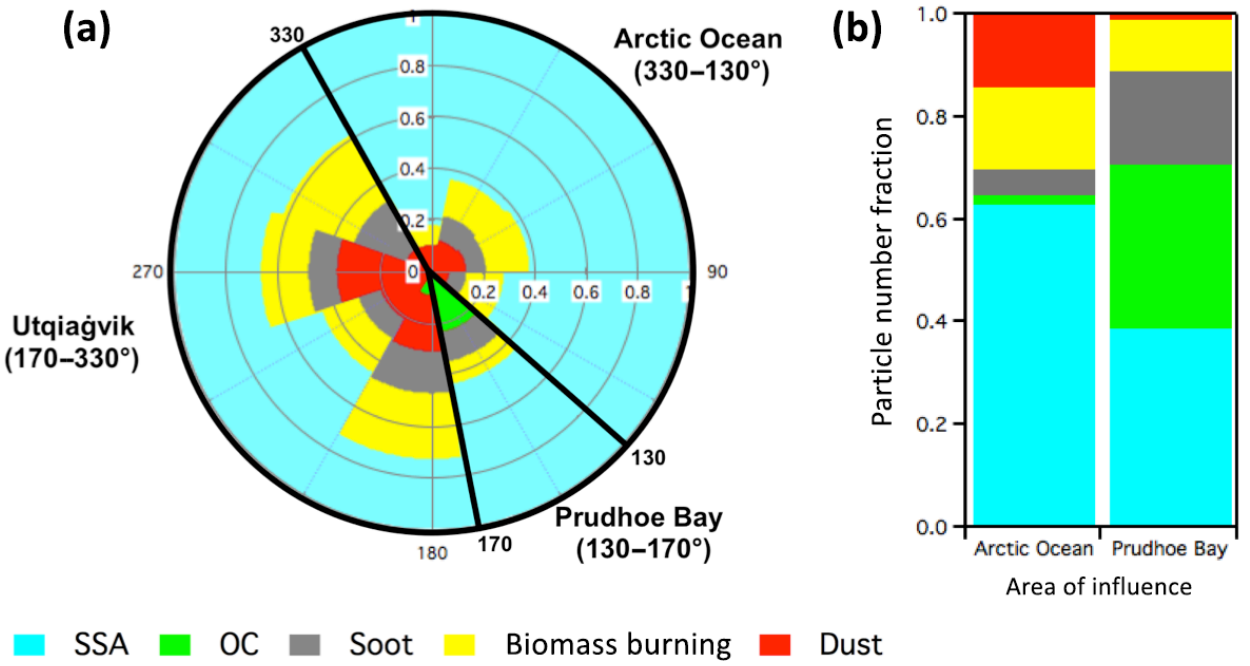

Figure 5.5. ATOFMS individual particle composition (0.2 – 1.5 µm) number fractions for 496 analyzed particles from September 8 – 20, 2015, based on wind direction (left) and air mass influence (right), determined by backward air mass trajectories. Data were binned every 40 degrees.

5.3.2. Single Particle Chemical Characterization

Analysis of the individual particle (0.1 – 4.0 µm) ATOFMS and CCSEM-EDX spectra resulted in the identification of five major single-particle types: sea spray aerosol (SSA), soot, organic carbon (OC), biomass burning, and mineral dust (Figure 5.4). Detailed descriptions of particle-type mass spectra and classifications can be found in the supplemental information. SSA internally mixed with nitrate (NO_2^- [*m/z* -46] or NO_3^- [*m/z* -62] using ATOFMS; N using EDX) and/or sulfate (SO_3^- [*m/z* -80] using ATOFMS; S using EDX) were sub-classified as partially

aged SSA (Qin et al., 2012; Gard et al., 1998) and are discussed further in Sections 5.3.2.1 and 5.3.2.2. Sulfate is identified as SO_3^- [*m/z* -80] in SSA due to mass spectral interference between HSO_4^- [*m/z* -97] and $NaCl_2^-$ [*m/z* -93,95,97] (Qin et al., 2012; Sultana et al., 2017). CCSEM-EDX identified a unique sulfur-rich particle type not observed by ATOFMS; this is consistent with previous ATOFMS studies, including an Arctic summer ship-based study (Sierau et al., 2014), that attributed a "missing" ATOFMS particle type to relatively pure ammonium sulfate or ocean-derived organic particles that scatter visible radiation, but are not ionized by 266 nm radiation (Wenzel et al., 2003; Spencer et al., 2008). CCSEM-EDX analysis identified these "missing" particles as sulfur particles, which comprised ~10 – 30% of the 0.13 – 1 μm particle number fraction during Arctic Ocean air mass influence, and ~10 – 20% of the 0.13 – 0.3 μm particle number fraction during Prudhoe Bay air mass influence (Figure 5.6). Accounting for these sulfur particles would reduce the reported ATOFMS fractions by ~5 – 15% for Arctic Ocean air mass influence, and ~5 – 10% for Prudhoe Bay air mass influence. Minor contributions were observed from biomass burning and mineral dust particles for Arctic Ocean (14 ± 4% and 14 ± 3%, respectively, by number) and Prudhoe Bay (10 ± 11% and 4 ± 7%, respectively, by number) influenced air masses (Figure 5.5). Wildfire smoke from on-going central Alaskan wildfires did not influence the site during the study based on air mass origin; therefore, biomass burning particles were likely from local residential heating or beach bonfires commonly seen around Utqiaġvik. The dirt roads and beaches near the field site are the likely source of the observed mineral dust. Both dust and biomass burning contributions were greatest when the wind was coming from Utqiaġvik.

5.3.2.1 Chemical Characterization of Aerosols during Arctic Ocean Air Mass Influence

Based on HYSPLIT backward air mass trajectories, periods of Arctic Ocean air mass influence occurred between September 8 – 12, 14 – 22 and 26 – 30. Fresh SSA contributed 80 – 100%, by number, to the measured 1 – 4 μm, as measured by CCSEM-EDX (Figure 5.6), consistent with previous Utqiaġvik measurements which demonstrated that SSA comprises approximately 70% of the summertime Arctic supermicron (1 – 10 μm) particle mass (Quinn et al., 2002). Approximately 20% of 0.13 – 0.4 μm and 40 – 70% of 0.4 – 1 μm particles, by number, were identified as fresh SSA, as determined by CCSEM-EDX, and in agreement with the measured ATOFMS number fraction of 63 ± 5% for 0.2 – 1.5 μm particles (Figure 5.5). Prominent chloride peaks, including Cl^- [*m/z* -35,37], $NaCl_2^-$ [*m/z* -93,95] and Na_2Cl^+ [*m/z* 81,83]

(Ault et al., 2014; Gard et al., 1998), were present in the ATOFMS SSA mass spectra. The majority of the identified supermicron SSA (>99%, by number) also showed little evidence of atmospheric processing through addition of nitrogen or sulfur, identified as nitrate and sulfate by ATOFMS (Figure 5.4), in part due to local SSA production. Minimal chloride depletion was observed for supermicron SSA particles during Arctic Ocean influence, with an average Cl/Na mole ratio of 0.99 for 1 – 4 μm (15% depletion) (Table 1 and Figure C.4), compared to the seawater Cl/Na ratio of 1.16 (Keene et al., 1986). Supermicron SSA particles also had low S/Na and N/Na mole ratios (0.15 and >0.1, respectively), indicating low contributions from sulfate and

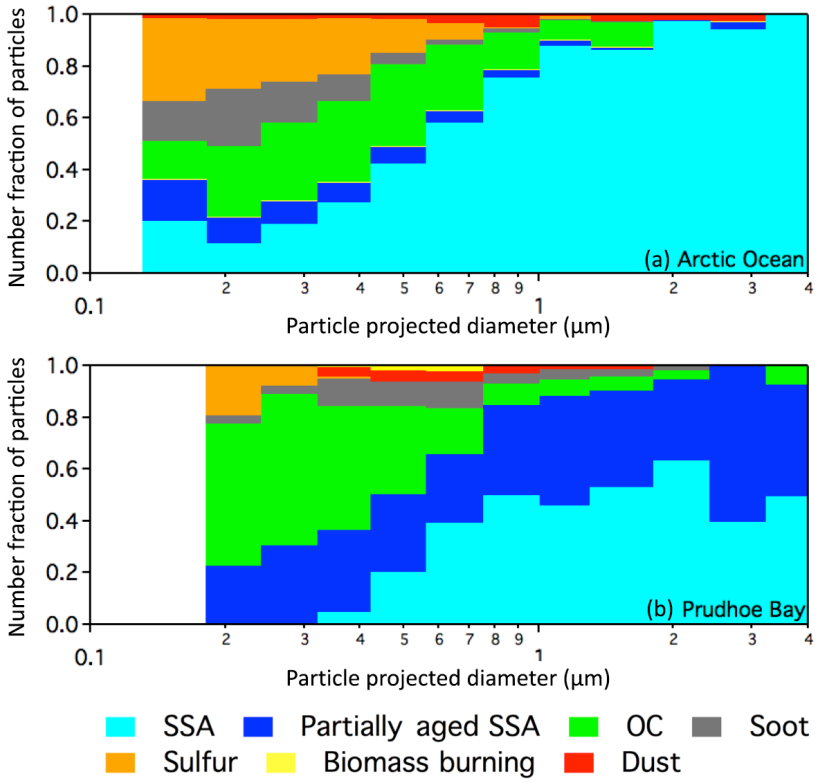

Figure 5.6. Size and chemical composition of individual particles measured by CCSEM-EDX during influence by (A) Arctic Ocean (2,869 particles analyzed) and (B) Prudhoe Bay (1,997 particles analyzed) air masses. For Arctic Ocean influenced periods, the following 8 h samples were analyzed: September 8, 2015 (00:00–08:00, 08:00 – 16:00), September 9, 2015 (00:00–08:00), September 15, 2015 (00:00–08:00). For Prudhoe Bay influenced periods, the following 8 h samples were analyzed: September 23, 2015 (00:00–08:00, 08:00–16:00). All times are in AKDT. A histogram of the number of particles analyzed in each bin can be found in the Supplemental Information (Figure C.6).

nitrate on the particles. In fact, the S/Na mole ratio of 0.15 for supermicron SSA is near the ratio expected of seawater (0.121) (Keene et al., 1986), indicating that very little atmospheric processing occurred, consistent with local SSA production. Comparatively, submicron (0.13 – 1 μm) SSA had a lower Cl/Na mole ratio (0.81, 30% depletion), as well as higher S/Na and N/Na mole ratios (0.36 and 0.27, respectively), indicating increased atmospheric processing (Williams et al., 2002; Gong et al., 2002; Laskin et al., 2002; Hopkins et al., 2008). As residence times for submicron particles are longer compared to supermicron particles, submicron SSA can be transported further, providing longer periods of atmospheric processing and leading to the observed increases in sulfate and nitrate, coincident with chloride depletion.

OC particles contributed 27%, by number, to 0.13 – 1 μm particles with minimal size dependence (Figure 5.6). OC contributed ~10%, by number, from 1 – 2 μm particles, with no OC particles measured between 2 and 4 μm. For the submicron OC particles, 94%, by number, were internally mixed with sulfur with an average atomic composition of 11% during Arctic Ocean influence (Table 5.1). Sulfur was identified as sulfate using ATOFMS spectral markers (Figure 5.4). The Arctic Ocean has previously been shown to be a significant source of biogenic sulfur in the form of dimethyl sulfide (DMS) (Ferek et al., 1995). DMS oxidizes in the atmosphere to form methanesulfonic acid (MSA), previously observed in Arctic aerosols (e.g. Sharma et al., 2012; Geng et al., 2010; Tjernström et al., 2014; Quinn et al., 2009; Quinn et al., 2007).

Table 5.1. Submicron and supermicron CCSEM-EDX number fractions and mole ratios for sulfate, nitrate, and chloride within individual SSA particles (SSA and partially aged SSA classes combined) during Arctic Ocean and Prudhoe Bay air masses. S, N, and Cl were confirmed as sulfate, nitrate, and chloride by ATOFMS.

SSA Projected Area Diameter	Sulfate (Number Fraction)	Nitrate (Number Fraction)	Chloride (Number Fraction)	S/Na	N/Na	Cl/Na
Arctic Ocean						
0.13 – 1 μm	0.77	0.33	0.81	0.36	0.27	0.81
1 – 4 μm	0.97	0.22	0.99	0.15	<0.1	0.99
Prudhoe Bay						
0.13 – 1 μm	0.86	0.40	0.87	0.53	0.54	0.67
1 – 4 μm	0.90	0.43	0.87	0.32	0.76	0.55

5.3.2.2 Chemical Characterization of Transported Prudhoe Bay Aerosols

For air masses influenced by Prudhoe Bay emissions, increased number fractions of soot, OC, and partially aged SSA particles were measured, with increased soot and OC expected based on previous estimates of soot (1.9 kt) and OC (2.0 kt) emissions from 2004 US Arctic oil and gas extraction activities, primarily at Prudhoe Bay (Peters et al., 2011). ATOFMS analyses identified 32 ± 18%, by number, of 0.2 – 1.5 μm particles as OC (Figure 5.5). CCSEM-EDX identified OC particles to comprise 60%, by number, of 0.13 – 0.3 μm particles, with contributions decreasing to 10%, by number, for 0.8 – 1 μm particles and 5%, by number, for supermicron (1 – 2 μm) particles (Figure 5.6). ATOFMS identified hydrocarbon markers within the OC particles (e.g. $C_2H_3^+$ [*m/z* 27], $C_3H_2^+$ [*m/z 37*], $C_4H_2^+$ [*m/z* 50]), similar to those detected in previous studies of vehicle combustion (Toner et al., 2008). The presence of oxidized OC was also identified ($C_2H_3O^+$ [*m/z 43*]) in these OC particles, suggesting secondary organic aerosol formation (Qin et al., 2012). However, as particle growth was not observed during Prudhoe Bay air mass influence (Section 5.3.1), it is likely that SOA contributions to particle mass were minor. Ammonium signal (NH_4^+ [*m/z* 18]) was also detected in the OC particles. Sulfur and nitrogen were identified in 60% and 28%, by number, respectively, of OC particles between 0.13 – 1 μm, confirmed as sulfate (HSO_4^- [*m/z* -97]) and nitrate (NO_3^- [*m/z* -62]), respectively, by ATOFMS (Figure 5.5.4) (Pratt and Prather, 2009). Internally mixed sulfate and nitrate have been shown to increase the hygroscopicity of organic particles and therefore enhance their CCN activity (Petters and Kreidenweis, 2007; Wang et al., 2010).

Similar number fractions of fine mode soot particles were observed by CCSEM-EDX during both Prudhoe Bay and Arctic Ocean periods (5 – 10% and 5 – 20%, by number, across 0.13 – 1 μm, respectively) (Figure 5.5.6). Soot was also identified by ATOFMS during Prudhoe Bay periods by C_n^+ clusters (C^+ [*m/z* 12], C_2^+ [*m/z* 24], C_3^+ [*m/z* 36], etc.). Elevated black carbon mass concentrations (up to 0.27 $\mu g/m^3$) were also measured by the aethalometer during the Prudhoe Bay air mass observed on August 25 (Figure C.5). Soot particles are primarily emitted through diesel combustion from heavy duty vehicles (Spencer et al., 2006) and ships (Ault et al., 2009). However, the majority of soot is expected to be less than 100 nm in diameter and therefore not chemically characterized in this study. During the 2012 ACCESS campaign off the coast of Norway, Roiger et al. (2015) observed increased soot mass concentrations <80 nm in

diameter while sampling near oil and gas extraction facilities, consistent with the observed elevated ultrafine particle number concentrations in the present study when under Prudhoe Bay air mass influence (Figure 5.2 and 5.3).

Since the air mass trajectory from Prudhoe Bay to Utqiaġvik crosses the Beaufort Sea, SSA particles were still a major contributor, making up over 90% of supermicron (1 – 4 μm) particles by number. However, unlike the Arctic Ocean air mass influence, ~60%, by number, of the supermicron SSA was classified as partially aged SSA. This is over three times the fraction compared to Arctic Ocean air masses (16%) due to atmospheric processing during 21 ± 7 hour transit over land before reaching Utqiaġvik. SSA shows 43% chloride depletion in the SSA EDX spectra (Cl/Na mole ratio of 0.66 compared to 1.16 in seawater (Keene et al., 1986)) (Table 5.1); ATOFMS chloride peak intensities ($NaCl_2^-$ [*m/z* -93,95], Cl^- [*m/z* -35,37]) are lower than during the Arctic Ocean influence for the SSA particles. Sulfur, identified as sulfate (SO_3^- [*m/z* -80]) in ATOFMS spectra (Pratt and Prather, 2009), was internally mixed with 86%, by number, of SSA (Table 5.1). For these particles, the S/Na mole ratio of the submicron (0.13 – 1 μm) SSA during Prudhoe Bay influence (0.53) is higher than expected from seawater (0.121), indicating contributions of secondary sulfate (Keene et al., 1986). Nitrogen, identified as nitrate (NO_2^-[*m/z* -46] and NO_3^-[*m/z* -62]) by ATOFMS (Liu et al., 2003), was observed in 40%, by number, of the SSA particles by CCSEM-EDX. Similar to S/Na mole ratios, submicron (0.13 – 1 μm) SSA N/Na ratios were substantially higher during Prudhoe Bay influence (0.54) compared to Arctic Ocean influenced SSA (0.27). In addition to longer atmospheric residence time for submicron particles leading to increased submicron atmospheric processing (Williams et al., 2002; Gong et al., 2002), models have found that secondary species such as sulfate and nitrate preferentially accumulate on submicron particles (Bassett and Seinfeld, 1984). These SSA particles were likely transported from the Arctic Ocean surrounding Prudhoe Bay, and underwent chloride displacement during transport due to multiphase reactions with N- and S- containing trace gases from precursor Prudhoe Bay combustion emissions (SO_2 and NO_x) leading to nitrate (Hara et al., 1999) and sulfate (Hara et al., 2003) formation. A previous ATOFMS study during the summertime in the high Arctic Ocean detected similar partially aged SSA particles containing nitrate and sulfate with low intensity chloride markers (Sierau et al., 2014).

5.4. Conclusions.

The chemical composition of individual atmospheric particles transported to Utqiaġvik, Alaska from the Arctic Ocean and Prudhoe Bay were measured from August 21 to September 30, 2015. During periods of Arctic Ocean influence, fresh SSA was a major contributor to both submicron (~20%, by number, from 0.13 – 0.4 μm, 40 – 70% between 0.4 – 1 μm) and supermicron (80 – 100%, by number, from 1 – 4 μm) particles with only 30% chloride depletion (average Cl/Na mole ratio of 0.81) for all submicron SSA and 15% chloride depletion (average Cl/Na mole ratio of 0.99) for all supermicron SSA. Submicron OC particles contributed an average of 27%, by number, from 0.13 – 1 μm with a minimum of 10%, by number, from 0.13 – 0.2 μm and were likely from a marine biogenic source. With complete summertime sea ice loss expected by 2050 (Wang and Overland, 2015; Overland and Wang, 2013), increasing aerosol and trace gas emissions from the open Arctic Ocean are expected (Browse et al., 2013; Struthers et al., 2011).

Increased total particle number concentrations (920 ± 4 particles cm^{-3}) and a smaller particle size mode of 27 ± 4 nm were observed during periods of Prudhoe Bay air mass influence, in comparison to Arctic Ocean air masses (130 ± 1 particles cm^{-3}, 76 ± 40 nm, respectively), due to transportation of ultrafine combustion particles from the Prudhoe Bay oil fields. Though not observed in the present study, these transported particles have the potential to grow (Kolesar et al., 2017) and serve as CCN, which would have a large impact on the low CCN concentrations currently in the Arctic (Mauritsen et al., 2011). During these periods, increased number fractions of partially aged SSA (28 ± 1%, by number, of particles 0.13 – 4 μm) and OC (60%, by number, of 0.13 – 0.3 μm particles with a minimum of 10%, by number, of 0.8 – 1 μm particles) were observed by CCSEM-EDX, with evidence of sulfate and nitrate internally mixed with SSA and OC particles due to heterogeneous reactions and gas-particle partitioning, respectively, during transport. Increased particle aging has been shown previously to increase the CCN activity of combustion particles (Furutani et al., 2008; Petzold et al., 2005). Therefore, increasing trace gas and aerosol emissions due to Arctic oil and gas extraction activities will contribute to further Arctic climate change (Law and Stohl, 2007).

5.5. Acknowledgements.

Matthew Gunsch ran the A-ATOFMS, SMPS, and MPS throughout the Utqiaġvik study. throughout the study, and analyzed A-ATOFMS and SMPS data. Rachel Kirpes collected and analyzed CCSEM-EDX data. Katheryn Kolesar analyzed the long-term number concentration

data. Tate Barrett and Rebecca Sheesley provided assistance throughout the field campaign. Swarup China and Alexander Laskin provided assistance collecting CCSEM-EDX data. Alfred Wiedensohler andThomas Tuch provided assistance with the TROPOS-type mobility particle size spectrometer. This study was supported by the NOAA Climate Program Office Atmospheric Chemistry, Carbon Cycle, and Climate Program, through NA14OAR4310149 (University of Michigan) and NA14OAR4310150 (Baylor University). Funding for housing and logistical support was provided by Department of Energy Atmospheric Radiation Measurements (DOE ARM) field campaign 2013-6660. UIC-Science and Department of Energy Atmospheric Radiation Measurement Climate Research Facility are thanked for logistics assistance in Utqiaġvik, AK. CCSEM-EDX analyses were performed at the Environmental Molecular Sciences Laboratory (EMSL), a national scientific user facility located at the Pacific Northwest National Laboratory (PNNL) and sponsored by the Office of Biological and Environmental Research of the U.S DOE. PNNL is operated for DOE by Battelle Memorial Institute under Contract No. DE-AC06-76RL0 1830. Travel funds to PNNL were provided by the University of Michigan Rackham Graduate School. Additional CCSEM-EDX analyses were carried out at the Michigan Center for Materials Characterization. Andrew Ault (University of Michigan) is thanked for discussions of aerosol sampling and CCSEM-EDX analysis. We also thank the National Oceanic and Atmospheric Administration (NOAA) Global Monitoring Division (including Anne Jefferson, staff at the Barrow Observatory, and Wolfram Birmili (Leibniz Institute for Tropospheric Research) for meteorological and long-term aerosol data.

5.6. References

Allen, J. O.: Quantitative analysis of aerosol time-of-flight mass spectrometry data using YAADA, California Environmental Protection Agency, Air Resources Board, Research Division, 2004.

Allison, E. H., and Bassett, H. R.: Climate change in the oceans: Human impacts and responses, Science, 350, 778-782, 2015.

Asmi, E., Kondratyev, V., Brus, D., Laurila, T., Lihavainen, H., Backman, J., Vakkari, V., Aurela, M., Hatakka, J., and Viisanen, Y.: Aerosol size distribution seasonal characteristics measured in Tiksi, Russian Arctic, Atmos. Chem. Phys., 16, 1271-1287, 2016.

Ault, A. P., Moore, M. J., Furutani, H., and Prather, K. A.: Impact of emissions from the Los Angeles port region on San Diego air quality during regional transport events, Environ. Sci. Technol., 43, 3500-3506, 2009.

Ault, A. P., Guasco, T. L., Ryder, O. S., Baltrusaitis, J., Cuadra-Rodriguez, L. A., Collins, D. B., Ruppel, M. J., Bertram, T. H., Prather, K. A., and Grassian, V. H.: Inside versus outside: Ion redistribution in nitric acid reacted sea spray aerosol particles as determined by single particle analysis, J. Am. Chem. Soc., 135, 14528-14531, 2013.

Ault, A. P., Guasco, T. L., Baltrusaitis, J., Ryder, O. S., Trueblood, J. V., Collins, D. B., Ruppel, M. J., Cuadra-Rodriguez, L. A., Prather, K. A., and Grassian, V. H.: Heterogeneous reactivity of nitric acid with nascent sea spray aerosol: Large differences observed between and within individual particles, J. Phys. Chem. Lett., 5, 2493-2500, 2014.

Barrett, T., Robinson, E., Usenko, S., and Sheesley, R.: Source contributions to wintertime elemental and organic carbon in the western arctic based on radiocarbon and tracer apportionment, Environ. Sci. Technol., 49, 11631-11639, 2015.

Bassett, M. E., and Seinfeld, J. H.: Atmospheric equilibrium model of sulfate and nitrate aerosols—II. Particle size analysis, Atmospheric Environment (1967), 18, 1163-1170, 1984.

Bond, T. C., Doherty, S. J., Fahey, D., Forster, P., Berntsen, T., DeAngelo, B., Flanner, M., Ghan, S., Kärcher, B., and Koch, D.: Bounding the role of black carbon in the climate system: A scientific assessment, J. Geophys. Res-Atmos., 118, 5380-5552, 2013.

Brock, C. A., Cozic, J., Bahreini, R., Froyd, K. D., Middlebrook, A. M., McComiskey, A., Brioude, J., Cooper, O., Stohl, A., and Aikin, K.: Characteristics, sources, and transport of aerosols measured in spring 2008 during the aerosol, radiation, and cloud processes affecting Arctic Climate (ARCPAC) Project, Atmos. Chem. Phys., 11, 2423-2453, 2011.

Browse, J., Carslaw, K., Schmidt, A., and Corbett, J.: Impact of future Arctic shipping on high‐latitude black carbon deposition, Geophys. Res. Lett., 40, 4459-4463, 2013.

Cappa, C. D., Onasch, T. B., Massoli, P., Worsnop, D. R., Bates, T. S., Cross, E. S., Davidovits, P., Hakala, J., Hayden, K. L., and Jobson, B. T.: Radiative absorption enhancements due to the mixing state of atmospheric black carbon, Science, 337, 1078-1081, 2012.

Chung, S. H., and Seinfeld, J. H.: Climate response of direct radiative forcing of anthropogenic black carbon, J. Geophys. Res-Atmos., 110, 2005.

Croft, B., Martin, R. V., Leaitch, W. R., Tunved, P., Breider, T. J., D'Andrea, S. D., and Pierce, J. R.: Processes controlling the annual cycle of Arctic aerosol number and size distributions, Atmos. Chem. Phys., 16, 3665-3682, 2016.

Dal Maso, M., Kulmala, M., Lehtinen, K., Mäkelä, J., Aalto, P., and O'Dowd, C.: Condensation and coagulation sinks and formation of nucleation mode particles in coastal and boreal forest boundary layers, J. Geophys. Res-Atmos., 107, 8097, 2002.

EIA: Top 100 U.S. Oil and Gas Fields, U.S. Department of Energy, 2015.

Ferek, R. J., Hobbs, P. V., Radke, L. F., Herring, J. A., Sturges, W. T., and Cota, G. F.: Dimethyl sulfide in the arctic atmosphere, J. Geophys. Res-Atmos., 100, 26093-26104, 1995.

Fierce, L., Riemer, N., and Bond, T. C.: Explaining variance in black carbon's aging timescale, Atmos. Chem. Phys., 15, 3173-3191, 2015.

Flanner, M. G., Zender, C. S., Randerson, J. T., and Rasch, P. J.: Present‐day climate forcing and response from black carbon in snow, J. Geophys. Res-Atmos., 112, 2007.

Flanner, M. G.: Arctic climate sensitivity to local black carbon, J. Geophys. Res-Atmos., 118, 1840-1851, 2013.

Furutani, H., Dall'osto, M., Roberts, G. C., and Prather, K. A.: Assessment of the relative importance of atmospheric aging on CCN activity derived from field observations, Atmos. Environ., 42, 3130-3142, 2008.

Gard, E. E., Kleeman, M. J., Gross, D. S., Hughes, L. S., Allen, J. O., Morrical, B. D., Fergenson, D. P., Dienes, T., Gälli, M. E., and Johnson, R. J.: Direct observation of heterogeneous chemistry in the atmosphere, Science, 279, 1184-1187, 1998.

Gautier, D. L., Bird, K. J., Charpentier, R. R., Grantz, A., Houseknecht, D. W., Klett, T. R., Moore, T. E., Pitman, J. K., Schenk, C. J., and Schuenemeyer, J. H.: Assessment of undiscovered oil and gas in the Arctic, Science, 324, 1175-1179, 2009.

Geng, H., Ryu, J., Jung, H.-J., Chung, H., Ahn, K.-H., and Ro, C.-U.: Single-particle characterization of summertime Arctic aerosols collected at Ny-Ålesund, Svalbard, Environ. Sci. Technol., 44, 2348-2353, 2010.

Gong, S., Barrie, L., and Lazare, M.: Canadian Aerosol Module (CAM): A size‐segregated simulation of atmospheric aerosol processes for climate and air quality models 2. Global sea‐salt aerosol and its budgets, J. Geophys. Res-Atmos., 107, 2002.

Hara, K., Osada, K., Hayashi, M., Matsunaga, K., Shibata, T., Iwasaka, Y., and Furuya, K.: Fractionation of inorganic nitrates in winter Arctic troposphere: Coarse aerosol particles containing inorganic nitrates, J. Geophys. Res-Atmos., 104, 23671-23679, 1999.

Hara, K., Yamagata, S., Yamanouchi, T., Sato, K., Herber, A., Iwasaka, Y., Nagatani, M., and Nakata, H.: Mixing states of individual aerosol particles in spring Arctic troposphere during ASTAR 2000 campaign, J. Geophys. Res-Atmos., 108, 2003.

Harsem, Ø., Heen, K., Rodrigues, J., and Vassdal, T.: Oil exploration and sea ice projections in the Arctic, Polar. Rec., 51, 91-106, 2015.

Haywood, J., and Boucher, O.: Estimates of the direct and indirect radiative forcing due to tropospheric aerosols: A review, Rev. Geophys., 38, 513-543, 2000.

Healy, R. M., Wang, J. M., Jeong, C. H., Lee, A. K., Willis, M. D., Jaroudi, E., Zimmerman, N., Hilker, N., Murphy, M., and Eckhardt, S.: Light‐absorbing properties of ambient black carbon and brown carbon from fossil fuel and biomass burning sources, J. Geophys. Res-Atmos., 120, 6619-6633, 2015.

Heintzenberg, J., Leck, C., and Tunved, P.: Potential source regions and processes of aerosol in the summer Arctic, Atmos. Chem. Phys, 15, 6487-6502, 2015.

Hopkins, R. J., Desyaterik, Y., Tivanski, A. V., Zaveri, R. A., Berkowitz, C. M., Tyliszczak, T., Gilles, M. K., and Laskin, A.: Chemical speciation of sulfur in marine cloud droplets and particles: Analysis of individual particles from the marine boundary layer over the California current, J. Geophys. Res-Atmos., 113, 2008.

Jacobson, M. Z.: Strong radiative heating due to the mixing state of black carbon in atmospheric aerosols, Nature, 409, 695-697, 2001.

Jaffe, D., Honrath, R., Furness, D., Conway, T., Dlugokencky, E., and Steele, L.: A determination of the CH4, NO x and CO2 emissions from the Prudhoe Bay, Alaska oil development, J. Atmos. Chem., 20, 213-227, 1995.

Jung, J., Miyazaki, Y., and Kawamura, K.: Different characteristics of new particle formation between urban and deciduous forest sites in Northern Japan during the summers of 2010–2011, Atmos. Chem. Phys., 13, 51-68, 2013.

Keene, W. C., Pszenny, A. A., Galloway, J. N., and Hawley, M. E.: Sea‐salt corrections and interpretation of constituent ratios in marine precipitation, J. Geophys. Res-Atmos., 91, 6647-6658, 1986.

Knox, A., Evans, G., Brook, J., Yao, X., Jeong, C.-H., Godri, K., Sabaliauskas, K., and Slowik, J.: Mass absorption cross-section of ambient black carbon aerosol in relation to chemical age, Aerosol. Sci. Technol., 43, 522-532, 2009.

Koch, D., Schulz, M., Kinne, S., McNaughton, C., Spackman, J., Balkanski, Y., Bauer, S., Berntsen, T., Bond, T. C., and Boucher, O.: Evaluation of black carbon estimations in global aerosol models, Atmos. Chem. Phys., 9, 9001-9026, 2009.

Kolesar, K. R., Cellini, J., Peterson, P. K., Jefferson, A., Tuch, T., Birmili, W., Wiedensohler, A., and Pratt, K. A.: Effect of Prudhoe Bay emissions on atmospheric aerosol growth events observed in Utqiaġvik (Barrow), Alaska, Atmos. Environ., 152, 146-155, 2017.

Kulmala, M., Hämeri, K., Aalto, P., Mäkelä, J., Pirjola, L., Nilsson, E. D., Buzorius, G., Rannik, Ü., Maso, M., and Seidl, W.: Overview of the international project on biogenic aerosol formation in the boreal forest (BIOFOR), Tellus B, 53, 324-343, 2001.

Kulmala, M., Vehkamäki, H., Petäjä, T., Dal Maso, M., Lauri, A., Kerminen, V.-M., Birmili, W., and McMurry, P. H.: Formation and growth rates of ultrafine atmospheric particles: a review of observations, J. Aerosol. Sci., 35, 143-176, 2004.

Laskin, A., Iedema, M. J., and Cowin, J. P.: Quantitative time-resolved monitoring of nitrate formation in sea salt particles using a CCSEM/EDX single particle analysis, Environ. Sci. Technol., 36, 4948-4955, 2002.

Laskin, A., Cowin, J. P., and Iedema, M. J.: Analysis of individual environmental particles using modern methods of electron microscopy and X-ray microanalysis, J. Electron. Spectrosc., 150, 260-274, 2006.

Laskin, A., Moffet, R. C., Gilles, M. K., Fast, J. D., Zaveri, R. A., Wang, B., Nigge, P., and Shutthanandan, J.: Tropospheric chemistry of internally mixed sea salt and organic particles: Surprising reactivity of NaCl with weak organic acids, J. Geophys. Res-Atmos., 117, 2012.

Law, K. S., and Stohl, A.: Arctic air pollution: Origins and impacts, Science, 315, 1537-1540, 2007.

Lehtinen, K. E., Korhonen, H., Maso, M., and Kulmala, M.: On the concept of condensation sink diameter, Boreal. Environ. Res., 8, 405-412, 2003.

Liggio, J., Li, S.-M., Hayden, K., Taha, Y. M., Stroud, C., Darlington, A., Drollette, B. D., Gordon, M., Lee, P., and Liu, P.: Oil sands operations as a large source of secondary organic aerosols, Nature, 534, 91-94, 2016.

Liu, D. Y., Wenzel, R. J., and Prather, K. A.: Aerosol time‐of‐flight mass spectrometry during the Atlanta Supersite Experiment: 1. Measurements, J. Geophys. Res-Atmos., 108, 2003.

Liu, S., Aiken, A. C., Gorkowski, K., Dubey, M. K., Cappa, C. D., Williams, L. R., Herndon, S. C., Massoli, P., Fortner, E. C., and Chhabra, P. S.: Enhanced light absorption by mixed source black and brown carbon particles in UK winter, Nat. Commun., 6, 2015.

Mauritsen, T., Sedlar, J., Tjernström, M., Leck, C., Martin, M., Shupe, M., Sjogren, S., Sierau, B., Persson, P., and Brooks, I.: An Arctic CCN-limited cloud-aerosol regime, Atmos. Chem. Phys., 11, 165-173, 2011.

Moffet, R. C., and Prather, K. A.: In-situ measurements of the mixing state and optical properties of soot with implications for radiative forcing estimates, Proc. Natl. Acad. Sci., 106, 11872-11877, 2009.

Neubauer, K. R., Johnston, M. V., and Wexler, A. S.: On-line analysis of aqueous aerosols by laser desorption ionization, Int. J. Mass. Spectrom., 163, 29-37, 1997.

Nguyen, Q. T., Glasius, M., Sørensen, L. L., Jensen, B., Skov, H., Birmili, W., Wiedensohler, A., Kristensson, A., Nøjgaard, J. K., and Massling, A.: Seasonal variation of atmospheric particle number concentrations, new particle formation and atmospheric oxidation capacity at the high Arctic site Villum Research Station, Station Nord, Atmos. Chem. Phys., 16, 11319-11336, 2016.

Overland, J. E., and Wang, M.: When will the summer Arctic be nearly sea ice free?, Geophys. Res. Lett., 40, 2097-2101, 2013.

Peters, G., Nilssen, T., Lindholt, L., Eide, M., Glomsrød, S., Eide, L., and Fuglestvedt, J.: Future emissions from shipping and petroleum activities in the Arctic, Atmos. Chem. Phys., 11, 5305-5320, 2011.

Petters, M., and Kreidenweis, S.: A single parameter representation of hygroscopic growth and cloud condensation nucleus activity, Atmos. Chem. Phys., 7, 1961-1971, 2007.

Petzold, A., Gysel, M., Vancassel, X., Hitzenberger, R., Puxbaum, H., Vrochticky, S., Weingartner, E., Baltensperger, U., and Mirabel, P.: On the effects of organic matter and sulphur-containing compounds on the CCN activation of combustion particles, Atmos. Chem. Phys., 5, 3187-3203, 2005.

Polissar, A., Hopke, P., Paatero, P., Kaufmann, Y., Hall, D., Bodhaine, B., Dutton, E., and Harris, J.: The aerosol at Barrow, Alaska: long-term trends and source locations, Atmos. Environ., 33, 2441-2458, 1999.

Polissar, A. V., Hopke, P. K., and Harris, J. M.: Source regions for atmospheric aerosol measured at Barrow, Alaska, Environ. Sci. Technol., 35, 4214-4226, 2001.

Pöschl, U.: Atmospheric Aerosols: Composition, Transformation, Climate and Health Effects, Angew. Chen. Int. Ed., 44, 7520 - 7540, 2005.

Prather, K. A., Hatch, C. D., and Grassian, V. H.: Analysis of atmospheric aerosols, Annu. Rev. Anal. Chem., 1, 485-514, 2008.

Pratt, K., Murphy, S., Subramanian, R., DeMott, P., Kok, G., Campos, T., Rogers, D., Prenni, A., Heymsfield, A., and Seinfeld, J.: Flight-based chemical characterization of biomass burning aerosols within two prescribed burn smoke plumes, Atmos. Chem. Phys., 11, 12549-12565, 2011.

Pratt, K. A., Mayer, J. E., Holecek, J. C., Moffet, R. C., Sanchez, R. O., Rebotier, T. P., Furutani, H., Gonin, M., Fuhrer, K., and Su, Y.: Development and characterization of an aircraft aerosol time-of-flight mass spectrometer, Anal. Chem., 81, 1792-1800, 2009.

Pratt, K. A., and Prather, K. A.: Real-time, single-particle volatility, size, and chemical composition measurements of aged urban aerosols, Environ. Sci. Technol., 43, 8276-8282, 2009.

Qin, X., Pratt, K. A., Shields, L. G., Toner, S. M., and Prather, K. A.: Seasonal comparisons of single-particle chemical mixing state in Riverside, CA, Atmos. Environ., 59, 587-596, 2012.

Quinn, P., Miller, T., Bates, T., Ogren, J., Andrews, E., and Shaw, G.: A 3 - year record of simultaneously measured aerosol chemical and optical properties at Barrow, Alaska, J. Geophys. Res-Atmos., 107, 2002.

Quinn, P., Shaw, G., Andrews, E., Dutton, E., Ruoho - Airola, T., and Gong, S.: Arctic haze: current trends and knowledge gaps, Tellus B, 59, 99-114, 2007.

Quinn, P., Bates, T., Schulz, K., and Shaw, G.: Decadal trends in aerosol chemical composition at Barrow, Alaska: 1976–2008, Atmos. Chem. Phys., 9, 8883-8888, 2009.

Ramanathan, V., and Carmichael, G.: Global and regional climate changes due to black carbon, Nat. Geosci., 1, 221-227, 2008.

Rehbein, P. J., Jeong, C.-H., McGuire, M. L., Yao, X., Corbin, J. C., and Evans, G. J.: Cloud and fog processing enhanced gas-to-particle partitioning of trimethylamine, Environ. Sci. Technol., 45, 4346-4352, 2011.

Roiger, A., Thomas, J.-L., Schlager, H., Law, K. S., Kim, J., Schäfler, A., Weinzierl, B., Dahlkötter, F., Krisch, I., and Marelle, L.: Quantifying emerging local anthropogenic

emissions in the Arctic region: The ACCESS aircraft campaign experiment, B. Am. Meteorol. Soc., 96, 441-460, 2015.

Sand, M., Berntsen, T. K., Kay, J. E., Lamarque, J. F., Seland, Ø., and Kirkevåg, A.: The Arctic response to remote and local forcing of black carbon, Atmos. Chem. Phys., 13, 211-224, 10.5194/acp-13-211-2013, 2013a.

Sand, M., Berntsen, T. K., Seland, Ø., and Kristjánsson, J. E.: Arctic surface temperature change to emissions of black carbon within Arctic or midlatitudes, J. Geophys. Res-Atmos., 118, 7788-7798, 2013b.

Searby, H. W., and Hunter, M.: Climate of the North Slope, Alaska, US Department of Commerce, National Oceanic and Atmospheric Administration, National Weather Service, Alaska Region, 1971.

Sharma, S., Chan, E., Ishizawa, M., Toom‐Sauntry, D., Gong, S., Li, S., Tarasick, D., Leaitch, W., Norman, A., and Quinn, P.: Influence of transport and ocean ice extent on biogenic aerosol sulfur in the Arctic atmosphere, J. Geophys. Res-Atmos., 117, 2012.

Sharma, S., Ishizawa, M., Chan, D., Lavoué, D., Andrews, E., Eleftheriadis, K., and Maksyutov, S.: 16‐year simulation of Arctic black carbon: Transport, source contribution, and sensitivity analysis on deposition, J. Geophys. Res-Atmos., 118, 943-964, 2013.

Sierau, B., Chang, R.-W., Leck, C., Paatero, J., and Lohmann, U.: Single-particle characterization of the high-Arctic summertime aerosol, Atmos. Chem. Phys., 14, 7409-7430, 2014.

Simpson, I., Blake, N., Barletta, B., Diskin, G., Fuelberg, H., Gorham, K., Huey, L., Meinardi, S., Rowland, F., and Vay, S.: Characterization of trace gases measured over Alberta oil sands mining operations: 76 speciated C 2–C 10 volatile organic compounds (VOCs), CO 2, CH 4, CO, NO, NO 2, NO y, O 3 and SO 2, Atmos. Chem. Phys., 10, 11931-11954, 2010.

Song, X.-H., Hopke, P. K., Fergenson, D. P., and Prather, K. A.: Classification of single particles analyzed by ATOFMS using an artificial neural network, ART-2A, Anal. Chem., 71, 860-865, 1999.

Spencer, M., Holecek, J., Corrigan, C., Ramanathan, V., and Prather, K.: Size‐resolved chemical composition of aerosol particles during a monsoonal transition period over the Indian Ocean, J. Geophys. Res-Atmos., 113, 2008.

Spencer, M. T., Shields, L. G., Sodeman, D. A., Toner, S. M., and Prather, K. A.: Comparison of oil and fuel particle chemical signatures with particle emissions from heavy and light duty vehicles, Atmos. Environ., 40, 5224-5235, 2006.

Stein, A., Draxler, R., Rolph, G., Stunder, B., Cohen, M., and Ngan, F.: NOAA's HYSPLIT atmospheric transport and dispersion modeling system, B. Am. Meteorol. Soc., 96, 2059-2077, 2015.

Stohl, A., Klimont, Z., Eckhardt, S., Kupiainen, K., Shevchenko, V., Kopeikin, V., and Novigatsky, A.: Black carbon in the Arctic: the underestimated role of gas flaring and residential combustion emissions, Atmos. Chem. Phys., 13, 8833-8855, 2013.

Struthers, H., Ekman, A., Glantz, P., Iversen, T., Kirkevåg, A., Mårtensson, E. M., Seland, Ø., and Nilsson, E.: The effect of sea ice loss on sea salt aerosol concentrations and the radiative balance in the Arctic, Atmos. Chem. Phys., 11, 3459-3477, 2011.

Sultana, C. M., Collins, D. B., and Prather, K. A.: Effect of Structural Heterogeneity in Chemical Composition on Online Single-Particle Mass Spectrometry Analysis of Sea Spray Aerosol Particles, Environ. Sci. Technol, 51, 3660-3668, 2017.

Tjernström, M., Leck, C., Birch, C. E., Bottenheim, J. W., Brooks, B. J., Brooks, I. M., Bäcklin, L., Chang, R.-W., de Leeuw, G., and Di Liberto, L.: The Arctic Summer Cloud Ocean Study (ASCOS): overview and experimental design, Atmos. Chem. Phys., 14, 2823-2869, 2014.

Toner, S. M., Shields, L. G., Sodeman, D. A., and Prather, K. A.: Using mass spectral source signatures to apportion exhaust particles from gasoline and diesel powered vehicles in a freeway study using UF-ATOFMS, Atmos. Environ., 42, 568-581, 2008.

Tunved, P., Ström, J., and Krejci, R.: Arctic aerosol life cycle: linking aerosol size distributions observed between 2000 and 2010 with air mass transport and precipitation at Zeppelin station, Ny-Ålesund, Svalbard, Atmos. Chem. Phys., 13, 3643-3660, 2013.

Volkamer, R., Jimenez, J. L., San Martini, F., Dzepina, K., Zhang, Q., Salcedo, D., Molina, L. T., Worsnop, D. R., and Molina, M. J.: Secondary organic aerosol formation from anthropogenic air pollution: Rapid and higher than expected, Geophys. Res. Lett., 33, 2006.

Wang, J., Cubison, M., Aiken, A., Jimenez, J., and Collins, D.: The importance of aerosol mixing state and size-resolved composition on CCN concentration and the variation of the importance with atmospheric aging of aerosols, Atmos. Chem. Phys., 10, 7267-7283, 2010.

Wang, M., and Overland, J. E.: Projected future duration of the sea-ice-free season in the Alaskan Arctic, Prog. Oceanogr., 136, 50-59, 2015.

Wenzel, R. J., Liu, D. Y., Edgerton, E. S., and Prather, K. A.: Aerosol time‐of‐flight mass spectrometry during the Atlanta Supersite Experiment: 2. Scaling procedures, J. Geophys. Res-Atmos., 108, 2003.

Wiedensohler, A., Birmili, W., Nowak, A., Sonntag, A., Weinhold, K., Merkel, M., Wehner, B., Tuch, T., Pfeifer, S., and Fiebig, M.: Mobility particle size spectrometers: harmonization of technical standards and data structure to facilitate high quality long-term observations of atmospheric particle number size distributions, Atmos. Meas. Tech., 5, 657-685, 2012.

Williams, J., Reus, M. d., Krejci, R., Fischer, H., and Ström, J.: Application of the variability-size relationship to atmospheric aerosol studies: estimating aerosol lifetimes and ages, Atmos. Chem. Phys., 2, 133-145, 2002.

Willis, R., Blanchard, F., and Conner, T.: Guidelines for the application of SEM/EDX analytical techniques to particulate matter samples, EPA. Washington, US, 2002.

Ziemba, L. D., Dibb, J. E., Griffin, R. J., Huey, L. G., and Beckman, P.: Observations of particle growth at a remote, Arctic site, Atmos. Environ., 44, 1649-1657, 2010.

Chapter 6.
Diesel and Natural Gas Combustion Contributions to Atmospheric Aerosols in an Arctic Oil Field

In preparation for submission to *Environ. Sci. Technol.*

6.1. Introduction

With Arctic surface temperatures increasing at nearly twice the global average (IPCC, 2013; Screen and Simmonds, 2010) and sea ice extent rapidly declining (Overland and Wang, 2013; Swart et al., 2015; Wang and Overland, 2015), the Arctic has become more accessible to oil and gas extraction infrastructure development (Allison and Bassett, 2015; Harsem et al., 2015). 30% of the world's undiscovered gas and 13% of the undiscovered oil are located in the Arctic (Gautier et al., 2009). In 2016, Alaska sold new leases for over 2,400 km^2 of land for oil and gas extraction on the North Slope of Alaska and in the Beaufort Sea; this was second largest sale since 1998 (Mack and Bluemink, 2016). Similar expansions are currently occurring elsewhere in the Arctic, particularly in Russia and Norway, where much of the undiscovered oil is thought to be located (Gautier et al., 2009).

Oil and gas extraction activities emit particulate matter (PM) (Law and Stohl, 2007; Peters et al., 2011), which has negative effects on air quality, climate, and human health (Pöschl, 2005). Depending on chemical composition, atmospheric particles can scatter or absorb incoming solar radiation, act as cloud condensation and ice nuclei, and alter the surface albedo of snow (Jacobson, 2004), all of which impact climate (IPCC, 2013). Peters et al. (2011) estimated that 47 kt of PM (15 kt black carbon, BC, 16 kt organic carbon, OC) emitted from Arctic oil and gas extraction activities in 2004. In addition, significant emissions of SO_2 (150 kt), NO_x ($NO + NO_2$, 160 kt), and non-methane volatile organic compounds (VOCs, 120 kt) were also emitted (Peters et al., 2011), and these trace gases can undergo oxidation, contribution to secondary aerosol

formation (Pöschl, 2005). Notably, local sources of BC within the Arctic are simulated to have as much as three times the impact on Arctic climate compared to transported sources of BC (Flanner, 2013). Further, Bond et al. (2013) found that BC is under-predicted by models by an average factor of 2.5 in the Arctic. Therefore, Law and Stohl (2007) stated the need for further measurements of soot in the Arctic to clarify the importance of various sources.

Few studies have examined emissions from Arctic oil and gas extraction (Brock et al., 2011; Brooks et al., 1997; Creamean et al., 2017; Gunsch et al., 2017; Jaffe et al., 1995; Maahn et al., 2017; Roiger et al., 2015; Stohl et al., 2013). The Arctic Climate Change, Economy, and Society (ACCESS) field campaign in the Norwegian Arctic identified increased NO_x, SO_2, and BC in plumes from local extraction facilities (Roiger et al., 2015). Increased BC, NO_x, SO_2, CO_2, and CH_4 have previously been measured during both ground and aircraft-based campaigns within the Prudhoe Bay oil fields (Brock et al., 2011; Brooks et al., 1997; Creamean et al., 2017; Jaffe et al., 1995; Maahn et al., 2017). Recent flight campaigns by Maahn et al. (2017) and Creamean et al. (2017) measured enhanced cloud condensation nuclei (CCN) concentration above Oliktok Point, within the Prudhoe Bay oil fields. Gas flaring within Arctic oil fields, in particular, is a direct source of NO_x and BC (Fawole et al., 2016; Li et al., 2016), contributing an estimated 42% of the annual surface BC levels in the Arctic (Stohl et al., 2013).

Atmospheric particle mixing state defines particle properties, such as optical properties (scattering/absorption), hygroscopicity, toxicity, and chemical reactivity (Moffet and Prather, 2009; Pöschl, 2005). For example, Sharma et al. (2013) stated that a limited understanding of BC mixing state has led to uncertainties about the climate impacts of BC in the Arctic. Single particle mass spectrometry can be used to identify the chemical composition and mixing state of individual particles using mass spectral "chemical fingerprints" unique to different sources (Pratt et al., 2009b; Pratt and Prather, 2012). To investigate the sources, chemical composition, and chemical mixing state of aerosols from oil and gas extraction activities within the Prudhoe Bay oil fields, an on-line aerosol time-of-flight mass spectrometer (ATOFMS) was used to measure individual particle size and chemical composition in real-time at Oliktok Point, Alaska during August and September 2016. These observations represent the first online aerosol chemical composition measurements of oil and gas extraction emissions in the Alaskan Arctic.

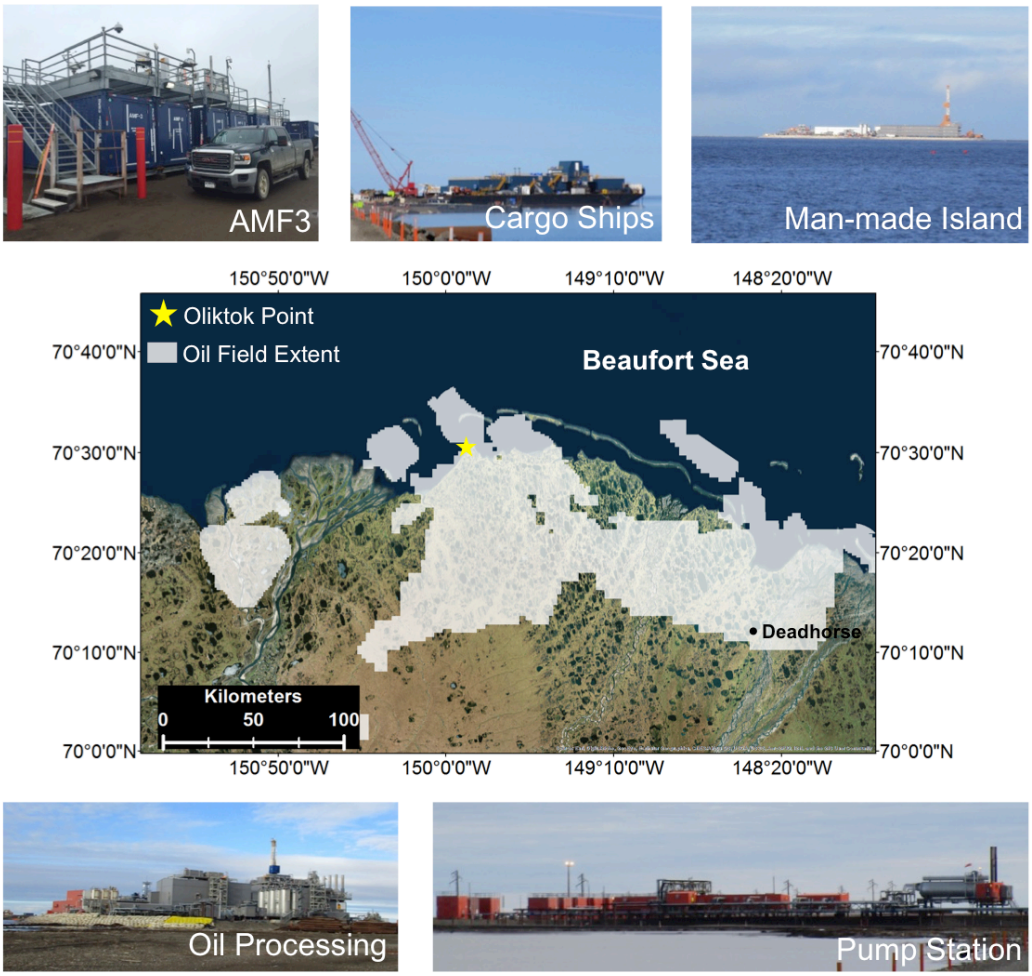

Figure 6.1. Map of Prudhoe Bay oil fields and images of local sources near AMF3 field site, as indicated by a yellow star. The map background was provided by ArcGIS 10.3.1 with the World Imagery basemap (Sources: Esri, DigitalGlobe, GeoEye, Earthstar Geographics, CNES/Airbus DS, USDA, USGS, AeroGRID, IGN, and the GIS User Community). Oil field extent obtained from http://dog.dnr.alaska.gov. Photo Credit: Matthew Gunsch.

6.2. Methods

6.2.1. Field Site and Instrumentation.

From August 22 – September 17, 2016, atmospheric measurements were conducted at the Atmospheric Radiation Measurement (ARM) Mobile Facility (AMF3) located at Oliktok Point, Alaska (70°29'41.4" N, 149°53'10.9" W). The surrounding Prudhoe Bay oil fields, located both on-shore and off-shore total over 14,000 km^2 of land (Figure 6.1, http://dog.dnr.alaska.gov). The Beaufort Sea is located ~0.5 km to the north, northwest, and northeast, as well as ~1 km to the east. Meteorological data, including wind speed, wind direction, relative humidity, and

temperature, were obtained from a Waisala WXT520 weather transmitter at a height of ~10 m. Radiation measurements were collected by the "Sky Radiation System", a collection of radiometers. Carbon dioxide (CO_2) levels were measured by a cavity ringdown spectrometer (model G2301, Picarro) from a height of ~10 m.

Within the ARM AMF3, air was sampled at a height of 5.4 m through a PM_{10} teflon-coated aluminum cyclone (URG Corporation) at a flow rate of 40 L min^{-1}. Downstream, a stainless steel cylindrical manifold split the flow into dedicated, foam-insulated copper sampling lines for each of the following instruments. An aerosol time-of-flight mass spectrometer (ATOFMS) measured the size and chemical composition of individual 0.07 – 1.6 μm particles (vacuum aerodynamic diameter) in real time (Section 6.2.2). Black carbon (BC) mass concentrations were measured by a seven wavelength aethalometer (model AE42, Magee Scientific). Aerosol particle size distributions (13 - 746 nm mobility diameter and 0.5 – 20 μm aerodynamic diameter) were measured using a scanning mobility particle sizer (SMPS, model 3082, TSI, Inc.) and an aerodynamic particle sizer (APS, model 3321, TSI, Inc.), respectively. Using the method of Khlystov et al. (2004), the SMPS and APS size distributions were combined into a single continuous particle size distribution from 0.013 – 2.5 μm (aerodynamic diameter), assuming a shape factor of 1 and density of 1.5 g cm^{-3}.

6.2.2. ATOFMS.

An ATOFMS, based on the design of Pratt et al. (2009b), measured the size and chemical composition of 32,880 individual aerosol particles (0.07 – 1.6 μm, vacuum aerodynamic diameter) in real-time. Briefly, particles were focused through an aerodynamic lens system and entered the sizing region as a narrow, collimated beam. Particle diameter, calibrated using polystyrene latex spheres (Polysciences, Inc.) of known diameter (0.09 – 2 μm) and density (1 g cm^{-3}), was calculated using the time each particle took to traverse two continuous wave lasers (50 mW 405 nm and 50 mW 488 nm, Coherent Technol.). The particles then entered a dual-polarity reflectron time-of-flight mass spectrometer (Tofwerk) and were individually desorbed and ionized by a 266 nm Nd:YAG pulsed laser (Centurion, Quantel, Inc.), operating at 0.8 – 1.2 mJ, resulting in positive and negative ion mass spectra. Prior to ATOFMS analysis, particles were dried in-line through two silica gel diffusion driers; however, negative ion mass spectra were collected for only 63% of particles, by number, due to the accumulation of water that

suppressed negative ion formation (Neubauer et al., 1997), a phenomenon commonly observed in other marine environments (Spencer et al., 2008).

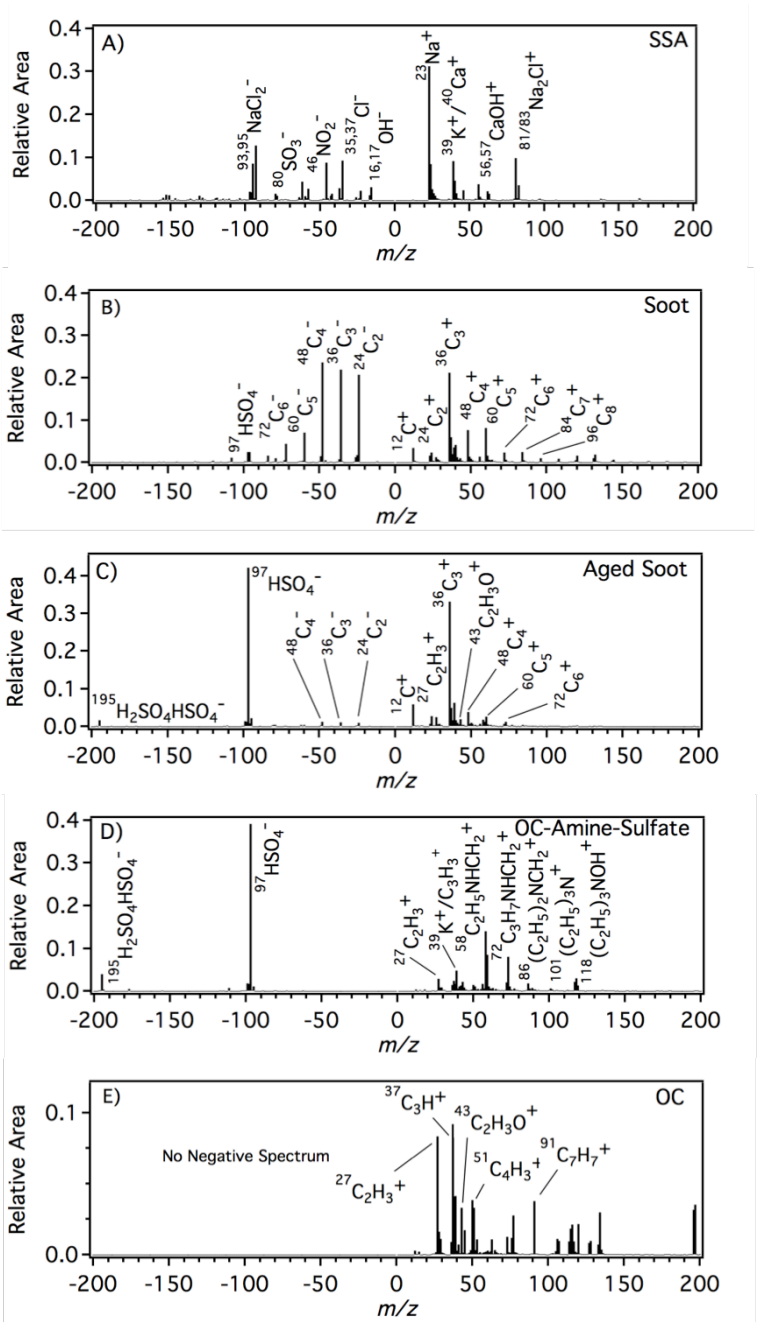

Figure 6.2. Average individual particle ATOFMS mass spectra for major particles types observed: **(A)** sea spray aerosol (SSA), **(B)** soot, **(C)** aged soot, **(D)** organic carbon (OC)-amine-sulfate, **(E)** OC.

Individual particle mass spectra were imported and analyzed in FATES, a custom single particle mass spectrometer analysis toolkit for MATLAB (MathWorks) (Sultana et al., 2017). Individual particle mass spectra were clustered based on the presence and intensity of ion peaks using an ART-2a neural network algorithm with a vigilance factor of 0.8 and a learning rate of 0.05 for 20 iterations (Song et al., 1999). The resulting clusters were grouped into eight unique clusters, each representing an individual particle type, based on the most likely *m/z* assignments, according to ion ratios and spectral identification from previous laboratory and field campaigns (Pratt and Prather, 2009). Using the method of Qin et al. (2006), ATOFMS particle numbers were scaled using the SMPS and APS data (converted to aerodynamic diameter, as described in Section 6.2.1.) to obtain chemically-resolved number and mass concentrations. A density of 1.4 g/cm^3 was assumed for organic carbon (OC), soot, OC-

amine-sulfate, aged soot, and incineration particles; a density of 2.1 g/cm^3 was used for mineral dust, and a density of 1.5 g/cm^3 was applied for biomass burning (BB) and sea spray aerosol (SSA) (Moffet et al., 2008; Qin et al., 2012; Spencer et al., 2007).

6.3. Results and Discussion

6.3.1. Single Particle Chemical Characterization.

From August 22 – September 17, 2016, eight unique individual particle types were identified by ATOFMS: sea spray aerosol (SSA), organic carbon (OC), soot, aged soot, organic carbon-amine-sulfate (OC-amine-sulfate), biomass burning (BB), mineral dust and incineration particles (Figures 6.2 and D.1). BB, dust, and incineration particles each contributed 8%, 3%, and 1% of the 0.07 – 1.6 μm particle number concentrations, respectively; therefore, analysis here focuses on the characteristics and contributions of the most abundant particle types: OC, soot, aged soot, OC-amine-sulfate, and SSA. Mass spectra of the minor particle types are shown and described in the supplemental information (Figure D.1). SSA was characterized by *m/z* 23 (Na^+) with minor ion peaks at *m/z* 39 (K^+), 40 (Ca^+), 56 (CaO^+), 57 ($CaOH^+$), and 81, 83 (Na_2Cl^+), as well as *m/z* -35, -37 (Cl^-), and -93, -95 ($NaCl_2^-$) (Prather et al., 2013). Individual OC particles were identified by characteristic organic carbon ion peaks at *m/z* 27 ($C_2H_3^+$), 37 (C_3H^+), and 43 ($C_2H_3O^+$) (Qin et al., 2012; Silva and Prather, 2000; Spencer et al., 2006); negative ion mass were not observed due to ion suppression from the accumulation of water (Neubauer et al., 1997) during atmospheric transport.

OC-amine-sulfate particles were characterized by organic carbon (*m/z* 27, $C_2H_3^+$) and sulfate (*m/z* -97, HSO_4^-) ion markers, as well as unique contributions from diethylamine (DEA, *m/z* 58, 73, $C_2H_5NHCH_2^+$, $C_3H_7NHCH_2^+$), trimethylamine (TMA, *m/z* 59, $N(CH_3)_3^+$), triethylamine (TEA, *m/z* 86, 101, $(C_2H_5)_2NCH_2^+$, $(C_2H_5)_3N^+$), and triethylamine-oxide (TEAO, *m/z* 118, $C_2H_5)_3NOH^+$) (Angelino et al., 2001). The OC-amine-sulfate particle mass spectra also included sulfuric acid cluster ions (*m/z* -195, $H_2SO_4HSO_4^-$), indicative of particle acidity (Pratt et al., 2009a), which could aid in the formation of aminium salts (Pratt et al., 2009a). While the presence of TMA can be associated with biogenic marine emissions (Köllner et al., 2017; Willis et al., 2016) the observed particles in the present study also have intense peaks corresponding to ethylamines, which are not associated with biogenic sources but instead with anthropogenic sources, including vehicular combustion and industrial processes (Angelino et al., 2001; Ge et

al., 2011; Huang et al., 2012). The OC-amine-sulfate mass spectral signature was consistent throughout the study, suggesting a single source for these amines. Ethylamines are commonly used in many oil and gas drilling processes as corrosion inhibitors, drilling fluid additives, and within solutions used to treat sour (high sulfur content) natural gas (Kadnar, 1999; Patel et al., 2007; Tam et al., 1990). These processes are currently used within Prudhoe Bay to treat sour gas, and will continue to be used as the Prudhoe Bay oil fields becomes more sour over time (Fingas, 2010). Therefore, these OC-amine-sulfate particles are most likely from natural gas extraction and treatment activities within the Prudhoe Bay oil fields.

Soot particle mass spectra featured both positive and negative carbon cluster ions ($C_n^{+/-}$) (Toner et al., 2008; Toner et al., 2006), with phosphate (*m/z* -79, PO_3^-), likely originating from diesel generators and heavy duty vehicles, due to phosphate-based additives in lubricating oils used for diesel engines (Spencer et al., 2006). Aged soot particles, also likely from diesel combustion, were identified by carbon cluster ions ($C_n^{+/-}$), as well as hydrocarbon peaks (*m/z* 27, $C_2H_3^+$, and 43, $C_2H_3O^+$), sulfate (*m/z* -97, HSO_4^-), and sulfuric acid (*m/z* -195, $H_2SO_4HSO_4^-$) (Moffet and Prather, 2009; Pratt et al., 2009a), The soot and aged soot average single particle mass spectra were compared to ATOFMS mass spectra previously collected during diesel source studies (Toner et al., 2008); A higher calculated dot product indicates greater similarity between the ambient and source particle mass spectra (dot product of 1 = identical), whereas a lower dot product indicates less similarity (dot product of 0 = no similarity) (Pratt and Prather, 2009). Both soot and aged soot showed a high degree of similarity (dot products of 0.71 and 0.45 for fresh and aged soot, respectively) compared to individual diesel particle mass spectra (Toner et al., 2008). Aged soot has a lower dot product due to the accumulation of secondary species, including sulfate (*m/z* -97, HSO_4^-) and oxidized organic carbon (*m/z* 43, $C_2H_3O^+$), which reduces the similarity compared to a freshly emitted particle (Pratt and Prather, 2009). It should be noted that fresh soot also has minor contributions from sulfate (Toner et al., 2008). If the secondary species were removed from the aged soot particles, the resulting mass spectra are expected to be identical to those of the fresh soot, resulting in an elevated dot product (Pratt and Prather, 2009). Comparing each of the carbonaceous particle types (OC and OC-amine-sulfate) to mass spectra from gasoline-powered combustion aerosol emissions (Toner et al., 2008) resulted in dot products less than 0.01, further confirming the lack of gasoline combustion activities within the oil field. Therefore, it is likely that the soot is from diesel combustion, and the aged soot particles

originated from diesel combustion and gained secondary aerosol mass during transport across the oil field.

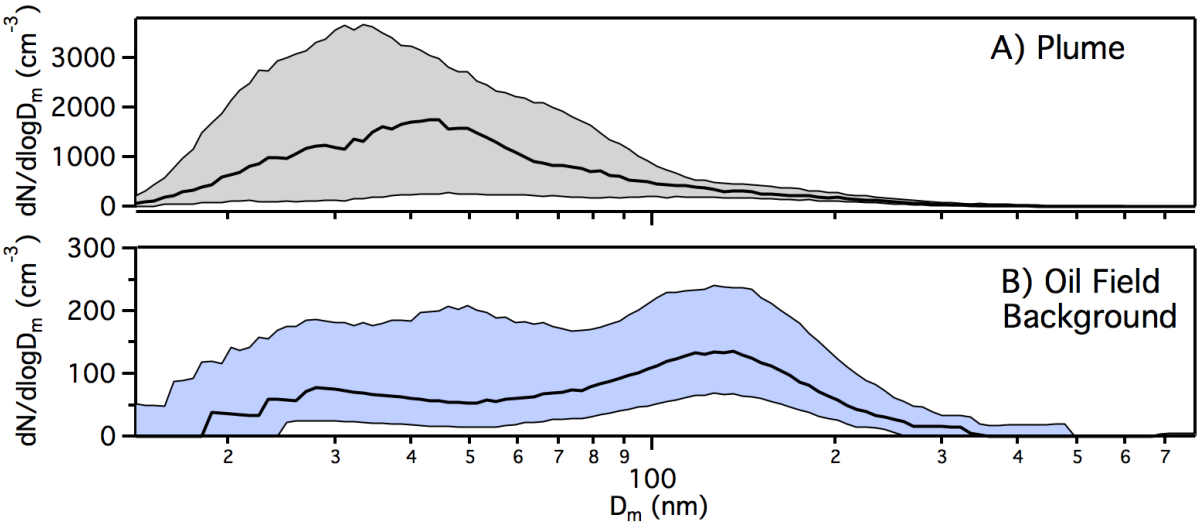

Figure 6.3. Median aerosol size-resolved number concentrations (13 - 746 nm mobility diameter, D_m) and 25th/75th percentiles, measured by SMPS, during **(A)** direct plume and **(B)** oil field background air mass periods at Oliktok Point, AK.

6.3.2. Oil Field Plume Characterization. Over the course of the study the field site was continually influenced by oil and gas extraction emissions from all directions (Figure 6.1). Frequently, the site was impacted by direct emission plumes, defined by elevated BC mass concentrations (greater than 0.2 μg/m^3) as measured by the aethalometer and/or CO_2 mole ratios (greater than 397 ppm). Both black carbon and CO_2, at these levels, are indicative of anthropogenic combustion from within the oil fields (Brooks et al., 1997; Jaffe et al., 1995). Plumes impacted the field site for 29% of the time between August 22 and September 17, 2016, with the remainder of the time classified as oil field background air mass periods, discussed in Section 6.3.3.

Within plume periods, elevated $PM_{2.5}$ aerosol number and mass concentrations were observed (average 1400 particles cm^{-3} and 2.6 μg/m^3). These increases in particle number and mass were driven mainly by the significant increase in sub-100 nm particles (average particle number mode of 50 nm, Figure 6.3 and D.4.), attributed to fresh combustion emissions (Wallace and Hobbs, 2006). A Kolmogorov-Smirnov goodness-of-fit statistical test shows that above 200 nm, the aerosol number distributions during plume and oil field background air mass periods

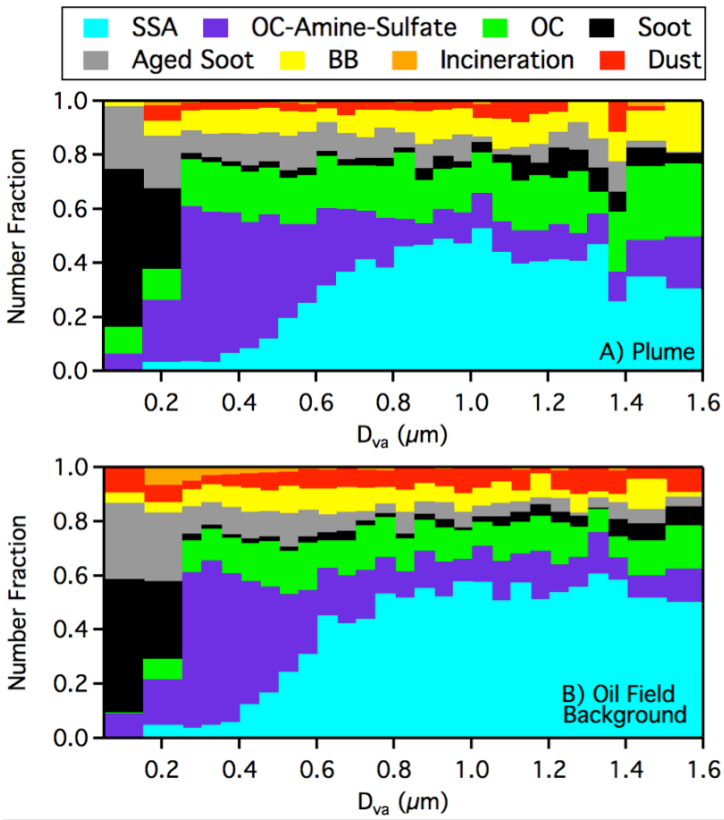

Figure 6.4. Size-resolved number fractions of ATOFMS individual particle types (0.07 – 1.6 μm), with 0.05 μm resolution bins shown between 0.25 – 1.4 μm and 0.1 μm resolution shown for < 0.25 μm and > 1.4 μm during (A) direct plume and (B) oil field background air mass periods at Oliktok Point, AK. Particle types include sea spray aerosol (SSA), organic carbon (OC)-amine-sulfate, organic carbon (OC), soot, aged soot, biomass burning (BB), incineration, and dust.

were statistically similar ($\sigma = 0.05$). While it is expected that during plumes particles will have increased condensed secondary species, these do not add enough mass to lead to a diameter change. This further indicates that the plumes are primarily adding ultrafine combustion particles to the oil field background aerosol distribution (Section 6.3.3).

From August 22 – September 17, 2016, 15,682 individual particles (0.07 – 1.6 μm) were chemically characterized by ATOFMS during direct emission plumes (Figure 6.4). During the maximum number concentration observed on August 27, ~80% of the 0.07 – 1.6 μm particles, by number, corresponded to fresh and aged soot (Figure 6.6); this was a relatively stagnant period with wind (3 m/s) shifting from the northerly ocean to the oil extraction facilities to the south/southwest (Figure D.3). Also on this day, heavy machinery was used to move an oil rig on the nearby road to the east over the course of 12 h during the day of August 27 and provided a significant local source of soot from diesel combustion. The 0.07 – 1.6 μm aerosol mass concentrations reached a maximum of ~5 μg/m^3 on August 29 due to significant contributions from SSA (1.6 μg/m^3) (Figure 6.6) produced from oceanic wave-breaking during a period of elevated wind speed (~10 m/s) with air arriving from the open ocean ~0.5 km to the north of the field site (Figure D.3).

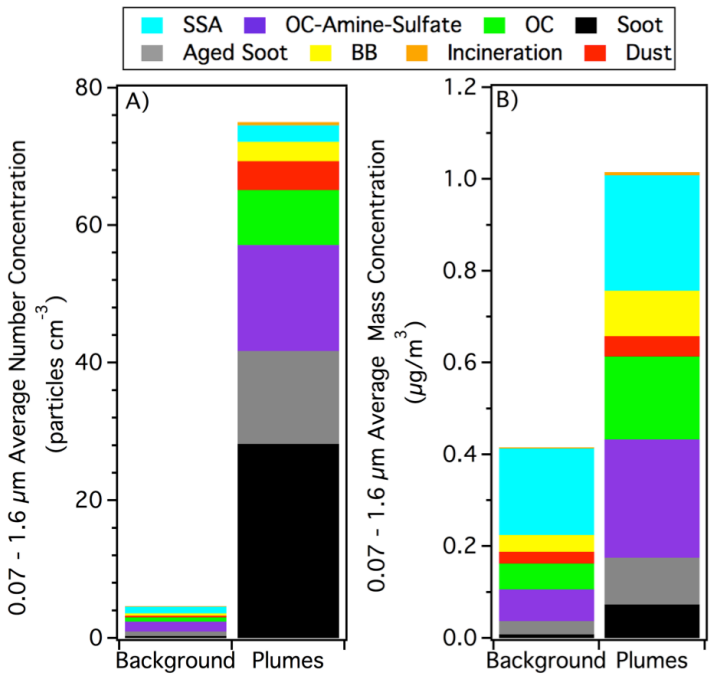

Figure 6.5. Chemically resolved average **(A)** number and **(B)** mass concentrations for 0.07 – 1.6 μm particles, measured by ATOFMS, during oil field background and direct plume air mass influence periods at Oliktok Point, AK.

Overall, the number concentrations were dominated by soot (38% fresh soot, 18% aged soot, by number) and organic carbon (11% OC, 21% OC-amine-sulfate, by number) particles from oil and gas extraction activities (Figures 6.5 and 6.6) involving diesel and natural gas combustion. Fresh soot particles were primarily less than 200 nm, and accounted for 40%, by number, of the 70 – 200 nm particles during both plume and oil field background periods (Figure 6.4). OC-amine-sulfate particles were primarily detected with diameters less than 700 nm and contributed ~60% of the particles, by number, between 300-500 nm during plumes (Figure 6.4). Increased average mass of soot (0.07 μg/m^3), aged soot (0.11 μg/m^3), OC (0.18 μg/m^3) and OC-amine-sulfate (0.26 μg/m^3) particles were also observed (Figure 6.5). $PM_{2.5}$ BC mass concentrations (aethalometer) averaged 0.39 ± 0.04 μg/m^3 (95% confidence interval) during plumes (with brief, extreme spikes in BC mass concentrations up to a maximum ~8 μg/m^3 on August 28), indicating that an average of ~0.2 μg/m^3 of soot was below the size cut (0.07 μm) of the A-ATOFMS during plume influence, further supporting the contribution of combustion emissions to the elevated ultrafine particle concentration.

During plumes, sulfate (HSO_4^-, *m/z* -97) was internally mixed with 97% of aged soot and 91% of OC-amine-sulfate particles, by number. Only 29% of the fresh soot particles, by number, contained sulfate, consistent with local emissions. In addition, ~60% of aged soot, ~50% of OC-amine-sulfate, and ~10% of OC particles, by number, were internally mixed with oxidized organic carbon (*m/z* 43, $C_2H_3O^+$) a marker of secondary organic aerosol (Qin et al., 2012), during

plumes. Soot and aged soot particles internally mixed with OC and sulfate may have increased light absorption characteristics (e.g. Jacobson, 2001; Moffet et al., 2008) that could impact Arctic warming (Flanner, 2013); however, the extent of the impact of these coatings on soot absorption properties is not clear (e.g. Cappa et al., 2012; Healy et al., 2015). Notably, soot particles internally mixed with nitrate and sulfate have been shown to have increased CCN activity (Bond et al., 2013).

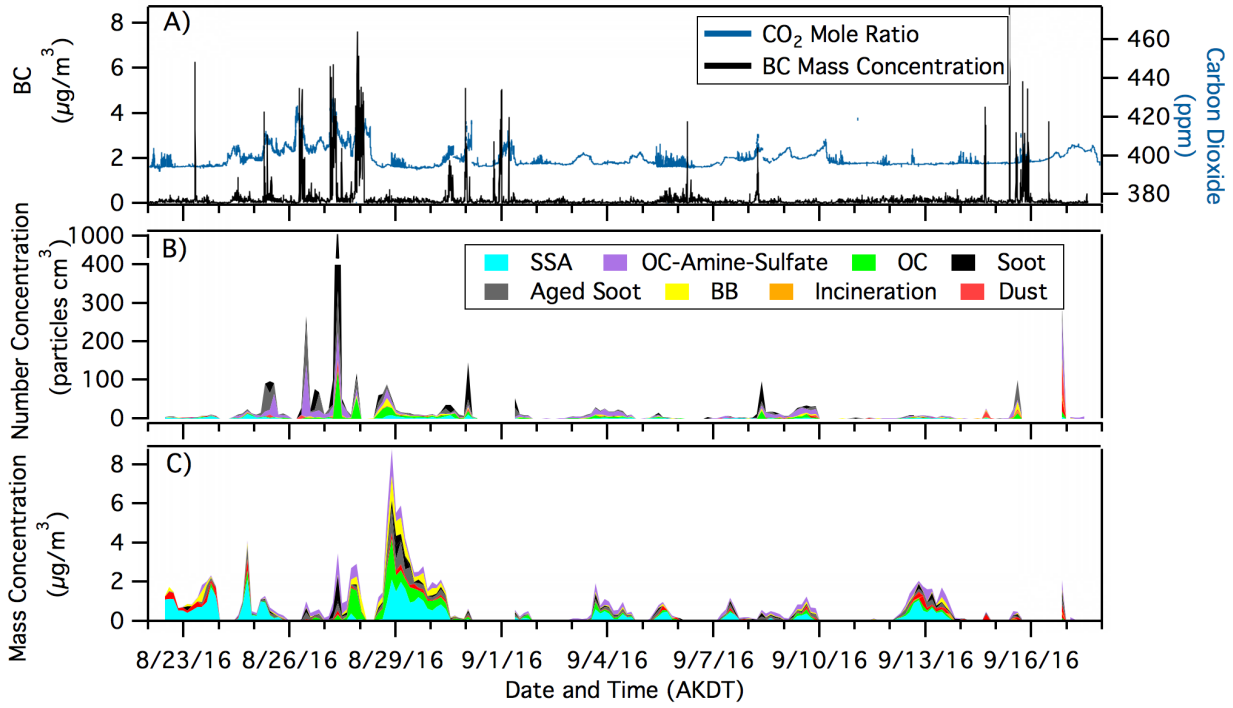

Figure 6.6. (A) Black carbon (BC) mass concentrations, CO_2 mole ratios, and 3 h time resolution chemically-resolved **(B)** number and **(C)** mass concentrations (0.07 – 1.6 μm), based on ATOFMS measurements.

Even within the plumes, SSA accounted for a significant portion (0.25 μg/m^3) of the total mass and contributed ~40%, by number, to the 0.8 – 1.6 μm particles (Figure 6.4). The SSA mass concentration was similar during background periods (0.19 μg/m^3, Section 6.3.3), with the local open water surrounding the field site from 230° - 20° episodically influencing both plume and background periods based on local winds. In order to investigate possible differences in SSA particle mass spectra during plume and oil field background periods, the average dual-polarity SSA spectrum from the plumes was subtracted from the average SSA mass spectra from the oil field background periods (Figure 6.7). This subtraction plot depicts increased intensity in sodium

nitrate (*m/z* -131, $NaNO_2NO_3^-$ and -147, $Na(NO_3)_2^-$) and sodium sulfate (*m/z* -119, $NaSO_4^-$ and +165, $Na_3SO_4^+$) ion peaks in the SSA particles present during plumes, as well as increased intensity in the nitrate (*m/z* -46, NO_2^-, and -62, NO_3^-) and sulfate (*m/z* -80, SO_2^-) ion markers, all indicative of atmospheric multi-phase processing of SSA (Ault et al., 2014; Gard et al., 1998). Consistent with this, during plume periods greater number fractions of SSA particles contained nitrate (77%, by number) and sulfate (40%, by number), both indicative of chloride displacement, due to multiphase reactions involving precursor combustion emission trace gases (SO_2 and NO_x) and their oxidation products (Gard et al., 1998; Hara et al., 1999; Hara et al., 2003). Note that *m/z* -80 is used to identify sulfate instead of *m/z* -97 due to an interference with $NaCl_2$ at *m/z* -97 (Qin et al., 2012).

6.3.3. Oil Field Background Aerosol Characterization.

During oil field background air mass periods, when direct plume emissions were not observed, winds primarily arrived from the north/northeast, the direction of the prevailing winds (Figure D.3). During these periods, average $PM_{2.5}$ number and concentrations were 307 particles cm^{-3} and 1.2 $\mu g/m^3$, respectively, with a particle number mode of 105 nm (Figure 6.3). The oil field background particle concentrations are higher than those observed during August – September at other Arctic locations, including Station Nord, Greenland (227 particles cm^{-3}, Nguyen et al., 2016), Tiksi, Russia (222 particles cm^{-3}, Asmi et al., 2016), Utqiaġvik, AK (190 particles cm^{-3} when under Arctic Ocean influence, Gunsch et al., 2017), and the central Arctic Ocean (90 - 210 particles cm^{-3}, Heintzenberg et al., 2015). $PM_{2.5}$ BC measurements (aethalometer) recorded an average mass concentration of 0.089 ± 0.002 $\mu g/m^3$ (95% confidence interval), nearly double the 0.05 $\mu g/m^3$ cut-off that is typically used when classifying clean marine environments (Gantt and Meskhidze, 2013). These data support that the "background" periods are more representative of regional Arctic oil field conditions, with the extent of nearby oil fields over 14,000 km^2 wide (Figure 6.1), than a "clean" Arctic background.

During oil field background periods, ATOFMS sampled 17,198 particles between 0.07 and 1.6 μm. The oil field background periods were primarily characterized by soot (soot and aged soot) and organic carbon (OC and OC-amine-sulfate) particles, by number (Figure 6.5), due to the regional influence from oil and gas extraction activities surrounding the field site. Sulfate and oxidized OC were internally mixed with 95% and 56% of the measured aged soot particles,

by number, and 89% and 50% of OC-amine-sulfate particles, by number, respectively. In addition, 12% of the fresh soot, by number, was internally mixed with sulfate. The number percentages of particles internally mixed with sulfate and oxidized OC were similar to the plume periods, further indicating that the field site was constantly under the influence of oil and gas extraction emissions.

During oil field background periods, 46%, of 0.07 – 1.6 μm particle mass was comprised of SSA (0.19 μg/m^3) due to the close proximity (0.5 km) of the site to open ocean. Markers of fresh SSA, including intense Na_xCl_y ion clusters at *m/z* 81, 83 (Na_2Cl^+), *m/z* 58, 60 ($NaCl^-$), *m/z* -93, -95 ($NaCl_2^-$), and *m/z* -151, -153, -155, -157 ($Na_2Cl_3^-$) as well as intense chloride peaks at *m/z* -35, -37 (Cl^-), are consistent with local SSA production (Figure 6.7). Some of these ion markers were also present in aged SSA, indicating that complete chloride displacement has not occurred, similar to previous observation in Utqiaġvik, AK during Prudhoe Bay influence (Gunsch et al., 2017). As shown in in Figure 6.7, the Na_xCl_y ion peaks were more intense in oil field background SSA particles compared to plume period SSA particles, indicative of less atmospheric aging. During the oil field background periods, 45% and 16% of the SSA, by number, were internally mixed with nitrate and sulfate, respectively, from chloride displacement (Ault et al., 2014; Gard et al., 1998; Hara et al., 1999; Hara et al., 2003).

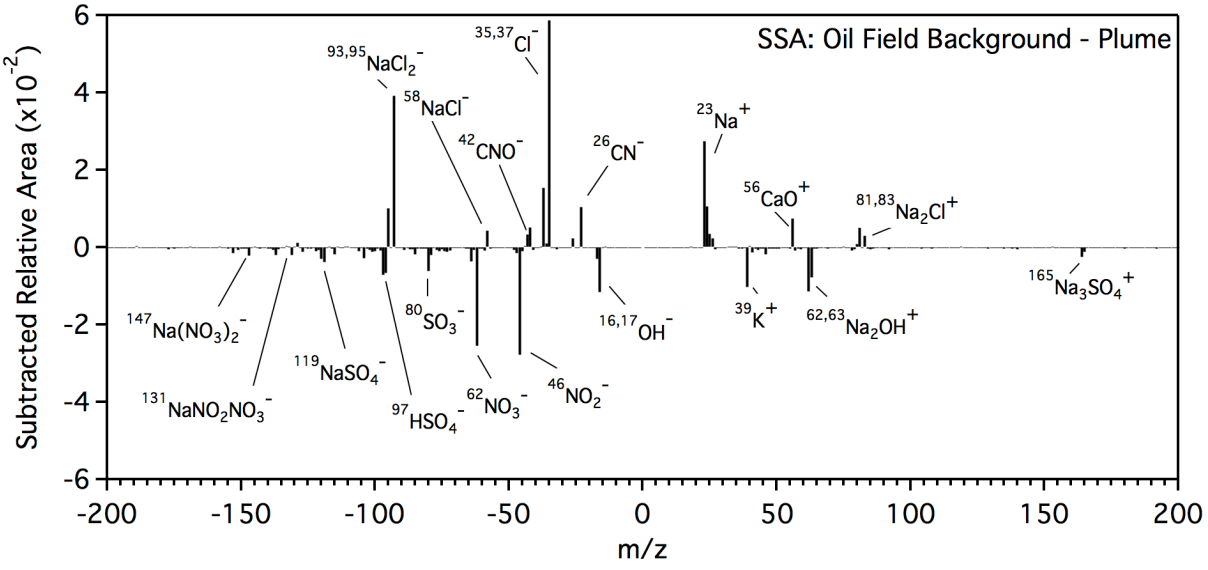

Figure 6.7. ATOFMS mass spectral subtraction plot of average individual SSA particle mass spectra during oil field background minus the corresponding direct plume air mass periods. Positive values show higher intensity *m/z* peaks during oil field background conditions, and negative values indicate greater intensities during direct plume periods.

6.3.4. Observed Aerosol Particle Growth.

A unique period of aerosol growth was observed between August 24 – 27 during an oil field background period(Figure D.2); this period was not included in the previously discussed background averages. Two individual events were observed, one from August 24 06:00 – August 25 20:00 AKDT and a second from August 26 06:00 – August 27 00:00. Wind direction did not shift during individual growth periods, suggesting that the observed aerosol growth was not associated with dilution in a shifting plume. During both events, winds were relatively stagnant (~4 m/s), with increased solar radiation (132 W/m^2) and temperature (9°C) compared to the study average (69 W/m^2 and 3°C, respectively). The events both had starting diameters ~20 nm and ending diameters ~50 nm, with growth rates of 0.8 nm/h and 1.6 nm/h, respectively. Both of these growth rates are lower than the average growth rate observed by Kolesar et al. (2017) during Prudhoe Bay influence (2.5 ± 2.7 nm/h), however this may be impacted by the limited sample size of the current study compared to six years of analysis by Kolesar et al. (2017) Both growth events occurred during condensation sink minima (~2 x 10^{-2} s^{-1}), compared to an average of 2 x 10^{-1} s^{-1} for the rest of the study (Figure D.5); these values were calculated using the methods of Dal Maso et al. (2002) using particle number size distributions. While this condensation sink is orders of magnitude higher than previously observed during aerosol growth in clean Arctic environments (2 x 10^{-3} s^{-1}; Kolesar et al., 2017), stagnant winds combined with elevated oxidants and condensable material from the surrounding oil and gas extraction activities likely contributed to the observed aerosol growth. Condensation sinks of ~2 x 10^{-2} s^{-1} were also observed between September 5 and September 10; however, elevated wind speeds during this period (~10 m/s) likely hindered aerosol growth from occurring. Notably, the number fraction of 0.07 – 1.6 μm OC-amine-sulfate particles increased as these events progressed, beginning at <10% and reaching a maximum of 68% at 11:00 AKDT on August 26, similar to previous observations of amine contributions to fine particles during ultrafine growth at a remote site in northern California (Creamean et al., 2011). Previous studies have found that amines contribute to new particle formation and growth (Almeida et al., 2013; Smith et al., 2010; Tao et al., 2016), with greater contributions expected in colder climates (Chen and Finlayson-Pitts, 2016).

6.4. Atmospheric Implications

Here we report the first single particle chemical characterization of atmospheric aerosols in the Prudhoe Bay oil fields, the third largest oil field in North America (EIA, 2015). Throughout the study, combustion emission plumes originating from nearby oil and gas extraction facilities were characterized, and at no time was the site not influenced by oil field emissions. The vast majority of particles observed within direct plumes (~90% of the number concentration) were ultrafine particles (sub-100 nm in diameter), attributed to fresh combustion. Plumes primarily consisted of soot and organic carbon particles, by both number and mass, as expected based on models of emissions by Peters et al. (2011), with >90% of these particles internally mixed with sulfate, attributed to SO_2 emissions from diesel and natural gas combustion processes within the oil field. The presence of sulfate and oxidized organic carbon in soot particles may increase absorption characteristics of the particles (e.g. Chung and Seinfeld, 2005; Jacobson, 2001; Knox et al., 2009; Liu et al., 2015; Moffet and Prather, 2009), though the extent is unclear. In addition, soot aging increases CCN activity (Bond et al., 2013). With on-going expansion of Arctic oil and gas extraction activities, these impacts will likely continue increasing. Aminium sulfate salts likely contributed to observed particle growth during oil field background air mass influence, and may explain the preferential aerosol growth observed by Kolesar et al. (2017) at Utqiaġvik, AK during Prudhoe Bay influenced air masses, compared to clean Arctic Ocean air masses. With the use of ethylamines expected to increase on the North Slope of Alaska due to planned liquefied natural gas pipelines (Ruester and Neumann, 2008) and carbon capture efforts (Rao and Rubin, 2002; Rochelle, 2009), the likely contribution of these compounds to new particle formation and growth should be considered in evaluating the climate impacts of the oil and gas extraction activities.

6.5. Acknowledgements

Matthew Gunsch ran the A-ATOFMS, SMPS, and APS throughout the study. Claire Moffett provided aethalometer data and assistance throughout the study. This study was supported by the NOAA Climate Program Office Atmospheric Chemistry, Carbon Cycle, and Climate Program through NA14OAR4310149 (University of Michigan) and NA14OAR4310150 (Baylor University). Funding for lodging and logistical support was provided by Department of Energy Atmospheric Radiation Measurement (DOE ARM) field campaign 2013-6660. Meteorological,

greenhouse gas, and ACSM data were obtained from the ARM Climate Research Facility, a U.S. Department of Energy Office of Science user facility sponsored by the Office of Biological and Environmental Research. DOE ARM, Sandia National Laboratory, AMF3 field operators, and the U.S. Air Force are thanked for logistical assistance at Oliktok Point, AK.

6.6. References

Allison, E.H., Bassett, H.R., 2015. Climate change in the oceans: Human impacts and responses. Science 350, 778-782.

Almeida, J., Schobesberger, S., Kürten, A., Ortega, I.K., Kupiainen-Määttä, O., Praplan, A.P., Adamov, A., Amorim, A., Bianchi, F., Breitenlechner, M., 2013. Molecular understanding of sulphuric acid-amine particle nucleation in the atmosphere. Nature 502, 359-363.

Angelino, S., Suess, D.T., Prather, K.A., 2001. Formation of aerosol particles from reactions of secondary and tertiary alkylamines: Characterization by aerosol time-of-flight mass spectrometry. Environ. Sci. Technol. 35, 3130-3138.

Asmi, E., Kondratyev, V., Brus, D., Laurila, T., Lihavainen, H., Backman, J., Vakkari, V., Aurela, M., Hatakka, J., Viisanen, Y., 2016. Aerosol size distribution seasonal characteristics measured in Tiksi, Russian Arctic. Atmos. Chem. Phys. 16, 1271-1287.

Ault, A.P., Guasco, T.L., Baltrusaitis, J., Ryder, O.S., Trueblood, J.V., Collins, D.B., Ruppel, M.J., Cuadra-Rodriguez, L.A., Prather, K.A., Grassian, V.H., 2014. Heterogeneous reactivity of nitric acid with nascent sea spray aerosol: Large differences observed between and within individual particles. J. Phys. Chem. Lett. 5, 2493-2500.

Bond, T.C., Doherty, S.J., Fahey, D., Forster, P., Berntsen, T., DeAngelo, B., Flanner, M., Ghan, S., Kärcher, B., Koch, D., 2013. Bounding the role of black carbon in the climate system: A scientific assessment. J. Geophys. Res-Atmos. 118, 5380-5552.

Brock, C.A., Cozic, J., Bahreini, R., Froyd, K.D., Middlebrook, A.M., McComiskey, A., Brioude, J., Cooper, O., Stohl, A., Aikin, K., 2011. Characteristics, sources, and transport of aerosols measured in spring 2008 during the aerosol, radiation, and cloud processes affecting Arctic Climate (ARCPAC) Project. Atmos. Chem. Phys. 11, 2423-2453.

Brooks, S.B., Crawford, T.L., Oechel, W.C., 1997. Measurement of carbon dioxide emissions plumes from Prudhoe Bay, Alaska oil fields. J. Atmos. Chem. 27, 197-207.

Cappa, C.D., Onasch, T.B., Massoli, P., Worsnop, D.R., Bates, T.S., Cross, E.S., Davidovits, P., Hakala, J., Hayden, K.L., Jobson, B.T., 2012. Radiative absorption enhancements due to the mixing state of atmospheric black carbon. Science 337, 1078-1081.

Chen, H., Finlayson-Pitts, B.J., 2016. New Particle Formation from Methanesulfonic Acid and Amines/Ammonia as a Function of Temperature. Environ. Sci. Technol. 51, 243-252.

Chung, S.H., Seinfeld, J.H., 2005. Climate response of direct radiative forcing of anthropogenic black carbon. J. Geophys. Res-Atmos. 110.

Creamean, J.M., Ault, A.P., Ten Hoeve, J.E., Jacobson, M.Z., Roberts, G.C., Prather, K.A., 2011. Measurements of Aerosol Chemistry during New Particle Formation Events at a Remote Rural Mountain Site. Environ. Sci. Technol. 45, 8208-8216.

Creamean, J.M., Maahn, M., de Boer, G., McComiskey, A., Sedlacek, A.J., Feng, Y., 2017. The influence of local oil exploration, regional wildfires, and long range transport on summer 2015 aerosol over the North Slope of Alaska. Atmos. Chem. Phys. Discuss. 2017, 1-27.

Dal Maso, M., Kulmala, M., Lehtinen, K., Mäkelä, J., Aalto, P., O'Dowd, C., 2002. Condensation and coagulation sinks and formation of nucleation mode particles in coastal and boreal forest boundary layers. J. Geophys. Res-Atmos. 107, 8097.

EIA, 2015. Top 100 U.S. Oil and Gas Fields. U.S. Department of Energy.

Fawole, O.G., Cai, X.-M., MacKenzie, A., 2016. Gas flaring and resultant air pollution: A review focusing on black carbon. Environmental Pollution 216, 182-197.

Fingas, M., 2010. Review of the North Slope Oil properties relevant to environmental assessment and prediction. Spill Science, Edmonton, Alberta, Canada.

Flanner, M.G., 2013. Arctic climate sensitivity to local black carbon. J. Geophys. Res-Atmos. 118, 1840-1851.

Gantt, B., Meskhidze, N., 2013. The physical and chemical characteristics of marine primary organic aerosol: a review. Atmos. Chem. Phys. 13, 3979-3996.

Gard, E.E., Kleeman, M.J., Gross, D.S., Hughes, L.S., Allen, J.O., Morrical, B.D., Fergenson, D.P., Dienes, T., Gälli, M.E., Johnson, R.J., 1998. Direct observation of heterogeneous chemistry in the atmosphere. Science 279, 1184-1187.

Gautier, D.L., Bird, K.J., Charpentier, R.R., Grantz, A., Houseknecht, D.W., Klett, T.R., Moore, T.E., Pitman, J.K., Schenk, C.J., Schuenemeyer, J.H., 2009. Assessment of undiscovered oil and gas in the Arctic. Science 324, 1175-1179.

Ge, X., Wexler, A.S., Clegg, S.L., 2011. Atmospheric amines–Part I. A review. Atmos. Environ. 45, 524-546.

Gunsch, M.J., Kirpes, R.M., Kolesar, K.R., Barrett, T.E., China, S., Sheesley, R.J., Laskin, A., Wiedensohler, A., Tuch, T., Pratt, K.A., 2017. Contributions of transported Prudhoe Bay oil field emissions to the aerosol population in Utqiaġvik, Alaska. Atmos. Chem. Phys. 17, 10879-10892.

Hara, K., Osada, K., Hayashi, M., Matsunaga, K., Shibata, T., Iwasaka, Y., Furuya, K., 1999. Fractionation of inorganic nitrates in winter Arctic troposphere: Coarse aerosol particles containing inorganic nitrates. J. Geophys. Res-Atmos. 104, 23671-23679.

Hara, K., Yamagata, S., Yamanouchi, T., Sato, K., Herber, A., Iwasaka, Y., Nagatani, M., Nakata, H., 2003. Mixing states of individual aerosol particles in spring Arctic troposphere during ASTAR 2000 campaign. J. Geophys. Res-Atmos. 108.

Harsem, Ø., Heen, K., Rodrigues, J., Vassdal, T., 2015. Oil exploration and sea ice projections in the Arctic. Polar. Rec. 51, 91-106.

Healy, R.M., Wang, J.M., Jeong, C.H., Lee, A.K., Willis, M.D., Jaroudi, E., Zimmerman, N., Hilker, N., Murphy, M., Eckhardt, S., 2015. Light‐absorbing properties of ambient black carbon and brown carbon from fossil fuel and biomass burning sources. J. Geophys. Res-Atmos. 120, 6619-6633.

Heintzenberg, J., Leck, C., Tunved, P., 2015. Potential source regions and processes of aerosol in the summer Arctic. Atmos. Chem. Phys 15, 6487-6502.

Huang, Y., Chen, H., Wang, L., Yang, X., Chen, J., 2012. Single particle analysis of amines in ambient aerosol in Shanghai. Environmental Chemistry 9, 202-210.

IPCC, 2013. IPCC, 2013: climate change 2013: the physical science basis. Contribution of working group I to the fifth assessment report of the intergovernmental panel on climate change. Cambridge University Press.

Jacobson, M.Z., 2001. Strong radiative heating due to the mixing state of black carbon in atmospheric aerosols. Nature 409, 695-697.

Jacobson, M.Z., 2004. Climate response of fossil fuel and biofuel soot, accounting for soot's feedback to snow and sea ice albedo and emissivity. J. Geophys. Res-Atmos. 109.

Jaffe, D., Honrath, R., Furness, D., Conway, T., Dlugokencky, E., Steele, L., 1995. A determination of the CH4, NO x and CO2 emissions from the Prudhoe Bay, Alaska oil development. J. Atmos. Chem. 20, 213-227.

Kadnar, R., 1999. Determination of amines used in the oil and gas industry (upstream section) by ion chromatography. Journal of Chromatography A 850, 289-295.

Khlystov, A., Stanier, C., Pandis, S., 2004. An algorithm for combining electrical mobility and aerodynamic size distributions data when measuring ambient aerosol. Aerosol. Sci. Technol. 38, 229-238.

Knox, A., Evans, G., Brook, J., Yao, X., Jeong, C.-H., Godri, K., Sabaliauskas, K., Slowik, J., 2009. Mass absorption cross-section of ambient black carbon aerosol in relation to chemical age. Aerosol. Sci. Technol. 43, 522-532.

Kolesar, K.R., Cellini, J., Peterson, P.K., Jefferson, A., Tuch, T., Birmili, W., Wiedensohler, A., Pratt, K.A., 2017. Effect of Prudhoe Bay emissions on atmospheric aerosol growth events observed in Utqiaġvik (Barrow), Alaska. Atmos. Environ. 152, 146-155.

Köllner, F., Schneider, J., Willis, M.D., Klimach, T., Helleis, F., Bozem, H., Kunkel, D., Hoor, P., Burkart, J., Leaitch, W.R., Aliabadi, A.A., Abbatt, J.P.D., Herber, A.B., Borrmann, S., 2017. Particulate trimethylamine in the summertime Canadian high Arctic lower troposphere. Atmos. Chem. Phys. Discuss. 2017, 1-28.

Law, K.S., Stohl, A., 2007. Arctic air pollution: Origins and impacts. Science 315, 1537-1540.

Li, C., Hsu, N.C., Sayer, A.M., Krotkov, N.A., Fu, J.S., Lamsal, L.N., Lee, J., Tsay, S.-C., 2016. Satellite observation of pollutant emissions from gas flaring activities near the Arctic. Atmos. Environ. 133, 1-11.

Liu, S., Aiken, A.C., Gorkowski, K., Dubey, M.K., Cappa, C.D., Williams, L.R., Herndon, S.C., Massoli, P., Fortner, E.C., Chhabra, P.S., 2015. Enhanced light absorption by mixed source black and brown carbon particles in UK winter. Nat. Commun. 6.

Maahn, M., de Boer, G., Creamean, J.M., Feingold, G., McFarquhar, G.M., Wu, W., Mei, F., 2017. The observed influence of local anthropogenic pollution on northern Alaskan cloud properties. Atmos. Chem. Phys. Discuss. 2017, 1-23.

Mack, A., Bluemink, E., 2016. State receives $17.8 million in oil and gas lease sales. State of Alaska Department of Natural Resources.

Moffet, R.C., Prather, K.A., 2009. In-situ measurements of the mixing state and optical properties of soot with implications for radiative forcing estimates. Proc. Natl. Acad. Sci. 106, 11872-11877.

Moffet, R.C., Qin, X., Rebotier, T., Furutani, H., Prather, K.A., 2008. Chemically segregated optical and microphysical properties of ambient aerosols measured in a single‐particle mass spectrometer. J. Geophys. Res-Atmos. 113, D12213.

Neubauer, K.R., Johnston, M.V., Wexler, A.S., 1997. On-line analysis of aqueous aerosols by laser desorption ionization. Int. J. Mass. Spectrom. 163, 29-37.

Nguyen, Q.T., Glasius, M., Sørensen, L.L., Jensen, B., Skov, H., Birmili, W., Wiedensohler, A., Kristensson, A., Nøjgaard, J.K., Massling, A., 2016. Seasonal variation of atmospheric particle number concentrations, new particle formation and atmospheric oxidation capacity at the high Arctic site Villum Research Station, Station Nord. Atmos. Chem. Phys. 16, 11319-11336.

Overland, J.E., Wang, M., 2013. When will the summer Arctic be nearly sea ice free? Geophys. Res. Lett. 40, 2097-2101.

Patel, A., Stamatakis, S., Young, S., Friedheim, J., 2007. Advances in inhibitive water-based drilling fluids—can they replace oil-based muds?, International Symposium on Oilfield Chemistry. Society of Petroleum Engineers.

Peters, G., Nilssen, T., Lindholt, L., Eide, M., Glomsrød, S., Eide, L., Fuglestvedt, J., 2011. Future emissions from shipping and petroleum activities in the Arctic. Atmos. Chem. Phys. 11, 5305-5320.

Pöschl, U., 2005. Atmospheric Aerosols: Composition, Transformation, Climate and Health Effects. Angew. Chen. Int. Ed. 44, 7520 - 7540.

Prather, K.A., Bertram, T.H., Grassian, V.H., Deane, G.B., Stokes, M.D., DeMott, P.J., Aluwihare, L.I., Palenik, B.P., Azam, F., Seinfeld, J.H., 2013. Bringing the ocean into the laboratory to probe the chemical complexity of sea spray aerosol. Proc. Natl. Acad. Sci. 110, 7550-7555.

Pratt, K.A., Hatch, L.E., Prather, K.A., 2009a. Seasonal volatility dependence of ambient particle phase amines. Environ. Sci. Technol. 43, 5276-5281.

Pratt, K.A., Mayer, J.E., Holecek, J.C., Moffet, R.C., Sanchez, R.O., Rebotier, T.P., Furutani, H., Gonin, M., Fuhrer, K., Su, Y., 2009b. Development and characterization of an aircraft aerosol time-of-flight mass spectrometer. Anal. Chem. 81, 1792-1800.

Pratt, K.A., Prather, K.A., 2009. Real-time, single-particle volatility, size, and chemical composition measurements of aged urban aerosols. Environ. Sci. Technol. 43, 8276-8282.

Pratt, K.A., Prather, K.A., 2012. Mass spectrometry of atmospheric aerosols—Recent developments and applications. Part II: On‐line mass spectrometry techniques. Mass Spectrom. Rev. 31, 17-48.

Qin, X., Bhave, P.V., Prather, K.A., 2006. Comparison of two methods for obtaining quantitative mass concentrations from aerosol time-of-flight mass spectrometry measurements. Anal. Chem. 78, 6169-6178.

Qin, X., Pratt, K.A., Shields, L.G., Toner, S.M., Prather, K.A., 2012. Seasonal comparisons of single-particle chemical mixing state in Riverside, CA. Atmos. Environ. 59, 587-596.

Rao, A.B., Rubin, E.S., 2002. A technical, economic, and environmental assessment of amine-based CO2 capture technology for power plant greenhouse gas control. Environ. Sci. Technol. 36, 4467-4475.

Rochelle, G.T., 2009. Amine scrubbing for CO2 capture. Science 325, 1652-1654.

Roiger, A., Thomas, J.-L., Schlager, H., Law, K.S., Kim, J., Schäfler, A., Weinzierl, B., Dahlkötter, F., Krisch, I., Marelle, L., 2015. Quantifying emerging local anthropogenic emissions in the Arctic region: The ACCESS aircraft campaign experiment. B. Am. Meteorol. Soc. 96, 441-460.

Ruester, S., Neumann, A., 2008. The prospects for liquefied natural gas development in the US. Energy Policy 36, 3160-3168.

Screen, J.A., Simmonds, I., 2010. The central role of diminishing sea ice in recent Arctic temperature amplification. Nature 464, 1334-1337.

Sharma, S., Ishizawa, M., Chan, D., Lavoué, D., Andrews, E., Eleftheriadis, K., Maksyutov, S., 2013. 16‐year simulation of Arctic black carbon: Transport, source contribution, and sensitivity analysis on deposition. J. Geophys. Res-Atmos. 118, 943-964.

Silva, P.J., Prather, K.A., 2000. Interpretation of mass spectra from organic compounds in aerosol time-of-flight mass spectrometry. Anal. Chem. 72, 3553-3562.

Smith, J.N., Barsanti, K.C., Friedli, H.R., Ehn, M., Kulmala, M., Collins, D.R., Scheckman, J.H., Williams, B.J., McMurry, P.H., 2010. Observations of aminium salts in atmospheric nanoparticles and possible climatic implications. Proc. Natl. Acad. Sci. 107, 6634-6639.

Song, X.-H., Hopke, P.K., Fergenson, D.P., Prather, K.A., 1999. Classification of single particles analyzed by ATOFMS using an artificial neural network, ART-2A. Anal. Chem. 71, 860-865.

Spencer, M., Holecek, J., Corrigan, C., Ramanathan, V., Prather, K., 2008. Size‐resolved chemical composition of aerosol particles during a monsoonal transition period over the Indian Ocean. J. Geophys. Res-Atmos. 113.

Spencer, M.T., Shields, L.G., Prather, K.A., 2007. Simultaneous measurement of the effective density and chemical composition of ambient aerosol particles. Environ. Sci. Technol. 41, 1303-1309.

Spencer, M.T., Shields, L.G., Sodeman, D.A., Toner, S.M., Prather, K.A., 2006. Comparison of oil and fuel particle chemical signatures with particle emissions from heavy and light duty vehicles. Atmos. Environ. 40, 5224-5235.

Stohl, A., Klimont, Z., Eckhardt, S., Kupiainen, K., Shevchenko, V., Kopeikin, V., Novigatsky, A., 2013. Black carbon in the Arctic: the underestimated role of gas flaring and residential combustion emissions. Atmos. Chem. Phys. 13, 8833-8855.

Sultana, C.M., Cornwell, G.C., Rodriguez, P., Prather, K.A., 2017. FATES: a flexible analysis toolkit for the exploration of single-particle mass spectrometer data. Atmos. Meas. Tech. 10, 1323-1334.

Swart, N.C., Fyfe, J.C., Hawkins, E., Kay, J.E., Jahn, A., 2015. Influence of internal variability on Arctic sea-ice trends. Nature Climate Change 5, 86.

Tam, P.S., Kittrell, J.R., Eldridge, J.W., 1990. Desulfurization of fuel oil by oxidation and extraction. 1. Enhancement of extraction oil yield. Industrial & Engineering Chemistry Research 29, 321-324.

Tao, Y., Ye, X., Jiang, S., Yang, X., Chen, J., Xie, Y., Wang, R., 2016. Effects of amines on particle growth observed in new particle formation events. J. Geophys. Res-Atmos. 121, 324-335.

Toner, S.M., Shields, L.G., Sodeman, D.A., Prather, K.A., 2008. Using mass spectral source signatures to apportion exhaust particles from gasoline and diesel powered vehicles in a freeway study using UF-ATOFMS. Atmos. Environ. 42, 568-581.

Toner, S.M., Sodeman, D.A., Prather, K.A., 2006. Single particle characterization of ultrafine and accumulation mode particles from heavy duty diesel vehicles using aerosol time-of-flight mass spectrometry. Environ. Sci. Technol. 40, 3912-3921.

Wallace, J.M., Hobbs, P.V., 2006. Atmospheric science: an introductory survey. Academic Press.

Wang, M., Overland, J.E., 2015. Projected future duration of the sea-ice-free season in the Alaskan Arctic. Prog. Oceanogr. 136, 50-59.

Willis, M.D., Burkart, J., Thomas, J.L., Köllner, F., Schneider, J., Bozem, H., Hoor, P.M., Aliabadi, A.A., Schulz, H., Herber, A.B., 2016. Growth of nucleation mode particles in the summertime Arctic: a case study. Atmos. Chem. Phys. 15, 7663-7679.

Chapter 7.
Conclusions and Future Directions

7.1. Conclusions

This dissertation describes the construction of a aerosol time-of-flight mass spectrometer (ATOFMS) as well as the chemical characterization of aerosol populations during three unique field campaigns in rural environments impacted by climate change. An updated aircraft aerosol time-of-flight mass spectrometer (A-ATOFMS) first was constructed with reduced weight (~23 kg less), power consumption (~600 W less) and an expanded size range (down to 70 nm). During 2014, we partook in a small campaign at the University of Michigan Biological Station, where we chemically characterized the aerosol population while under the influence of long-range transported pollutants from Canadian wildfires and regional urban areas, finding major contributions from heavily aged biomass burning particles coated with SOA. During 2015, the newly built aircraft-capable aerosol time-of-flight mass spectrometer (A-ATOFMS) and a particle impactor for off-line SEM-EDX analysis were deployed to Utqiaġvik, AK in order to investigate the impacts on a remote aerosol population from transported Arctic oil and gas extraction emissions from Prudhoe Bay, located hundreds of kilometers to the east. During Prudhoe Bay air masses, the A-ATOFMS combined with off-line SEM-EDX chemically characterized increased combustion emissions (organic carbon, soot) as well as aged SSA. This was compared to the clean Arctic Ocean air masses, consisting primarily of fresh SSA. During 2016, we took the A-ATOFMS into the Prudhoe Bay oilfields to investigate contributions nearby to these oil and gas extraction sources within both direct plumes and the overall oil field background population. During plumes, the A-ATOFMS chemically characterized increased soot and organic carbon, including a unique amine-containing organic carbon attributed to natural gas purification processes. The oil field background was also characterized and had these same anthropogenic influences, in stark contrast to the typical clean Arctic background.

Chapter 2 detailed the design and construction of the A-ATOFMS, based on the previous version of the A-ATOFMS described by of Pratt et al. (2009). The newest A-ATOFMS

underwent a near complete electronic overhaul, with updated turbomolecular and scroll pumps, pressure gauges, lasers, timing circuit, and computer. This led to instrument weight reduction and increased performance. Notably, due to using lower wavelength lasers and an internally black anodized particle sizing region, the lower limit of particle characterization has improved to 70 nm. As the number concentration mode for ambient aerosols is less than 100 nm (Seinfeld and Pandis, 2016), the ability to chemically characterize these smaller particles will lead to a more representative characterization of the aerosol population. In addition, due to the upgraded computer and 100 Hz 266 nm DI laser, the theoretical maximum spectral acquisition rate doubled from 30 Hz to 67 Hz, providing increased data acquisition capability, particularly in polluted environments where ambient particle concentration may be elevated or within a fast-moving aircraft. This newly built A-ATOFMS has already been deployed on two field campaigns to northern Alaska and used in many laboratory studies, with many more planned for the future.

Chapter 3 detailed single particle chemical characterization efforts of long-range transported Canadian wildfire smoke on northern Michigan using the TSI 3800 ATOFMS, an earlier commercial version of our A-ATOFMS discussed in Chapter 2. Summer of 2014 was one of the most active burning seasons for Canada in the past 20 years with a total of 10,643 km^2 of land burned (CIFFC, 2017). This smoke was transported to our field site in northern Michigan, where we classified ~90%, by number, of the 0.5 – 2.0 μm particles as aged biomass burning particles, internally mixed with sulfate and oxidized organics. These particles were likely primarily SOA by mass, as 90% of the non-refractory PM_1 mass was identified as organics by aerosol mass spectrometry. In the United States, biomass burning is the largest combustion contributor by mass of SOA (Jathar et al., 2014). As OC is currently underpredicted in the midwest United States (Napelenok et al., 2013; Spak and Holloway, 2009), it is likely much of the missing mass is from these SOA contributions. As Canadian wildfires are expected to increase in intensity and frequency due to climate change (Gillett et al., 2004; Knorr et al., 2016; Liu et al., 2010; Veira et al., 2016), contributions from SOA from biomass burning are likely to continue increasing in the future.

Chapter 4 discussed particle growth events and how they were influenced by both regional and transported air masses during the summer 2014 northern Michigan field campaign. Particle growth was observed during three unique air mass classifications: urban-influence,

wildfire-influence, and regional-influence. Growth events during urban influenced air masses occurred during the daytime, and a combination of elevated oxidants and solar radiation likely led to OH oxidation of BVOCs and production of condensable organics. Wildfire-influenced growth events only occurred during the nighttime. Increased NO_x from the wildfires likely led to NO_3 oxidation of SO_2 and BVOCs, particularly monoterpenes, and subsequent particle growth. Finally, two multi-day growth events occurred during stagnant air masses, likely influenced by regional BVOC oxidation. Particles analyzed by TEM-EDX during all growth events contained sulfur, oxygen, and carbon, consistent with H_2SO_4 and organics contributing to the observed particle growth.

Chapter 5 discussed results of our field campaign near Utqiaġvik, AK, where we used A-ATOFMS and CCSEM-EDX to chemically characterize the clean Arctic background aerosol population and influences from the Prudhoe Bay oil fields, located hundreds of kilometers to the southeast. During Prudhoe Bay air masses, particle number concentrations were nearly 10 times the level of the clean Arctic background and the particle mode decreased from 76 nm down to 27 nm, likely due to the contribution of transported combustion particles. In addition, SSA had higher internal mixtures with sulfate and nitrate due to chloride depletion during atmospheric processing. Increased number fractions of organic carbon particles, internally mixed mixtures with sulfate and nitrate, were also observed. During the clean Arctic background, SSA was identified as the major contributor to both submicron and supermicron particles, and showed minimal chloride depletion. Particle aging has been previously shown to increase CCN activities of certain particle types (Furutani et al., 2008), and these combustion particles are likely to contribute to the on-going Arctic warming and lead to a further decrease in sea ice extent.

Chapter 6 detailed the results of our second field campaign to Alaska, using the A-ATOFMS within the Prudhoe Bay oil fields. The field site was influenced by direct plumes from nearby point sources. Background air masses periods were unique as they differed from the traditional "clean" Arctic background previously measured (Chapter 5), due to the 360 degree influence from both on-shore and off-shore oil and gas extraction emissions. During plumes, $PM_{2.5}$ number and mass concentration were ~4 and ~2 times higher than background oil field conditions. The majority (90%) of these particles were less than 100 nm in diameter and were attributed to fresh combustion, similar to the transported particles from the Prudhoe Bay oil fields detailed in Chapter 5. During both plumes and oil field background periods, the majority

of particles were chemically characterized as soot, aged soot, or organic carbon. A unique OC particle type consisting primarily of amines was also measured during these periods, attributed to solutions used in natural gas production processes (Kadnar, 1999; Patel et al., 2007; Tam et al., 1990). These measurements are also the first reported single particle chemical characterization conducted within the Prudhoe Bay oilfields.

7.2. Future Directions

While the A-ATOFMS has been fully constructed, characterized, and successfully operated in the field, improvements can still be made to the instrument. Notably, as mentioned in Chapter 2, our updated timing circuit was built with additional output channels with the ability to output the waveforms of the scattered laser collected by the PMT during particle sizing. This waveform can be used to calculate chemically-resolved single particle measurements of density and refractive index (Moffet and Prather, 2005; Moffet et al., 2008). In addition, further software improvements, specifically accurately timing the trigger to collect this scattered light waveform need to be completed before this additional feature can be fully implemented within the instrument.

The results of the field campaigns detailed in Chapters 3-6 have led to further questions that can be investigated. For example, most of the organic carbon particles measured at UMBS and described in Chapter 3 had markers for SOA but also potassium, commonly used to identify biomass burning. It is likely that these OC particles were highly aged biomass burning particles coated with a large mass of SOA, however in order to confirm this we would need to identify the particle core. Recently, a thermodenuder based on the design of Huffman et al. (2008) was constructed in the Pratt Lab, and this thermodenuder could be used to investigate semi-volatile and non-volatile aerosol components of these particles. ,If we were to return to UMBS and measure a similar air mass using the thermodenuder, we could volatilize the SOA and reveal the non-volatile particle core, similarly to the study by Pratt and Prather (2009) in an urban environment. We'd expect the SOA to volatize and the markers to no longer appear in the spectra, with just the expected non-volatile biomass burning particle mass spectral "fingerprint" remaining (Pratt and Prather, 2009).

One of the limitations of the A-ATOFMS is the inability to chemically characterize pure sulfate particles, as these particles do not absorb the 266 nm radiation used for particle

desorption and ionization. This has been a well known ATOFMS limitation and is not unique to our updated A-ATOFMS (e.g. Sierau et al., 2014; Wenzel et al., 2003). During our field campaign to Utqiaġvik, AK described in Chapter 5, CCSEM-EDX detected a sulfur particle type that made up ~10 – 30% of the particle number fraction, varying by size (0.1 – 4 μm projected area diameter). The A-ATOFMS could scatter these particles but could not ionize them well due to the limitations of the 266 nm laser; a few very weak negative spectra showed a single sulfate peak at *m/z* -97 (HSO_4^-). However, if the A-ATOFMS was fit with a lower wavelength laser, it may be possible to detect these sulfur particles in future studies. Ideally, the A-ATOFMS would need a 193 nm excimer laser installed to be able to characterize these sulfate particles, either replacing the 266 nm laser or installed in parallel with some mechanism to switch between the two lasers. A downside to using a 193 nm excimer laser would be increased organic ion fragmentation, limiting the chemical information gained. Recently, Quantel Inc. began manufacturing a 213 nm Ultra CFR laser, similar to the design of the laser used on the original A-ATOFMS but at a lower wavelength. This would be easier to retrofit onto the current A-ATOFMS than an eximer laser, and would result in less fragmentation than the 193 nm laser. Using a 213 nm laser would require new optics to transmit the beam, therefore the laser could not simply be installed in place of the 266 nm laser. Ideally, the 213 nm laser would be installed next to the 266 nm laser, and aligned to a unique laser path. The ionization energy of the 213 nm laser is only 5.83 eV, ~25% higher than 266 nm (4.66 eV), but still less than the 193 nm laser (6.42 eV). Accounting for two-photon ionization, the ionization energy of 266 nm (9.32 eV total) and 213 nm (11.66 eV total) would still be less than the ionization energy required for sulfuric acid (12.4 eV) (Snow and Thomas, 1990). However, previous studies have shown that coating sulfate-rich particles with small amounts UV-absorbing compounds, such as organics, can increase ablation efficiency (Kane and Johnston, 2001). Therefore, if sulfate-rich compounds were internally mixed with even small amounts of UV-absorbing compounds, it may be possible to successfully ionize them with the 213 nm laser.

Finally, during the Prudhoe Bay campaign described in Chapter 6, many days were foggy, suggesting the potential for aqueous-phase reactions. Previous single particle mass spectrometer studies have identified hydroxymethanesulfonate (HMS), which appears at *m/z* -111 ($HOCH_2SO_3^-$), as a marker for fog processing (e.g. Dall'Osto et al., 2009; Rehbein et al., 2011; Whiteaker and Prather, 2003). Preliminary data analysis shows many periods throughout

the study with high particle counts and particle number fractions containing HMS, particularly during periods of on-going fog. Work is on-going within our lab to further characterize the fog processing within this dataset, using not only our single particle data, but also other data from instruments within the ARM AMF3 and AOS, both operating throughout our field campaign.

7.3. References

Canadian Interagency Forest Fire Centre, National Wildland Fire Situation Report. Accessed July 2016. http://www.ciffc.ca.

Dall'Osto, M., Harrison, R., Coe, H., Williams, P., 2009. Real-time secondary aerosol formation during a fog event in London. Atmos. Chem. Phys. 9, 2459-2469.

Furutani, H., Dall'osto, M., Roberts, G.C., Prather, K.A., 2008. Assessment of the relative importance of atmospheric aging on CCN activity derived from field observations. Atmos. Environ. 42, 3130-3142.

Gillett, N., Weaver, A., Zwiers, F., Flannigan, M., 2004. Detecting the effect of climate change on Canadian forest fires. Geophys. Res. Lett. 31, L18211.

Huffman, J.A., Ziemann, P.J., Jayne, J.T., Worsnop, D.R., Jimenez, J.L., 2008. Development and characterization of a fast-stepping/scanning thermodenuder for chemically-resolved aerosol volatility measurements. Aerosol. Sci. Technol. 42, 395-407.

Jathar, S.H., Gordon, T.D., Hennigan, C.J., Pye, H.O., Pouliot, G., Adams, P.J., Donahue, N.M., Robinson, A.L., 2014. Unspeciated organic emissions from combustion sources and their influence on the secondary organic aerosol budget in the United States. Proc. Natl. Acad. Sci. 111, 10473-10478.

Kadnar, R., 1999. Determination of amines used in the oil and gas industry (upstream section) by ion chromatography. Journal of Chromatography A 850, 289-295.

Kane, D.B., Johnston, M.V., 2001. Enhancing the detection of sulfate particles for laser ablation aerosol mass spectrometry. Anal. Chem. 73, 5365-5369.

Knorr, W., Jiang, L., Arneth, A., 2016. Climate, CO2 and human population impacts on global wildfire emissions. Biogeosciences 13, 267-282.

Liu, Y., Stanturf, J., Goodrick, S., 2010. Trends in global wildfire potential in a changing climate. Forest. Ecol. Manag. 259, 685-697.

Moffet, R.C., Prather, K.A., 2005. Extending ATOFMS measurements to include refractive index and density. Anal. Chem. 77, 6535-6541.

Moffet, R.C., Qin, X., Rebotier, T., Furutani, H., Prather, K.A., 2008. Chemically segregated optical and microphysical properties of ambient aerosols measured in a single‐particle mass spectrometer. J. Geophys. Res-Atmos. 113, D12213.

Napelenok, S.L., Simon, H., Bhave, P.V., Pye, H.O., Pouliot, G.A., Sheesley, R.J., Schauer, J.J., 2013. Diagnostic air quality model evaluation of source-specific primary and secondary fine particulate carbon. Environ. Sci. Technol. 48, 464-473.

Patel, A., Stamatakis, S., Young, S., Friedheim, J., 2007. Advances in inhibitive water-based drilling fluids—can they replace oil-based muds?, International Symposium on Oilfield Chemistry. Society of Petroleum Engineers.

Pratt, K.A., Mayer, J.E., Holecek, J.C., Moffet, R.C., Sanchez, R.O., Rebotier, T.P., Furutani, H., Gonin, M., Fuhrer, K., Su, Y., 2009. Development and characterization of an aircraft aerosol time-of-flight mass spectrometer. Anal. Chem. 81, 1792-1800.

Pratt, K.A., Prather, K.A., 2009. Real-time, single-particle volatility, size, and chemical composition measurements of aged urban aerosols. Environ. Sci. Technol. 43, 8276-8282.

Rehbein, P.J., Jeong, C.-H., McGuire, M.L., Yao, X., Corbin, J.C., Evans, G.J., 2011. Cloud and fog processing enhanced gas-to-particle partitioning of trimethylamine. Environ. Sci. Technol. 45, 4346-4352.

Seinfeld, J.H., Pandis, S.N., 2016. Atmospheric chemistry and physics: from air pollution to climate change. John Wiley & Sons, Hoboken, New Jersey.

Sierau, B., Chang, R.-W., Leck, C., Paatero, J., Lohmann, U., 2014. Single-particle characterization of the high-Arctic summertime aerosol. Atmos. Chem. Phys. 14, 7409-7430.

Snow, K.B., Thomas, T.F., 1990. Mass spectrum, ionization potential, and appearance potentials for fragment ions of sulfuric acid vapor. Int. J. Mass. Spectrom. 96, 49-68.

Spak, S.N., Holloway, T., 2009. Seasonality of speciated aerosol transport over the Great Lakes region. J. Geophys. Res-Atmos. 114, D08302.

Tam, P.S., Kittrell, J.R., Eldridge, J.W., 1990. Desulfurization of fuel oil by oxidation and extraction. 1. Enhancement of extraction oil yield. Industrial & Engineering Chemistry Research 29, 321-324.

Veira, A., Lasslop, G., Kloster, S., 2016. Wildfires in a warmer climate: Emission fluxes, emission heights, and black carbon concentrations in 2090–2099. J. Geophys. Res-Atmos. 121, 3195-3223.

Wenzel, R.J., Liu, D.Y., Edgerton, E.S., Prather, K.A., 2003. Aerosol time‐of‐flight mass spectrometry during the Atlanta Supersite Experiment: 2. Scaling procedures. J. Geophys. Res-Atmos. 108.

Whiteaker, J.R., Prather, K.A., 2003. Hydroxymethanesulfonate as a tracer for fog processing of individual aerosol particles. Atmos. Environ. 37, 1033-1043.

Appendix A.

Ubiquitous Influence of Wildfire Emissions and Secondary Organic Aerosol on Summertime Atmospheric Aerosol in the Forested Great Lakes Region Supplemental Information

A.1.Supporting Measurements

Meteorological data (Figure A.1.), including wind direction, wind speed, relative humidity, and temperature, were collected by a Vaisala WXT510 weather sensor located at the top of the PROPHET tower. Variations in meteorological conditions throughout the study, and average meteorological conditions during each period of influence, are discussed in the main text. In order to determine the origin of the influential air masses (Figure A.2.), backward air mass trajectories were calculated using the NOAA Hybrid Single Particle Lagrangian Integrated Trajectory (HYSPLIT) Model (Stein et al., 2015). A final altitude of 500 m AGL was used for the field site, with each trajectory modeling the proceeding 72 h. During each of the three influence air mass locations, median, was well as 25^{th} and 75^{th} percentile aerosol number and size distributions were calculated based on SMPS measurements (Figure A.3.).

A.2.References

Stein, A., Draxler, R., Rolph, G., Stunder, B., Cohen, M., Ngan, F., 2015. NOAA's HYSPLIT atmospheric transport and dispersion modeling system. B. Am. Meteorol. Soc. 96, 2059-2077.

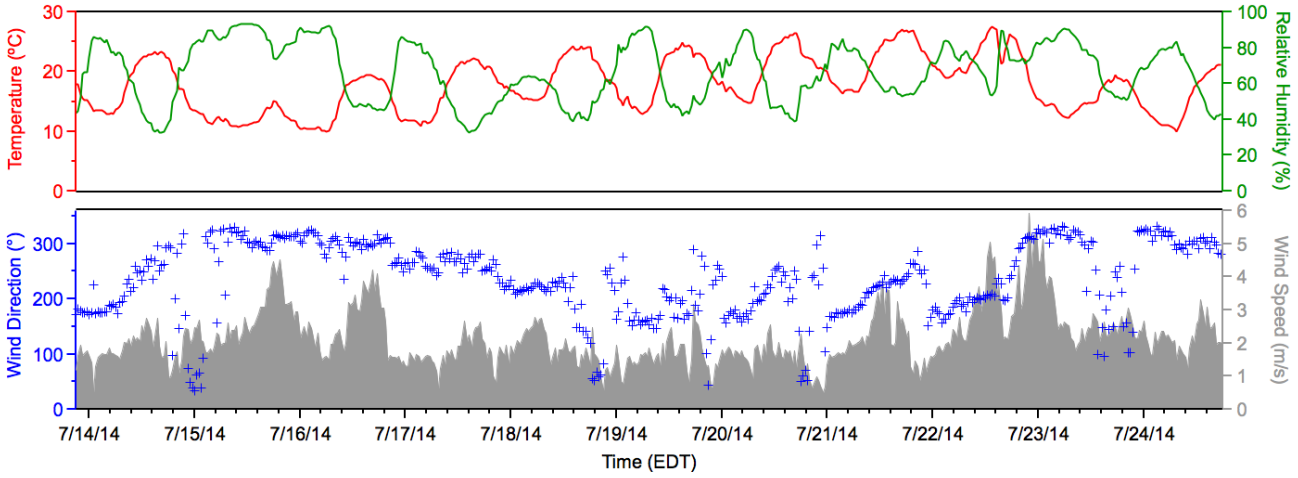

Figure A.1. Meteorological conditions measured from a height of ~30 m at the UMBS PROPHET Tower.

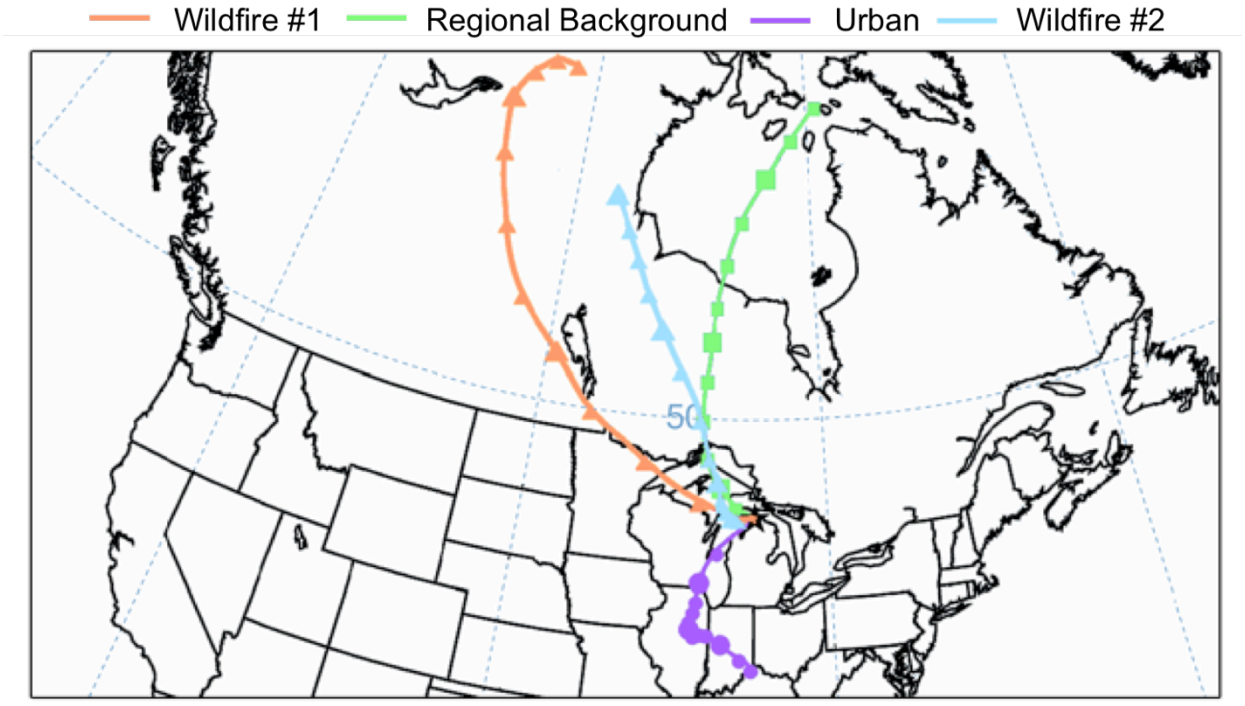

Figure A.2. Representative 72 h HYSPLIT back trajectories with a final altitude of 500 m for the four air mass influences, with markers indicating 6 h intervals. Trajectory start times were: Wildfire #1: 7/14/2014 07:00 EDT, Regional Background: 7/17/2014 07:00 EDT, Urban: 7/21/2014 07:00 EDT, Wildfire #2: 7/24/14 07:00 EDT. Colors correspond to the air mass of influence indicated in Figure 3.3.

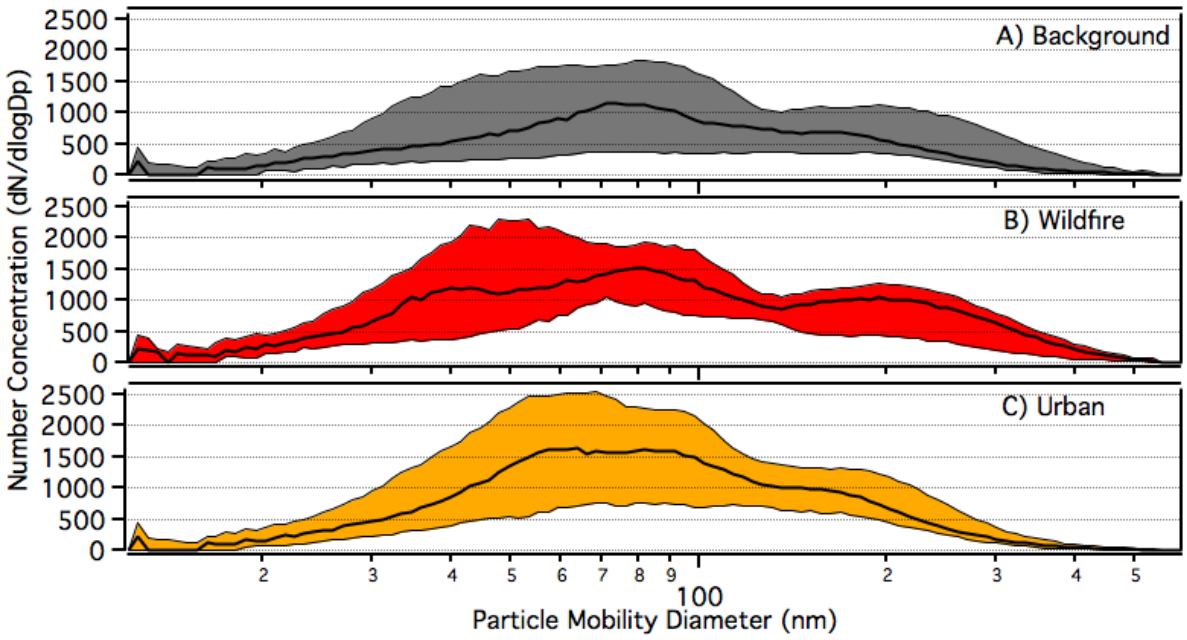

Figure A.3. Median and 25th/75th percentiles of particle number and mobility diameter distributions during the three time periods of interest (described in the main text) as measured by SMPS: (A) Background, (B) Wildfire, and (C) Urban.

Appendix B.

Particle Growth in an Isoprene-Rich Forest: Influences of Urban, Wildfire, and Biogenic Precursors Supplemental Information

B.1. SMPS Correction Factor

From July 11-22, 2014, both an SMPS 3938 and SMPS 3936 were present at the field site. The SMPS 3938 sampled above the canopy (~ 34 m) and the SMPS 3936 sampled at ground level (~5 m) (Figure S1). In order to directly compare the number concentrations reported by both instruments, both instruments sampled from the same inlet at ground level (~5 m) for ~6 h on July 10, 2014. These data were then averaged for the duration of the sampling period for each individual size bin for each instrument. A ratio was then made between the two instruments, resulting in a correction factor (Figure S2) to apply to the SMPS 3936, as it had, on average, undercounted the number concentration. This corrected number concentration was used for the analysis present in this paper.

B.2. Additional Factors Contributing to Particle Growth

In general, growth events than began at a smaller particle size had an increased growth rate compared to those beginning at larger sizes (Figure S3). A linear fit of particle starting diameter versus particle growth shows a weak inverse correlation with an R^2 of 0.37, however a trend can still be observed. In addition, daytime growth events were typically observed during periods of increased solar radiation (Figure S4) and generally during increased transported NO_2 (Figure S5) indicative of photochemical reactions occurring under the influence of transported urban emissions, discussed further in the main text (Section 3.1).

B.3. Meteorological Conditions

Meteorological data (Figure S6) were obtained from the AmeriFlux tower at UMBS, located 100 m northeast of the PROPHET tower. Temperature and relative humidity were

collected by a Rotronic HPO-43 probe. Wind speed and wind direction were measured by a Campbell Scientific CSAT3 sonic anemometer. Total solar radiation (400-1100 nm) was measured by a LI-COR pyranometer (LI-200) located on a Great Lake Observing System buoy on Douglas Lake, 4 km northeast of PROPHET.

B.4. Wildfire Contributions to Particle Growth

Throughout particle growth events observed during the nighttime, the field site was under the influence of transported wildfire air masses from northwestern Canada (Section 3.2, main text). Using NOAA HMS smoke products, direct wildfire influence was observed (Figure 5, S7, with the remaining provided in Gunsch et al. (2017)). In addition, particle growth observed in Kanawade et al. (2011) also likely occurred during wildfire influence, and NOAA HMS smoke product maps are provided for these days in Figure S8.

B.5. Bi-modal Growth During Forested/Stagnant (Multiday) Events

During event #1 occurring during stagnant conditions (Section 3.3, main text) on June 25, a second mode appeared in the evening at 25 nm and continued to growth until the morning on June 26 (Figure S9). Due to the substantial growth observed from this second mode, this was classified as event #2.

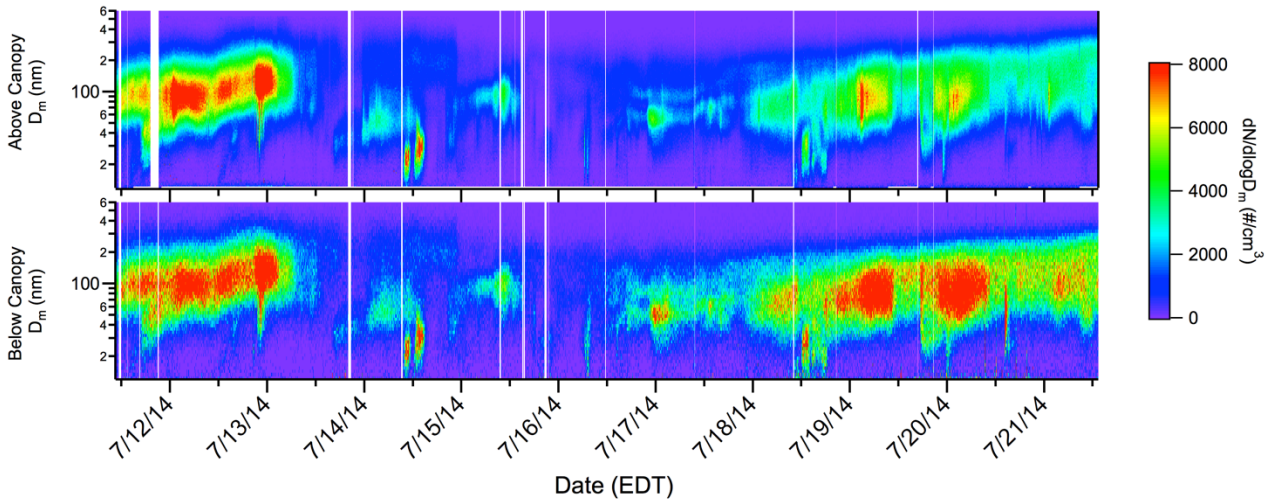

Figure B.1. Comparison of above canopy (34 m) and below canopy (3 m) corrected particle size distributions measured by the two SMPS instruments.

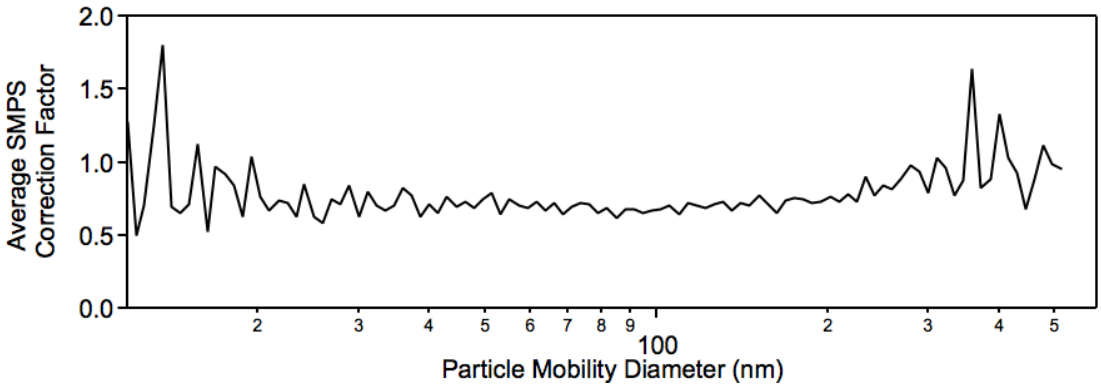

Figure B.2. Average correction factor applied to the SMPS 3936 to allow direct comparison with the SMPS 3938.

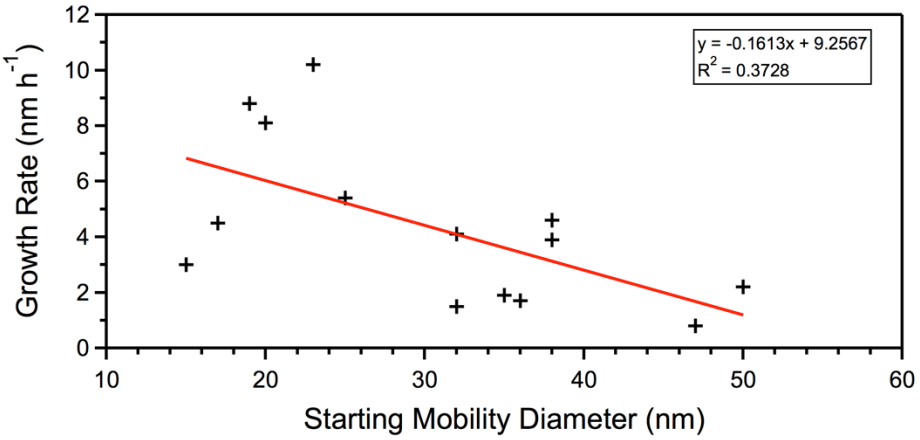

Figure B.3. Particle starting diameter mode compared to growth rate for all 14 particle growth events.

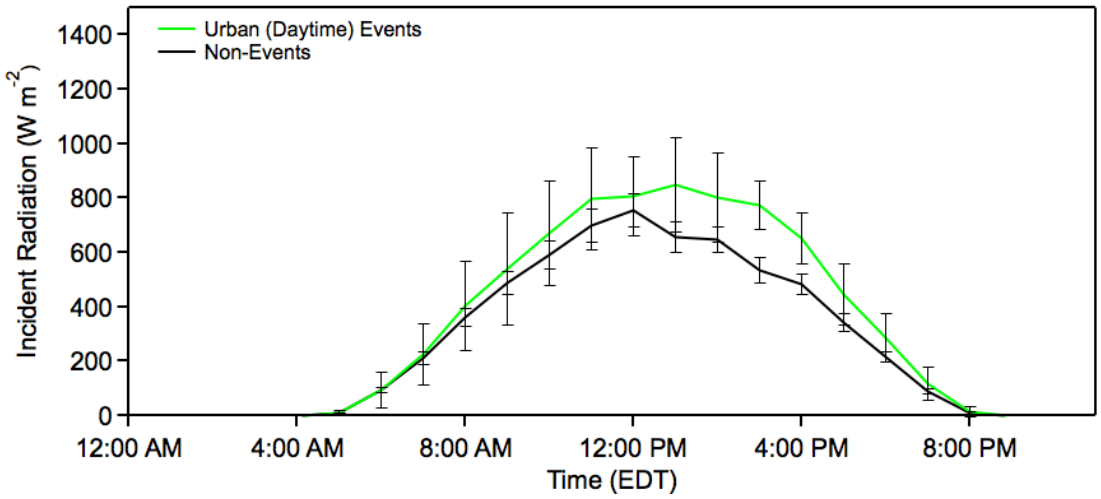

Figure B.4. Average incident solar radiation for daytime event (green) and non-event periods (black). Error bars depict the 95% confidence interval for each point. Anomalous data from June 29 11:00 – 13:00 EDT are not included due to a brief but intense rainstorm with heavy cloud coverage.

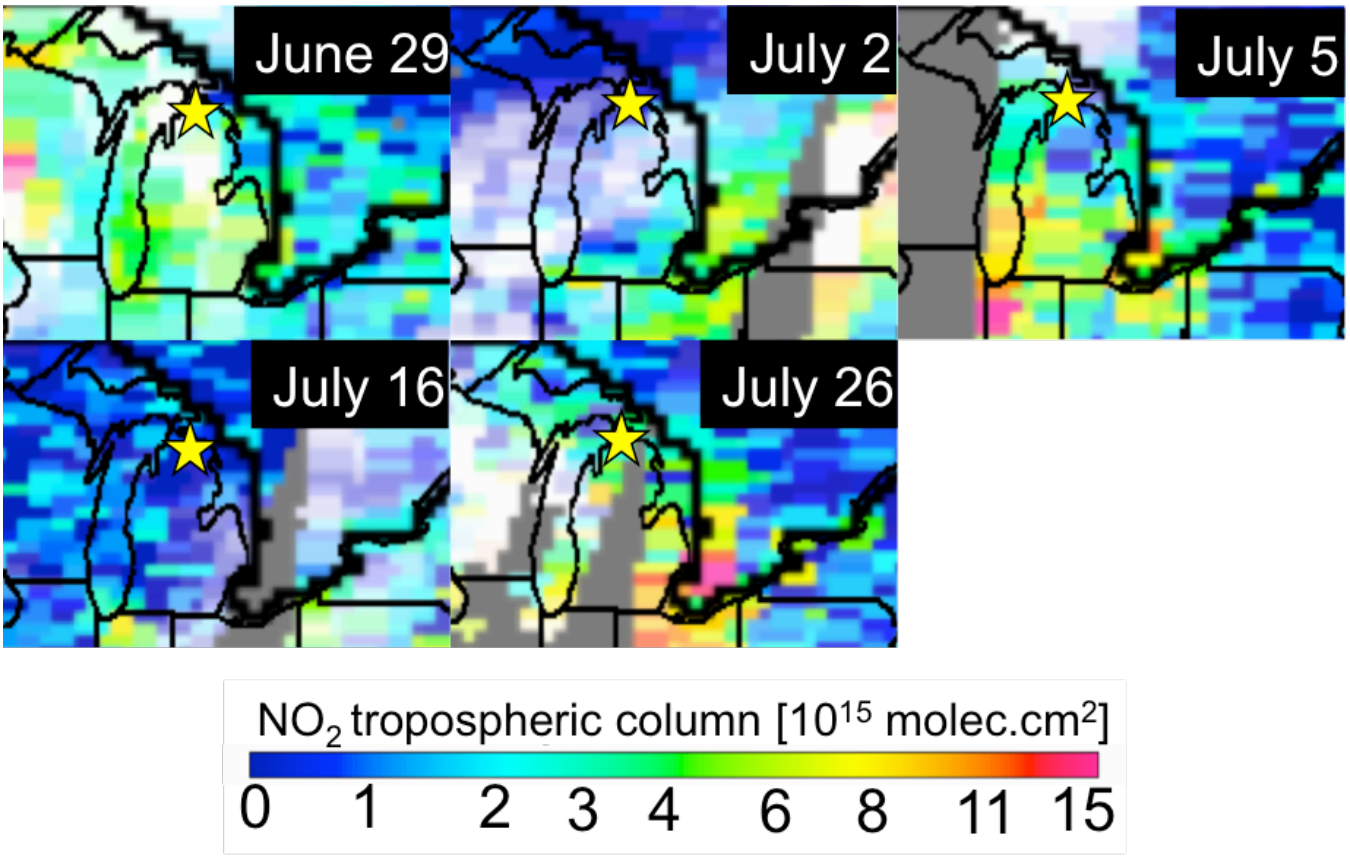

Figure B.5. Tropospheric column NO_2 from TEMIS OMI on June 29, July 2, July 5, July 16, and July 26. Field site is indicated by a yellow star.

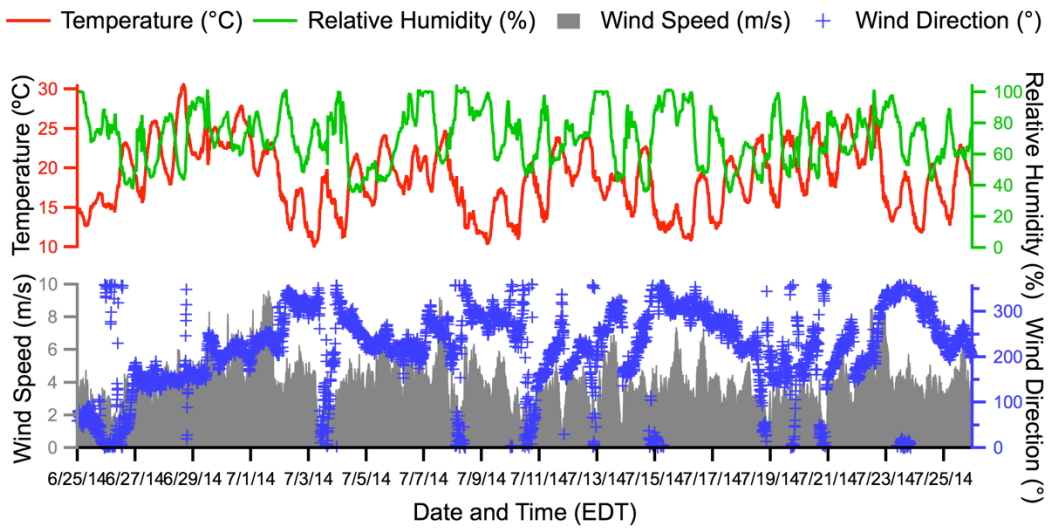

Figure B.6. Meteorological conditions for the duration of the UMBS field campaign. Wind speed, wind direction, and relative humidity were collected from the Ameriflux tower at a height of 46 m located 100 m northeast of PROPHET.

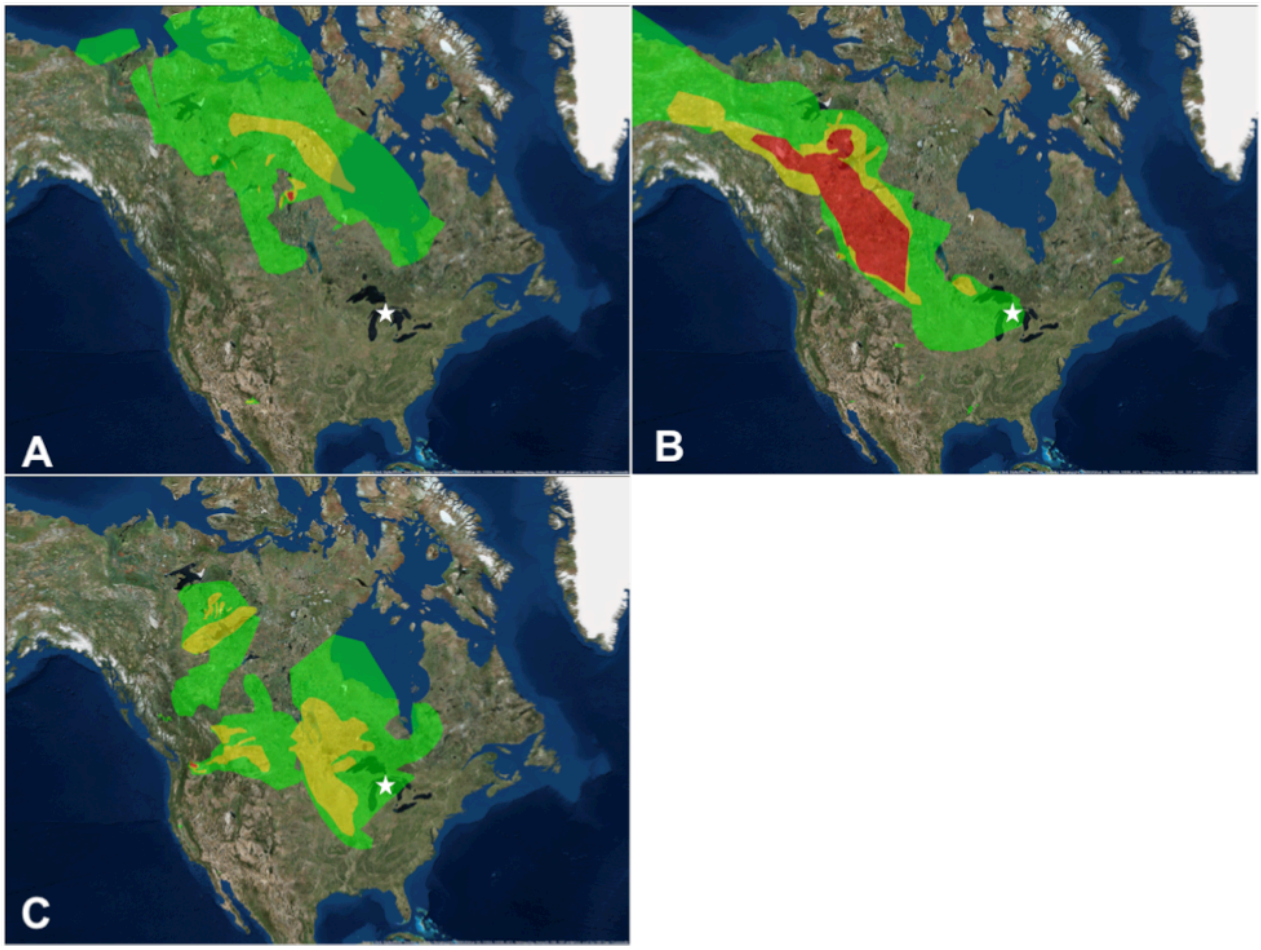

Figure B.7. NOAA HMS smoke maps for three nighttime growth events on **(A)** June 25, **(B)** July 7, and **(C)** July 9, with the remaining nighttime growth event smoke maps provided by Gunsch et al., 2017. Smoke coverage is categorized as heavy (red), medium (yellow), and light (green). UMBS is marked on each map by a white star. Map imagery were provided by ArcGIS 10.3.1 with World Imagery basemap (Sources: Esri, DigitalGlobe, GeoEye, Earthstar Geographics, CNES/Airbus DS, USDA, USGS, AeroGRID, IGN, and the GIS User Community).

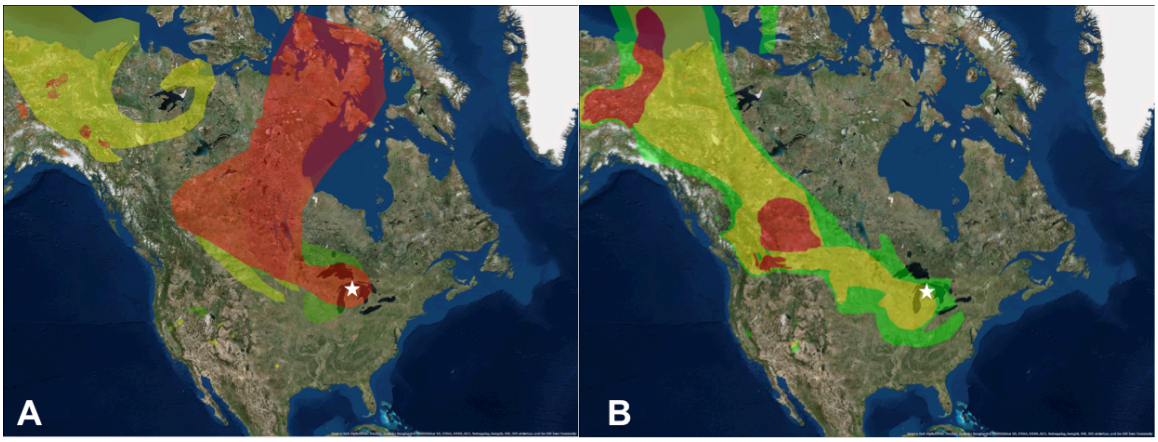

Figure B.8. NOAA HMS smoke maps for two nighttime growth events, described by Kanawade et al, (2011), on (A) July 16, 2009 and (B) August 2, 2009. Smoke coverage is categorized as heavy (red), medium (yellow), and light (green). UMBS is marked on each map by a star. Map imagery was provided by ArcGIS 10.3.1 with World Imagery basemap (Sources: Esri, DigitalGlobe, GeoEye, Earthstar Geographics, CNES/Airbus DS, USDA, USGS, AeroGRID, IGN, and the GIS User Community).

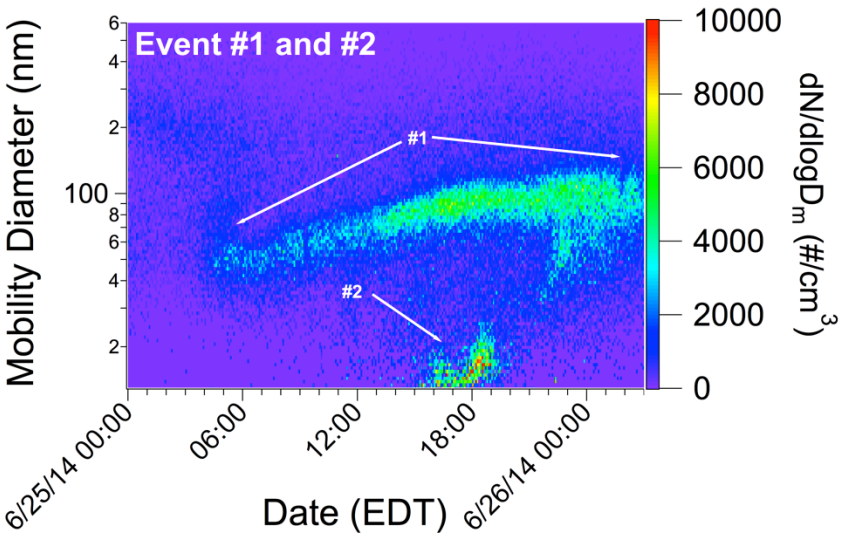

Figure B.9. Time-resolved aerosol size distribution for Event #1 and #2.

Appendix C.

Contributions of Transported Prudhoe Bay Oil Field Emissions to the Aerosol Population in Utqiaġvik, Alaska Supplemental Information

C.1. Particle Type Classification

SSA was characterized by an intense peak at *m/z* 23, corresponding to Na^+, and less intense peaks at *m/z* 39 (K^+), 81 (Na_2Cl^+), -35/37 (Cl^-) and -93/95 (Na_2Cl^-) (Ault et al., 2013). Spectra that also contained intense markers for nitrate (*m/z* -46, -62) or sulfate (*m/z* -64, -80) was sub-classified as aged SSA. Organic carbon (OC) was characterized by intense peaks at *m/z* 37 (C_3H^+) and 27 ($C_2H_3^+$) and are attributed to combustion (Toner et al., 2008). A sub-classification of OC was characterized by an intense peak at *m/z* 59 ($N(CH_3)_3^+$), which is characteristic of the presence of trimethylamine (TMA) (Rehbein et al., 2011) and has been detected previously in the Arctic (Willis et al., 2016). Rehbein et al. (2011) found that TMA was exclusively found during high relative humidity or fog events when gas phase TMA partitioned onto the particles or fog droplets. Relative humidity was high throughout the duration of the study (average of 91%), thus partitioning of TMA to the particle-phase is likely to occur. Due to the small number of TMA-containing particles, both OC particle types were grouped into a single OC class. Soot particles were characterized by elemental carbon C_n^+ fragment peaks, observed at *m/z* 12[C^+], 24[C_2^+], 36[C_3^+], 48[C_4^+], etc. that are typical of incomplete combustion (Toner et al., 2008). Biomass burning (BB) particles were characterized by an intense peak at *m/z* 39 (K^+) and *m/z* -97 (HSO_4^-) with less intense peaks at *m/*z 43 ($C_3H_2O^+$), 27 ($C_2H_3^+$) and 12 (C^+) (Pratt et al., 2011). Dust was present in two different forms: calcium-rich and iron-rich. Calcium-rich dust (Ca-Dust) was characterized by an intense peak at *m/z* 40 (Ca^+) with less intense peaks at *m/*z 23 (Na^+), 24 (Mg^+) and 56/57 ($CaOH^+$/$CaOH_2^+$). Iron-rich dust (Fe-dust) was characterized by intense peaks at *m/z* 54/56 (Fe^+). All dust particle types were combined into a single cluster, as the majority

likely originated from the nearby beaches, dirt roads and soil. Average spectra for each particle type are shown in Figure 2.

Particle types were identified based on observed morphology from SEM as well as composition and atomic percentages calculated from the EDX spectra. These classes are based on prior SEM-EDX studies, which established EDX spectra for fresh and aged SSA (Ault et al., 2013; Hara et al., 2003), organic carbon aerosol (Laskin et al., 2006; Moffet et al., 2010), soot (Jiang et al., 2011), biomass burning aerosol (Li et al., 2003; Pósfai et al., 2003), and mineral dust (Coz et al., 2009; Sobanska et al., 2003). Fresh SSA was characterized by large amounts Na and Cl, with Na/Mg and Na/Cl ratios close to those found in seawater. Aged SSA was characterized by Na and S and/or N > Cl, indicative of chlorine displacement by heterogeneous reactions (Laskin et al., 2003; Laskin et al., 2002). OC particles were round and contained large amounts of C and O with the majority also containing small fractions of S and/or N (Moffet et al., 2010). Soot was primarily carbon in composition and had a chain-like agglomerate morphology (Quennehen et al., 2012; Weinbruch et al., 2012). Dust particles were characterized by large fractions of Al and Si, in addition to trace metals such as Fe (Coz et al., 2009; Sobanska et al., 2003). Some fly ash particles, primarily aluminum and silicon oxides, may also be present in this class, but due to similarities in chemical composition between fly ash and dust accompanied by low abundance, fly ash and dust will be considered together. Minor contributions from BB were also identified, characterized by large amounts of K and Cl but little Na (Pósfai et al., 2003). A sulfur-rich particle type was identified by greater amounts of S as compared to C and O. This is likely the "missing" particle type unable to be characterized by the ATOFMS in this study, as well as the previous ATOFMS study by Sierau et al. (2014). Wenzel et al. (2003) previously attributed scattered, but not ionized particles by ATOFMS, as relatively pure ammonium sulfate particles.

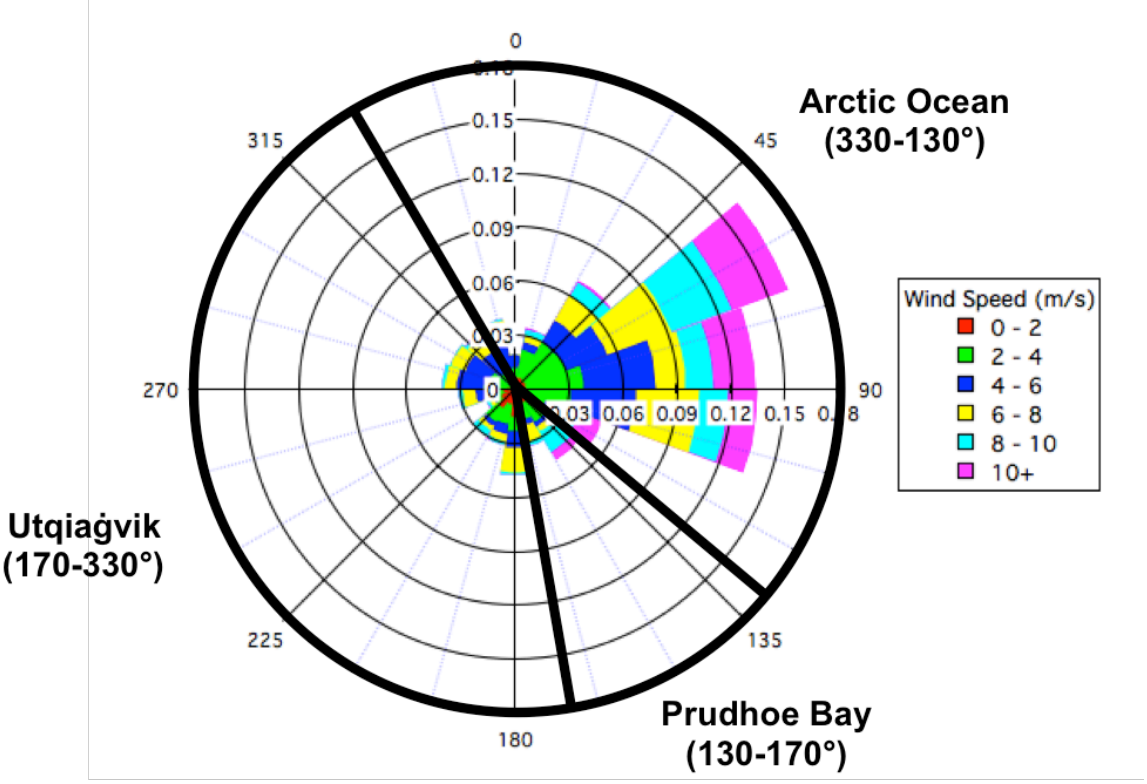

Figure C.1. Wind rose from August 21–September 30, 2015 measured at the NOAA Barrow Observatory. Wind speed is binned by 2 m/s, and wind direction is binned by 20 degrees, with the radial axes representing the fraction of the study under those wind conditions.

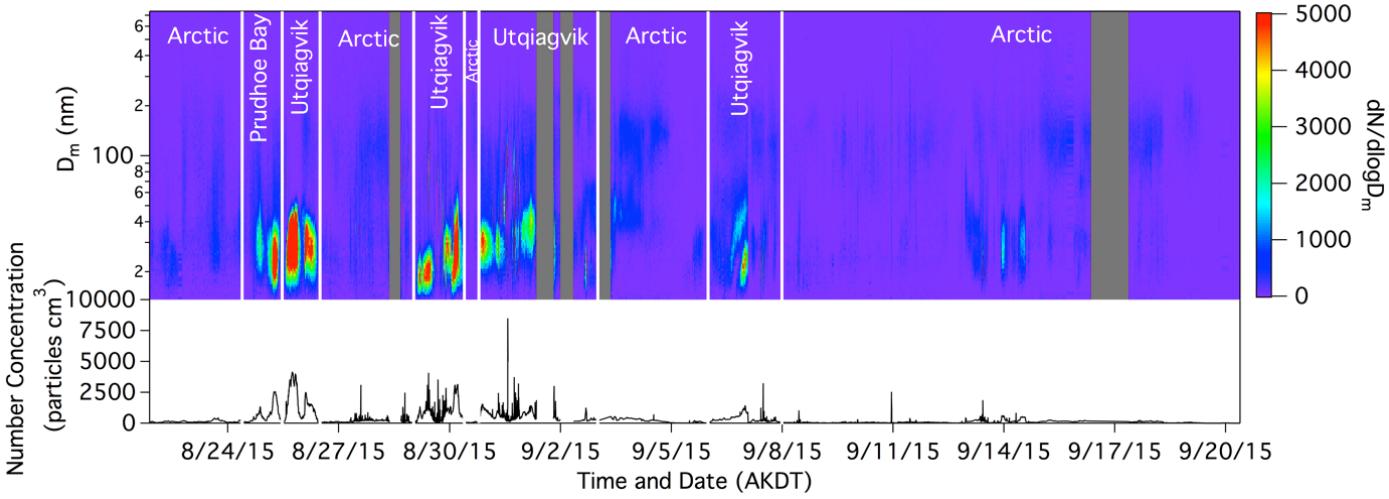

Figure C.2. Aerosol size-resolved number concentrations (mobility diameter) measured by the SMPS from August 21-September 20, 2015. Identified air mass source regions, determined based on wind direction and backward air mass trajectories, are labeled and divided by white lines in the time series. Periods lacking data are indicated in gray. The total particle (0.013 – 746 nm) number concentration is also shown.

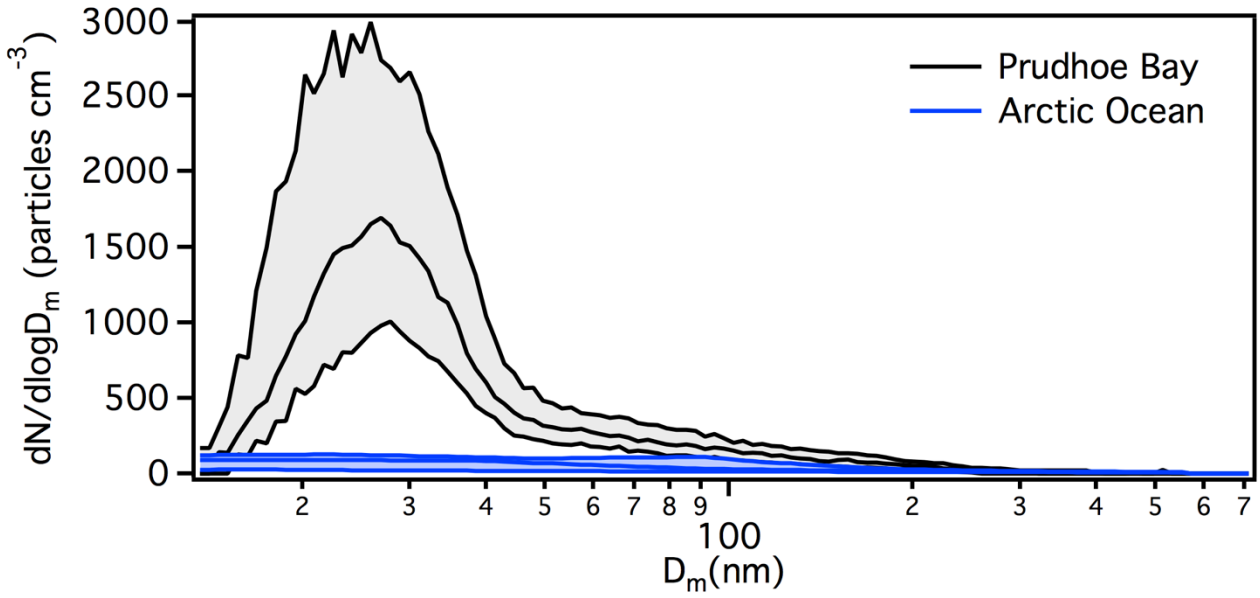

Figure C.3. Median, as well as 25th and 75th percentile, particle size distributions during Prudhoe Bay and Arctic Ocean influenced air masses from August 21–September 20, 2015.

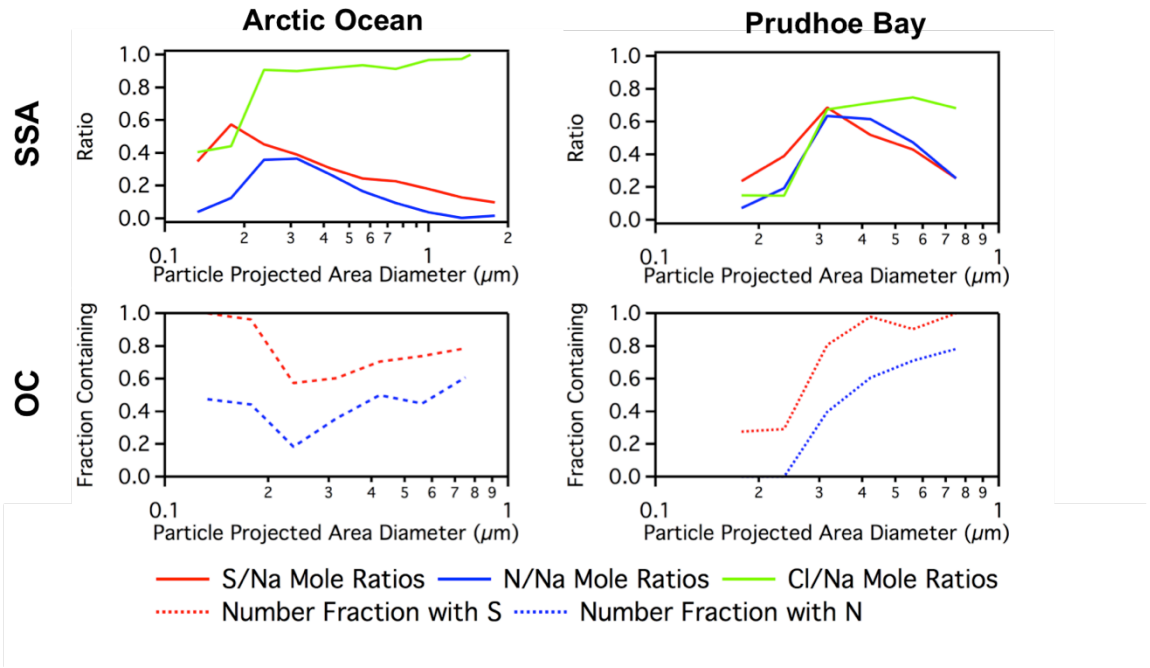

Figure C.4. S/Na, N/Na, Cl/Na mole ratios of individual SSA (top) and fraction of OC particles (bottom) containing S, N, and/or Cl, measured by CCSEM-EDX for Arctic Ocean and Prudhoe Bay influenced air masses. Size bins with less than 25 particles are not displayed.

C.2. References

Ault, A.P., Guasco, T.L., Ryder, O.S., Baltrusaitis, J., Cuadra-Rodriguez, L.A., Collins, D.B., Ruppel, M.J., Bertram, T.H., Prather, K.A., Grassian, V.H., 2013. Inside versus outside: Ion redistribution in nitric acid reacted sea spray aerosol particles as determined by single particle analysis. J. Am. Chem. Soc. 135, 14528-14531.

Coz, E., Gómez-Moreno, F.J., Pujadas, M., Casuccio, G.S., Lersch, T.L., Artíñano, B., 2009. Individual particle characteristics of North African dust under different long-range transport scenarios. Atmos. Environ. 43, 1850-1863.

Hara, K., Yamagata, S., Yamanouchi, T., Sato, K., Herber, A., Iwasaka, Y., Nagatani, M., Nakata, H., 2003. Mixing states of individual aerosol particles in spring Arctic troposphere during ASTAR 2000 campaign. J. Geophys. Res-Atmos. 108.

Jiang, M.Y., Li, J.Q., Wu, Y.Q., Lin, N.T., Wang, X.M., Fu, F.F., 2011. Chemical characterization of nanometer-sized elemental carbon particles emitted from diesel vehicles. J. Aerosol. Sci. 42, 365-371.

Laskin, A., Cowin, J.P., Iedema, M.J., 2006. Analysis of individual environmental particles using modern methods of electron microscopy and X-ray microanalysis. J. Electron. Spectrosc. 150, 260-274.

Laskin, A., Gaspar, D.J., Wang, W., Hunt, S.W., Cowin, J.P., Colson, S.D., Finlayson-Pitts, B.J., 2003. Reactions at interfaces as a source of sulfate formation in sea-salt particles. Science 301, 340-344.

Laskin, A., Iedema, M.J., Cowin, J.P., 2002. Quantitative time-resolved monitoring of nitrate formation in sea salt particles using a CCSEM/EDX single particle analysis. Environ. Sci. Technol. 36, 4948-4955.

Li, J., Pósfai, M., Hobbs, P.V., Buseck, P.R., 2003. Individual aerosol particles from biomass burning in southern Africa: 2, Compositions and aging of inorganic particles. J. Geophys. Res-Atmos. 108.

Moffet, R.C., Henn, T., Laskin, A., Gilles, M.K., 2010. Automated Chemical Analysis of Internally Mixed Aerosol Particles Using X-ray Spectromicroscopy at the Carbon K-Edge†. Anal. Chem. 82, 7906-7914.

Pósfai, M., Simonics, R., Li, J., Hobbs, P.V., Buseck, P.R., 2003. Individual aerosol particles from biomass burning in southern Africa: 1. Compositions and size distributions of carbonaceous particles. J. Geophys. Res-Atmos. 108.

Pratt, K., Murphy, S., Subramanian, R., DeMott, P., Kok, G., Campos, T., Rogers, D., Prenni, A., Heymsfield, A., Seinfeld, J., 2011. Flight-based chemical characterization of biomass burning aerosols within two prescribed burn smoke plumes. Atmos. Chem. Phys. 11, 12549-12565.

Quennehen, B., Schwarzenboeck, A., Matsuki, A., Burkhart, J., Stohl, A., Ancellet, G., Law, K.S., 2012. Anthropogenic and forest fire pollution aerosol transported to the Arctic: observations from the POLARCAT-France spring campaign. Atmos. Chem. Phys. 12, 6437-6454.

Rehbein, P.J., Jeong, C.-H., McGuire, M.L., Yao, X., Corbin, J.C., Evans, G.J., 2011. Cloud and fog processing enhanced gas-to-particle partitioning of trimethylamine. Environ. Sci. Technol. 45, 4346-4352.

Sierau, B., Chang, R.-W., Leck, C., Paatero, J., Lohmann, U., 2014. Single-particle characterization of the high-Arctic summertime aerosol. Atmos. Chem. Phys. 14, 7409-7430.

Sobanska, S., Coeur, C., Maenhaut, W., Adams, F., 2003. SEM-EDX characterisation of tropospheric aerosols in the Negev desert (Israel). J. Atmos. Chem. 44, 299-322.

Toner, S.M., Shields, L.G., Sodeman, D.A., Prather, K.A., 2008. Using mass spectral source signatures to apportion exhaust particles from gasoline and diesel powered vehicles in a freeway study using UF-ATOFMS. Atmos. Environ. 42, 568-581.

Weinbruch, S., Wiesemann, D., Ebert, M., Schütze, K., Kallenborn, R., Ström, J., 2012. Chemical composition and sources of aerosol particles at Zeppelin Mountain (Ny Ålesund, Svalbard): An electron microscopy study. Atmos. Environ. 49, 142-150.

Wenzel, R.J., Liu, D.Y., Edgerton, E.S., Prather, K.A., 2003. Aerosol time‐of‐flight mass spectrometry during the Atlanta Supersite Experiment: 2. Scaling procedures. J. Geophys. Res-Atmos. 108.

Willis, M.D., Burkart, J., Thomas, J.L., Köllner, F., Schneider, J., Bozem, H., Hoor, P.M., Aliabadi, A.A., Schulz, H., Herber, A.B., 2016. Growth of nucleation mode particles in the summertime Arctic: a case study.

Appendix D.

Diesel and Natural Gas Combustion Contributions to Atmospheric Aerosols in an Arctic Oil Field Supplemental Information

D.1.Particle Type Classification

Biomass burning (BB) particles were characterized by an intense peak at *m/z* 39 (K^+), with less intense peaks at *m/z* 27 ($C_2H_3^+$), 37 (C_3H^+), 51 ($C_4H_3^+$), and 73 (C_6H^+) (Pratt et al., 2010). BB particles did not contain any negatives, likely due to the accumulation of water during transport (Neubauer et al., 1997), which indicates a non-local source. A potassium chloride-rich particle type, classified as incineration, was also identified by an intense *m/z* 39 (K^+), with less intense peaks at *m/z* 63, 65 (Cu^+) and *m/z* 113, 115, 117 ($K_2Cl^{+/-}$), as well as nitrate identified at *m/z* -46 (NO_2^-) and -62 (NO_3^-). This particle type was attributed to a local incinerator located to the north, as these particles were only present during brief periods when air was coming directly from this location; the mass spectra are similar to previously reported fly ash and incineration particles (Moffet et al., 2008; Spencer et al., 2008), and was therefore classified as an incineration particle type. Mineral dust was identified by strong Fe^+ (*m/z* 56), Ca^+ (*m/z* 40), and Na^+ (*m/z* 23) peaks and is attributed to lofting from nearby dirt roads and beaches surrounding the site.

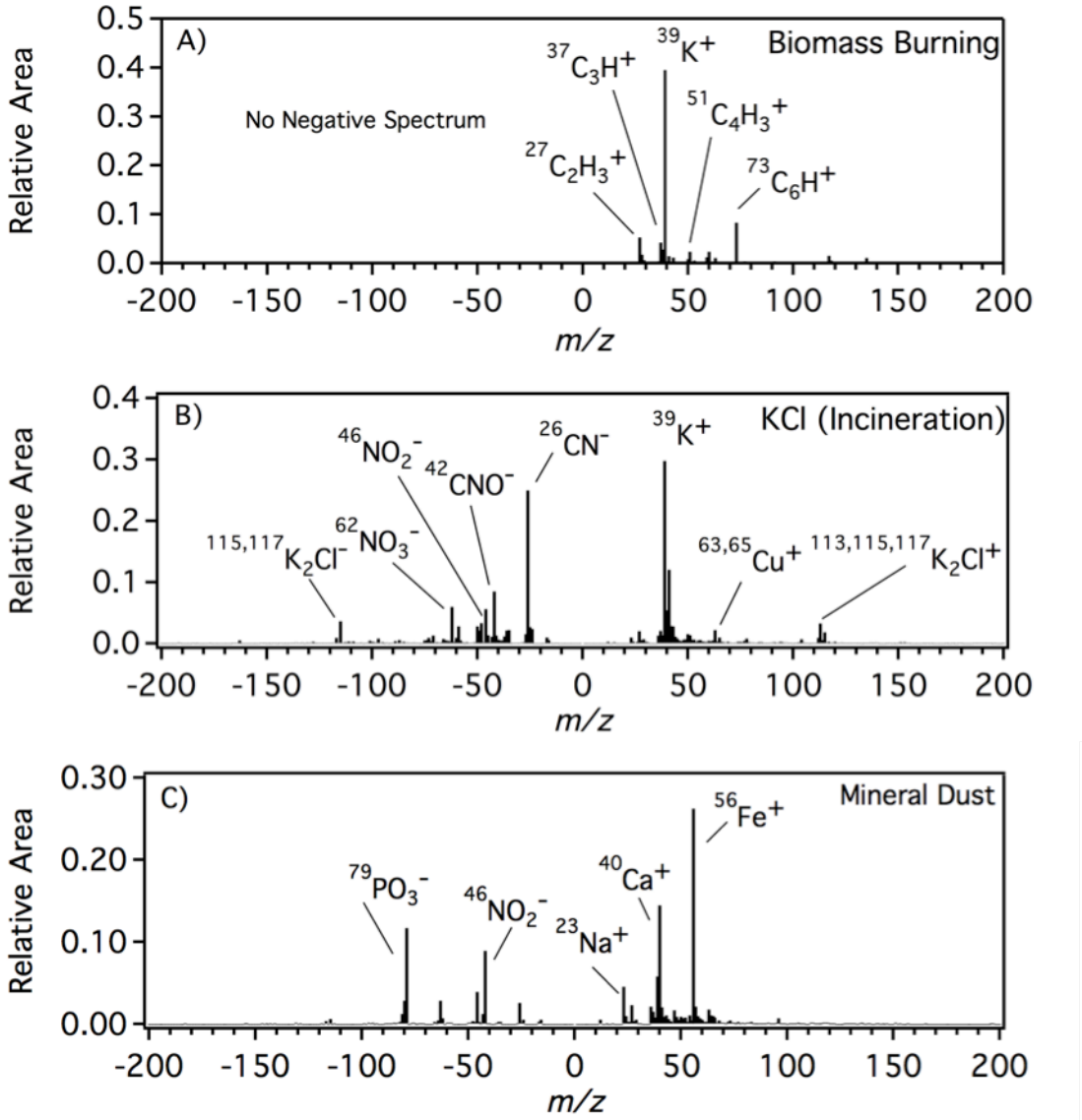

Figure D.1. Average A-ATOFMS mass spectra for particles types observed: **(A)** biomass burning, **(B)** incineration, and **(C)** mineral dust**.**

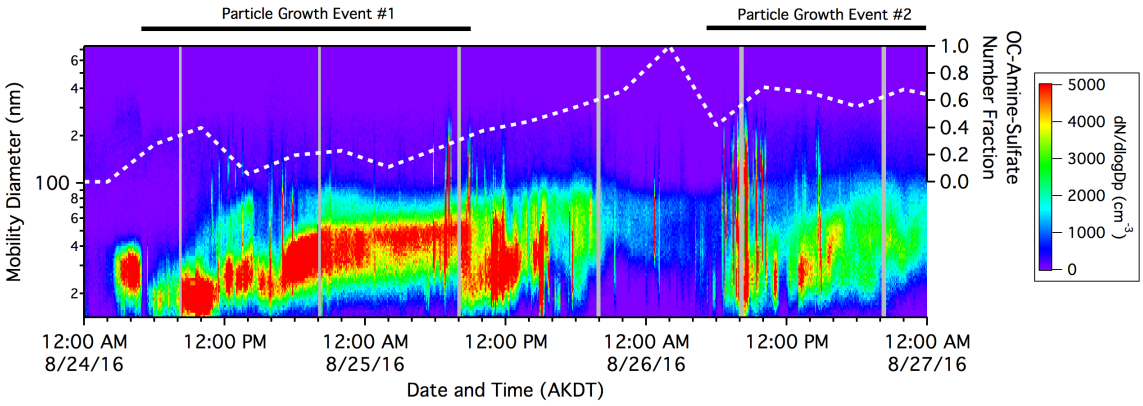

Figure D.2. SMPS size distribution (14 – 740 nm) during two particle growth events that occurred from August 24 06:00 – August 25 20:00 AKDT and August 26 06:00 – August 27 00:00. OC-Amine-Sulfate number fraction is plotted as a dotted white line for comparison.

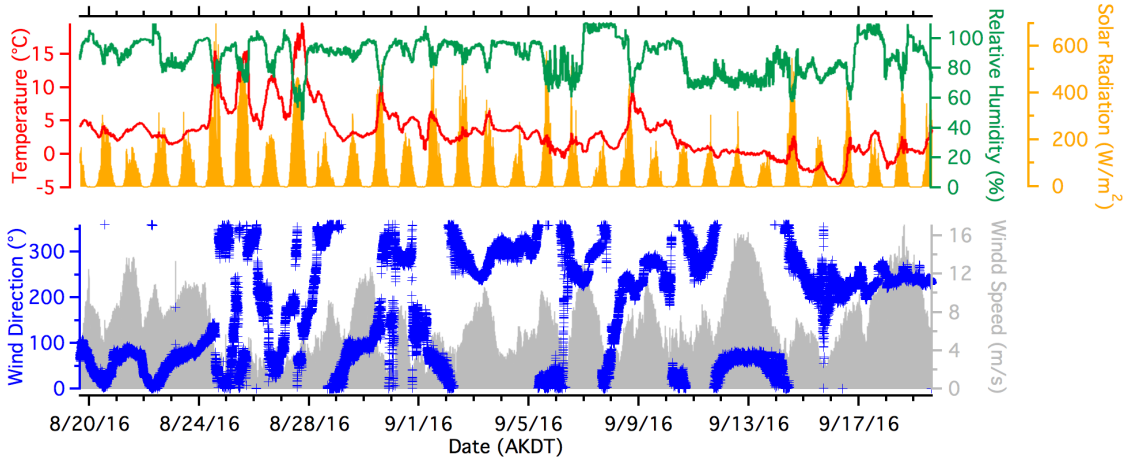

Figure D.3. Meteorological conditions at the Oliktok Point field site collected from a height of 10 m.

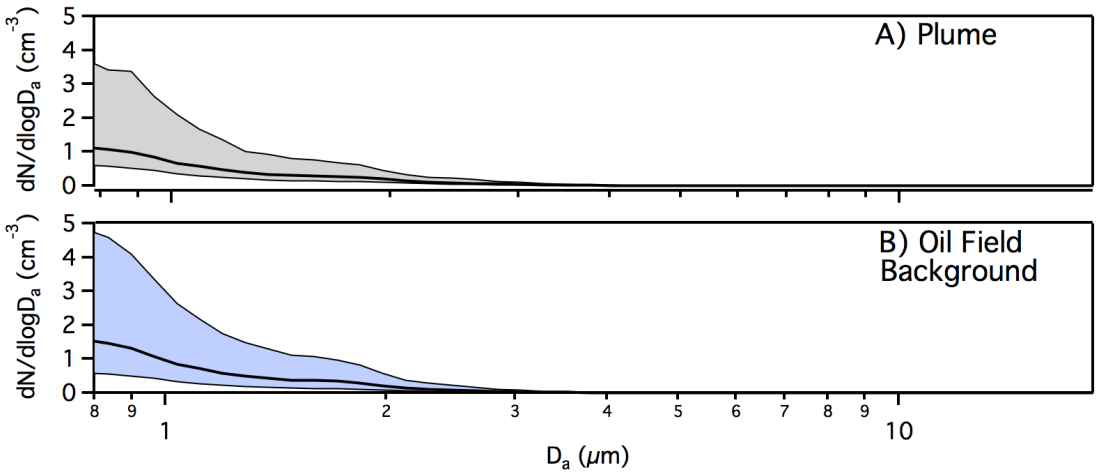

Figure D.4. Median aerosol size-resolved number concentrations (0.746 – 718 μm aerodynamic diameter) and 25th/75th percentiles, measured by APS, during **(A)** direct plume and **(B)** oil field background air mass periods at Oliktok Point, AK.

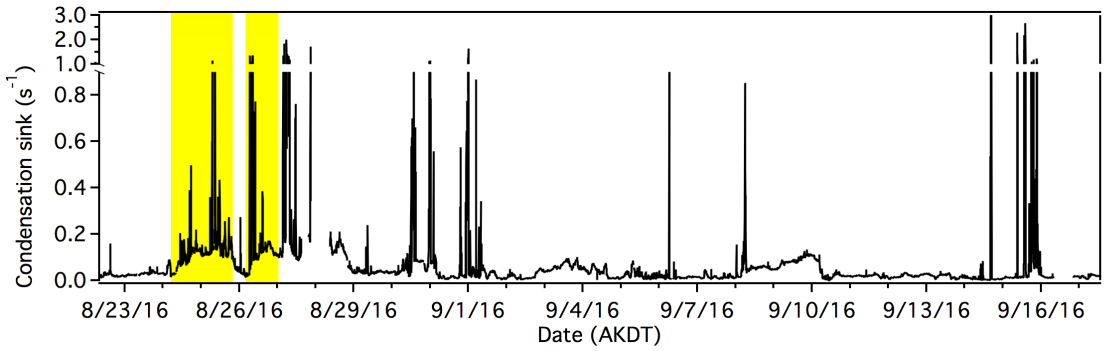

Figure D.5. Condensation sink, calculated using the combined SMPS and APS particle size number distribution, for the duration of the study. Periods of particle growth are highlighted in yellow.

D.2.References

Moffet, R.C., Qin, X., Rebotier, T., Furutani, H., Prather, K.A., 2008. Chemically segregated optical and microphysical properties of ambient aerosols measured in a single‐particle mass spectrometer. J. Geophys. Res-Atmos. 113, D12213.

Neubauer, K.R., Johnston, M.V., Wexler, A.S., 1997. On-line analysis of aqueous aerosols by laser desorption ionization. Int. J. Mass. Spectrom. 163, 29-37.

Pratt, K.A., Heymsfield, A.J., Twohy, C.H., Murphy, S.M., DeMott, P.J., Hudson, J.G., Subramanian, R., Wang, Z., Seinfeld, J.H., Prather, K.A., 2010. In situ chemical characterization of aged biomass-burning aerosols impacting cold wave clouds. J. Atmos. Sci. 67, 2451-2468.

Spencer, M., Holecek, J., Corrigan, C., Ramanathan, V., Prather, K., 2008. Size‐resolved chemical composition of aerosol particles during a monsoonal transition period over the Indian Ocean. J. Geophys. Res-Atmos. 113.

Toner, S.M., Shields, L.G., Sodeman, D.A., Prather, K.A., 2008. Using mass spectral source signatures to apportion exhaust particles from gasoline and diesel powered vehicles in a freeway study using UF-ATOFMS. Atmos. Environ. 42, 568-581.